Université des Sciences et Technologies de Lille

Ecole Doctorale

Sciences de la Matière, du Rayonnement et de l'Environnement

Thèse pour obtenir le titre de

Docteur de l'Université des Sciences et Technologies de Lille

Molécules et Matière Condensée

Thomas Lukowicz

Synergistic Solubilisation of Fragrances in Binary Surfactant Systems and Prediction of their EACN Value with COSMO-RS

Thèse dirigée par :

Pr. Jean-Marie Aubry, Directeur

Pr. Véronique Nardello-Rataj, Co-Directrice

Soutenue le 12 Octobre 2015

Membres du Jury

Dr. Thomas Sottmann	Université de Stuttgart	**Rapporteur**
Dr. Fabienne Testard	CEA Saclay	**Rapporteur**
Dr. Liudmila Mokrushina	Université de Erlangen-Nuremberg	**Examinateur, Président**
Pr. Jean-Marie Aubry	ENSCL	**Directeur**
Pr. Véronique Nardello-Rataj	Université de Lille 1	**Co-Directrice**

Acknowledgments

Without the support of so many people, this research project would have not been possible.

In this context I would like to express my gratitude to my supervisor Professor Jean-Marie Aubry for creating such an interesting project. The discussions were always very fruitful and enthusiastic. Very often they resulted in the development of new ideas and experiments. Especially his eagerness for COSMO-RS, convinced me to dare the step into the – to me previously unknown - world of computational modelling.

Furthermore I would like to thank my co-supervisor Professor Véronique Nardello-Rataj for her interesting advices and her constant support during my thesis. Especially the helpful improvements during the creation of the manuscript were well appreciated.

I would like to thank the members of the committee Dr. Thomas Sottmann, Dr. Fabienne Testard and Dr. Liudmila Mokrushina for the kindness and time to judge my work, as well as for taking the trouble to come to Lille for my defense.

Moreover I would like to express my sincere gratitude to Dr. Christel Pierlot, Dr. Raphael Lebeuf and Dr. Valérie Molinier for their extremely valuable assistance concerning emulsions, organic synthesis and NMR spectroscopy.

My gratitude goes as well to Dr. Andreas Klamt - the creator of COSMO-RS - for his extremely helpful advices concerning the σ-moments, which led to the publishing of scientific work.

A special thanks goes to my friend Dr. Fabio Manca, who invested a lot time in explaining me the principals of multilinear regression analysis and statistics.

I owe my deepest respect to Dr. Fermin Jesus Ontiveros for his help concerning surfactant/oil/water systems, to Dr. Adrien Benazzouz for his effort in explaining COSMO-RS to me, as well as to Dr. Delphine Blonde for her help in organizing the sensorial testing.

I want to express my sincere gratitude also to the rest of my colleagues for their time and help during the last three years: Adrien Mouret, Andrea Mühlbauer, Benjamin Joosen, Bing Hong, Bingyu Yang, Christoph Penverne, Laura Dubrulle, Laurianne Moity, Loic Leclercq, Maxime Nollet, Maxime Royer, Mike Ortega, Roberto Company Maldonado, Romain Guitard.

For their excellent work, I want to thank also my student apprentices Lison Podevin and Blandine Couchouron.

At last I wish to thank my family, who always supported and encouraged me, even in bad times. Their support was invaluable and highlighted their importance to me.

In the same way I can only express my deepest gratitude to Estelle Illous, my love, who was always there for me. Who always encouraged me and motivated me, but as well put my mind at ease, when I started to lose my head!

Resumé

Les "solvo-surfactants" appartiennent à une nouvelle classe de molécules amphiphiles qui présentent à la fois les propriétés de tensiaoctifs et de solvants. Ils sont en effet capables de former des agrégats et peuvent ainsi solubiliser des composés hydrophobes. De plus, ces molécules présentent une volatilité importante, ce qui les rend particulièrement intéressantes pour des applications où cette propriété est décisive, notamment au cours de la solubilisation aqueuse de parfums. Les comportements de phase et d'agrégation de "solvo-surfactants" en solution aqueuse sont ici étudiés. L'influence de tensioactifs ioniques est aussi considérée afin de mettre en évidence une synergie avec les amphiphiles non ioniques. Il est montré que des faibles quantités (traces) de tensioactifs ioniques permettent d'augmenter significativement la miscibilité des "solvo-surfactants" dans l'eau, particulièrement pour les systèmes riches en eau. Dans un système solvo-surfactant/huile/eau (SHE), le comportement de phase est fortement influencé par l'hydrophobicité de l'huile. Le nombre équivalent de carbones d'alcane (EACN) de différentes huiles polaires telles que dialkyléthers, 2-alcanones, 1-chloroalcanes etc... est ainsi étudié. La diminution de l'EACN en comparaison avec les *n*-alcanes est reliée à leur fonctionnalisation. L'ordre suivant est déterminé : *n*-Alcanes > 1-alkylcyclohexanes > 1-alcenes > dialkylethers ≈ 1-chloroalcanes > 1-alcylbenzenes ≈ ethyl alcanoates ≈ 1-alcynes > alcanenitriles > 2-alcanones. La diminution de l'EACN est rationnalisée grâce au paramètre d'empilement effectif pour chaque type d'huile correspondante. Les EACN de 94 huiles différentes ont été utilisés dans une analyse de régression multilinéaire basée sur les sigma moments de COSMO-RS, dans le but d'établir un modèle QSPR capable de prédire l'EACN d'hydrocarbones qui ne contiennent pas de groupement donneur de liaison hydrogène. Enfin, l'influence de tensioactifs ioniques sur un système SHE est déterminée avec plusieurs huiles d'EACN différents. Il est montré que le tensioactif ionique augmente fortement la température de stabilité du pseudo système ternaire de même que l'efficacité de solubilisation de l'huile. Cependant, cette efficacité atteint un maximum à un certain ratio molaire en tensioactif ionique car ce dernier empêche le système de s'inverser. Ainsi, une microémulsion bicontinue, connue pour solubiliser une grande quantité d'huile et d'eau, ne peut pas être formée.

Mots clés: Solubilisation de parfum, Microémulsion, Solvo-surfactant, EACN, Synergie entre des tensioactifs, COSMO-RS, Sigma-moments, Paramètre d'empilement

Abstract

Solvo-surfactants are a relatively new class of amphiphiles, which exhibit properties of both, surfactants and solvents. They are able to form aggregates, wherein they can solubilise hydrophobic compounds. Furthermore they exhibit volatile characteristics, which make them interesting for applications where volatility is a key factor, such as aqueous fragrance solubilisations. In this context the phase and aggregation behaviour of solvo-surfactants in aqueous solution is investigated. Furthermore the influence of ionic surfactants is determined, in order to highlight the synergistic effects between non-ionic amphiphile and ionic surfactant. It was shown that traces of ionic surfactants are able to strongly increase the miscibility of the solvo-surfactant in water, especially for water-rich systems. In a solvo-surfactant/oil/water (SOW) system, the phase behaviour is strongly influenced by the hydrophobicity of the oil. Therefore the equivalent alkane carbon number (EACN) of several polar oils, such as dialkylethers, 2-alkanones, 1-chloroalkanes etc. were investigated and the decrease in EACN with respect to *n*-alkanes was related to its functionalization. Following order was found: *n*-Alkanes > 1-alkylcyclohexanes > 1-alkenes > dialkylethers ≈ 1-chloroalkanes > 1-alkylbenzenes ≈ ethyl alkanoates ≈ 1-alkynes > alkanenitriles > 2-alkanones. The decrease in EACN was rationalised with the effective packing parameter for each corresponding type of oil. The EACN of all 94 oils were then used in a multilinear regression analysis, based on COSMO-RS σ-moments, in order to establish a QSPR model, which is able to predict the EACN of any hydrocarbon oil, which contains no hydrogen bond donors. The influence of ionic surfactants was finally investigated in a SOW system, with various oils of different EACN. It was found that the ionic surfactant increases strongly the temperature stability of the (pseudo-)ternary system, as well as the efficiency to solubilise the oil. However the efficiency undergoes a maximum for a certain molar fraction of ionic surfactant, since the latter prevents the system to inverse. Thus a bicontinuous microemulsion cannot be formed, which is known to solubilise high amounts of oil and water.

Keywords: Fragrance Solubilisation, Microemulsion, Solvo-surfactant, EACN, Surfactant synergy, COSMO-RS, Sigma-moments, Packing parameter

Abbreviations

A	alcohol mass concentration
a	alcohol specific coefficient
α	weight fraction of oil within water and oil
α_1	non-ionic surfactant molar fraction within the binary surfactant mixture
ACN	Alkane Carbon Number
b	salt specific coefficient
β	interaction parameter
CAC	critical aggregation concentration
CAC*	critical aggregation concentration of the mixed surfactant system
Cc	characteristic curvature ionic surfactant
Ccn	characteristic curvature non-ionic surfactant
cep_α	critical endpoint α
cep_β	critical endpoint β
cp_α	critical point α
cp_β	critical point β
c_{T}	surfactant specific temperature coefficient
d	number of descriptors
δ	salt mass fraction in water
ε	ionic surfactant mass fraction within water
EACN	Equivalent Alkane Carbon Number
FIT	fitness
γ	surfactant mass fraction within the mixture
γ^*	critical surfactant mass fraction within the mixture
HLB	Hydrophilic-Lipophilic Balance
HLD	Hydrophilic-Lipophilic Deviation
k	oil specific coefficient
l	surfactant tail length
M_i^X	*ith* σ-moment of compound X
$\mathrm{N_{Carbon}}$	carbon chain length
ν_o	molecular volume of the oil
ν_s	molecular volume of the surfactant
Non-VOC	non-volatile organic compound
o/w	oil in water
P	packing parameter

$\bar{P}$	effective packing parameter
PIT	phase inversion temperature
QSPR	quantitative structure property relationship
R_h	hydrodynamic radius
R^2	coefficient of determination
S	salinity
S*	Optimal salinity
SEE	Standard Error of the Estimate
SO	surfactant/oil
SOR	surfactant-to-oil ratio
SOW	surfactant/oil/water
SVOC	semi-volatile organic compound
SW	surfactant/water
SWR	surfactant-to-water ratio
σ_s	equilibrium area of the surfactant
σ_o	equilibrium area of the oil
T	temperature
T*	fish-tail temperature / optimal temperature
T_α	critical temperture α
T_β	critical temperture β / cloud point
τ	number of oil molecules in relation to surfactant molecules at the interface
VOC	volatile organic compound
w	weight fraction of non-ionic amphiphile in water
w*	critical composition in a binary surfactant/water phase diagram
WOR	water-to-oil ratio
w/o	water in oil
x	weight fraction of oil within the mixture
x*	maximum solubilisation / efficiency
ξ	fragrance mass fraction within fragrance mixture

Table of content

Introduction

The history of fragrances began already 10.000 BC when in the old Egypt people used scented oils and ointments. Due to the suited climate around the river Nil with its tides, the region offered a high botanical variety, with various flowers, bushes and herbs, which represented the basis for the ancient Egyptians to explore the odorous properties of these plants. They developed the knowledge to apply various methods to create perfumed compositions by combining plants, oils and fats. Perfumes were predominantly used for religious purpose in temples, rituals, ceremonies and festivals. The use of perfumed materials were of importance in such processions, because many of their deities were directly connected to perfumes, such as Nefertem, “lord of perfume”, whose symbol is a lotus. It was during the Hellenistic era (300 BC – 30 BC) when the manufacture of perfumes attained its peak. The ateliers were mostly found in Alexandria and the variety of raw materials were supplemented by those of Arabia, Persia, India and China. During this time detailed recipes for some perfume creations were inscribed in hieroglyphs on walls, which were found and decoded by archaeologists. The perfumes of these times were mostly relatively simple, with few oils mixed together. For example Tutankhamun’s perfume, which was found in his tomb, contained only coconut oil, with several drops of the essential oils of spikenard and frankincense.[1,2] However despite the simplicity of ingredients, the Egyptians made big effort in obtaining them. They invented the process of Enfleurage, which was still used in the 20th century to obtain fragrance oils.[3] Thereby natural materials are placed on a layer of odourless fat, allowing them to diffuse their fragrances into it. These oils were then directly applied on the skin, or mixed with grease from animals and plants in order to form pastures.

Much of the knowledge concerning perfumery was lost during the following centuries and it was only during the renaissance, when major steps in the perfume creation were achieved and more and more liquid compositions were available, instead of solid ones. In the 19th century the first synthetic compounds were created, which gave a new dimension to the composition of perfumes, which in turn resulted in the appearance of great and popular formulations, such as Chanel N°5 by Ernest Beaux (1921) or Shalimar by Jacques Guerlain (1925). In the 20th century perfumes became finally a product for the mass market and fragrances were increasingly used in all types of home and personnel care products. The progress in synthesizing fragrances and determining their structure by spectroscopic methods, resulted in the creation of a whole industry, which specialised in the synthesis and solubilisation of odorant molecules. The biggest flavours and fragrances companies are Givaudan with 21% and Firmenich with 12% market share, closely followed by IFF and Symrise with 12%, respectively 10% market share (**Figure 1**). These highly specialised companies deliver odorant compounds to home and personnel care companies, which use them in their products. Furthermore they are responsible for the creation of many perfumes, which are advertised in the media. Unlike widely assumed, brands like Calvin Klein, Hugo Boss etc. have no laboratories wherein they formulate their perfumes. In most cases, the compositions are created by these specialised enterprises and then sold under the brand name. There are only few exceptions, like Chanel, which creates their own perfumes.

Figure 1 Market-share of the leading companies in the segment flavours and fragrances in 2010.[4]

From the evolution of solid and/or oily pastures, to the solubilisation in solvents, perfumes underwent since then only slight advances in their molecular appearance. In the context of the "green revolution" which is taking place in chemistry and industry, it is desired to use substances and methods, which leave a better environmental footprint. The perfume industry is not excluded from this trend. Especially with regards to the EU regulations, which desire to reduce the amount of volatile organic carbon (VOC) compounds in order to protect the environment and the health of human beings. Most fragrance compositions are solubilised in ethanol, which is a VOC. Although ethanol is no greenhouse gas, as well as no ozone killer, it may have negative effects on the health of organisms if it comes in contact with the skin or inhaled to the respiratory system. It is thus desired to replace ethanol with a volatile compound, which falls not under the restrictions made by the European Parliament. The evident candidate is water, since it is eco-friendly, inexpensive and of course not harmful to human being. However the problematic is the immiscibility of fragrances in water, which in turn emerges the necessity of a solubiliser. The latter can be a surfactant, which is able to solubilise the hydrophobic fragrances in a microemulsion. A microemulsion is a thermodynamically stable and isotropic mixture of two non-miscible compounds and an amphiphile.[5] Thereby a nanostructered interface is formed between the non-miscible liquids, which are usually water and oil. The size of its aggregates varies between 1 and 100 nm. If the surfactant has a stronger affinity for the water phase, an oil-in-water (o/w) microemulsion is formed, where the water represents the continuous phase and the oil is dispersed in the surfactant aggregates. A higher affinity for the oil phase, results in an inverse structural behaviour, with the oil as continuous phase and the water enclosed by the surfactants, namely a w/o microemulsion. Same affinity leads to the formation of a bicontinuous microemulsion, wherein the water and oil domains are interconnected and only separated by a surfactant film of zero curvature. A water-based perfume, which is an o/w microeumsion offers the possibility to solubilise high amounts of fragrance with only 10 – 20 wt.% of amphiphile, which represents much less organic compound than the usual 60 – 80 wt.% of ethanol or other organic solvents. Such systems were already investigated with long chain poly(ethylene) glycol monoalkyl ethers, since they are very interesting for personnel care products, where only small amounts of fragrance are used. However, for the creation of low-viscous and volatile water-based perfumes, they are barely useful, since the formation of liquid crystals and the leaving of residues contradicts the demands for an appropriate solubiliser.

It is thus part of this thesis to find and apply amphiphiles, which meet the requirements for the use in water-based perfumes. These requirements can be summarized as follows:

- The amphiphile has to be volatile, up to a temperature limit, which is defined by the least volatile and frequently used compounds in applications, where the absence of residues is a key factor, i.e. perfumes, hard surface cleansers.
- It has to be efficient in solubilising fragrances with only few amounts of amphiphile. Ideally more than 5 wt.% fragrance with less than 10 wt.% amphiphile.
- The o/w microemulsion must be stable over a huge temperature range. Ideally between 5 – 50 °C.
- There shall be no formation of liquid crystalline phases, since they may impose an inhomogeneity in phase composition and viscosity to the system.
- Must not be toxic and irritant. Ideally listed in REACH.

In the second chapter the volatility characteristics of short-chain amphiphiles were investigated via thermo gravimetric analysis. Thereby the amphiphiles were classified according to their volatility in VOC, semi-VOC, and non-VOC. Furthermore their amphiphilicity was determined by comparing their influence on the phase inversion temperature (PIT) of the reference system $C_{10}E_4$/*n*-octane/NaCl(aq). This so-called PIT Slope method was developed by Ontiveros *et al.* and is based on the PIT phenomena discovered by Shinoda in 1964.[6–8] The mixing of ionic and non-ionic surfactant results in the formation of mixed micelles. In 1979 a non-ideal mixing theory was developed by Rubingh and Holland, which enables the determination of the interaction parameter β between surfactants.[9] This method was used to describe the synergy between several short-chain amphiphiles and sodium dodecyl sulfate (SDS). Furthermore the influence of traces of ionic surfactants on the aqueous phase behaviour of short-chain amphiphiles was investigated.

The third chapter deals with the hydrophobicity of polar oils. The solubilisation of fragrances in aqueous amphiphile solution depends on various formulation variables, such as the hydrophilic-lipophilic nature of the surfactant, salt and alcohol content, temperature and the hydrophobicity of the oil. Especially the latter has an important influence on the phase behaviour of a SOW system. Fragrances exist in various forms, with many different functional groups. Usually fragrance molecules are rather small with $M \lesssim 300\ g/mol$, since volatility requires a limited amount of intermolecular interactions. In **Figure 2** a summary of several types of fragrances can be seen. It illustrates very well the vast variety of structural and functional possibilities, which can be found in a fragrance molecule.

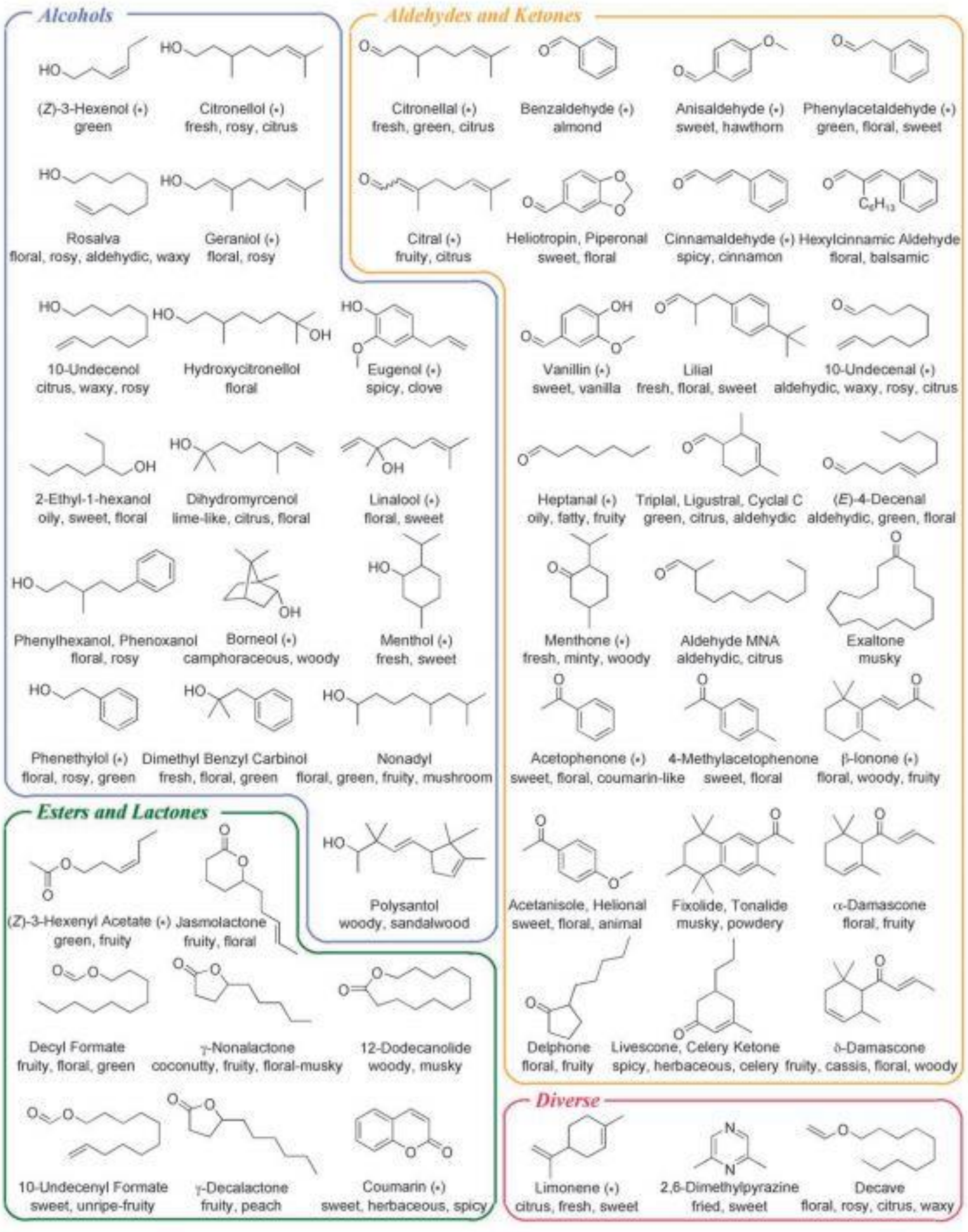

Figure 2 Typical fragrance molecules based on different functional groups, such as alcohols, aldehydes, ketones and esters.[10]

The hydrophobicity of an oil can be ranked according to its equivalent alkane carbon number (EACN), which relates the phase behaviour of an oil in a SOW system to those of linear alkanes. The EACN was determined for 46 oils, ranging from linear functionalised hydrocarbons, such as 2-alkanones, 1-alkynes, etc. to complex multifunctionalised fragrances, such as methyl jasmonate, ethylene brassylate. Together with values from literature, the influence of the functional group on the hydrophobicity was analysed and rationalised with the effective packing parameter. Since the whole procedure of EACN determination is quite time-consuming, a quantitative-structure-property relationship (QSPR) model was developed with COSMO-RS σ-moments, in order to predict the EACN of hydrocarbon oils.

Knowing the hydrophilic-lipophilic nature of the amphiphiles and the EACN of the fragrance, the optimum formulation of the system can be anticipated. Thus in the forth chapter the water-rich corner in the temperature dependent SOW phase prism is investigated and the influence of the polar oil and the ionic surfactant on the expansion of the monophasic region is determined. Furthermore an alternative system is studied, consisting of the bio-sourced amphiphile monopentyl glycerol. The efficiency and temperature stability of this system is compared to those containing poly(ethylene) glycol monoalkylethers. Since monodisperse amphiphiles are rarely used in industry, the differences in aqueous fragrance solubilisation between the well-defined tetraethylene glycol monooctyl ether (C_8E_4) and its commercial counterpart Dehydol O4 are investigated. Although these surfactants are not volatile, the findings can show the usefulness of polydisperse short-chain amphiphiles for aqueous fragrance solubilisation.

This thesis starts with an overview of several concepts, which found application in the formulation of micro- and macro-emulsions. Furthermore the ternary SOW-T phase prism is explained, with its dependence from the binary phase diagrams. In the following the relevant phase cuts are presented as well as their location in the phase prism.

Chapter 1

General theory regarding the phase behaviour of Surfactant/Oil/Water (SOW) systems

1.1. Physico-chemical concepts for the description of hydrophilic and lipophilic characteristics of amphphiles.

During the last century several concepts were established, which describe the preferences of amphiphiles according to the solubilisation of hydrophilic and hydrophobic compounds. In consequence it was figured out, that the formulation of micro- and macroemulsions depends on various formulation variables, such as the hydrophilic/hydrophobic properties of the surfactant, the hydrophobicity of the oil, the salt and alcohol content, as well as temperature and pressure. In the following the most important concepts are described and their advantages and inconveniences are discussed.

1.1.1. The hydrophilic-lipophilic balance (HLB) of Griffin and Davies

The hydrophilic-lipophilic balance (HLB) of surfactants was first introduced by Griffin in 1949.[11,12] The method quantifies the affinity of a surfactant or surfactant mixture for an aqueous and non-aqueous phase, which are not miscible with each other. This method allows to classify surfactants according to their HLB value and thus to compare them among themselves. The HLB value can be experimentally determined or calculated. Following relationship is valid for (poly)ethoxylated glycol ethers:

Table 1 Group contribution of several hydrophilic and hydrophobic groups for the HLB calculation according to Davies. Rather hydrophilic groups are positive, whereas hydrophobic groups have a negative contribution.[11]

Hydrophilic groups	
$-SO_4Na$	38.7
-COOK	21.1
COONa	19.1
N (tertiary amine)	9.4
Ester (sorbitan ring)	6.8
Ester (free)	2.4
-COOH	2.1
-OH (free)	1.9
-O-	1.3
-OH (sorbitan ring)	0.5
Lipophilic groups	
-CH- $-CH_2-$ CH_3- =CH-	-0.475
Derived groups	
$-(CH_2-CH_2-O)-$	0.33
$-(CH_2-CH_2-CH_2-O)-$	-0.15

$$HLB = \frac{E}{5} \qquad \textbf{(1)}$$

…wherein E signifies the weight percentage of the hydrophilic head group in the surfactant. In general, values between 1 and 20 are obtained, which distinguish surfactants in lipophilic (< 10), respectively hydrophilic surfactants (> 10). In 1957 Davies proposed an alternative approach to calculate the HLB-value via group contribution.[13]

$$HLB = 7 \cdot \Sigma(hydrophilic\ group) - \Sigma(hydrophobic\ group) \qquad \textbf{(2)}$$

This method has the advantage that the various strengths in hydrophilicity of the polar head groups is considered. In **Table 1**, several values for hydrophilic and hydrophobic groups can be seen. Thereby negative values represent a rather hydrophobic part and positive values a hydrophilic part of the surfactant.

The HLB is today widely used in industry, since it is easy applicable and it offers the possibility to assign a number to an emulsifier. This number may help to choose the appropriate surfactant for certain types of applications. In **Figure 3** a scheme of the HLB scale is shown, wherein the HLB regions are indicated, which correspond to a certain function of the surfactant in an application. According to this scheme, very hydrophilic agents are needed for solubilisation (15-18) and for the use as a detergent (13-15). In the mid-range between 7 and 9, the surfactants are very good for surface wetting. On the other hand antifoaming agents have to be very hydrophobic (2-3). With surfactants, which contain a HLB value between 8 and 18, o/w emulsions are formed, whereas w/o emulsions are obtained with surfactants with an HLB value between 4 and 6. Despite the common use in industry, the HLB method is an approximate method, which allocates only an empirical found value to a surfactant, and is thus not based on a thermodynamic background. Furthermore the method considers only the surfactant and is consequently not adapted to temperature and additive effects, such as salt or alcohols, which influence strongly the phase behaviour of amphiphiles.

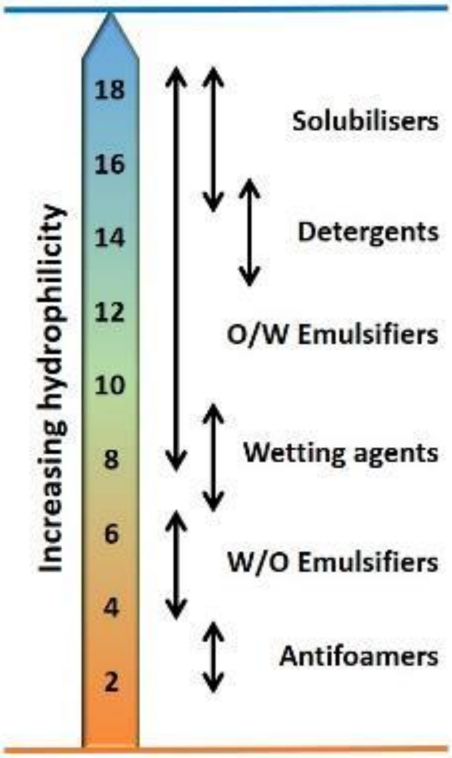

Figure 3 HLB scale for surfactants.

1.1.2. The R-ratio of Winsor

Winsor introduced in 1948 the R-ratio, which considers the interaction energy at the interface between the surfactant and the oil phase, as well as the surfactant and the aqueous phase.[14] Depending on the strength of these interactions, the interfacial film is either curved around the oil phase (R < 1) or around the water phase (R > 1). The balanced state (R = 1) describes thereby a bicontinuous microemulsion, wherein the surfactant has same affinity for both, the aqueous and oil phase. The R-ratio is defined as follows:

$$R = \frac{A_{CO}}{A_{CW}} = \frac{A_{Lco} + A_{Hco}}{A_{Lcw} + A_{Hcw}} \tag{3}$$

…where A_{co} describes the interaction energy between surfactant and oil, whereas A_{cw} between the surfactant and water. This terms can be split into two contributions, namely the hydrophilic (A_{Hco}, A_{Hcw}; hydrogen bonding) and the lipophilic contributions (A_{Lco}, A_{Lcw}; van der Waals forces). In 1954 Winsor modified his equation, in order to add the interactions between the oils (A_{oo}) and the water (A_{ww}).[15] With regards to the attractive interactions between surfactant and oil, respectively water, these energies are negative, because they favour phase separation. Finally Bourrel *et al.* modified the equation by introducing as well the interaction energies between the surfactant tails (A_{ll}) and head groups (A_{hh}).[16]

$$R = \frac{A_{co} - A_{oo} - A_{ll}}{A_{cw} - A_{ww} - A_{hh}} \tag{4}$$

A schematic representation of the interactions at the interface between the various constituents can be seen in **Figure 4**.

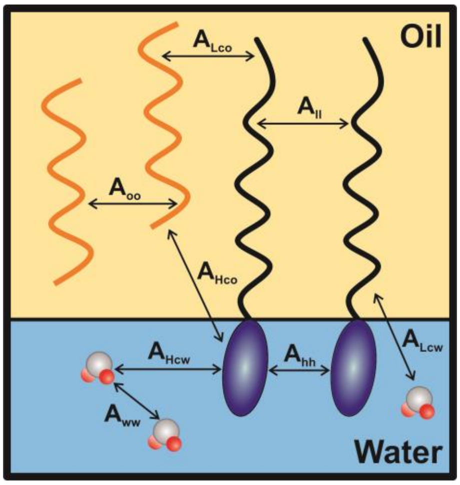

Figure 4 Schematic representation of the interaction energies between surfactant, water and oil at the interface.

According to the R-ratio, an equilibrated surfactant/oil/water (SOW) system can exist in four states, which are known under the denominations Winsor type I-IV microemulsions, and are abbreviated as WI, WII, WII and WIV (**Figure 5**).[14] WI is an o/w microemulsion with an excess oil phase. It is obtained for R < 1. Thus the hydrophilic interactions dominate and the interface curves around the oil droplets. For a non-ionic surfactant, it is always obtained at lower temperatures with regards to the w/o microemulsion (WII). This phase behaviour is determined by a strong hydrophobic interaction between the interfacial film and the oil phase. The process of phase inversion from WI to WII is often linked to the appearance of a WIII or WIV phase. WIII is a bicontinuous microemulsion with an excess oil and water phase. For this system R = 1, and thus the surfactant is in a balanced state. WIV is obtained for increased surfactant concentration with respect to WIII. Consequently it represents a bicontinuous monophasic mixture.

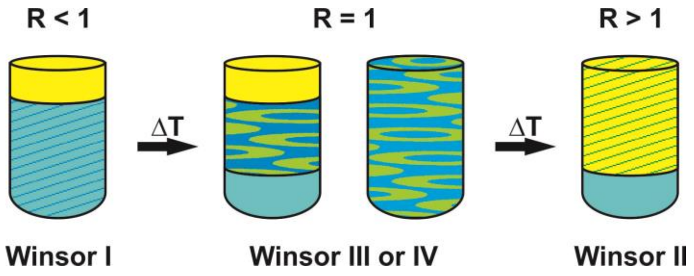

Figure 5 The Winsor phases: Winsor I represents an o/w microemulsion with excess oil phase. For higher temperatures a w/o microemulsion is obtained (Winsor II). In the balanced state a Winsor III phase is obtained, consisting of a bicontinuous microemulsion with excess oil and water phase, whereas a monophasic microemulsion is described as a Winsor IV phase.

As shown in **Figure 5**, the phase inversion can be obtained by increasing the temperature. However for ionic surfactants the phase inversion is obtained with the addition of salts, since temperature has barely an effect on its curvature.[17,18] In general any changes in the phase behaviour of a SOW mixture can be explained according to **Equation 4**.[14] Increasing the polarity of the oil, augments the interaction with the surfactant (A_{co}). Consequently R is augmenting and the system is inverting from WI to WII. Same happens if the surfactant is replaced with a more hydrophobic one. The addition of a salt induces a screening effect at the interface, which in turn reduces A_{cw}. An inversion from WI to WII is the result. The effect of salt is thereby much stronger on ionic surfactants than non-ionic surfactants. In order to obtain a phase inversion from WII to WI, the surfactant has to be increased in hydrophilicity. Hence the interaction A_{cw} augments, which can be attributed to a stronger hydration of the polar head groups.

The R-ratio is a useful tool, to describe the phase behaviour of SOW systems. It considers all the interaction energies at the interface, which can possibly appear in such a system, as well as it considers temperature effects, since the energies depend on it. However this concept is rather a pedagogic way to explain the phase behaviour of SOW system, since it is not possible to measure the discrete interaction energies.

1.1.3. The concept of phase inversion temperature of Shinoda

In 1964 Shinoda proposed a more accessible method to determine, whether the surfactant has a rather hydrophilic or a hydrophobic affinity for the interface.[6] The method is based on the measurement of the phase inversion temperature (PIT) of poly(ethoxylated) amphiphiles under temperature alteration and agitation. Under stirring the mixture forms an o/w or w/o emulsion, which is clearly turbid. However at a certain temperature, the so called PIT, the surfactant has same affinity for the aqueous and oil phase. Visually it can be recognized by a less distinctive appearance of the turbidity, which may - depending on the system – look almost clear. A more precise method to determine the PIT is via conductivity measurements.[19,20] Thereby the aqueous phase contains small amounts of salt, so that it is possible to measure the conductivity when the continuous phase is represented by water (o/w emulsion). With increasing temperature the ethoxy groups of the surfactants are dehydrating, which in turn increases its affinity for the oil phase. Thus at the PIT, the emulsion inverts and the continuous phase is represented by the oil. Since the salt is not soluble in oil, an extreme decline in conductivity can be observed. This decline happens usually within a small temperature interval, which in turn offers an easy accessible way to determine precisely the PIT.

The PIT concept takes into account all the formulation variables (surfactant, oil, salt, co-surfactant), since each of them influences the phase behaviour and thus the PIT of the SOW system.[7] Consequently it offers a rapid way to determine the hydrophilic-lipophilic characteristics of a surfactant with a given oil. However the concept is only applicable to poly(ethoxylated) surfactants, which bear a high temperature sensitivity. Hence the method has its limitations in determining the PIT of ionic surfactants, or other non-ionic surfactants, such as monoalkyl glycerols.

1.1.4. The Hydrophilic-Lipophilic Deviation (HLD) theory of Salager

The Hydrophilic-Lipophilic Deviation (HLD) was introduced by Salager in the 1970s, after several investigations concerning the improvement of oil recovery.[21–24] The HLD combines in a linear equation all the formulation variables and defines the deviation from the optimum formulation (HLD = 0). The optimum formulation represents thereby a system of zero curvature, with a minimum in interfacial tension ($< 10^{-3}$ mN/m). At this point the surfactant has same affinity for both, the aqueous and oil phase. The HLD equation exists for non-ionic and ionic surfactants.

Non-ionic: $$HLD = Ccn + b \cdot S - k \cdot ACN + c_T(T - 25) + a \cdot A \quad \textbf{(5)}$$

Ionic: $$HLD = Cc + \ln S - k \cdot ACN + c_T(T - 25) + a \cdot A \quad \textbf{(6)}$$

k and c_T are characteristic coefficients, which can be found for various surfactants in literature.[25–27] *b* represents the characteristic constant for a given salt, whereas *a* stands for the alcohol. *S* is the salt concentration in water in weight percentage and *A* the alcohol weight percentage in the mixture. *ACN* means alkane carbon number, i.e. 6 for hexane etc. It can be replaced by the equivalent alkane carbon number (*EACN*) for non-linear alkanes and functionalised oils. *T* represents the temperature, which is reduced by the reference temperature (25 °C). *Ccn* and *Cc* is the characteristic curvature of the non-ionic, respectively ionic surfactant.[28,29] It describes the hydrophilic-lipophilic nature of the amphiphile.

The optimum formulation of a SOW system is determined by observing the equilibrated phases, while altering one formulation variable. Increasing temperature and salt augments the HLD, whereas polar oils have a decreasing effect on the optimum formulation.[25,26] In **Figure 6** a schematic representation of the phase behaviour of a SOW system is shown with increasing HLD. Thereby the middle phase represents the microemulsion, which is solubilising further oil and simultaneously rejecting water with augmenting HLD. At HLD = 0, the excess phases have the same volume, which represents the optimum formulation. The middle phase consists of a bicontinuous microemulsion with zero curvature. In general such a formulation scan is done with same volumes of water and oil, so that the three phase region stays constant with increasing HLD. However very polar oils may solubilise huge quantities of surfactant monomerically, which in turn may falsify the determination of the optimum formulation.

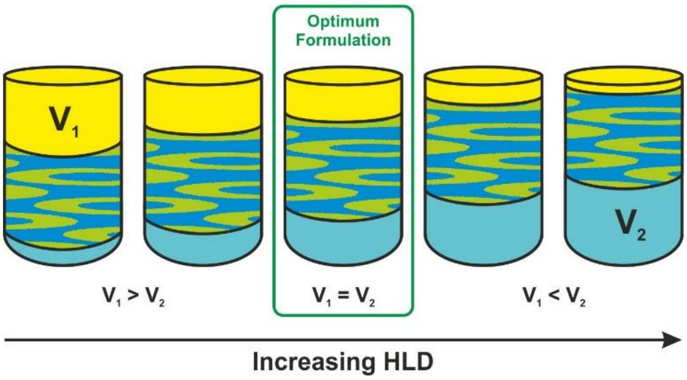

Figure 6 Evolution of the phase volumes with increasing HLD. The optimum formulation is obtained at $V_1 = V_2$.

Nevertheless the HLD theory is a very useful tool for the formulation of micro- and macroemulsions, since it is able to consider all the variables, which may influence the formulation. It is thus applied in various different domains, such as detergency, oil recovery, pesticides and paints.[30–32]

1.1.5. The packing parameter P of Israelichvili

The packing parameter *P* is a geometrical concept, which describes the arrangement of surfactants according to their geometric structure. It was first introduced by Israelichvili in 1976 to describe the shape of micelles.[33] In its easiest form, the packing parameter of an aggregate is given by…

$$P = \frac{v_0}{a_0 l} \tag{7}$$

…where v_0 describes the volume of the hydrophobic tail and l its length. a_0 is the equilibrium area of the polar head group at the interface. It is often misinterpreted as a constant value, which only depends on the type of polar head group. However a_0 depends strongly from formulation variables such as temperature or salt content.[34,35] Furthermore it depends on the surfactant concentration, since at higher content, a transition from spherical to rod-like micelles is possible.[36] In **Table 2** the micellar shapes are shown, which can be obtained for certain *P* values.

Above all spherical micelles are formed at low concentrations with a surfactant, which consists of a huge, respectively strongly hydrated polar head group, such as in the case of sodium dodecyl sulfate (SDS). Rod and disc-like micelles are obtained for higher surfactant concentrations, smaller a_0 or a bigger v_0/l to a_0 ratio. Cetyltrimethylammonium bromide can form such structures in aqueous NaBr solution.[37] Vesicles and flexible bilayers were frequently observed for catanionics in salt solution.[38,39] A packing parameter equal to 1 is obtained for various different non-ionic surfactants at higher surfactant concentration. Usually those arrangements lead to the formation of liquid lamellar crystalline phases. Inverted micelles are only obtained for highly concentrated aqueous non-ionic surfactant solutions. However in non-aqueous solvents even ionic surfactants may aggregate as inverse micelles.[40,41]

Table 2 The intervals of the packing parameter *P*, their corresponding surfactant shape and the preferred aggregation form.

Packing parameter *P*	Shape	Aggregates
< 1/3	Cone	Spherical micelles
1/3 – 1/2	Truncated cone	Rod & disc-like micelles
1/2 – 1	Truncated	Flexible bilayers and vesicles
1	Cylinder	Planar bilayers
>1	Inverted truncated cone	Inverted micelles

According to **Equation 7**, the packing parameter depends only on a_0, since v_0 and l are constant for a given surfactant. The volume v_0 can be approximated with the volume v of a hydrocarbon chain, according to following equation:

$$v = 0.027(n_C + n_{Me}) \quad [nm^3] \qquad \textbf{(8)}$$

Thereby n_c describes the number of $–CH_2-$ groups and n_{Me} the number of methyl groups. The hydrocarbon tail length can be estimated from..

$$l = 0.15 + 0.127 \cdot n_C \quad [nm] \qquad \textbf{(9)}$$

Thus the structure of the micelle is determined by a_0, which considers the hydration shell around the polar head group. The packing parameter can be used to explain the type of aggregation in a SOW system, according to the influence of formulation variables on this equilibrium area. In **Figure 7** the evolution of the packing parameter of a SOW system is shown. A strongly hydrated head group results in a big a_0, which in turn favours the formation of o/w droplets ($P < 1$). The increase in temperature or the addition of salt promotes the dehydration of the head group. Consequently a_0 is decreasing and a bicontinuous microemulsion is obtained at $P = 1$. Further change in formulation inverts finally the microemulsion and w/o droplets are obtained ($P > 1$).

Unfortunately the nano-scaled parameters of **Equation 7** are not easily accessible and advanced methods, such as scattering techniques, are required to obtain them. Furthermore Nagajaran showed that for spherical micelles, a_0 depends on the surfactant tail length.[42] However the concept of packing parameter still gives a useful qualitative overview of the geometric shape of aggregates, as well as a theoretical description of the alterations in the spontaneous curvature upon temperature and/or salt content change. This basic concept was extended by Tchakalova *et al.* to the effective packing parameter, which considers also the effect of oil penetration on the interfacial curvature.[43,44]

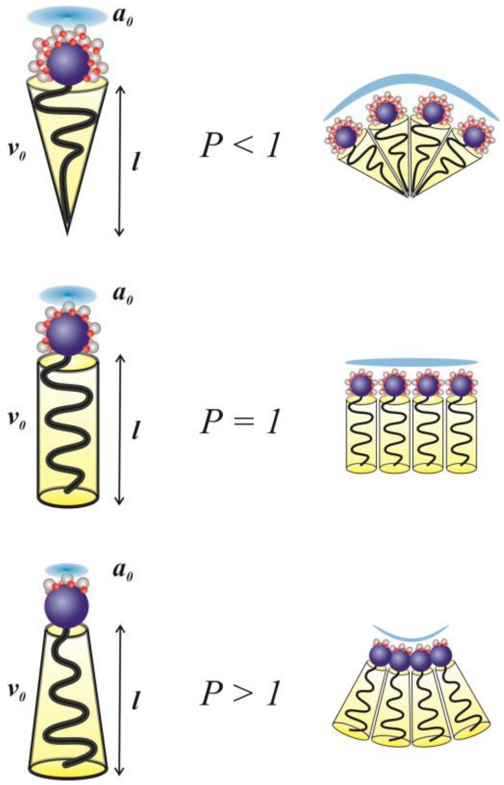

Figure 7 Evolution of the packing parameter in a SOW system. A strongly hydrated polar head group results in a big equilibrium area a_0 and thus in a positive curvature (P < 1). A zero curvature is obtained for a lesser hydrated head group (P = 1). Further dehydration results in inverted aggregates with negative curvature (P > 1).

1.1.6. The PIT-Slope method

Recently Ontiveros *et al.* reported a method to classify the hydrophilic-lipophilic nature of a surfactant via conductivity according to a reference system.[8] The PIT-Slope method is closely related to the PIT method of Shinoda. However it can also be used for ionic surfactants and other non-ionic surfactants, such as alkylglycerols, alkylisosorbides etc. The reference system consists of $C_{10}E_4$/octane/0.01 M NaCl(aq), which possess a PIT of 24 °C. The stepwise addition of a second surfactant, results in a change in the PIT, which can be approximated with a linear curve. The slope of the curve is thereby a measure for the effect of the second surfactant on the interface. It is negative for surfactants which are more hydrophobic than $C_{10}E_4$, and positive for more hydrophilic surfactants.

The PIT-Slope method was already used to classify several different surfactants, such as alkyltrimethylammonium bromides, commercial surfactants (TWEEN®, Brij®) or bio-based surfactants.[8,45] However the linear behaviour may deviate for certain kinds of surfactants, imposing a slight concentration dependency on the PIT-Slope method.

1.2. Graphical representations of phase diagrams

Due to their amphiphilicity, surfactants are usually used in a multicomponent system, which consists of water and oil, and often also additives such as co-surfactants. Each constituent in the mixture, results in a more complicated system, which becomes increasingly difficult to describe in a graphical representation. A system constituting of two compounds can be described with a two-dimensional binary phase diagram. A 3-compound system in a 3-dimensional representation, or even better in a ternary phase diagram. A forth compound can be represented either in a ternary phase prism or a 3-dimensional phase pyramid. However these representation become increasingly complicated in drawing and the reading off exact values becomes quite interpretative. Therefore often one compound or a ratio between two compounds is kept constant, which in turn transforms binary and ternary diagrams into pseudobinary and –ternary representations.

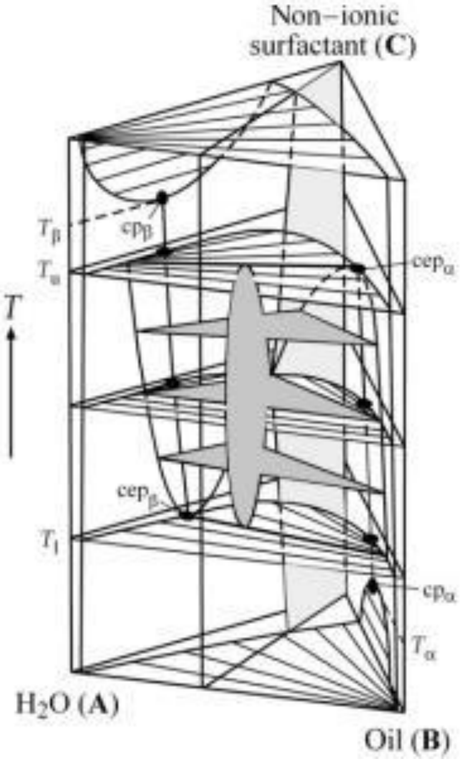

Figure 8 The temperature dependent non-ionic SOW phase prism. The phase behaviour is determined by the superposition of the three binary phase diagrams. A three phase region is formed when the critical points line "breaks" between cep_α and cep_β.[49,51]

The temperature dependent phase behaviour of a non-ionic SOW mixture can be completely represented in a SOW-T phase prism (**Figure 8**). Based on the fundamental work of Schreinemakers[46], Kahlweit *et al.* described in detail the origin of the three-phase region and its dependence from the critical points of the binary surfactant/water (SW) and surfactant/oil (SO) phase diagrams.[47–49] Thereby he showed that the three-phase region depends on the miscibility of the amphiphile in the water and oil phase. It appears between the critical endpoints cep_α and cep_β, which originate from the critical points cp_α and cp_β in the binary phase diagrams. Consequently the closer the critical temperatures T_α and T_β, the bigger the expansion of the three phase body. If the amphiphile solubilises very well in oil and water, T_β is very high, whereas T_α is very low and consequently the critical endpoints approach. By augmenting the polarity of the oil, T_α can be reduced until the critical points merge in the tricritcal point and the three-phase region disappears.[50]

The critical points line, which traverses the phase prism, connects the critical points cp_α of the binary phase diagram SO and cp_β of SW. The possible number of phases in equilibrium is thereby given by the Gibb’s phase rule:

$$F = C - P + 2 \qquad \textbf{(10)}$$

Thereby F represents the degrees of freedom, C the number of compounds and P the number of phases which are in thermodynamic equilibrium. In the SOW-T prism, the pressure is constant, which substracts a degree of freedom from **Equation 10**.

$$F = C - P + 1 \qquad \textbf{(11)}$$

The composition of the mixture in the prism is given by the mass fraction of the three components. Thus defining two of them, defines automatically the third. Consequently a monophasic region has three degrees of freedom, namely two composition variables and the temperature. In a two-phasic region, F = 2, since the composition is already determined by one composition variable and the temperature, whereas in the three-phasic region, temperature is the only degree of freedom. The composition of the three phases is fixed, independently of the total composition and only the ratios change.

Additives, such as salts, ionic surfactants or co-surfactants influence the critical points and have thus a distinctive effect on the critical points line in the ternary phase prism. Knowing the alterations of such additives in the binary phase diagrams can thus help to conclude their effects on the phase behaviour in the Gibb’s triangle.

In the last century several types of two-dimensional diagrams appeared, which turned out to give a characteristic representation of the phase behaviour of SOW mixtures. These “cuts” emerge from the temperature dependent SOW phase prism, wherein a compound, or the ratio between two compounds is held constant.

1.2.1. The Gibb’s triangle

The Gibb’s triangle, also known as ternary phase diagram or Δ cut, is the most frequently used representation for a three-component mixture. The isothermal and –baric diagram depends on the three composition variables of surfactant, oil and water. It offers a complete overview of the phase behaviour of a three-component mixture at given temperature and pressure.

In **Figure 9**, a schematic representation of three non-ionic SOW phase diagrams is shown, as well as its location in the SOW-T phase prism. In the balanced state at R = 1, the phase diagram shows a relatively symmetric appearance with a three-phase region, whose sides are connected to a WII lobe on the left and a WI lobe on the right. Adjacent to its base a two-phasic region appears, where the surfactant is solubilised monomerically in the oil and water phase. The diagram contains two critical points. They are connected to the WI and WII phase, and are the origin of the tie lines, which dictate the composition of their phases. There where all the Winsor phases meet lies the characteristic point, which describes the balanced state, at which the surfactant has same affinity for water and oil. With decreasing temperature, the balanced state is obtained at higher water and lower oil content, which in turn results in a movement of the characteristic point towards the critical point of the WII lobe, until they merge and the WII and WIII region disappear. For higher temperature, the inverse happens. Water is squeezed out of the bicontinuous microemulsion and further oil is solubilised. Thus the characteristic point moves towards the right part of the diagram, until the WI and WIII region disappear.[52,53]

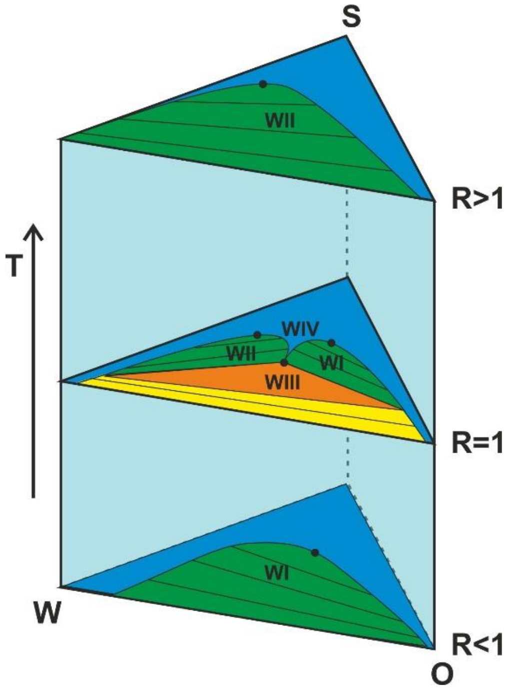

Figure 9 The ternary phase diagram in dependence of the R-ratio and its location in the SOW-T phase prism.

The appearance of the three-phase region depends furthermore on the miscibility of the surfactant in the oil and water phase. A high solubility in those phases may lead to no formation of the three-phase region.

Tracing a ternary phase diagram can be very time-consuming, since the phase borders cannot be obtained by changing a formulation variable. The composition has to be changed, which in turn results in the preparation of huge amounts of tubes. A more elegant way to construct such diagrams, is the composition determination of all phases via gas-chromatographic or spectroscopic measurements. Since multi-phasic systems diphase along their tie lines, it is sufficient to analyse the composition of one three-phase system and several two-phase system, in order to trace their phase boundaries.

1.2.2. The fish cut

A good possibility to trace the three phase region of a SOW mixture is the fish cut, also known as γ-cut or Kahlweit cut.[54] The temperature dependent two-dimensional diagram is usually prepared at a water-to-oil ratio (WOR) equal to one ($\alpha = 0.5$), with rising mass fractions of surfactant (γ). α and γ are defined as follows:

$$\alpha = \frac{m(oil)}{m(oil) + m(water)} \qquad \textbf{(12)}$$

$$\gamma = \frac{m(surfactant)}{m(mixture)} \qquad \textbf{(13)}$$

In **Figure 10**, a schematic representation of the fish cut can be seen, as well as its location in the SOW-T phase prism. The obtained phase borders align usually in a shape, which resembles a fish. In literature they can be found as well in different WORs.[55,56] The big advantage of a fish cut, is the characteristic information which it holds. The intersection at which all the Winsor phases meet, is characterised by the fish tail temperature T* and the critical composition γ*. The latter describes the minimum amount of surfactant necessary to solubilise same amount of oil and water. Thereby T* indicates the temperature at which the system inverts from WI to WII. T_l and T_u give the lower and upper frontier of the three-phase region. These borders stay the same for different WORs throughout the ternary phase prism. With increasing WOR the characteristic point moves towards T_l, until it merges with cp_β at the critical endpoint cep_β. For higher temperatures the inverse happens. The characteristic point moves towards T_u, until it merges with cp_α at cep_α (**see Figure 8**).

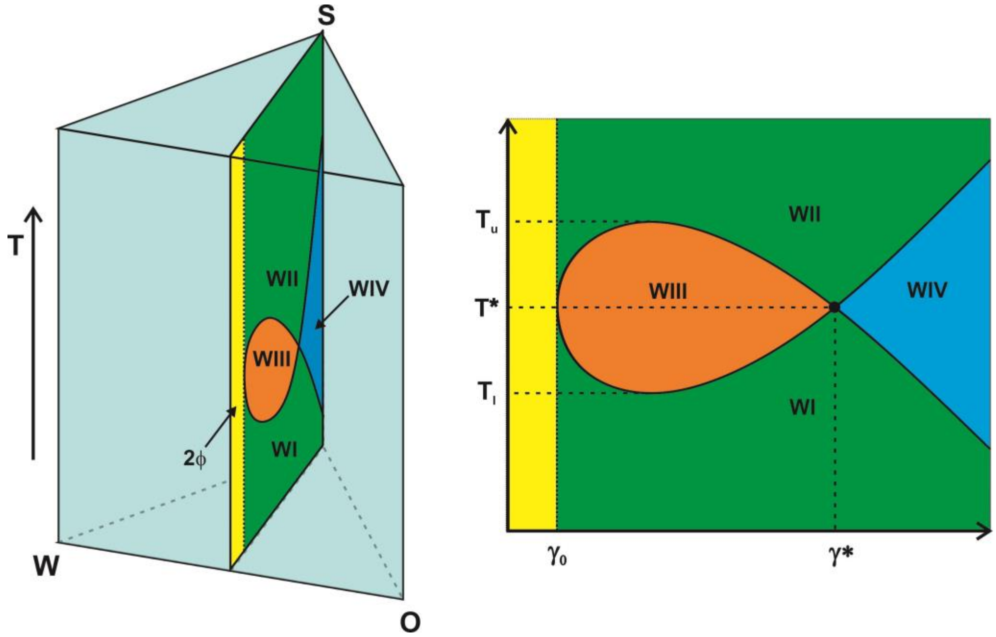

Figure 10 Left: The fish cut at WOR = 1 and its location in the SOW-T phase prism. Right: The fish cut representation. T*,γ* defines the fish tail, whereas γ_0 the monomeric solubility of the surfactant in water and oil. T_u and T_l describes the upper, respectively lower temperature border, which encloses the three-phase region throughout the phase prism.

Another important point of the fish cut is the monomeric solubility γ_0 (or γ_{mon}), which describes the point at which the three-phase region appears. Consequently γ_0 indicates the amount of surfactant which is lost to the excess phases and not able to solubilise water and oil. Especially in industry it is undesired, since a high γ_0, results in a smaller efficiency of the system to solubilise oil and water and thus in higher costs for the company. In general the monomeric solubility is elevated for short-chain amphiphiles and polar oils.[56–58] The preparation of the fish cut is quite easy, since the WOR is held constant. Same volumes of oil and water can be applied rapidly with micro pipettes, which is also valid if the fish cut is traced at same mass content of oil and water, providing that the density of the oil is known. After addition of the surfactant, the phase borders can be obtained by changing the temperature.

1.2.3. The χ cut

The χ ("kai") cut represents a temperature dependent cut through the phase prism at constant surfactant weight fraction. Thereby α is varied between 0 and 1. Two representations of their location in the SOW-T phase prism can be seen in **Figure 11**. If the cut is performed at elevated surfactant content, a monophasic channel can be observed, which extends from the lower left corner to the upper right. In this channel the aggregation changes from an o/w to a bicontinuous microemulsion around α =0.5 and inverts eventually to a w/o microemulsion for higher α-values. This inversion can be seen better, if the cut is performed at low amounts of surfactant, since the three-phase region appears. Thereby two characteristic points appear, at which the monophasic water-rich bicontinuous microemulsion turns into a WIII phase, and where the latter reunites into a monophasic oil-rich bicontinuous microemulsion.

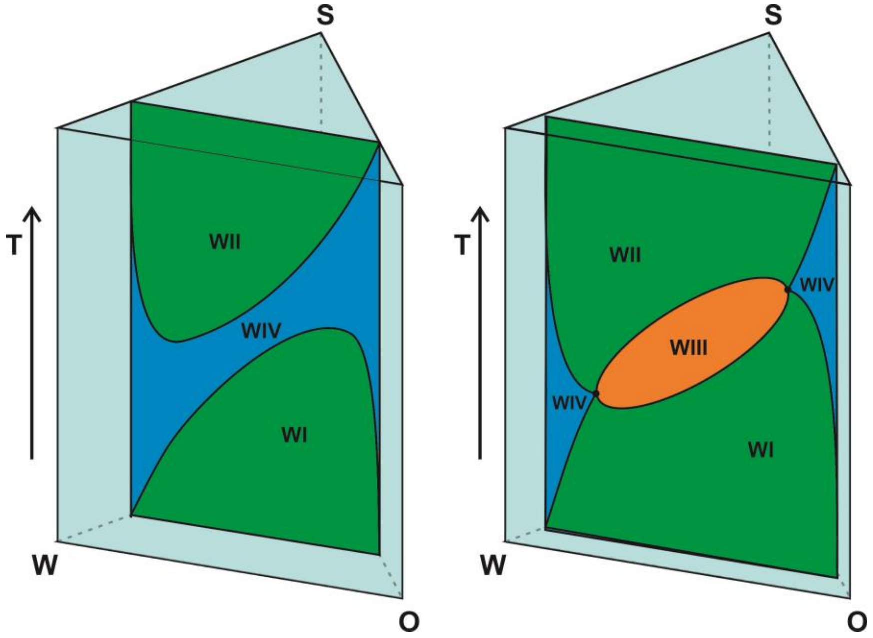

Figure 11 Left: The χ-cut at relatively high surfactant concentration. The elongated monophasic region traverses the diagram from the lower left to the upper right corner. Right: If the surfactant concentration is relatively low, a three phase region is obtained in the centre of the diagram.

The χ-cut is a good representation if someone wants to know how much oil can be solubilised in water with a fixed mass fraction of surfactant, or vice versa. However the preparation of this diagram is more work intensive than the fish cut, since various tubes with different WOR have to be prepared and the surfactant mass fraction must be held constant in each tube.

1.2.4. The lund cut

The temperature dependent section through the phase prism at constant surfactant-to-water ratio (SWR) or surfactant-to-oil ratio (SOR) can be seen in **Figure 12**. In literature it is also known as lund cut, named after a group from the University of Lund in Sweden.[59,60] In terms of simplicity, we use same denomination to describe this cut through the phase prism. The phase diagram resembles the fish cut. However it originates from the SW, respectively SO side of the prism. Thus the initial phase borders are directly connected to the miscibility gaps of the SW and SO systems. The diagrams contain a characteristic point at which all the Winsor phase meet. Its temperature is always lower than T* in the fish cut for same system at constant SWR, whereas it is higher for constant SOR. With the addition of oil, respectively water, the surfactant is diluted, which consequently leads to the appearance of a two-phase region with monomerically solubilised surfactant.

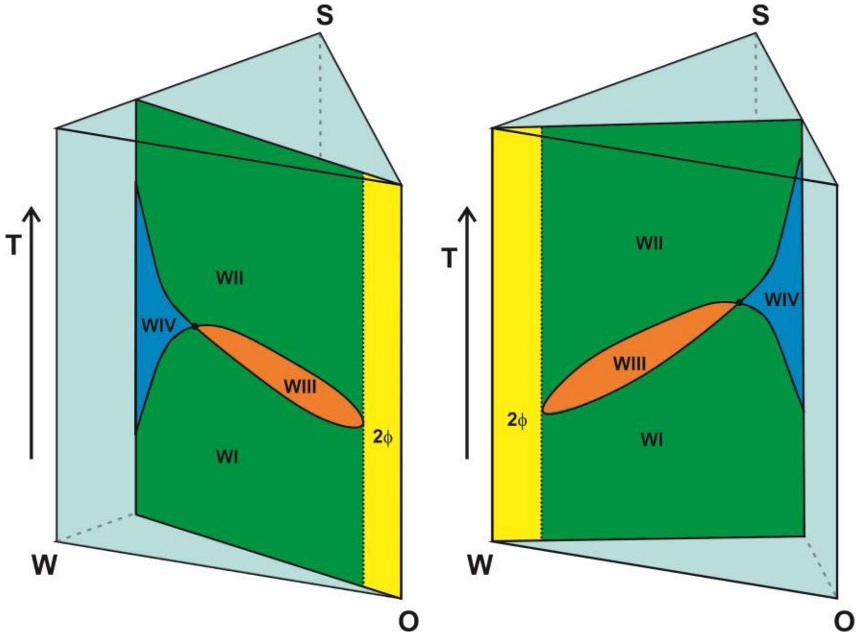

Figure 12 Lund cut at constant SWR (left) and SOR (right). The phase borders are directly connected to the binary SW, respectively SO diagrams.

The Lund Cut is a very useful representation, if one wants to investigate the phase behaviour of water- or oil-rich formulations. It is especially useful to determine the maximum solubilisation of an aqueous or oily surfactant solution. Since SWR and SOR is constant, a stock solution can be prepared, which is distributed to several tubes with rising amount of oil. Consequently the tracing of this cut is very simple and rapid.

This work concentrates on the aqueous solubilisation of hydrophobic compounds, so that in the following only the cut at constant SWR is investigated and any use of the term “lund cut” refers to this kind of diagram.

1.3. Fragrances and their solubilisation in SOW systems.

Fragrances are widely used in industry. They can be found in almost all cosmetic products, as well as in laundry detergents, etc. **Table 3** summarises several home and personnel care products, as well as their fragrance and amphiphile content. In these products they can be usually found in quantities between 0.1 to 1.2 wt.%, which may appear as not much. However due to their various functionalizations, which impose a strong polarity to most of the fragrances, they can penetrate into the interface of a SOW system, and consequently alter dramatically the temperature stability and efficiency of the system.[61] It is known that already small amounts of alcohols, may drastically decrease the optimum formulation of a SOW system.[23] This was also shown by Ontiveros *et al.* for perfume alcohols.[62] Thereby he used the PIT-Slope method to classify the influence of the terpene alcohols on the interface of a Brij30/octane/NaCl(aq) system in dependence of its strength. It was shown that small aromatic alcohols, such as thymol have the strongest effect on the interface, followed by rather linear terpene alcohols, such as linalool or eugenol. Relatively small – but still important - influence on the interface is imposed by non-alcoholic terpenoids, such as esters, ketones etc.

Table 3 Several home and personnel products, as well as their fragrance and amphiphile content.[63]

Home/Personnel Care Product	wt.% Fragrance	wt.% Amphiphile
Shampoo	0.3 – 1.2	10.0 – 30.0
Cream	0.1 – 0.3	5.0 – 10.0
Laundry Detergent	0.3 – 0.6	15.0 – 25.0
Toothpaste	0.5 – 1.0	0.5 – 2.0

Unfortunately the effect of fragrances on the phase behaviour of SOW system is only limited documented in literature. Friberg *et al*. performed pioneering work, concerning the vapour pressure of fragrances in micellar solution, as well as their amphiphilic aggregation structures.[64–68] Saito *et al.* showed by a dynamic headspace method that the volatility of fragrances is reduced in an aqueous polymer solution.[69] In 1994 Tokuoka *et al.* investigated the solubilisation of fragrances in various (poly)ethylene glycol monohexadecylethers.[70] He discussed in particular the interactions between surfactant and hydrophobic compound in the micellar region, since these highly concentrated surfactant solution are especially interesting for industrial applications, such as cosmetics or detergency. He showed that in general it is easier to solubilise very polar fragrances such as eugenol than terpenes like limonene. Kanei *et al*. performed several lund cuts with several fragrances of varying polarity in the system $C_{12}E_8$/fragrance/water, and he concluded that the optimum formulation is decreasing with increasing penetration of the fragrance into the interfacial layer.[61] Such temperature-dependent investigations in the water-rich corner of the ternary phase prism are rarely performed in literature, and to the best of our knowledge it is the only reported study with perfumes. Literature which deals with aqueous perfume solubilisation is more frequently found in patents.[71–73] Consequently, so far only few research has been performed on the solubilisation of fragrances in water-rich microemulsions. The requirements for such formulation, which are compatible with the high demands of the fine-perfumery, leave only little space in the choice of an appropriate amphiphile. Therefore it is important to find systems, which show superior properties, due to synergism between their constituents. Thus in our group we focus on non-ionic short-chain amphiphiles, whose properties are boosted by addition of small quantities of ionic surfactant. Although mixed ionic/non-ionic systems are widely described in literature[74–76], there is up to this date no study, which treats the effect of less than 1.wt% ionic surfactant on aqueous formulations.

Chapter 2

Solvo-surfactants: State of the art, synthesis and properties

2.1. Hydrotropes versus solvo-surfactants

The term "hydrotrope" was used for the first time in 1916 by Carl Neuberg, who tried to explain a phenomenon, which he encountered while he was trying to extract a colorant from bull urine, when it turned out that his usually non-miscible mixture of water and 1-pentanol became monophasic.[77] After further research he concluded that the salts, such as sodium benzoate or salicylate, contained in the urine were responsible for the solubilisation of hydrophobic compounds in water.

In 1946 McKee noticed that the solubilisation of organic compounds by small non-ionic amphiphiles was similar to the one obtained by salts.[78] Thus he suggested that short amphiphilic molecules, which he named hydrotropes afterwards, were able to solubilise organic compounds in water by a mechanism of complexation. As a result of further evidences, which confirmed the observations of McKee, Friberg started to compare hydrotropes with surfactants and came to the conclusion that the solubilisation mechanism of hydrotropes resembles to that of surfactants, with the difference that the structures are less organised.[79] Although the denomination as hydrotrope is now well-accepted, the mechanism which is responsible for the solubilisation of hydrophobic compounds in aqueous solution is controversy up to this date. In 1985 Saleh proposed a mechanism which implies a sort of stacking between the aromatic rings of non-ionic or ionic hydrotropes.[80] This was confirmed by Balasubramanian *et al.* and proceeded further to the description of lamellaric structures which are able to solubilise the organic compounds between the layers.[81] Srinivas *et al.* suggested in 1997 that hydrotropes arrange in cells, where the packing happens according to the electrostatic preferences of the hydrophilic and hydrophobic part of the hydrotrope. Hydrophobic compounds may then enter the layered structure and in turn stabilize it by a cooperative solubilizing isotherm (**Figure 13**).[82]

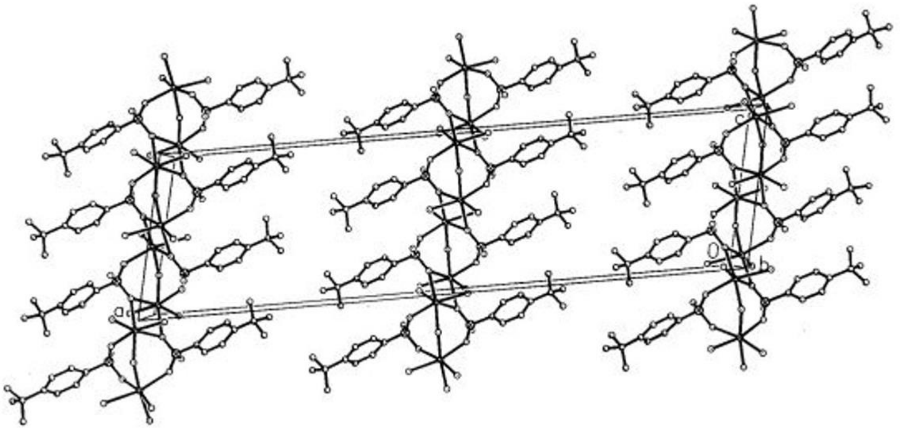

Figure 13 Cell packing for sodium *p*-tert-butylbenzenesulfonate dehydrate. The hydrotropes arrange in cells with their benzene rings next to each other.[82]

The observations made by Balasubramanian and Srinivas can also explain that in some cases the hydrotropic solubilisation of oils may be more efficient than surfactant solubilisation at same concentration. This can be explained with the lamellaric structure which can exhibit more solubilisation sites than micelles and taking into account the findings of Srinivas, a solute may have even a stabilising effect on the layers. However Arrigo *et al.* performed in 2003 small angle neutron scattering (SANS) measurements and classified - amongst others - short-chain amphiphiles of the type C_iE_j into groups according to their capability to form micellar aggregates.[83] According to these findings it can be considered that the aggregation of compounds with such a small amphiphilicity as it is the case for hydrotropes, may be particularly sensible to interaction forces between themselves and thus drive them, depending on their structure, to assemblies which lower their energy the most efficient. Consequently there might not be one mechanism for the aggregation behaviour of hydrotropes. Rather smooth transitions from a co-solvent to a hydrotrope which assembles in layers to one which develops weakly aggregated micelles to ending up with real surfactants with a sharp break in surface adsorption.

The physico-chemical properties of hydrotropes are closely related to surfactants. As the latter, they possess a critical aggregation concentration (CAC), which is located at rather high concentrations of the amphiphile. In **Figure 14** the adsorption isotherm of several short chain C_iE_j's can be seen. The adsorption isotherm proceeds thereby flatter than the curve of strong amphiphilic compounds, indicating a weaker aggregation.[84] The lower the amphiphilicity of the compound, the smoother the break in the curve, until it disappears completely for non-amphiphilic compounds, such as ethylene glycol.

Other possibilities to obtain the CAC are diffusion measurements or photo-physical measurements.[81,85] Furthermore hydrotropes serve as solubilising agents for hydrophobic compounds in hydrophilic media or vice versa. Adding hydrotrope to a mixture of non-miscible compounds can result in a monophasic solution. The concentration at which this transition occurs is denoted as the minimum hydrotropic concentration (MHC).[81] In literature it is also sometimes used to describe the aggregation concentration in aqueous solution without solutes. In order to anticipate misunderstandings, we use in this work CAC to describe the aggregation of hydrotropes in water.

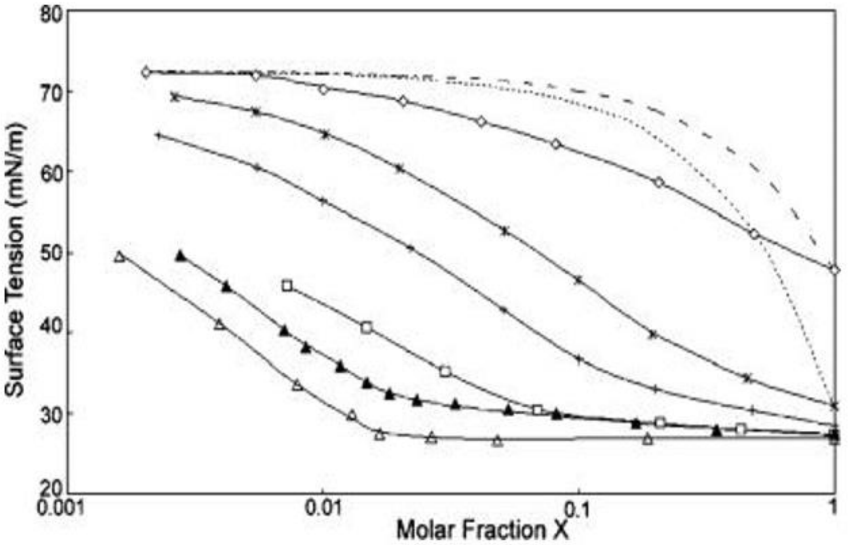

Figure 14 Surface tension in dependence of molar fraction for (from left to right): C_4E_1, C_3COE_1, C_3E_1, C_2E_1, C_1E_1 and E_1. The dashed and pointed line represent ideal mixtures.[84]

From a scientific point of view, the fundamental properties of hydrotropes, *e.g.* aggregation and solubilisation, are barely known and a clear distinction between hydrotropes and surfactants does not exist. Still hydrotropes are widely used in various industrial applications, ranging from household detergents and industrial cleansers to personal care products and paints.

Since Neuberg has introduced the term hydrotrope in 1916, a huge amount of compounds have been found, which show a hydrotropic behaviour. Many of them are non-ionic and volatile, which can be of interest for certain applications, since apart from their efficiency to solubilise hydrophobic organic compounds in water, they leave no residues. As examples, we can cite window cleansers in order to obtain clean streak-free surfaces or water-based perfumes.

In 2004, Lunkenheimer and Kunz introduced the new term **"solvo-surfactant"** to describe these volatile, non-ionic hydrotropes.[86] Solvo-surfactants are an interesting class of amphiphiles since they combine properties of both surfactants and solvents. On the one hand, they exhibit characteristics of a solvent, which is due to their relatively high volatility, as well as their capacity to solubilise molecularly hydrocarbon compounds. On the other hand, they also show properties which are related to surfactants, as a critical aggregation concentration and the solubilisation of hydrophobic compounds in aggregates, which yield a higher efficiency in solubilising oil in water or vice versa. The solubilisation mechanism can thus be generalised as a hydrotropic solubilisation mechanism, though hydrotropes are not compulsory solvo-surfactants. Hydrotropes are a class of amphiphilic ionic or non-ionic organic compounds, which are capable of effective solubilisation due to aggregation. This implies that volatility is not an obligatory property of these compounds, since this class contains also ionic compounds *i.e.*. sodium xylenesulfonate (SXS).

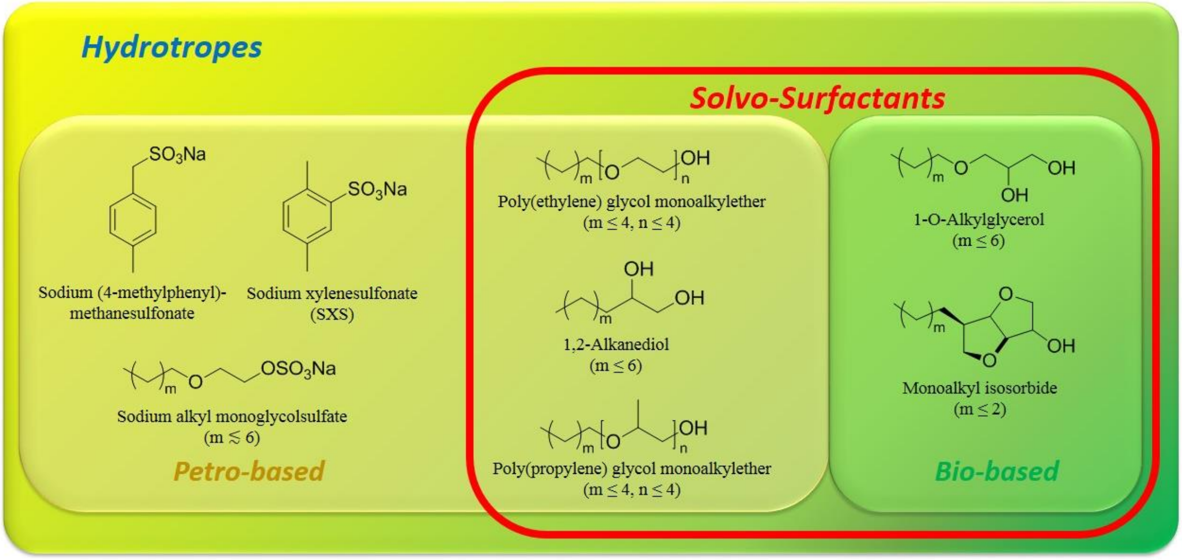

Figure 15 Summary of several classes of hydrotropes. The petro-based ionic hydrotropes are not volatile, whereas the non-ionic short-chain amphiphiles are volatile. Lately volatile bio-based hydrotropes were synthesized and characterized. Together with the non-ionic petro-based hydrotropes, they form the class of solvo-surfactants.

There exists a huge variety of solvo-surfactant classes, which have been in the centre of research in the last years. Some of them are petro-based like sodium alkyl monoglycolsulfate, others are bio-based like 1-O-alkylglycerols. Several classes are shown in **Figure 15**, where they are distinguished, according to petro- or bio-based, as well as their volatility. In the following sections an overview of the most important classes is given.

2.1.1. Glycol ethers

The most known and also used class of solvo-surfactants are the **short chain (poly)ethylene or (poly)propylene glycol monoalkylethers** abbreviated as C_iE_j or C_iP_j respectively (**Figure 16**).

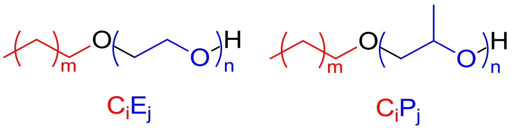

Figure 16 Basic structure of poly(ethylene) and poly(propylene) glycol monoalkylether. The red part represent the alkyl chain (C_i), whereas the blue part represent the ethoxy group (E_j), respectively the propoxy group (P_j).

Many of these molecules have been studied in detail and their properties are well known. Most of them are soluble in water at ambient temperature and due to their ethoxy/propoxy groups, they exhibit also a lower and upper miscibility gap. There are two classes of glycol ethers. The (poly)ethylene glycol monoalkylethers are usually constituted of an alkyl chain with 1 – 6 carbons and 1 – 4 ethoxy groups. Zhu *et al.* studied the hydrotropic properties of C_3E_1 and C_4E_1 and suggested that C_3E_1 is treated rather as a solvent, since its solubilisation capability resembles more a solvent in ternary amphiphile/water/oil systems.[84] In industry, short chain C_iE_j are widely used for numerous applications. The first amphiphilic glycol was C_1E_1, introduced under the commercial name methylcellosolve in 1930, it was used as a solvent for varnish. Nowadays short-chain C_iE_j's are used as solubilising agents in coatings[87] or in combination with other compounds in cleansers to form azeotropes with lower volatility.[88] Furthermore, they can be found in adhesives, pesticides, fracturing fluids and cosmetics. In 1985, it was figured out that C_1E_1 and C_2E_1 were genotoxic[89], which promoted the search for alternatives. These were found in (poly)propylene glycol monoalkylethers C_iP_j which consists usually of an alkyl chain with 1 – 4 carbons and 1 – 2 propoxy groups. Their head group contain one carbon more per propoxy unit than their smaller homologues, which makes them more hydrophobic in comparison to the ethoxy glycols. Due to their low toxicity, they became increasingly interesting in replacing poly(ethylene) glycol ethers. Nowadays they can be found in various applications, *e.g.* as dispersant in industrial cleaners[90] or solvent in perfumes[91].

Unfortunately ethoxy and propoxy glycols are petro-based compounds. Worldwide millions of tons of glycol ethers are produced each year (*e.g.* 161.000 tons of C_4E_1 per year). Thus the search for green alternatives is at the moment particularly pursued.

2.1.2. 1,2-Alkanediols

Another class of solvo-surfactants is represented by the **1,2-alkanediols** (**Figure 17**).

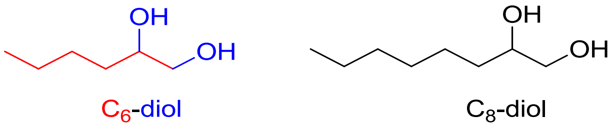

Figure 17 1,2-Hexanediol (C_6-diol) and 1,2-octanediol (C_8-diol). They can be found in a huge variety of different cosmetic products and antimicrobial products.

The most known is 1,2-ethanediol, which is also known under its trivial name glycol, since it is used as building block for poly(ethylene) glycol ethers. Due to its lack in amphiphilicity, it is classified as a solvent. More interesting are its longer homologues which are frequently used in personal care products, e.g. as softening agent in cosmetic compositions such as lotions or creams.[92] 1,2-Hexanediol turned out to be very mild to the skin[93], which made it particularly interesting as a solvent for ethanol-free aqueous perfume compositions.[72] Furthermore it is used in antimicrobial products, especially with 1,2-octanediol, since together they show synergy in comprising the antimicrobial properties of active agents.[94,95]

As glycolethers, 1,2-alkanediols are petro-based compounds. 1,2-Butanediol is a by-product of the production of 1,4-butanediol from butadiene with acetic acid.[96] 1,2-Propylenediol is produced from propylene oxide. There is also a possibility to synthesize it from the sugar alcohol *D*-mannitol, but with the drawback of using the very toxic lead(IV) acetate as reagent.[97]

2.1.3. Monoalkyl glycerols

A bio-based alternative to the petro-based glycol ethers and 1,2-alkanediols are the 1-O-monoalkyl glycerols (**Figure 18**).

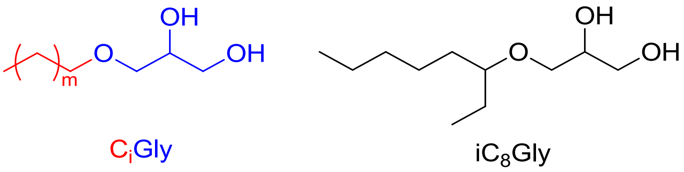

Figure 18 1-O-Monoalkyl glycerols consists of an alkylchain (C_i) and a glycerol head group (Gly). There exist also branched amphiphiles, such as ethylhexylglycerol (iC_8Gly)

In the last years, these compounds were intensively studied, since they may have the potential to replace C_iE_j's and C_iP_j's. At lab-scale, monoalkyl ethers can be synthesized according to a two-step reaction, consisting of an etherification between an alcohol and epibromohydrin, followed by a hydrolysis.[98] However, this type of reaction has a bad environmental footprint, since it has limited yields and a strong base is needed in order to deprotonate the alcohol. A greener alternative, which can be also up-scaled, is the catalytic reductive alkylation of polyols starting from aldehydes[99,100], ketones[101] or carboxylic acids[102].

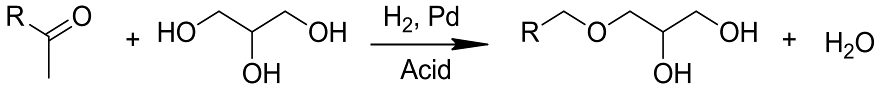

Figure 19 Catalytic reductive alkylation of glycerol. This green alternative, which can be up-scaled, produces only water as by-product.

There exist two isomers of monoalkyl glycerols. If the alkyl chain is attached to the first oxygen atom, it receives the denomination 1-O-alkyl glycerol, whereas 2-O-alkyl glycerol if the chain is located at the second oxygen atom. The alkyl chain can constitute of various length or constitutional isomers, which implies branching or cyclisation. Also the addition of a benzene ring as hydrophobic part of the glycerol ether is possible.[98]

2.1.4. Monoalkyl isosorbide

Isosorbide is obtained from the sugar alcohol sorbitol via double dehydration. Isosorbide contains two hydroxyl groups, whereon alkyl chains can be attached. There exist dialkylated and monoalkylated isosorbides. The latter exist in two conformations, since there exist two hydroxyl groups in the isosorbide (**Figure 20**).

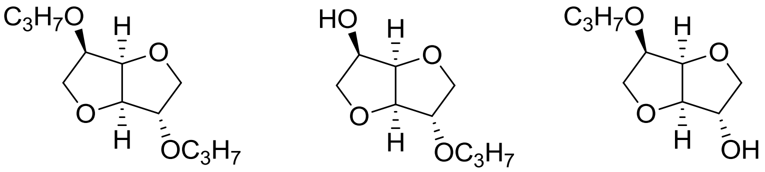

Figure 20 From left to right: Dipropylene isosorbide, 2-O-propyl isosorbide, 5-O-propyl isosorbide.

In this work only 5-O-alkyl isosorbides were used. No monoalkyl isosorbides were synthesized in this work. The investigated compounds were synthesized by Laurianne Moity during her Ph.D. thesis.[103]

2.1.5. Miscellaneous

Previously the most important and studied solvo-surfactants were presented, but there exist of course many other solvo-surfactants which are used in industry or are at the moment in the centre of research. In 2008 a paper was published which studied the properties of **dipropylene glycol isobornyl ether**, which belongs to the class of C_iP_j, but contains an uncommon hydrophobic part. It is sold under the name Pribelance® by CABB and it is a low-toxic anti-foaming solvo-surfactant with excellent co-surfactant properties[104]. **Glycerol monoalkanoates** and **glycerol carbonate alkanoates** are other types of amphiphiles, which can be obtained from esterification of glycerol. These types of molecules turned out to induce superhydrophilicity on surfaces, which makes them interesting for surface protection.[105,106] The possibility to functionalise glycerol in many different ways opens the door to a huge variety of other solvo-surfactants. The above stated are shown in **Figure 21**.

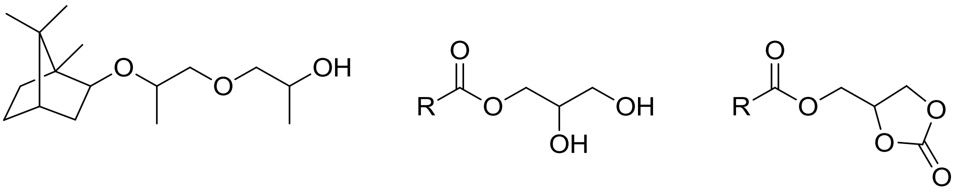

Figure 21 Several solvo-surfactants. Left: Pribleance®, a C_iP_j type amphiphile with a bicyclic tail. Centre: Glycerol monoalkanoate solvo-surfactants. R represents the alkyl chain. Right: The amphiphile glycerol carbonate alkanoate contains a cycle in its polar head group.

This chapter gives a complete overview of the most important solvo-surfactant classes. However there might exist other less known compounds, which meet the criteria of these amphiphiles. In general one can think of several different types of molecules which exhibit an amphiphilicity and are volatile. However more important than the actual existence of these compounds is the question about the cost- and eco-effectiveness of their production, as well as the question if their properties are superior to those, which are widely used in industry. Thus the search for further alternatives is not over and other solvo-surfactants are expected to appear in nearby future.

2.2. Synthesis of solvo-surfactants based on ethylene glycol and glycerol

2.2.1. Poly(ethylene) glycol monoalkylethers C_iE_j

The reaction to obtain poly(ethylene) glycol monoalkylethers C_iE_j is known under the name "Williamson Ether Synthesis". All C_iE_j were synthesized according to a known procedure (**Figure 22**).[107] After the reaction, the crude product was extracted and eventually distilled in order to obtain a pure product.

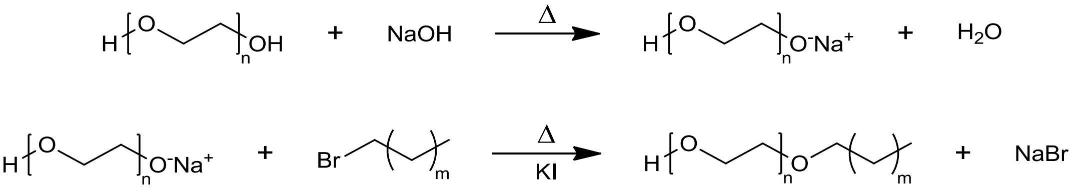

Figure 22 Synthesis of poly(ethylene) glycol monoalkylethers. Several amphiphiles were synthesised according to this procedure, such as the solvo-surfactants C_5E_3, C_5E_4, C_6E_3, C_6E_4 and C_8E_3, as well as the surfactants C_8E_4 and $C_{10}E_4$.

The purity of all synthesised glycols was verified with GC-FID and NMR spectroscopy. All of them have a purity of $\geq$ 97%.

2.2.2. 1-O-Alkylglycerols

The reaction to obtain 1-O-alkylglycerols C_iGly is a two-step reaction (**Figure 23**).[103] The first step represents a "Williamson Ether Synthesis" between an alcoholate and epibromohydrin. After purification the cycle is then opened in a hydrolysis reaction. The big advantage of the hydrolysis, is that no purification has to be made and the product can be obtained directly after water removal. Alternatively the second step can be accelerated by adding small amounts of hydrogen chloride. However the product has then to be purified.

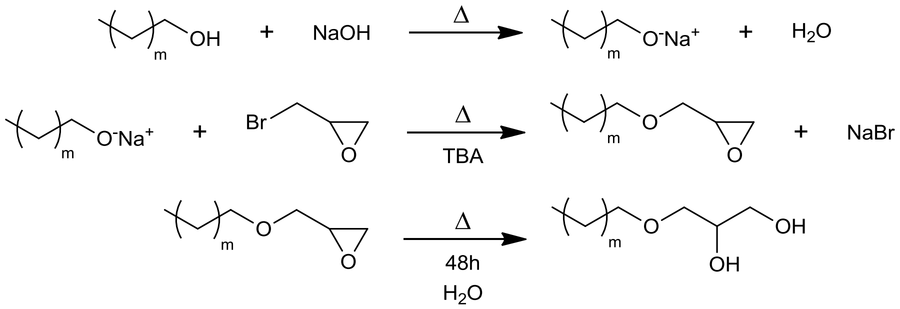

Figure 23 Synthesis of 1-O-alkylglycerols (C_iGly). Two amphiphiles (C_4Gly and C_5Gly) were synthesised according to this procedure.

The purity of all synthesised glycerols was verified with GC-FID and NMR spectroscopy. All of them have a purity of ≥ 98%.

2.3. Surfactant properties of solvo-surfactants

In this section the surfactant properties of solvo-surfactants are investigated. Thereby their aqueous phase behaviour is studied, as well as their hydrophilic-lipophilic nature.

2.3.1. Binary phase behaviour of solvo-surfactants in water

In order to understand the phase behaviour of a surfactant/oil/water (SOW) system, the phase behaviour of the binary system surfactant/water (SW) and surfactant/oil (SO) has to be well-known. Indeed, the ternary phase behaviour is a result of the interplay of the lower miscibility gap of the system WO with the lower gap of the system SO and the upper miscibility gap of the system SW (**Figure 24**). Since water and oil are not miscible between 0 and 100 °C, its upper critical points lie well above the boiling point of the mixture. Thus the phase behaviour is mainly determined by the binary phase diagrams SW and SO. The upper critical solution temperature T_α of the SO miscibility gap is usually located around 0 °C. However, relatively polar oils as they are used in fragrance compositions strongly decrease T_α, since the interaction between the hydrophilic part of the surfactant and the oil is less unfavourable as it is for linear alkanes. Thus many of these oils cannot be used for the investigation of their SO binary system. On the other hand C_iE_j's show mostly a miscibility gap between 0 and 100 °C in the SW binary phase diagram. This so called clouding phenomenon, describes the phase separation of a micellar solution with increasing temperature. It depends on the length of the carbon chain as well as on the number of ethoxy groups in the amphiphile. The appearance of the upper miscibility gap is a consequence of the dehydration of the ethoxy groups by increasing temperature.[108,109] It is widely accepted that the clouding phenomenon arises from the balance of intermicellar van der Waals attraction and hydration repulsion, with the latter decreasing with increasing temperature. Augmenting the temperature dehydrates the aggregates to some extent, which results in an increasing intermicellar interaction and thus results in a phase separation. The critical point cp_β of the mixture, at which the clouding behaviour is initiated, is described by the critical temperature T_β and the critical amphiphile

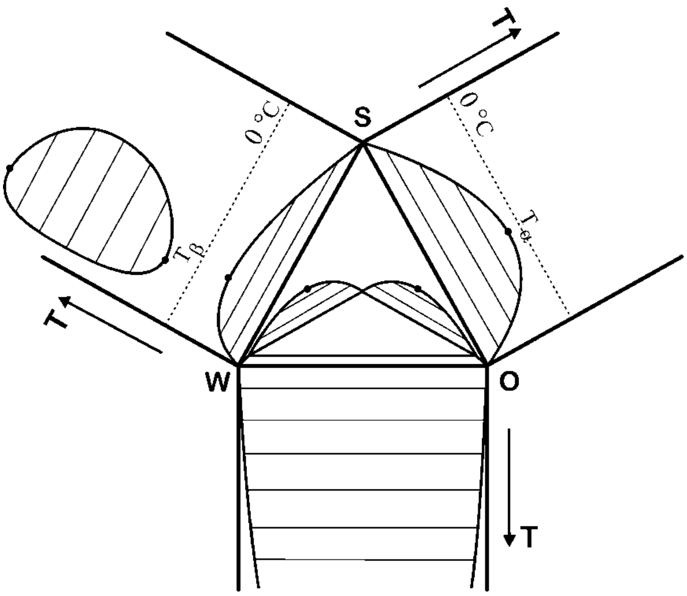

Figure 24 Schematic representation of the three binary phase diagrams (SW, SO and WO), which assemble the ternary SOW phase diagram. The dashed regions represent the miscibility gaps.

weight fraction w_β. Schubert *et al.* proposed a purification technique for poly(ethylene) glycol monoalkylethers based on the temperature dependence of the hydrophilic-lipophilic nature of C_iE_j's.[110] The amphiphile is given into oil and water (WOR = 1) and depending on the temperature and the hydrophilic-lipophilic balance of the amphiphile, a WI or WII phase is formed. The excess phase, which contain water or oil soluble impurities is then removed and same volume of pure excess phase is added. Then the temperature is changed until the amphiphile migrates into the other phase and the excess phase is removed. This procedure is repeated several times and results is highly pure glycol amphiphiles. Within this work, he showed the influence of impurities on the binary phase behaviour in water and concluded that impurities left over from synthesis decrease the miscibility gap towards lower temperatures.

In our work, several binary phase diagrams of short- and middle-chain amphiphiles were constructed, which can be seen in **Figure 25**. Thereby *w* signifies the weight fraction of amphiphile in the mixture. The curves separate the monophasic region from the upper miscibility gap, which lies at higher temperatures. The critical temperature T_β of the amphiphile is represented by the corresponding filled symbol. It can be seen that the higher the quantity of ethoxy groups in the amphiphile, the higher is the location of the upper miscibility gap, whereas an increase in carbon chain lengths diminishes T_β. These results are in accordance with literature.[108,110,111] The critical weight fraction w_β augments with increasing ethoxy number and decreasing carbon chain number length, which is a result of the high monomerical solubilisation of short chain amphiphiles in water. This indicates the dual solubilisation mechanism of short chain amphiphiles. On the one hand they may solubilise molecularly hydrophobic compounds, whereas on the other hand at a certain concentration they form as well aggregates, which permit them to solubilise compounds in their interior.

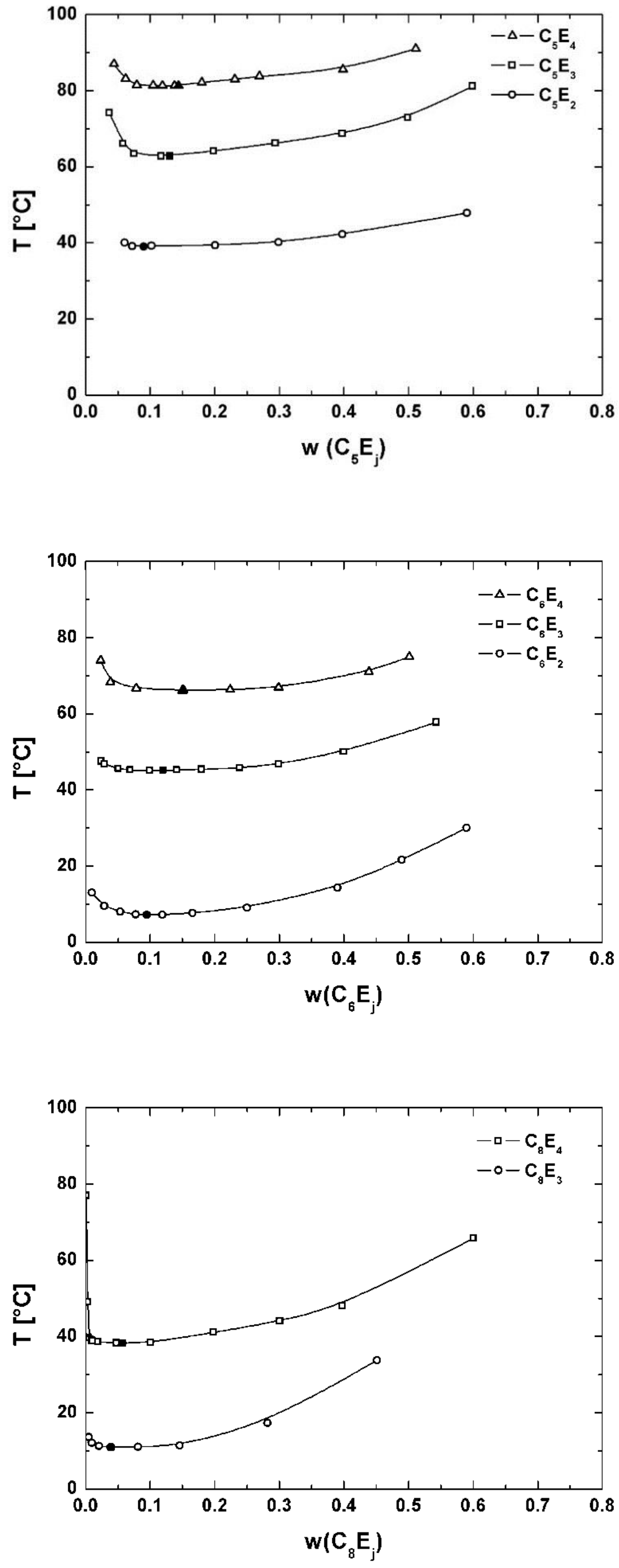

Figure 25 Binary phase diagrams of C_iE_j in water. The filled symbol represents the critical point cp_β. Top: Binary phase diagrams of C_5E_j (j =2,3,4). Centre: Binary phase diagrams of C_6E_j (j = 3,4). Bottom: Binary phase diagrams of C_8E_j (j = 3,4).

If the nature of the water phase stays unchanged (no salts, alcohols, etc.), the binary phase behaviour of poly(ethylene) glycol monoalkylethers depends, besides on the temperature and pressure, on i and j, which represents the length of the carbon chain and the number of ethoxy groups in the non-ionic amphiphile. It is an interesting question, if the aqueous properties of short-chain amphiphiles can be compared to those of long-chain surfactants. Therefore a relationship between T_β and i/j of several short, medium and long-chain amphiphiles was established, which is shown in **Figure 26**. Full circles represent surfactants, whose values were obtained from literature.[108,110] Empty circles represent solvo-surfactants, whose T_β values were determined in this work. A strong linear correlation can be seen, and it can be considered that T_β is decreasing with increasing i/j, thus for amphiphiles which are considered as rather hydrophobic. There is one distinct outlier, which is located far above the expected temperature. The value for C_4E_1 was obtained from literature[112] and verified rapidly in our laboratory. Kahlweit *et al.* investigated the transitions from weakly to strongly structured mixtures using several techniques and methods such as SAXS, wetting, surface adsorption, etc.[113] The authors concluded that C_4E_1 is a weak amphiphile, resulting in a strong monomeric solubilisation in water, which may be the reason for the huge displacement. Same deviation is obtained for C_4E_2, which is miscible with water between 0-100 °C. However its T_β value is expected to be between 40-60 °C according to **Figure 26**. Nevertheless other solvo-surfactants lie within the linear correlation. Kahlweit *et al.* stated that amphiphiles with a pentyl- or hexyl chain lie within a transition zone between weak amphiphiles (C_4E_j) and amphiphiles with a distinct break in surface adsorption (C_8E_j).[113] Thus the aqueous phase behaviour of solvo-surfactants with i ≥ 5 can be compared to those of real surfactants. According to the following relationship, T_β of (poly)ethylene glycol monoalkylethers with i ≥ 5 can be calculated:

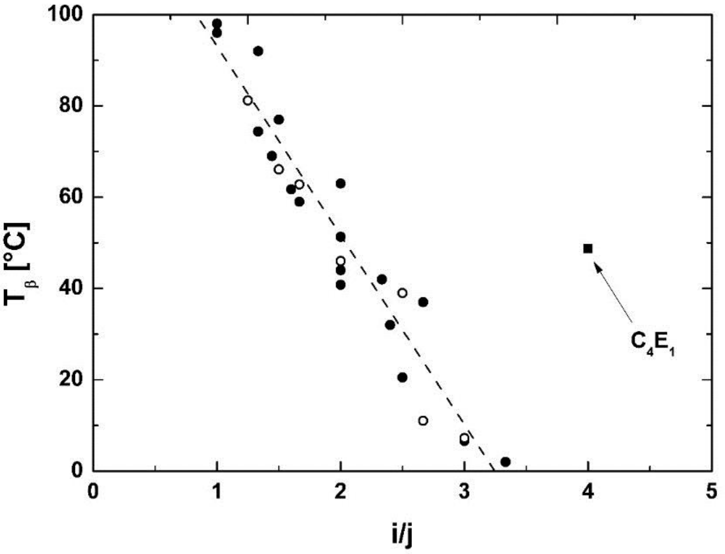

Figure 26 Correlation between the critical temperature T_β and the divider between the carbon chain length i and ethoxy number j. Full symbols signify surfactants, whereas empty symbol solvo-surfactants. C_4E_1 deviates strongly from the other C_iE_j.

$$T_\beta = 134.5 - 41.4 \times \frac{i}{j} \tag{14}$$

Table 4 summarizes all relevant solvo-surfactants as well as their abbreviation, their critical temperature T_β and critical mass fraction $w*$.

Table 4 Summary of the critical temperature T_β and the critical amphiphile mass fraction $w*$ for all in this work relevant solvo-surfactants.[110,112,116]

Compound	Abbreviation	T_β [°C]	$w*$
(Poly)ethylene glycol monoalkylethers C_iE_j			
Ethylene glycol monobutylether[a]	C_4E_1	48.7	0.290
Diethylene glycol monobutylether	C_4E_2	> 100	-
Ethylene glycol monopentylether[a]	C_5E_1	< 0	-
Diethylene glycol monopentylether	C_5E_2	39.0	0.090
Triethylene glycol monopentylether	C_5E_3	62.8	0.131
Tetraethylene glycol monopentylether	C_5E_4	81.3	0.144
Diethylene glycol monohexylether	C_6E_2	7.2	0.095
Triethylene glycol monohexylether	C_6E_3	45.1/46.0 [b]	0.120/0.146 [b]
Tetraethylene glycol monohexylether	C_6E_4	66.1/66.1 [b]	0.150/0.164 [b]
Diethylene glycol monooctylether	C_8E_2	< 0	-
Triethylene glycol monooctylether	C_8E_3	10.9/11.0 [b]	0.040/0.052 [b]
Tetraethylene glycol monooctylether	C_8E_4	38.3/40.8[b]	0.058/0.071 [b]
Propylene glycol monopropylether[a]	C_3P_1	33.0	~0.45
Propylene glycol monobutylether[a]	C_4P_1	< 0	-
Alkylglycerols C_iGly			
Butylglycerol[a]	C_4Gly	> 100	-
Pentylglycerol[a]	C_5Gly	> 100	-
Isopentylglycerol[a]	iC_5Gly	> 100	-
Hexylglycerol[a]	C_6Gly	< 0	-
Ethylhexylglycerol	iC_8Gly	< 0	-
Alkylisosorbides C_iIso			
Monopropylisosorbide	C_3Iso	> 100	-
Monopentylisosorbide[c]	C_5Iso	39.3	~0.25
Alkanediols C_i-diol			
1,2-Hexanediol	C_6-diol	> 100	-
1,2-Octanediol	C_8-diol	< 0	-

[a]see reference [112],[b]see reference [110],[c]see reference [116]

C_8E_4 and C_5Iso are no solvo-surfactants (see **Chapter 2.4.1.),** but were anyways investigated in this work. The glycerol and the alkanediol derivatives show no clouding behaviour between 0 and 100 °C, and only a slight temperature dependency due to their two hydroxyl groups which can undergo stronger hydrogen bond interactions than glycol ethers.

2.3.2. Influence of ionic surfactants on the critical temperature of C_iE_j solvo-surfactants

Ionic amphiphiles are less affected by temperature than non-ionic amphiphiles, which makes them interesting for the formulation of temperature insensitive mixtures. Together with non-ionic surfactants, they are able to form monophasic microemulsions within a huge temperature interval.[76,114,115] However the effect of varying small amounts of different ionic surfactants is barely understood. In order to attain this goal, first the influence of ionic surfactants on the binary phase behaviour of non-ionic amphiphiles in water has to be studied. The used ionic surfactants can be seen in **Figure 27**.

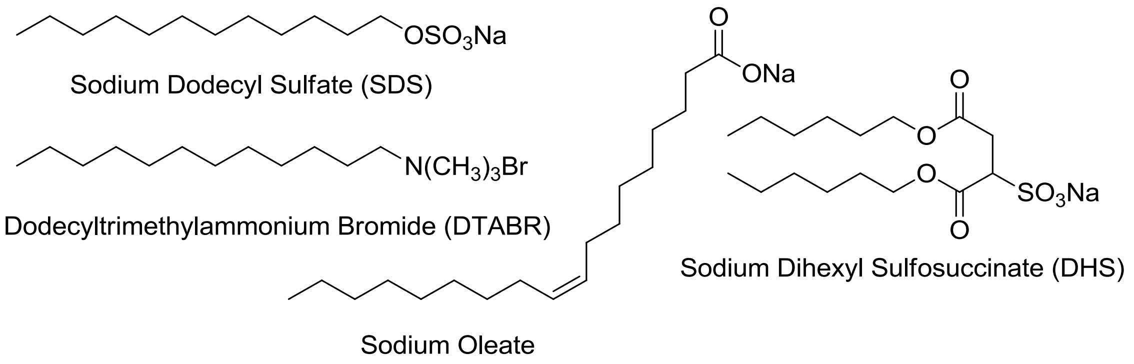

Figure 27 Several ionic surfactants, which were used in this work. The anionic sodium dodecyl sulfate, the cationic dodecyltrimethylammonium bromide, the bio-sourced anionic sodium oleate and the two-tailed anionic sodium dihexyl sulfosuccinate.

Thereby the effect of small amounts of ionic surfactant on the critical temperature of several solvo-surfactants was investigated by constructing their temperature depending pseudo-binary phase diagrams. Varying amounts of ionic surfactant were solubilised in water and mixed with different amounts of solvo-surfactant. The molar fraction ε of ionic surfactant is defined according to following relationship:

$$\varepsilon = \frac{n(IS)}{n(IS) + n(H_2O)} \tag{15}$$

The weight fraction of solvo-surfactant in the pseudo-binary mixture is defined as follows..

$$w(Solvo - surfactant) = \frac{m(Solvo - surfactant)}{m(Solvo - surfactant) + m(IS(aq))} \tag{16}$$

..where *IS*(*aq*) stands for the aqueous ionic surfactant solution. The phase behaviour was then determined by visual observation under temperature increase at a rate of 0.2 °C per minute, until the mixture dephased. It was verified for several samples if a hysteresis appears upon cooling and if the values deviate if the samples were left for equilibration at fixed temperature. Fortunately there were only marginal deviations (≤ 0.2 °C), which can be explained with the relatively small amphiphilicity of the solvo-surfactants. Thus alterations in the phase behaviour appear immediate.

In **Figure 28**, the phase diagrams of C_6E_2/DHS(aq) as well as C_6E_3/DHS(aq) are shown with increasing quantity of DHS in the aqueous phase. For low solvo-surfactant concentration, the effect of DHS on the phase separation is very strong whereas it is not significant for high concentrations of solvo-surfactant (> 0.5). Therefore cp_β shifts to higher mass fractions of solvo-surfactant. The pseudo binary diagrams of C_6E_2 and C_6E_3 resemble each other strongly. Indeed C_6E_3 is just shifted to higher temperatures, which can be attributed to the higher number of ethoxy groups in C_6E_3 compared to C_6E_2.

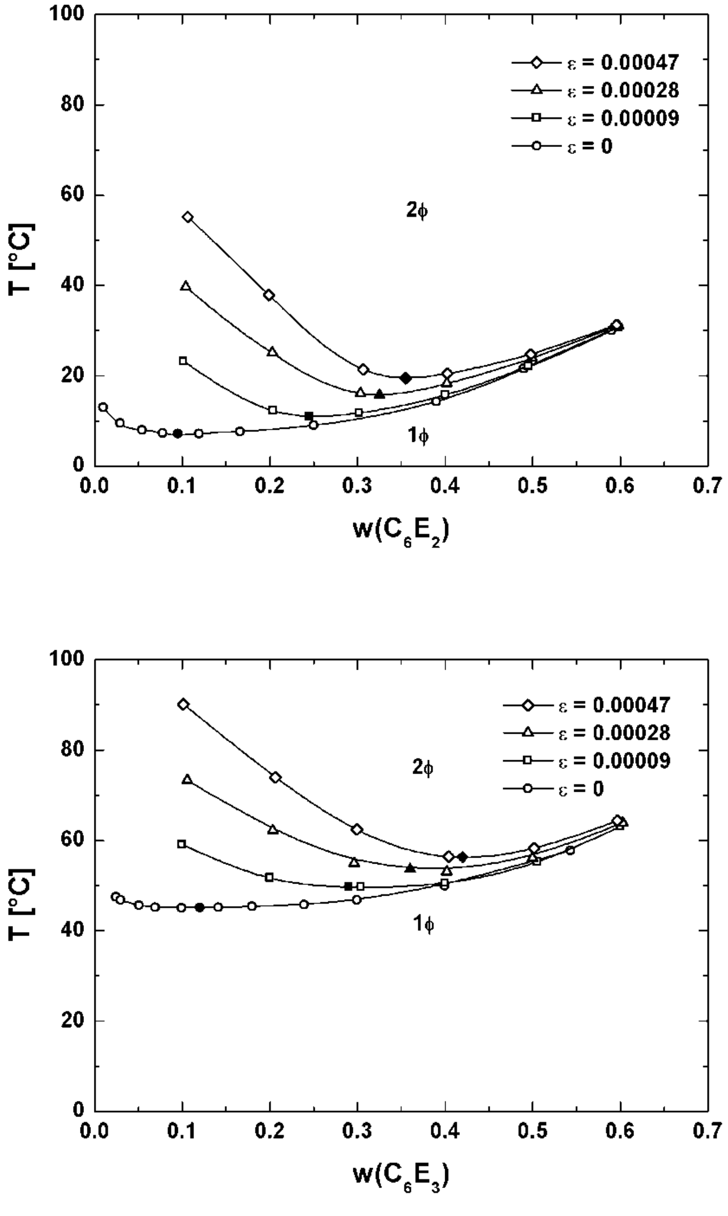

Figure 28 The influence of the ionic surfactant DHS on the binary phase behaviour of solvo-surfactants in water. Top: The system C_6E_2/DHS(sq). Bottom: The system C_6E_3/DHS(aq).

Same experiments were performed for C_6E_3 in aqueous SDS solutions. The results can be seen in **Figure 29**. Same behaviour as for DHS is thereby observed. T_β increases with augmenting SDS molar fraction. The effect on the upper miscibility gap is thereby stronger for small than for higher solvo-surfactant mass fractions. This causes a shift of the critical point cp_β towards higher solvo-surfactant mass fractions.

In **Figure 30** the influence of the ionic surfactant molar fraction on the critical temperature T_β can be seen. Thereby T_β of the solvo-surfactant is subtracted from the critical temperature T_β^ε at a given ε. Consequently the relative increase in temperature stability of the binary SW in dependence of ε(IS) is shown. It can be seen, that the effect of DHS on C_6E_2 and C_6E_3 is quite the same. Thus the interaction between C_6E_2 and DHS, as well as between C_6E_3 and DHS is assumed to be the same. On the other hand SDS has a stronger effect on the critical temperature than DHS. In can thus be concluded that the interaction between a C_iE_j and an ionic surfactant is rather determined by the latter and the strength of the interaction of the ionic head group with the non-ionic ethoxy group.

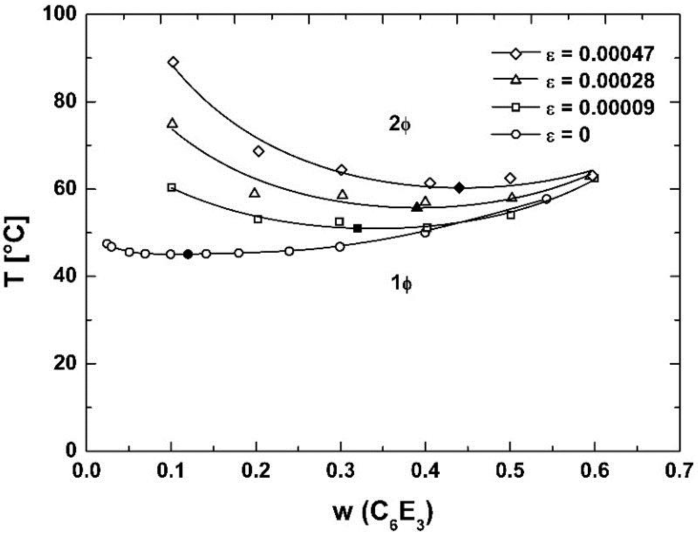

Figure 29 The influence of the ionic surfactant SDS on the binary phase behaviour of C_6E_3 in water.

Generally spoken, the addition of an ionic surfactant to a non-ionic surfactant results in the formation of mixed micelles.[9,117,118] At low mass fraction of solvo-surfactant, the number of micelles is relatively low, which results in more ionic surfactant molecules per micelle. The addition of DHS to the water phase charges the micelles and thus more energy in form of temperature increase has to be added to overcome – besides the dehydration of ethoxy groups - the electrostatic repulsion between micelles, until phase separation occurs.[119–121] Therefore, the critical temperature T_β evolves towards higher temperatures, as well as higher mass fraction of solvo-surfactant. Since at low non-ionic amphiphile content, more ionic surfactant is available, and thus more of it is distributed to each micelle, the increase is more pronounced in this region. With increasing amounts of solvo-surfactant, the curve passes through a minimum and eventually the dehydration of the ethoxy groups dominates again, as in the case without ionic surfactant.

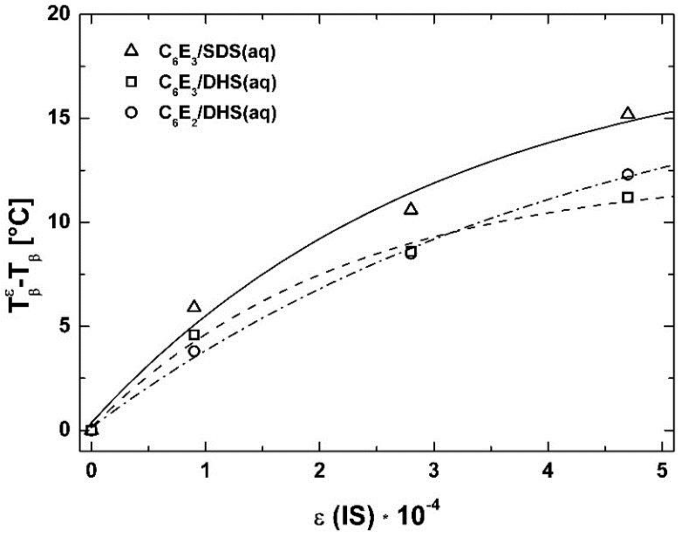

Figure 30 The influence of the molar fraction ε(IS) on the relative increase of the critical temperature $T_\beta^\varepsilon - T_\beta$.

The influence of other ionic surfactants on the phase behaviour of C_6E_2 in water was investigated. Among them, the cationic surfactant dodecyltrimethylammoniumbromide (DTABR) and the bio-sourced anionic surfactant sodium oleate. Results are shown in **Figure 31**.

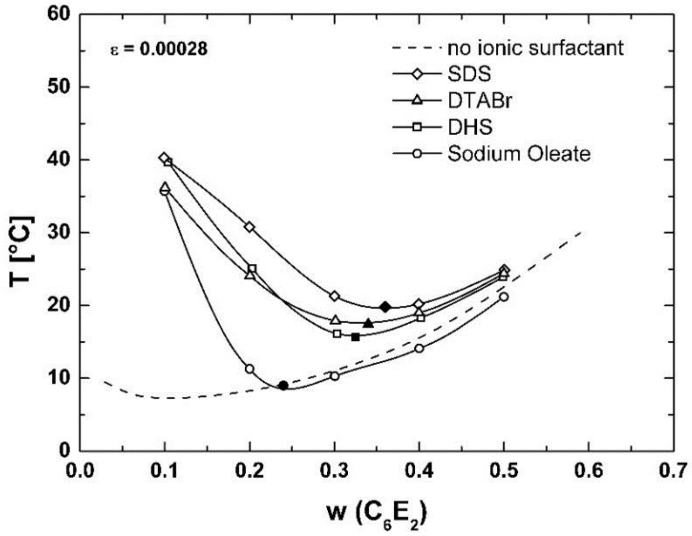

Figure 31 Influence of several ionic surfactants on the binary phase behaviour of C_6E_2 in water. The full symbols signify the location of the critical point cp_β. $\varepsilon = 2.8*10^{-4}$.

Thereby several aqueous ionic surfactant solutions were prepared with same molar fraction of ionic surfactant in water ($\varepsilon = 2.8*10^{-4}$). As already shown previously, the influence of the ionic amphiphiles is the strongest for low C_6E_2 mass fraction. SDS and DHS have approximately the same influence on the temperature stability at *w* = 0.1, whereas DTABr and sodium oleate – which show as well a similar behaviour at said mass fraction – have a slightly smaller effect. With increasing weight concentration of C_6E_2, the pseudo-phase behaviour differs strongly, especially by comparing the critical temperature T_β.

The influence on the cloud point can be ranked this way: sodium oleate << DHS < DTABr < SDS. According to this rqnking, SDS has the biggest influence among the studied ionic surfactants on T_β, whereas sodium oleate has only a slight effect, and shows even a negative effect for high concentrations of C_6E_2. The determination of the interaction parameter between an ionic and non-ionic surfactant via surface adsorption was investigated in literature for quite a lot of systems. Thereby it was found that the interaction tend to be smaller for cationic/non-ionic than for anionic/non-ionic systems.[9] This explains the stronger effect of SDS on the cloud point compared to DTABr. However DHS, which is also anionic has a slightly weaker effect. Probably the two ester groups in the molecule affect the interaction between the non-ionic surfactant and the SO_3^- head group. On the other hand sodium oleate do barely change the cloud point, which might be connected with its longer alkyl chain and consequently stronger hydrophobicity.

In the context of solubilising oil in water, in particular fragrances, the increase in temperature stability induced by the addition of small amounts of ionic surfactant at low non-ionic amphiphile weight fraction, is very interesting since it may promote the solubilisation of oil in a monophasic microemulsion in the water rich corner of the ternary SOW phase prism. It is known, that the phase behaviour in a phase prism is the result of the overlapping of the miscibility gaps of its binary phase diagrams. Consequently it is expected that the increase in temperature stability in the SW binary phase diagram, will have a distinct effect on the phase behaviour in a SOW system, particularly in the water rich corner. This effect is investigated in **Chapter 4**.

2.3.3. Aggregation behaviour of pure solvo-surfactants and mixtures with anionic surfactants

The aggregation behaviour of solvo-surfactants was already described in the beginning of this chapter. In this part it is compared to real surfactants and in the following the aggregation behaviour with SDS is investigated to show if the formation of mixed micelles results in a synergism in their CAC.

a. Pure solvo-surfactants

The aggregation behaviour of several solvo-surfactants was studied and their critical micelle/aggregation concentrations were compared to those of real C_iE_j surfactants (*i.e.* $i \geq 8$). As it can be seen in **Figure 32**, the surface tension *versus* concentration curve of C_5E_3 resembles the one of C_5E_4. The latter has a slightly bigger critical aggregation concentration (264 mM compared to 257 mM). However at these high concentrations it is quite difficult to determine an exact value, which is also affected by the rather smooth break in the adsorption isotherm. Nevertheless it can be shown that there is strong difference in the CAC between C_5E_j and C_6E_j. C_6E_3 and C_6E_4 have a CAC of 81 mM, respectively 84 mM. It is still relatively elevated compared to real surfactants (< 1 mM). However for oil solubilisation, where it can be assumed that the CAC represents approximately the monomeric solubility of the amphiphile in the water phase, a lower value is highly appreciated. As an example, in a

10 wt.% aqueous solution of C_5E_4 and C_6E_4, in the first case 6.3 wt.% is lost monomerically solubilised in water, whereas in the latter case only 2.1 wt.%, which is three times less. A huge CAC is also observed for 1-O-pentylglycerol (220 mM, 3.2 wt.%). The loss is not that high compared to C_5E_j, since its molecular weight is lower. Furthermore it decreases stronger the surface tension in comparison to the C_iE_j (27.5 mN/m *vs* 30.3 to 32.4 mN/m).

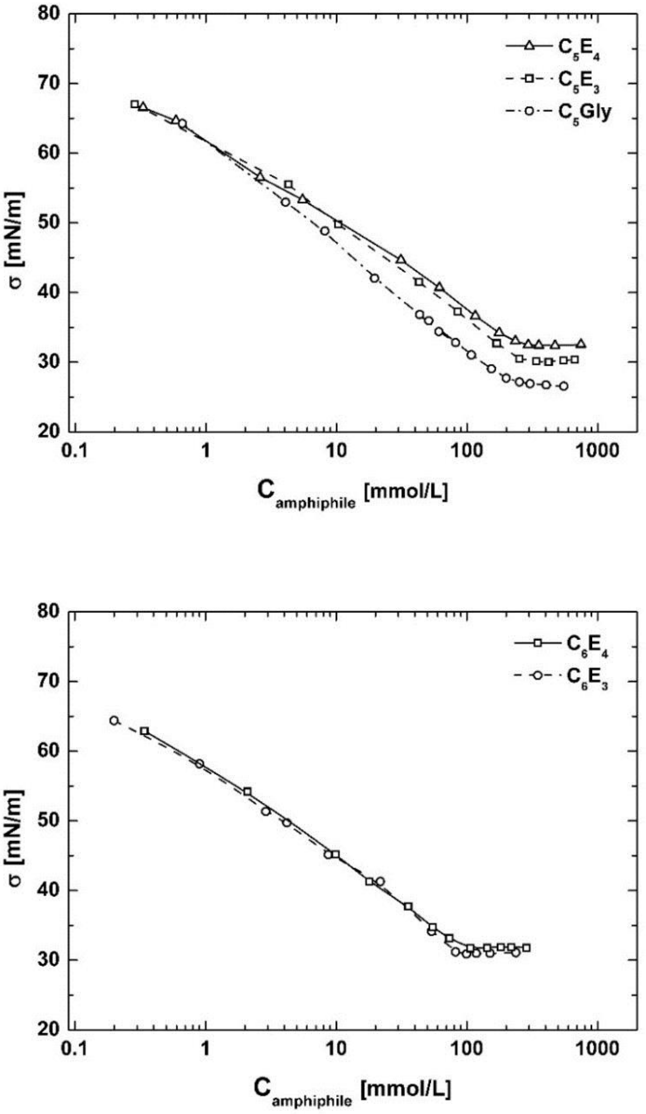

Figure 32 Surface tension versus concentration of amphiphile in water. The break in curve determines the critical aggregation concentration (CAC). Top: Adsorption isotherm of C_5E_j, with j = 3,4 and of C_5Gly. Bottom: Adsorption isotherm of C_6E_j, with j = 3,4.

Table 5 gathers the CAC of various solvo-surfactants investigated in the present work and in literature. As expected, the longer the hydrocarbon chain is, the lower the CAC. Furthermore, a bigger quantity of ethoxy units results in a slightly higher CAC (compare C_6E_3 *vs* C_6E_4 or C_4E_1 *vs* C_4E_2). Glycerol based solvo-surfactants show a smaller CAC compared to C_iE_j counterpart. The highest values are obtained for C_3P_1 and C_3E_1. However despite their amphiphilic structure, they may appear rather as a solvent. Furthermore at this high concentrations, it can be assumed that the activity and concentration is fairly different. Hence the CAC, which was found during the measurement may disappear if the effective concentration is calculated.

Table 5 Summary of all critical aggregation concentrations for solvo-surfactants as well as their surface tension σ_{CAC}.

Solvo-Surfactant	CAC [mmol/L]	σ_{CAC} [mN/m]
C_6E_3	81	31.0
C_6E_4	84	31.7
C_5E_3	257	30.3
C_5E_4	264	32.4
C_4E_1[a]	830	27.2
C_4E_2[a]	880	28.0
C_3E_1[a]	1220	33.4
C_3P_1[a]	1560	26.5
C_5Gly	220	27.5
iC_5Gly[a]	360	25.3
C_4Gly[a]	600	28.6

[a] see reference [110]

Short-chain amphiphiles are known to have high values for the aggregation concentration. Ethoxy groups have only a slight influence on the CAC, whereas the carbon chain length is the key factor for the magnitude of the aggregation concentration. In **Figure 33**, the CAC's of polyethylene glycol monoalkylethers C_iE_3, C_iE_4 and C_iE_5 are reported as a function of i. Values were measured for C_5E_3, C_5E_4, C_6E_3, C_6E_4 and C_8E_4 whereas the remaining were obtained from literature.[110,122–124] There is a linear relationship between the logarithm of the CAC and the carbon chain length i. Only for $C_{14}E_5$ and C_4E_3 slight deviations are obtained, which may have been caused by an error in the preparation of samples with ultra-low concentrations, respectively by the difficulty to clearly determine the CAC for weak amphiphiles.

Considering the results from **Figure 32**, it can be stated, that short-chain amphiphiles can be very well compared to long-chain surfactants. There is a logharitmic relationship between the carbon chain length i and the CAC of the amphiphile. Their properties concerning surface adsorption and - as previously seen - clouding behaviour can thus be extrapolated to those of real surfactants. Only C_4-amphiphiles seem to behave differently, which was already seen in **Section 2.3.1.**

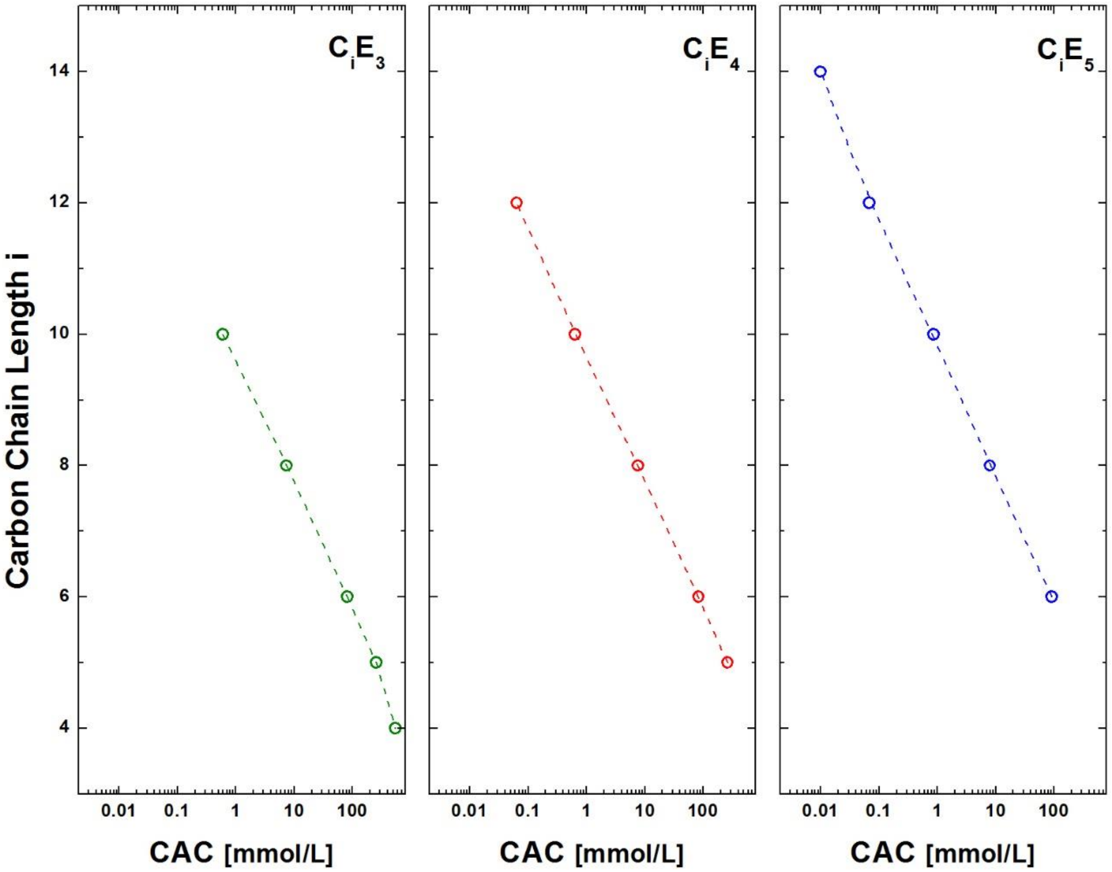

Figure 33 Evolution of the critical aggregation concentrations (CAC) of non-ionic (poly)ethylene glycol monoalkylethers C_iE_3, C_iE_4 and C_iE_5 as a function of i. The curves progress practically parallel. There are only slight deviations for C_4E_3 and $C_{14}E_5$. The effect of an ethoxy group on the aggregation is marginal.

b. Aggregation behaviour of solvo-surfactants with SDS

The surface adsorption of anionic/non-ionic mixed amphiphile systems was studied, in order to determine their critical aggregation concentration, which in turn enables the calculation of the interaction parameter β between a non-ionic and ionic surfactant. From a theoretical point of view, mixed surfactant systems first form mixed monolayers at the air-water interface and then, once the surface is saturated, they aggregate in the bulk phase to form mixed micelles. According to Holland and Rubingh, the critical aggregation concentration of a surfactant mixture (CAC) is given by the subsequent equation.[9]

$$\frac{1}{CAC^*} = \sum_{i=1}^{n} \left(\frac{\alpha_i}{f_i CAC_i} \right) \qquad \textbf{(17)}$$

Where α_i, CAC_i and f_i are respectively the stoichiometric mole fraction, the critical aggregation concentration (CAC) and the activity coefficient of the i^th component in the mixture (i = 1 for the nonionic surfactant and 2 for the ionic surfactant). From **Equation 17**, the CAC of an ideal mixture (f_i = 1), noted CAC^*_{calc}, can be calculated. When the experimental CAC^* is lower than CAC^*_{calc}, the system exhibits a non-ideal behaviour corresponding to a synergistic effect (i.e. f_i < 1). It results from an attractive interaction between the two surfactants located in the surface monolayer of the mixed micelle.[125–127] In this case, the regular solution theory must be invoked and the activity coefficient f_i of the i^th surfactant is expressed as follows[128]:

$$lnf_i = \beta(1 - X_i)^2 \qquad \textbf{(18)}$$

Where X_i is the mole fraction of the i^th surfactant in the mixed micelle and β is an interaction parameter related to the molecular interactions between the surfactant molecules in the mixed micelles. The interaction parameter β is an indication of the degree of interaction between the two surfactants. A negative β value indicates a synergism, indicating that the attractive interaction between the two different surfactants is stronger than the one between identical molecules of surfactants. From **Equations 17** and **18**, the following relationship can be deduced[129]:

$$CAC^* = \frac{CAC_1 CAC_2 e^{\beta(-1+X_1)^2+\beta X_1^2}}{\alpha_1\left(CAC_2 e^{\beta X_1^2} - CAC_1 e^{\beta(-1+X_1)^2}\right) + CAC_1 e^{\beta(-1+X_1)^2}} \qquad \textbf{(19)}$$

Moreover, the mole fraction of the ionic surfactant in the aggregated pseudo-phase, X_1,can be solved iteratively for each α_1 from **Equation 20.**[125,128]

$$\frac{X_1^2 \ln\left(\frac{\alpha_1 CAC^*}{X_1 CAC_1}\right)}{(1 - X_1)^2 ln\left[\frac{(1-\alpha_1)CAC^*}{(1-X_1)CAC_2}\right]} = 1 \qquad \textbf{(20)}$$

Hence, for each α_1, the theoretical CAC^* can be calculated, from **Equation 18** and **19**, in order to determine X_1 and consequently fit the adjustable parameters (β) with an algorithm.

The surface tensions of aqueous solutions containing different ratios of a solvo-surfactant and SDS have been measured as a function of amphiphile concentration. Three systems were studied: C_6E_3/SDS, C_6E_4/SDS and C_5Gly/SDS. As shown in the previous section, the solvo-surfactants have very high critical concentrations, for which reason we associate them rather a critical aggregation concentration than a critical micelle concentration. SDS, on the other hand, has a low critical concentration, with a sharp break in the adsorption phenomenon, indicating the so-called critical micelle concentration.

The adsorption isotherms of C_5Gly/SDS are shown in **Figure 34** for different molar fractions α_1. Small amounts of SDS in the surfactant mixture induce a strong decrease of the CAC. Indeed, the CAC decreases from 220.0 mM for pure C_5Gly to 41.0 mM for $\alpha_1 = 0.971$. Further decreasing of α_1 to 0.54 approximates the critical concentration (9.2 mM) to that of pure SDS (7.9 mM), with the difference that the surface tension is lower than that of pure SDS (36 mN/m *vs* 39 mN/m). This is desirable for processes like emulsification, solubilisation or surface wetting, where a low surface tension is preferred.

It can be clearly seen in **Figure 34**, how the curves are approximating the adsorption isotherm of SDS with decreasing α_1. This signifies that the system adopts more and more the surface characteristics of SDS, although a huge amount of C_5Gly is still present in the system.

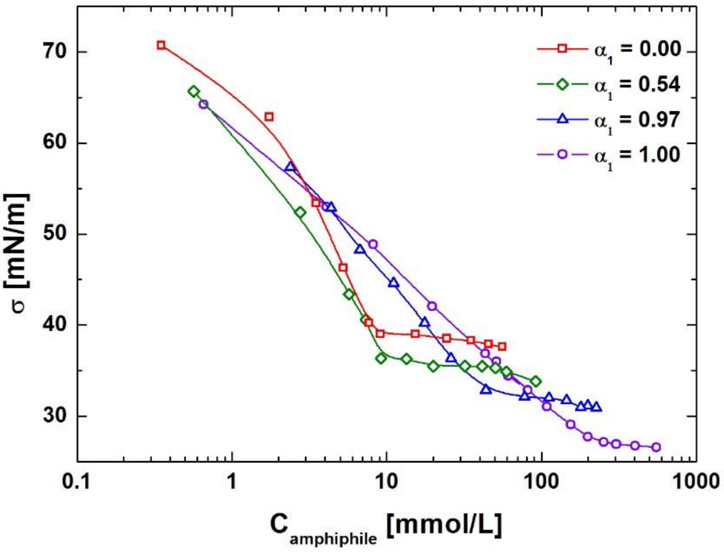

Figure 34 The adsorption isotherms of different molar ratios of C_5Gly (violet) and SDS (red). The increase in SDS results in an increasing surface tension and a lower CAC. In terms of clarity not all measured curves are shown here.

A summary of all critical aggregation concentrations is shown in **Figure 35**, where CAC* is shown in dependence of the molar fraction α_1 of the solvo-surfactant. The dashed lines represent the ideal case, where f =1. Each investigated surfactant mixture shows a non-ideal behaviour. It can be seen that the decline is the strongest for the system SDS/C_5Gly, whereas the systems C_6E_4/SDS and C_6E_3/SDS exhibit a similar development of the curve. With decreasing α_1 values, the curves approximate, since the adsorption behaviour is then rather determined by SDS than by the solvo-surfactant.

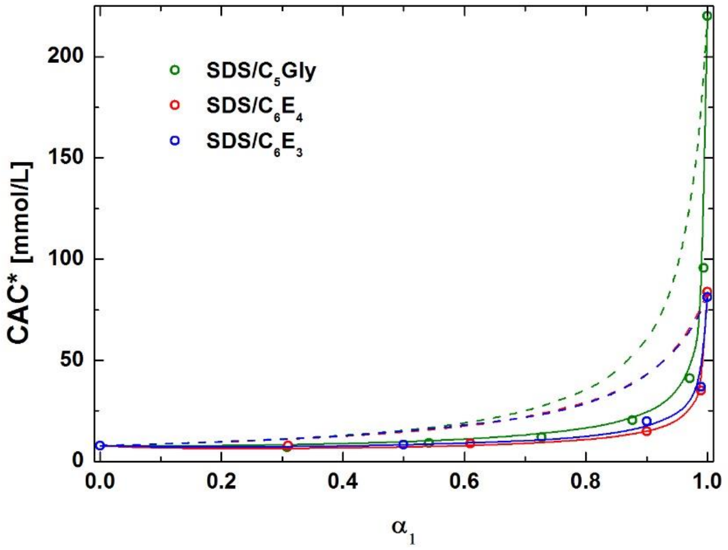

Figure 35 The critical micelle concentration of three binary surfactant systems, in dependence of a. The dashed lines represent the ideal mixing curve, whereas the solid lines represent the best fit, according to the non-ideal mixing theory.

The interaction parameter β, which was obtained by an interactive solution of **Equation 19** and **20**, is -4.2 for the binary surfactant system C_6E_4/SDS, indicating a strong interaction between these two amphiphiles. C_6E_3/SDS has a slightly weaker interaction parameter of -3.7, which may be a result of the lower quantity of ethoxy groups compared to C_6E_4. However Lange and Beck have reported a value of -4.1 for C_8E_6/SDS; -3.9 for $C_{12}E_8$/SDS and -4.3 for $C_{10}E_6$/sodium pentadecylsulfate.[128,130] Rubingh and Holland found a β value of -3.6 for $C_{10}E_4$/SDS and -4.1 for C_8E_4/sodium decyl sulfate respectively.[131] Although chain lengths and number of ethoxy units of the C_iE_j vary between 6-12 and 3-8 respectively, β changes only slightly and remains between -3.6 and -4.2. This indicates that the interaction between SDS and C_iE_j is more affected by the nature of the polar head group of the ionic surfactant rather than by the lengths of the hydrophilic and hydrophobic parts of C_iE_j.

Indeed, the interaction parameter β of C_8E_4 with decyltrimethylammonium bromide is equal to -1.8 which is quite different from the above values.[9] Surprisingly β between SDS and C_5Gly is -4.0, hence the interaction between them is comparable to those of C_iE_j/SDS systems. Although C_5Gly has a higher CAC than C_6E_3 and C_6E_4, in combination with SDS, it shows a comparable aggregation behaviour in aqueous solution as the glycols. At $\alpha_1 = 0.9$, the aggregation concentration can be found for all three binary surfactant systems between 15 – 24 mM, whereas for the pure solvo-surfactant systems, the concentration difference between glycols and glycerol is approximately 140 mM.

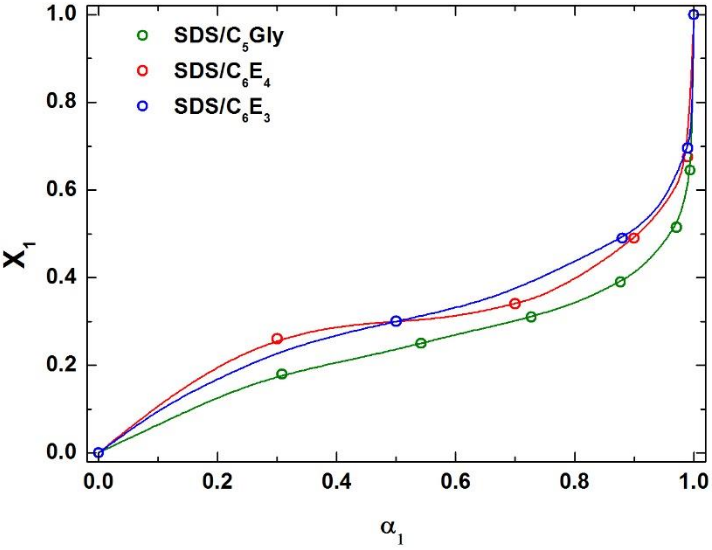

Figure 36 The micellar composition of the binary surfactant system in dependence of α_1. In all three cases the decrease in X_1 is very steep for already small amounts of SDS.

The composition of the mixed micelles can be seen in **Figure 36**. X_1 is the molar fraction of the solvo-surfactant in the micelle. It is obtained by iterative solution of **Equation 20**. Already small amounts of SDS severely decrease the molar fraction of solvo-surfactant in the micelle in all the three cases. This is somehow bizarre, since it can be assumed that solvo-surfactants form rather small aggregates. The ionic surfactant must then according to the findings in **Figure 36** further decrease the size of the micelle. However the inverse is expected. It must be noted that for high concentrations of amphiphile in water, normally the activities should be considered and not the concentrations. Strey *et al.* showed that the break in the adsorption isotherm can disappear, if it is considered that the activity coefficients are not unity.[132] However the authors used ethanol and *n*-propanol, solvents whose amphiphilicity is rather small, and thus the magnitude of concentrations is one order higher than is these cases here. Nevertheless, the evolution of the micellar composition is questionable and must be further investigated with dynamic light scattering experiments, in order to verify the size of the aggregates with and without SDS.

Nevertheless, taking into account the strong decrease of *CAC** with decreasing α_1, it can be concluded that the mixed micellar system resembles already at low SDS content more in its aggregation behaviour to the ionic surfactant than to the solvo-surfactant. It is thus interesting to see how the oil solubilisation characteristics of an aqueous solvo-surfactant solution behaves in the presence of small quantities of ionic surfactant, and if the mixture adopts, as in the case here, already for those little quantities any properties, which are clearly linked to an ionic surfactant (see **Chapter 4**).

2.3.4. The hydrophilic-lipophilic nature of solvo-surfactants, classified according to the PIT-Slope method

a. The PIT-Slope method

The phase behaviour of a ternary non-ionic surfactant/oil/water (SOW) systems is determined by the quantities of the constituents, the applied temperature and pressure, the hydrophilic-lipophilic nature of the surfactant and the hydrophobicity of the oil.[50,133,134] In 1949 Griffin proposed a method to determine, whether a surfactant is more hydrophilic or hydrophobic.[11,12] The so-called hydrophilic-lipophilic balance (HLB) was developed further by Davies[13] in 1957. These methods are based on empirical calculations and are commonly used in industry, but can be inappropriate for complex systems. Lately Ontiveros *et al.* published a more scientific approach and still relatively rapid way to determine the hydrophilic-lipophilic nature of an amphiphile, known as PIT-Slope method.[8] This method uses the reference system $C_{10}E_4$/n-octane/NaCl(aq) with $\delta = 0.01$ M and measures via conductivity under stirring the alterations in the phase inversion temperature (PIT) obtained by addition of a second amphiphile. Thereby several additions are made, and in general the change in PIT is linearly increasing or decreasing. Thereby the molar fraction x_2 of the added amphiphile in the amphiphile mixture is defined as follows:

$$x_2 = \frac{n_2}{n_2 + n_1} \qquad \textbf{(21)}$$

.. where n_2 signifies the molarity of the added amphiphile and n_1 the molarity of reference surfactant $C_{10}E_4$. An amphiphile which increases the PIT, is classified as a hydrophilic amphiphile, with respect to the reference system, whereas a decreasing slope of the curve, classifies the amphiphile as a hydrophobic amphiphile (**Figure 37**).

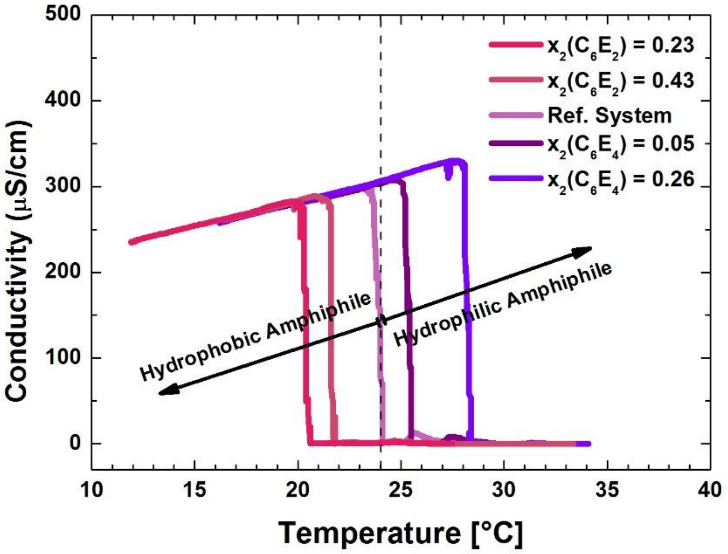

Figure 37 Temperature dependent conductivity profile for some molar fractions of C_6E_4 and C_6E_2. The reference system is marked with a dashed line. Hydrophilic amphiphiles increase the PIT, whereas hydrophobic decrease it.

The drop in conductivity is due to the inversion of the o/w emulsion to a w/o emulsion. Since the salt is dissolved in the water phase, a high conductivity is only obtained if the continuous phase is represented by water. In a w/o emulsion, the water – and thus the salt – is trapped in the micellar core, and thus no free moving ions are available, which may build up a conduction.

The alterations in the PIT depend thereby only on the hydrophilic-lipophilic nature of the second amphiphile, since the reference system is always used with WOR = 1 and 3.0 wt.% $C_{10}E_4$. Its PIT is between 23.9 °C and 24.0 °C, which locates the method in an accessible temperature interval. The PIT can be fitted linearly in dependence of the molar fraction x_2 of the investigated amphiphile in the surfactant mixture. The derivate of the linear equation gives the slope $dPIT/dx_2$ of the curve, which can be used as a measure to classify amphiphiles according to their hydrophilic-lipophilic nature.

In literature this method was already used to classify several pure C_iE_j's, ionic surfactants as well as cosmetic surfactants, such as sucrose esters.[8,45] Commercial surfactant mixtures, where no exact molar mass is known, can be classifies according to *dPIT/dC*, where *C* represents the mass concentration in wt.% of the investigated surfactant in the whole mixture. Furthermore it was used to investigate the influence of linear alcohols and fragrance alcohols on the interface.[62]

b. The $dPIT/dx_2$ value of solvo-surfactants

In this work, the PIT-Slope method is used to determine its applicability to solvo-surfactants, since the high monomeric solubility of these compounds, may have a falsifying effect on $dPIT/dx_2$. In **Table 6** a summary of all investigated amphiphiles can be seen, as well as several C_iE_j's, which were classified by Ontiveros *et al.* Furthermore the influence of triethylene glycol and tetraethylene glycol on the interface was determined.

Table 6 Summary of the *dPIT/dx* of all investigated amphiphiles and (poly)ethylene glycols. 3 wt.% $C_{10}E_4$/*n*-octane/NaCl (aq) δ = 0.01 M was used as the reference system. The values for the 1-alcohols and surfactants were obtained from literature.[8,62]

Compound	Structure	*dPIT/dx₂* [°C]
	Solvo-surfactants & Hydrotropes	
C_3P_1	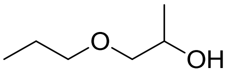	-2.0
C_4P_1	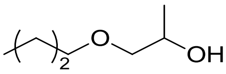	-7.9
C_4E_1	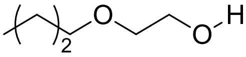	-1.8
C_4E_2	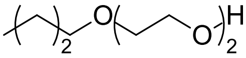	5.1
C_4Gly	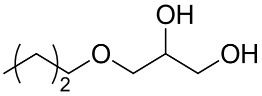	9.6
C_5E_1	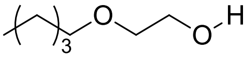	-10.4
C_5E_2	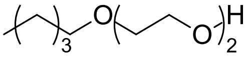	1.6
C_5E_3	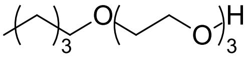	9.8
C_5E_4	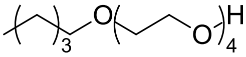	14.2
C_5Gly	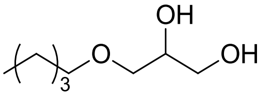	5.5
C_5Iso	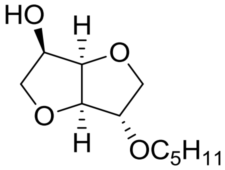	0.5
C_6E_2	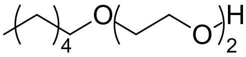	-7.7
C_6E_3	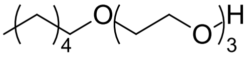	8.8
C_6E_4	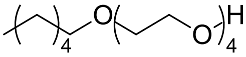	28.4
1,2-C_6-diol	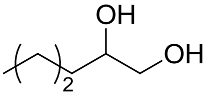	10.0
C_8E_3	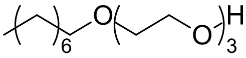	-4.3
1,2-C_8-diol	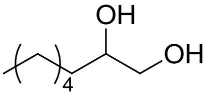	-10.6
iC_8Gly	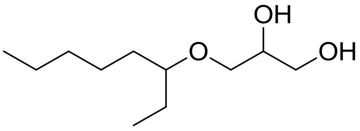	-29.0
	Surfactants	
C_8E_4	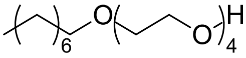	13.8
C_8E_5^{a}	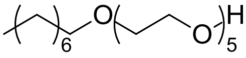	34.0

$C_{10}E_4$[a]	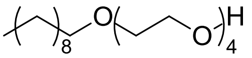	0.0
$C_{10}E_5$[a]		22.0
$C_{12}E_2$[a]		-34
$C_{12}E_3$[a]	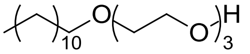	-27
$C_{12}E_4$[a]	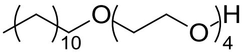	-9.2
$C_{12}E_5$[a]	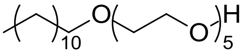	6.8
(Poly)ethylene glycols		
E_3	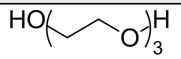	-1.9
E_4	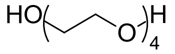	-1.8

[a] see reference [8,62]

In **Figure 38** the evolution of the PIT in dependence of x_2 for amphiphiles with three or four hydrocarbons in the alkyl chain are shown. The influence of the investigated amphiphile is relatively small, especially for C_3P_1, C_4E_1 and C_4E_2. Additionally the diol C_4Gly shows a rather non-linear behaviour.

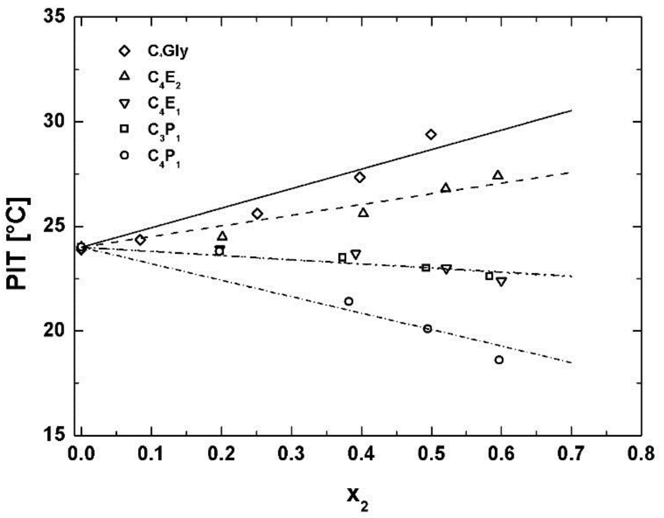

Figure 38 The evolution of the PIT in dependence of the molar fraction x_2 of the investigated amphiphile. In this diagram amphiphiles with three or four hydrocarbons in the alkyl-chain are shown.

This was already observed for alcohols in literature, which resulted in a decrease of the optimum formulation.[23,62] An alcohol can partition between the water phase, the interface or the oil phase, depending on the length of its alkyl-chain. If the alcohol solubilises in the interface, the optimal formulation decreases strongly, until the interface is saturated and further alcohol migrate into the micellar core. Consequently the decline of the optimal temperature, respectively the PIT flattens. In the case of C_4Gly, an inverse behaviour is obtained. In the beginning the increase in PIT is rather low, whereas at higher x_2 it starts to increase exponentially. This may happen, if the amphiphile is highly soluble in the water and/or oil phase, which in turn results in a low concentration of the amphiphile in the interface in the beginning. With increasing x_2, the oil and/or water phase becomes saturated and the amphiphile migrates to the interface, which results in a stronger increase of the PIT.

Amphiphiles with five hydrocarbons in the alkyl chain, are shown in **Figure 39**. Compared to **Figure 38**, the fitted curves are stronger scattered towards higher and lower phase inversion temperatures, which can be attributed to the stronger amphiphility of C_5-amphiphiles.

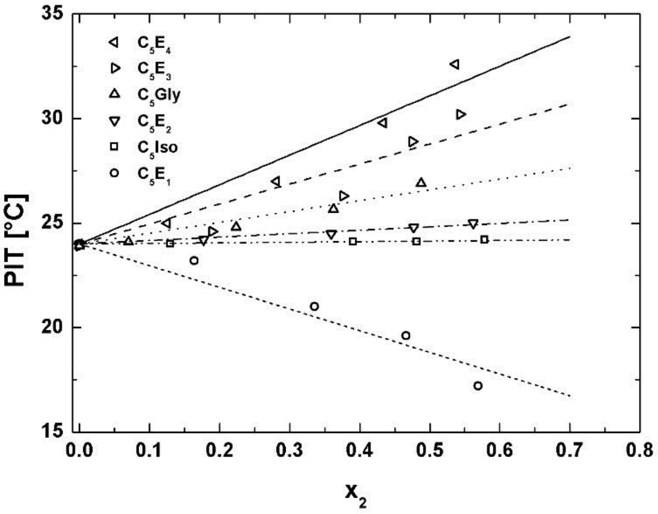

Figure 39 The evolution of PIT in dependence of the molar fraction x_2 of the investigated amphiphile. In this diagram amphiphiles with five hydrocarbons in the alkyl-chain are shown.

C_5E_4 and C_5E_1 have a quite non-linear behaviour, which may have been caused by their high monomeric solubility in the water and/or oil phase. As in the case of C_4Gly, they first start to solubilise predominantly in the interfacial layer, when the water and oil phase is saturated with monomerically solubilised amphiphile. However it is striking, that a distinct non-linearity is not obtained for C_5E_2, C_5Gly etc. Probably this can be explained with an amphiphility, which is close to the one of the reference system. Even if the amphiphile starts to solubilise predominantly in the interface, the effect on the curvature of the aggregates is rather small, which in turn results in no or a smaller deviation from linearity.

Figure 40 presents the results obtained with C_6-amphiphiles, such as C_6E_4 or 1,2-hexanediol. In general the PIT alterations upon increase in amphiphile molar fraction behave linearly, with one exception. The diol shows a non-linear increase due to same reasons as stated above. Compared to its smaller homologue from **Figure 39**, C_6E_4 has a linear relationship between x_2 and PIT. It can be thus considered that the monomeric solubility of C_6E_4 is much lower compared to C_5E_4, and the amphiphile starts to migrate much earlier predominantly into the interfacial layer. In **Section 2.3.2.a.** a critical aggregation concentration of 84 mM for C_6E_4 was obtained, whereas 264 mM for C_5E_4, indicating the strong difference in their monomeric solubility.

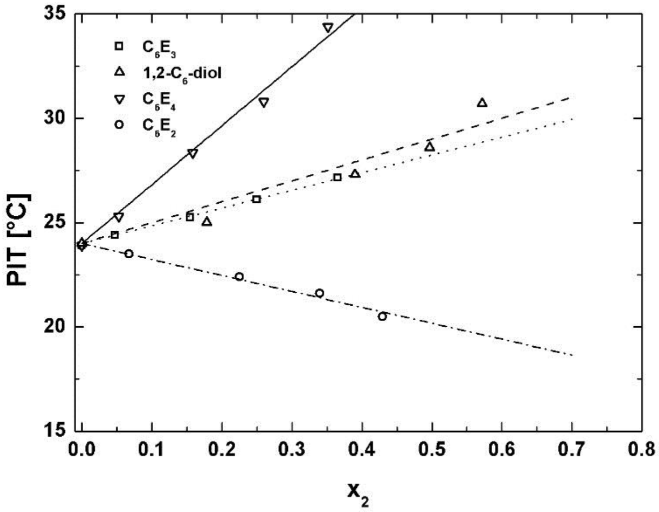

Figure 40 The evolution of PIT in dependence of the molar fraction *x₂* of the investigated amphiphile. In this diagram amphiphiles with six hydrocarbons in the alkyl-chain are shown.

In **Figure 41** the evolution of the PIT for C_8-amphiphiles is shown. Again a linear behaviour can be obtained for the glycol amphiphiles, whereas the diols, 1,2-octanediol and ethylhexyl glycerol show a non-linear behaviour, which can be attributed to same reason as previously described. Furthermore the curves are scattered over a bigger temperature interval, which can be attributed to their stronger amphiphility, due to a longer hydrocarbon chain.

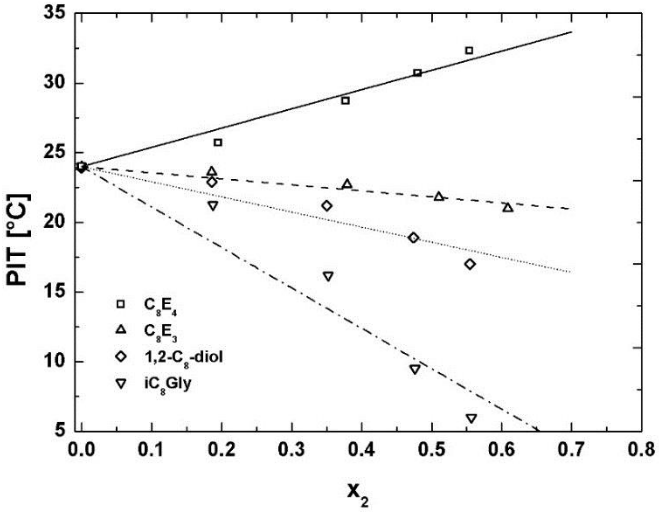

Figure 41 The evolution of PIT in dependence of the molar fraction *x₂* of the investigated amphiphile. In this diagram amphiphiles with eight hydrocarbons in the alkyl-chain are shown.

In can be concluded that the PIT–Slope method is applicable for amphiphiles with an alkyl carbon chain of six and higher. Shorter amphiphiles have an elevated monomeric solubility in the water and oil phase, which results in a non-linear dependence of the PIT from x_2 for very hydrophilic or hydrophobic amphiphiles. Those with a moderate preference for either water or oil, induce only slight changes to the reference system. Such behaviour may appear either because the amphiphile's hydrophilic-lipophilic nature is close to the one of $C_{10}E_4$, or because the amphiphile has an extremely elevated monomeric solubility in water and/or oil. Consequently the PIT Slope method may lead to misinterpretations concerning very short chain amphiphiles and shall only be used for those with an alkyl chain of six and higher. Furthermore diols turned out to behave nonlinearly, which makes their values highly questionable, since their slope depends strongly from the last measured point.

c. Influence of the monomeric solubility of the amphiphile on *dPIT/dx₂*

The influence of the monomeric solubility on the mass fraction of amphiphile at the interface is particular important for small quantities of $C_{10}E_4$, since all amphiphile may solubilise in the water and oil phase, before it can even act at the interface. If the mass concentration of $C_{10}E_4$ is increased to 7 wt.%, more of the second amphiphile has to be added, compared to the case with only 3 wt.% $C_{10}E_4$. However the amount of monomerically solubilised amphiphile remains the same. Consequently in the case of high monomeric solubility, different $dPIT/dx_2$ values are obtained for 3 and 7 wt.% $C_{10}E_4$. Thus it can be evaluated if the monomeric solubility of the amphiphile is too elevated to give a $dPIT/dx_2$ value which is independent of $C_{10}E_4$ mass concentration. In **Figure 42** the solvo-surfactants C_4Gly, C_5Gly and C_6E_4 were investigated with the reference system at 3.0 and 7.0 wt.% $C_{10}E_4$. Furthermore their $dPIT/dx_2$ values are summarized in **Table 7**.

Table 7 ***dPIT/dx₂*** **values for C_4Gly, C_5Gly and C_6E_4, obtained in the reference system with 3.0 and 7.0 wt.% $C_{10}E_4$.**

$dPIT/dx_2$ [°C]	C_4Gly	C_5Gly	C_6E_4
3.0 wt.% $C_{10}E_4$	8.1	5.5	28.4
7.0 wt.% $C_{10}E_4$	17.6	9.6	30.5

It can be seen that there is a huge difference in the slope for the two curves of C_4Gly (8.1 *vs* 17.6). C_5Gly shows as well a considerable deviation between the two measurements (5.5 *vs* 9.6), whereas the measurements made with C_6E_4 gave almost congruent results. The reference systems consists of a water and oil phase, as well as of an interface, wherein the second amphiphile can be solubilized. The glycerols have a high CAC, which indicates, that a high amount of them is solubilsed in water. At 7 wt.% $C_{10}E_4$, the amount of added glycerols is bigger, whereas the monomerically solubilised quantity of C_4Gly, respectively C_5Gly remains constant. Thus more amphiphile is at interface, which in turn results in a bigger change of the PIT and consequently in a different $dPIT/dx_2$ value. Despite the also relatively high CAC of C_6E_4, it solubilizes preferably in the interface, since in both cases $dPIT/dx_2$ is approximately the same (28.4 *vs* 30.5). Consequently small short-chain amphiphiles of the type C_iGly ($i \leq 5$) impose a concentration dependency onto the PIT-Slope method.

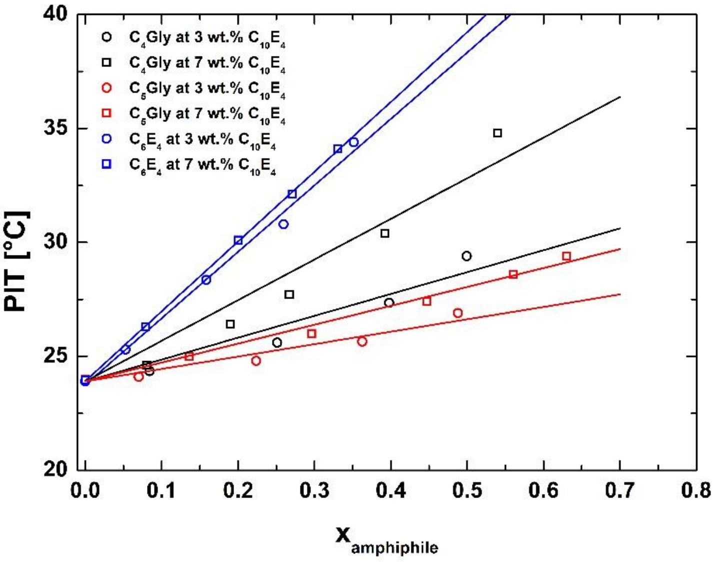

Figure 42 The PIT Slope method applied to C_4Gly, C_5Gly and C_6E_4 at 3.0 and 7.0 wt.% $C_{10}E_4$. There is a non-negligible difference between their curves for C_4Gly and C_5Gly, whereas C_6E_4 gave quite convenient results.

It is also expected that the monomeric solubility of other amphiphiles, such as glycols and isosorbides with i ≤ 5 is too elevated. Unlike 1-O-monoalkyl-glycerols, these compounds possess usually a cloud point between 0 – 100 °C. Thus their T_β can be compared with *$dPIT/dx_2$*, in order to verify if C_5-amphiphiles deviate from long-chain amphiphiles. In **Figure 43**, *$dPIT/dx_2$* is shown in dependence of the critical temperature T_β for several amphiphiles, mainly C_iE_j's. Shinoda already showed that the PIT of SOW systems is related to the critical temperature T_β of poly(ethylene) glycol ethers.[6]

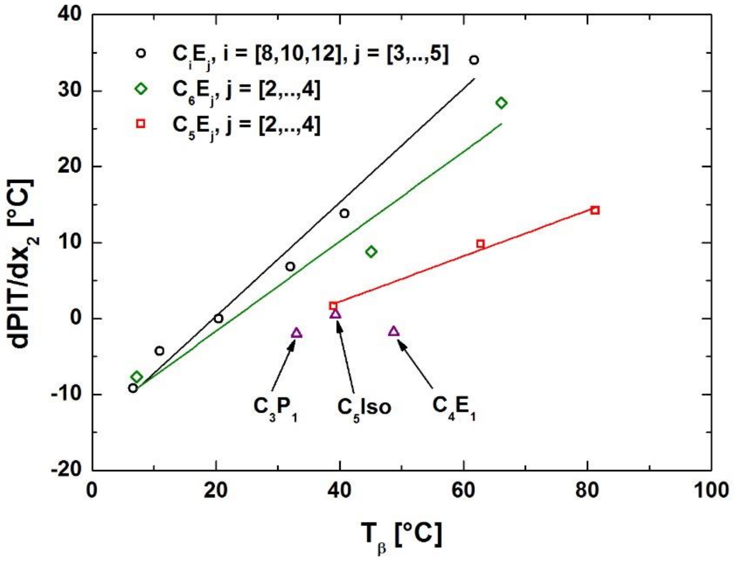

Figure 43 The dependence of *$dPIT/dx_2$* from the critical temperature T_β. While C_6E_j deviates only slightly from long-chain surfactants, the C_5-amphiphiles deviate strongly. Furthermore the highly monomeric soluble compounds C_3P_1, C_5Iso and C_4E_1 have independent of their structure, barely an effect on the interface.

Furthermore Ontiveros *et al.* stated that there is a linear relationship between the critical temperature and *dPIT/dx*$_2$ for long-chain C_iE_j's.[8] This is not completely valid for solvo-surfactants. It can be seen that the C_6E_j's are slightly dislocated from the C_iE_j's with 8,10 or 12 hydrocarbons in the alkyl chain. They have still a quite high CAC, and compared to the C_iE_j's with $i \geq 8$, there is probably still a not negligible amount of amphiphile solubilised in the water and/or oil phase. However the C_5E_j's deviate even stronger, which can be attributed to the loss of monomerically solubilised amphiphile. With regards to the previous results concerning alkylglycerols, it can be concluded that short-chain amphiphiles, with $i \leq 5$ solubilise rather in the oil and water phase, until saturation. This explains the strong deviation of C_5E_j's from the black curve. In this context it is not surprisingly that the highly oil and water soluble amphiphiles C_3P_1, C_5Iso as well as C_4E_1 have almost no influence on the interface.

d. The dependency of *dPIT/dx*$_2$ from carbon chain length *i* and ethoxy group number *j*

The here obtained results are combined with those from literature[8,62,135], in order to evaluate the dependence of *dPIT/dx*$_2$ from the carbon chain length and ethoxy group number of several (poly)ethylene glycol monoalkylethers. In this context 1-alcohols can be seen as homologues without any ethoxy group and are thus abbreviated as C_iE_0 in **Figure 44**. Furthermore the influence of triethylene glycol (E_3) and tetraethylene glycol (E_4) on the interface was determined. It can be seen that the influence of the amphiphile on the interface in the $C_{10}E_4$/*n*-octane/NaCl(aq) system is increasing with augmenting carbon chain length i, independent of the number of ethoxy groups. Each series of amphiphiles contains a maximum, which represents the biggest hydrophilic influence on the interface for these types of molecules. Thereby the strength of this effect increases as follows:

$$\mathbf{C_2E_0 < (C_3E_1) < C_4E_2 < C_5E_3 < C_6E_4 < (C_7E_5)}$$

C_3E_1 and C_7E_5 are in parenthesis, since their values were not measured. However following the progression of the curves, it can be concluded that they position according to that order. In general the smaller the hydrocarbon chain, the more hydrophilic is the compound. Very short-chained amphiphiles are found predominantly in the water phase and not at the interface. With increasing i, the amphiphile starts to penetrate into the interface and depending on the number of ethoxy groups, it has a curvature increasing or decreasing effect. Alcohols have a very small head group and thus decrease the curvature strongly, which in turn results in an early and small maximum for ethanol and consequently in a steep decrease of *dPIT/dx*$_2$ for $i \geq 3$. With increasing number of ethoxy groups, the head group is augmenting in size, which in turn has an augmenting effect on the curvature and consequently *dPIT/dx*$_2$ increases. The influence of the amphiphile on the interfacial layer is thus an interplay of the length of the hydrophilic and hydrophobic group. In general it can be summarized that small amphiphiles have barely an effect on the interface, independent of their structure, whereas big amphiphiles may decrease or increase *dPIT/dx*$_2$ strongly. The obtained maximum for C_6E_4 is remarkable, since it is particularly different from the adjacent C_5E_4. Considering C_6E_3 and C_5E_3, where the difference is marginal, the addition of one carbon to the alkyl chain of C_5E_4 promotes a strong migration of the amphiphile to the interface, which in turn has a remarkable curvature increasing effect. Consequently, of all here investigated solvo-surfactants, C_6E_4 is the most hydrophilic and thus very interesting for the solubilisation of fragrances. The latter are usually very polar hydrophobic compounds, which decrease the optimum formulation towards low temperatures. Hence a hydrophilic amphiphile is able to counteract this tendency, by increasing the optimal temperature.

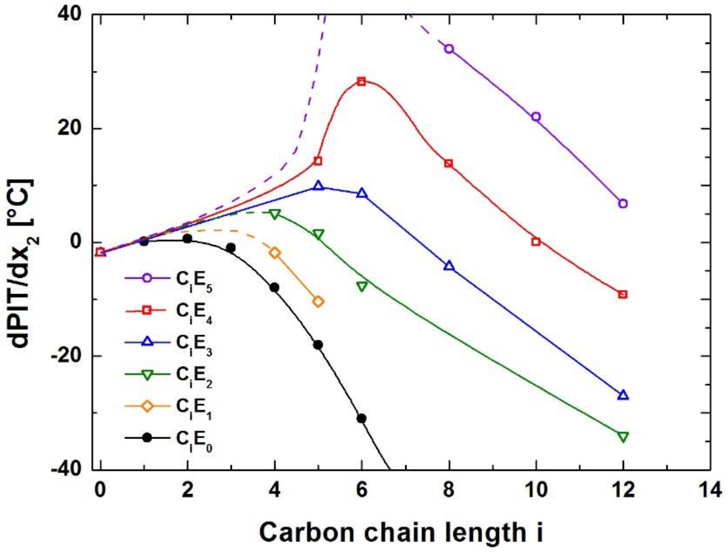

Figure 44 The evolution of *dPIT/dx₂* in dependence of the carbon chain length i. With increasing i, the curves undergo a maximum, which is particularly distinct for C_iE_4.

e. The PIT of C_6E_4/eucalyptol/water

In this context a fish cut of the system C_6E_4/eucalyptol/water was constructed and its PIT was determined by conductivity measurements. Eucalyptol is a fragrance which contains an inter-cyclic ether functionality. Consequently it is very polar compared to usual alkane oils, and in order to obtain a three-phase region, a very hydrophilic amphiphile has to be chosen. As in the previous conductivity measurements, 0.01 M NaCl was present in the aqueous phase, and the PIT was measured after each addition of C_6E_4. The phase diagram was constructed without NaCl. It is assumed that small quantities of salt have barely an effect on the phase behaviour of non-ionic C_iE_j amphiphiles. In **Figure 45**, the fish cut and the results from the conductivity measurement can be seen. The PIT curve lies within the three-phase body of the equilibrated system and it depends barely from the mass fraction γ of the amphiphile in the mixture. The green curve represents simultaneously the optimal formulation of the system, at which the amphiphile has same affinity for both, the oil and the water phase.

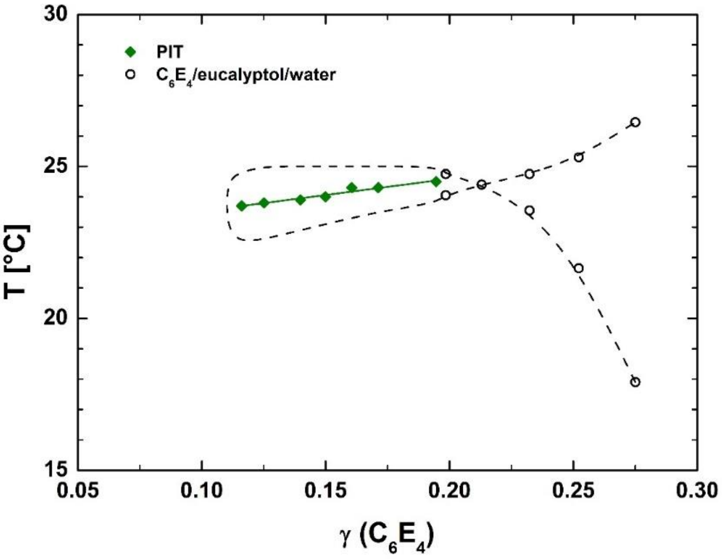

Figure 45 Fish cut of the system C_6E_4/eucalyptol/water and the PIT curve obtained from conductivity. Note that for the conductivity measurements, the aqueous phase contained 0.01 M of NaCl.

2.4. Solvent properties of the solvo-surfactants

In this section the solvent properties of solvo-surfactants are investigated. Thereby the volatility of these amphiphiles are studied as well as their olfactory properties.

2.4.1. Volatility of solvo-surfactants

The volatility of a surfactant can be of great importance for many consumer or industrial products, since for certain applications it is necessary that no residues are left, *e.g.* perfumes, hard surface cleaning. However the European Union desires to reduce the emission of volatile organic compounds (VOCs), since it can be harmful for public health and contributes to the local and trans boundary formation of photochemical oxidants in the boundary layer of the troposphere.[136] In the Council Directive 1999/13/EC, the European Union defined a volatile organic compound as an organic compound, which has at 293.15 K a vapour pressure of 0.01 kPa and more, or which has a corresponding volatility under the particular conditions of use. Thereby the European Union discussed also the possibility of reducing or substituting potential harmful chemicals by partially less harmful chemicals.

In the field of fine perfumery, ethanol, which is used as the principal solvent for fragrance solubilisation, falls under this regulation. Although it has no negative effect on the environment, effects on the human health have been observed. In a world where more and more chemicals are used in the products which surround our everyday live, people with negative reaction to those are steadily increasing. One illness which describes these reactions to inhaled chemicals, is the sensory hyperreactivity (SHR)[137], a syndrome which results in cough, breathing difficulty, phlegm, rhinorrhoea and thus in an impaired quality of life.[138] It is kind of impossible to avoid the inhalation of chemicals in everyday life. Especially in bureaus, which are meant to be clean places, the accumulation of chemicals in the air can rapidly increase in bad ventilated rooms. Millqvist *et al.* showed that the reaction of patients with SHR to the provocation with capsaicin is increased in the presence of ethanol, suggesting that the combination of ethanol and perfumes may augment an airway reaction in these individuals.[139] Furthermore, ethanol is known to cause irritations and skin drying.[140] The application of a perfume directly on the skin can thus be harmful for the skin, resulting in redness and itching. Throughout the internet, it is therefore advised to apply perfumes on clothes or the hair, which can nevertheless not avoid that the airy dispersion gets in contact with the skin.

Within this context and because it is expected to be a property of our solvo-surfactants, the volatility of several compounds have been investigated by thermo gravimetric analysis (TGA) with a TA Instruments TGA Q50 apparatus. Thereby the $T_{50\%}$ value was defined, which describes the temperature at which 50 wt.% of the initial mass is evaporated. This $T_{50\%}$ value correlates very well with the boiling point, as it can be seen in **Figure 46** for 1-alkohols. Since the thermo gravimetric analysis is a rapid and precise method, it was used in this work to discuss the volatility of short-chain amphiphiles.

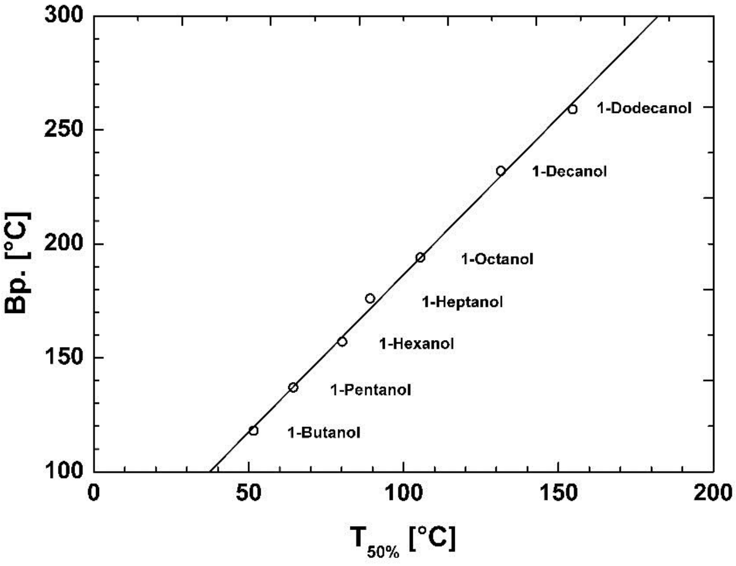

Figure 46 The boiling point of 1-alcohols in dependence of the $T_{50\%}$ value. There is a perfect linear relationship between both.

The thermo gravimetric profiles of 29 amphiphilic compounds were then measured and their temperature $T_{50\%}$, was determined and compared to dimethyl isosorbide (DMI). This solvent has been chosen as a reference since it is known that DMI is closely located to the VOC limit[141] (b.p. = 236°C and P_{vap} = 4.1 Pa at 25°C). In **Figure 47** the thermo gravimetric profile of several compounds can be seen. The $T_{50\%}$ value of C_4Gly is lower than the one of DMI, whereas all the other compounds have higher values. In perfumery, volatility is most important, however triethyl citrate, which has a $T_{50\%}$ value above DMI (180 °C *vs* 140 °C) is frequently used as a solvent.[142–144] At the same time it is not classified as a VOC and thus it is not touched by EU regulations. Amphiphiles which bear a volatility between DMI and triethyl citrate are thus very interesting for water-based perfumes or any other water-based applications, such as cleansers since they are not classified as VOC and show comparable volatility characteristics to other compounds which are used in perfumery. In order to distinguish them from non-VOCs and underline their particular interest for application, we denominate them here as **Semi-Volatile Organic Compounds** (SVOCs). Thereby, the maximum border is no fixed value. In fact, the value orientates on the volatility of solvents which are frequently and to a greater extend used in products, where evaporation is a key property, *i.e.* perfumes, hard surface cleansers. The border set by triethyl citrate represents thus the lowest acceptable volatility, which we have found according to the solvents used in industry and may represent the maximum, or at least a value close to the maximum.

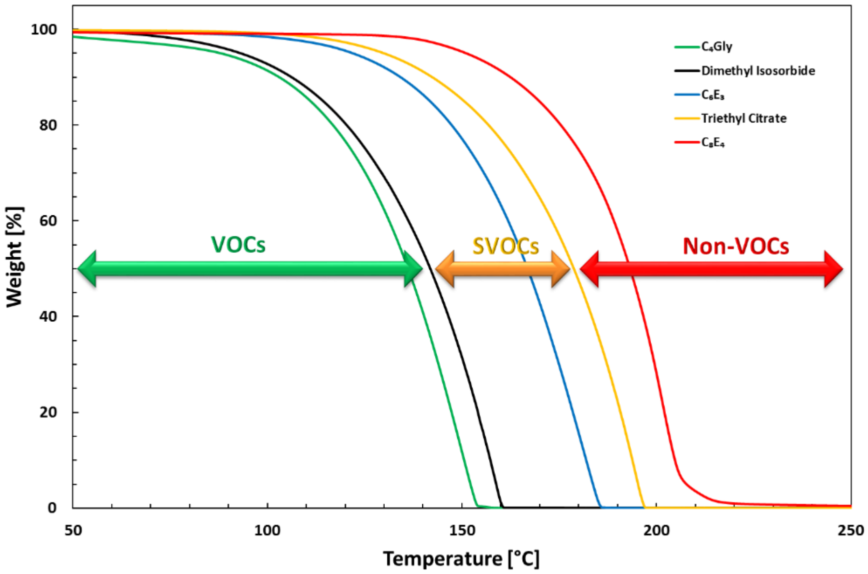

Figure 47 Thermo gravimetric analysis of several compounds and classification into volatile organic compound (VOC), semi-volatile organic compound (SVOC) and non-volatile organic compound (Non-VOC).

In **Figure 48**, the $T_{50\%}$-value is shown against the carbon chain length i. Several short-chain glycol ethers, alkyl glycerols, alkyl isosorbides as well as linear alcohols and 1,2-alkanediols were investigated.

The increase in $T_{50\%}$ with increasing carbon chain for a sequence of molecules is the result of augmenting van-der-Waals interactions between the alkane chains. The lowest values relative to its chain length are obtained for alcohols, which is understandable, since they contain only one hydroxyl group to undergo strong acceptor-donor interactions with each other. With increasing ethoxy number, $T_{50\%}$ increases as well. The highest values relative to the carbon chain length are obtained for the monoalkyle isosorbides. A general order can be obtained $\mathbf{C_iE_0 < C_iE_1 \approx C_iP_1 < C_iE_2 \approx C_i\text{-diol} < C_iE_3 < C_iGly < C_iE_4Me < C_iE_4 < C_iIso}$. The order roughly follows the molecular weight of the compound. Furthermore it can be generalised that the more oxygen atoms in the compound, the higher $T_{50\%}$. This can be explained by the strong hydrogen bond acceptor-donor interactions between the molecules. Thereby hydroxyl groups undergo stronger interactions than ethers, which can be seen by comparing the results of C_iE_4Me and C_iE_4. The methylated tetraethylene glycol monoalkyl ethers loose a hydrogen, which could otherwise serve as a hydrogen bond donor.

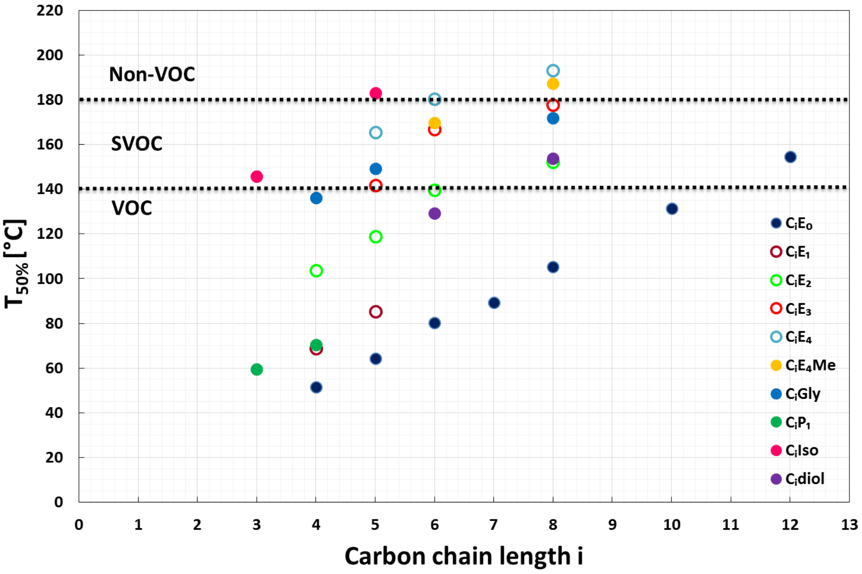

Figure 48 $T_{50\%}$ **in dependence of the carbon chain length i. The dashed lines separate the Non-VOCs from the SVOCs and the SVOCs from the VOCs.**

The thermo gravimetric results of all investigated compounds are summarised in **Table 8** and according to their $T_{50\%}$ value they are classified in either VOC, SVOC or Non-VOC. Furthermore the solubiliser LRI was used as a reference system, since it is used in industry to create water-based perfumes.[145,146] It is an aqueous dispersion of the polymer PPG-26 buteth-26 and the surfactant PEG-40 hydrogenated castor oil. The results from the thermo gravimetric analysis showed that there was virtual no evaporation and the slight changes can be attributed to the small amount of water in the mixture.

2.4.2. Sensorial analysis of solvo-surfactants

Whether in food, cosmetics or in fine perfumery, determining the sensorial properties of the final product is essential. Otherwise there will be little input about the quality of the product with regards to the end consumer's opinion. Therefore a proper sensorial analysis is very important to validate a product. Sensory tests exist for as long as there have been human beings evaluating the quality of food, water and other consumer products. However scientists have only recently developed sensory testing as a formalised and structured methodology, which yields reproducible results. The interest in developing methods of sensorial analysis is clearly economical driven, since the testing can validate the acceptability of a certain product by the end consumer. Therefore a sensorial analysis should provide reliable data on which thorough decisions can be made.[147] Unlike the measurement of physical properties of a sample, where devices based on physics and mathematics are used as a measurement instrument, panellists are used to evaluate a sample during a sensorial analysis. Testers vary over time, are very variable among themselves as well as they are highly prone to bias. In order to reduce these sources of error, the sensory analysis has to follow some general rules.[147,148]

Table 8 $T_{50\%}$-values of several amphiphilic compounds and classification into VOC, SVOC and Non-VOC according to the previously made considerations.

Compound	$T_{50\%}$ [°C]	Molar Mass [g/mol]	VOC / SVOC / Non-VOC
C_4E_0	52	74.12	VOC
C_5E_0	54	88.15	VOC
C_6E_0	80	102.18	VOC
C_7E_0	89	116.21	VOC
C_8E_0	105	130.24	VOC
$C_{10}E_0$	131	158.28	VOC
$C_{12}E_0$	155	186.28	SVOC
C_4E_1	69	118.17	VOC
C_5E_1	85	132.20	VOC
C_4E_2	104	162.23	VOC
C_5E_2	119	176.25	VOC
C_6E_2	140	190.28	SVOC
C_8E_2	152	218.33	SVOC
C_5E_3	142	220.31	SVOC
C_6E_3	167	234.33	SVOC
C_8E_3	178	262.21	SVOC
C_5E_4	166	264.37	SVOC
C_6E_4	180	278.39	SVOC
C_8E_4	193	306.09	Non-VOC
C_6E_4Me	170	292.41	SVOC
C_8E_4Me	187	320.11	Non-VOC
C_4Gly	136	148.20	VOC
C_5Gly	149	162.23	SVOC
iC_8Gly	172	204.31	SVOC
C_3P_1	59	118.17	VOC
C4P_1	70	132.20	VOC
C_3Iso	146	188.22	SVOC
C_5Iso	183	216.27	Non-VOC
C_6-diol	129	118.17	VOC
C_8-diol	154	146.23	SVOC
LRI	>300	-	Non-VOC

1) The definition of the problem must be as precise as possible so that the panellist understands what he has to do.
2) The test design must leave no room for subjectivity and bias. Coloured samples may influence the evaluation of the panellist. Furthermore the tester shall not be influenced by the surrounding setting and the testing time has to be minimized, especially in olfactory tests, where the receptors can saturate over time.
3) Test subjects must be selected and trained in order to give reproducible results.
4) The results must be interpreted statistically correct. A duplicate helps to separate the reproducible from the non-reproducible panellists.

Following these rules, a proper analysis shall be performed with enough panellists (20-50) in a spacious neutral room under calm conditions. The samples shall be tested randomly and the quantity shall be minimised. Furthermore the testers are not allowed to interchange with each other throughout the project.[149]

The process of sensory testing is seen as a one-step process, where the panellists evaluate the sample directly after stimulus. In fact there are three steps implicated in this process.[150] First the sense organ is stimulated by the sample, which transforms it into a nerve signal, which travels through the nerve system to the brain. There the tester interprets the signal by considering previous experiences which are stored in the brain, and eventually converts the information in perception. The evaluation process is then finished when the panellists formulates a response based on this perception. In the case of a sensory analysis which is based on the evaluation of odours, a good working olfactory system is necessary.

a. The olfactory system

The olfactory organ is located in the nasal mucous membrane which is covering the nasal cavity (**Figure 49**). It consists of tiny hair-like projections (cilia), constituted of 6 - 10 million olfactory cells.[151] The odour molecules are aspirated through the nose and dissolve in the nasal mucosa (wherein the olfactory epithelium is located), exciting cilia. Their membrane is composed of many different sensory neurons, which consist of seven helix transmembrane proteins and which are able to recognize a huge variety of odorants. An electrical signal is triggered then, causing a series of chemical and electrical reactions, which transmits the information via the olfactory bulb and nerve to the temporal lobe of the brain, where they are decoded by approximately 1000 genes.[152] The stimulation of the receptor depends strongly on the volatility of the compound, which is proportional to the concentration of the odour and thus the signal which is transmitted, as well as on the structure of the molecule. Today it is known that a human being can distinguish up to 10 000 odours[153] with his olfactory receptor cells. Nevertheless the relation “one receptor = one odour” cannot be applied, since the way the olfactory system is able to discriminate odours is much more elaborated.[151]

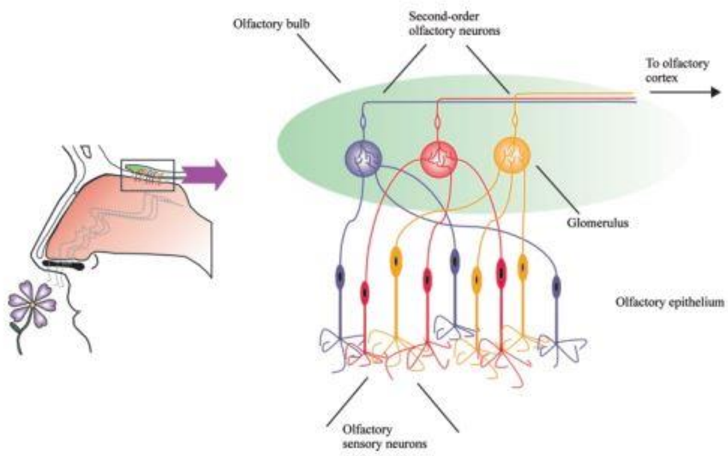

Figure 49 The location of the olfactory system in the nasal cavity. The olfactory receptors are located in the olfactory epithelium. A stimulus is conversed into a signal and send via the olfactory bulb to the cortex.[152]

Olfactory receptors are part of the family of G protein-coupled receptors (GPCR).[154] These receptors are traversing the membrane seven times, each representing one domain of the receptor (**Figure 50**). The three central transmembrane domains vary from one receptor to the other, while the four other domains are conserved in all family members of the GPCR's. So in the central area of the receptor lies the diversity of olfactory receptors that allow the detection of so many odours. Indeed, studies in the structure of the three variable domains suggest that they are positioned to form a cavity in which odour molecules are accommodated. Thus any change in the central area will produce a different cavity to adapt to a different odorant molecule.[155]

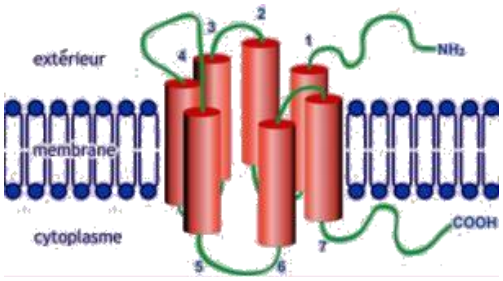

Figure 50 Schematically representation of a G protein-coupled receptor (GPCR). The membrane is traversed 7 times, forming a cavity with various binding sites.[155]

In addition, the sensitivity of an olfactory receptor is not limited to the mere receipt of a given geometry within its cavity. The detection of odours can be seen as a key-lock system (**Figure 51**). However this system stays fairly flexible, that is a lock can accept several keys and a key can activate several locks. Thus a fragrant molecule cannot be associated with a single odorant receptor. Indeed, the identification of an odour by the organism is a stimulus which is based on the specific combination of the signals transmitted by the receptors which were activated by the molecule.[156]

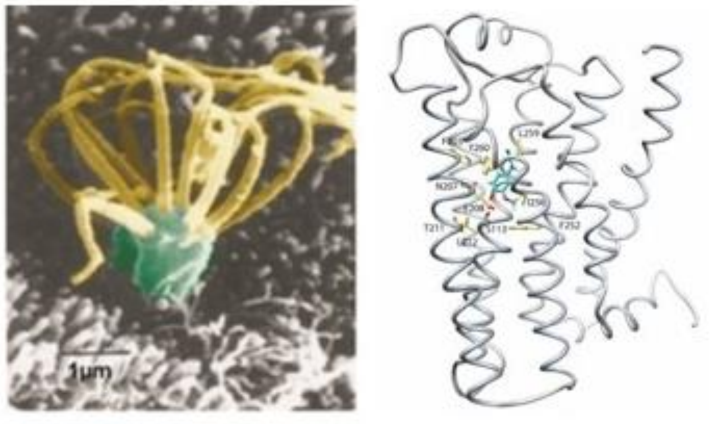

Figure 51 Left: Electro-microscopic picture of an olfactory cell with dendrite (green) and cilia (yellow).[157] Right: Modelling of eugenol in the cavity of an olfactory GPCR.[158] The perfume molecule arranges according to the binding sites of the receptor, like a "key" in a "lock".

It can be considered that the intensity and the pleasantness of an odour depends strongly on the interaction of the odorant at the binding sites of the cavity. The complexity of these kind of processes lead to the development of modelling software which describes the interaction and binding sites between a receptor and a perfume molecule, though there is no general pattern which allows the attribution of a type of scent to a type of molecule structure. In the group of Rodrigues *et al.* group contribution methods have been applied to predict odour intensities of perfume mixtures.[159] Depending on the model (UNIFAC, ASOG, UNIFAC Dortmund, A-UNIFAC), average relative deviations of 24 – 35% from experimental values were obtained. Quite remarkable, if it is pointed out, that the experimental results were determined by sensorial testing with human beings. Another model was developed by Chastrette and De Sainte Laumer *et al.* for the prediction of the musk odour of nitrobenzene derivatives with 77% correctness. However up to this date, despite intensive research on structure-odour relationships, the prediction of an odour remains statistical exercise and models only provide a probability of the character, threshold and intensity. Moreover recent advances in the understanding of the olfactory mechanism suggest that the ability to predict odour properties will not improve significantly in the near future.[160] Thus the procedure of sensorial testing stays until now the only reproducible method to determine the odour of a molecule.

b. Procedure

Considering the results from the thermo gravimetric analysis, several VOCs and SVOCs were chosen for a sensorial analysis in order to verify their odour intensity and pleasantness with panellists. Furthermore they were asked to evaluate several descriptors, which describe the odour of the solvo-surfactant. For the sensory testing, 10 amphiphilic compounds were chosen, 9 solvo-surfactants (C_4E_2, C_5E_4, C_6E_2, C_6E_3, C_6E_4, C_8E_3, C_4Gly, C_5Gly, 1,2-hexanediol,) and LRI, a non-VOC which is used in industry for the solubilisation of fragrances. 10 wt.% of each compound was solubilised in water, in order to test their odour characteristics. Initially a small group of ten persons was asked to describe the smell of each sample. Out of all propositions eight descriptors were chosen, which were mentioned the most frequently by the panellists and which attribute either a pleasant, neutral or unpleasant odour to the amphiphile. The pleasant descriptors are fruity, flowery and woody, whereas the notes acrid, rancid and greasy are defined as unpleasant descriptors. The two remaining descriptors "acid" and "solvent" are assigned as neutral, since depending on the panellist, these notes of a solvo-surfactant were attributed to a pleasant or unpleasant odour. The proper sensorial analysis was performed two weeks later on two different days, with one day gap in between. 12 samples were prepared, thereof 2 which represent a duplicate. On day one 30 panellists were asked to indicate the intensity of each sample. Two panellists at once were requested into the study room. Two set of samples were prepared on a big table and the panellists were separated by a screen, in order to guarantee that they do not influence each other. Each participant evaluated 5 samples, thereof one duplicate and indicated the intensity between 0 - for no intensity - and 10 - for strong intensity - on a questionnaire. It was explained to the panellists that the intensity shall be evaluated independent of the pleasantness of an odour. The order of the samples was random and comparison between the samples was allowed. In the end each samples was evaluated 12 times. On the second day, same procedure was applied. Again 30 panellists were asked to evaluate the same samples, but this time the odour should be evaluated according to a pleasant or unpleasant perception. Thereby 10 signifies very pleasant and 0 very unpleasant. Since the initial impression was of importance, comparison was not allowed. Afterwards in a second part, the panellists had to evaluate the intensity of the 8 descriptors which were previously determined for the same samples they had previously sensed. As on day one, the evaluation was performed between 0 and 10. Since the intensity had to be noted with respect to each sample, comparison was again allowed.

c. The odour intensity and pleasantness verified by panellists

In **Figure 52** the odour intensity is mapped against $T_{50\%}$. The diagram is divided in four parts. On the left hand side the compounds with low odour intensity are shown, whereas compounds with a strong odour intensity are shown on the right. Furthermore it is distinguished between SVOCs and VOCs. In general it is expected that a smaller $T_{50\%}$-value results in a stronger odour intensity. If the compounds are compared according to a diagonal, the location of C_4Gly is remarkable, since it is much less intense in his odour smell than expected according to its volatility. Same happens for C_5Gly, but in the other direction. Its odour intensity is much bigger than expected. A big gap is as well observed for C_6E_2. However the slope of the diagonal is set arbitrate, since the highest and lowest intensity values cannot be attributed to a clear $T_{50\%}$-value. Nevertheless it can be seen, that there is a remarkable difference between the two glycerol derivatives, which cannot be explained by their mass difference. LRI has a $T_{50\%}$-value above 300 °C. However an intensity value of 3.5 could be allocated by the panellists. Since it is an industrial produced mixture, volatile impurities may cause this relatively high value.

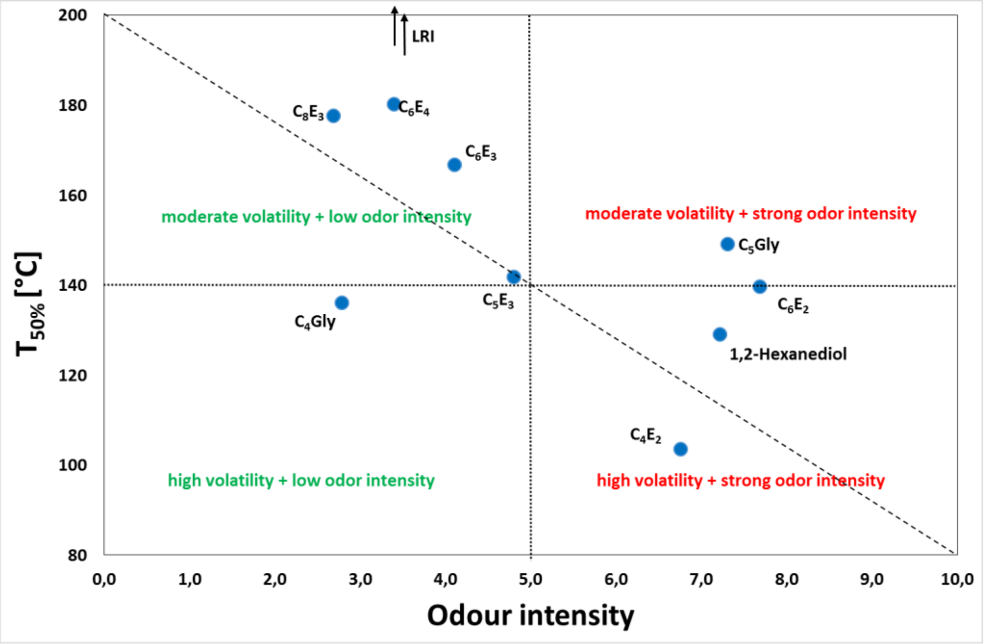

Figure 52 The perceived intensity versus $T_{50\%}$. The diagram is divided in four regions, which describe the volatile and olfactory properties of the amphiphiles. The border at 140°C represents the VOC limit. The virtual diagonal serves as a support to identify compounds, whose intensity characteristics deviates strongly from expectation.

Used in a water based perfume, a solvo-surfactant shall have an odour intensity as weak as possible and an odour signature which is perceived as pleasant as possible. In **Figure 53** the odour intensity is shown against the odour pleasantness. The diagram is divided in four parts, which are classified in positive, neutral and negative according to the colours green, orange and red. Furthermore the VOCs are displayed in orange, the SVOCs in green and LRI, which represents the non-VOCs in red. In general the odour signature of the solvo-surfactants is located around 5 ± 0.5, which describes an odour as neutral, neither pleasant, nor unpleasant. C_4E_2 and C_6E_2 is located slightly under this border and as a lonely exception C_5Gly turned out to be very unpleasant.

The difference between C_4Gly and C_5Gly according to its pleasantness is remarkable, since the C_iE_j compounds are located relatively close to each other. The difference is probably due to the interaction of the molecule with the receptor binding sites. C_4Gly activates receptors which give combined a pleasant, at least neutral, impression of the odour, whereas C_5Gly activates predominantly the receptors which are linked to an unpleasant impression of the scent. That the change in a carbon chain length may cause such a difference in the perceived odour, can be experienced in everyday life. Acetic acid is found in almost every household and frequently used in the preparation of salads. His longer homologue is also perceived frequently, but due to its unpleasant smell it is one of the reasons why people take a shower. Bacteria on the skin manufacture enzymes which break down lipids into smaller molecules, such as propionic acid, which results in unpleasant body odour.

For applications, such as a water-based perfume, C_5E_3, C_6E_3, C_6E_4, C_8E_3 are with regards to the odour pleasantness and their classification as SVOC's particularly interesting. C_4Gly and 1,2-hexanediol may be also acceptable, though due to their low volatility, they are touched by EU regulations. The strong unpleasant odour of C_5Gly is a pity, since it is a SVOC and bio-sourced, which is demanded by the industry. Masking of the scent may turn this solvo-surfactant still interesting for applications, such as hard surface cleaning.

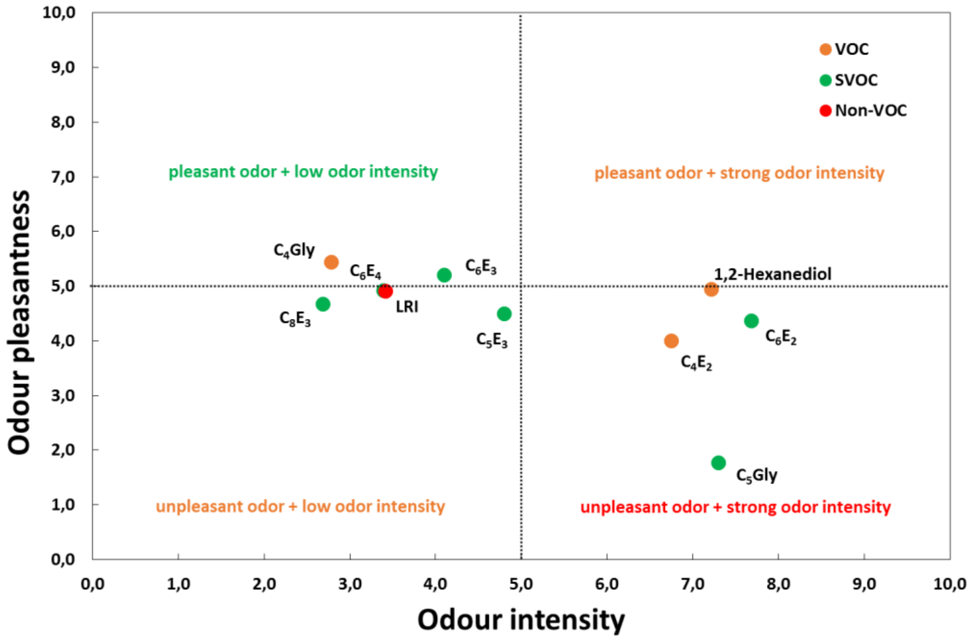

Figure 53 The odour pleasantness mapped against the odour intensity. All compounds can be found between 4 and 6 in odour pleasantness, which describes an odour as rather neutral in its convenience. In contrast C_5Gly deviates strongly from the rest.

d. The odour signature mapped with descriptors

As described previously, several descriptors of a scent were identified and used for the description of the odour signature of the solvo-surfactants and the reference system LRI. As in the previous sensorial analysis, the panellist had to identify the duplicate in order to validate his reproducibility. Thereby the results from the duplicates were correlated between the whole ranges, from 0 to 10 and if the correlation was equal or better than 80%, the panellist was regarded as confident. If it was smaller, the given data of this specific panellist was excluded.

In **Figure 54** the results are mapped in form of star diagrams. The centre is defined as zero intensity. The bigger the area which is spanned over the diagram, the stronger is the perceived intensity of the odour. Notes which are displayed in the upper part of the diagram meant to be pleasant notes of an odour, horizontal notes depend on the preferences of the panellist, so that they are described here as neutral, whereas the notes located in the lower part are assigned to unpleasant odours. In **Figure 54a** the star diagrams of C_6E_j ($j = 2 – 4$) are displayed. The higher the volatility of the compound, the bigger is the area which is covering the diagram. C_6E_2 has a $T_{50\%}$ value of 140 °C and shows thus the biggest expansion. The covered area is almost circular, which indicates either a broad distribution of several different notes or the here shown descriptors do not cover the whole spectrum of notes which were emitted from the sample and the panellists associated pleasant and unpleasant notes randomly with the corresponding descriptors. C_6E_3 with a $T_{50\%}$ value of 167 °C has already a decreased expansion due to

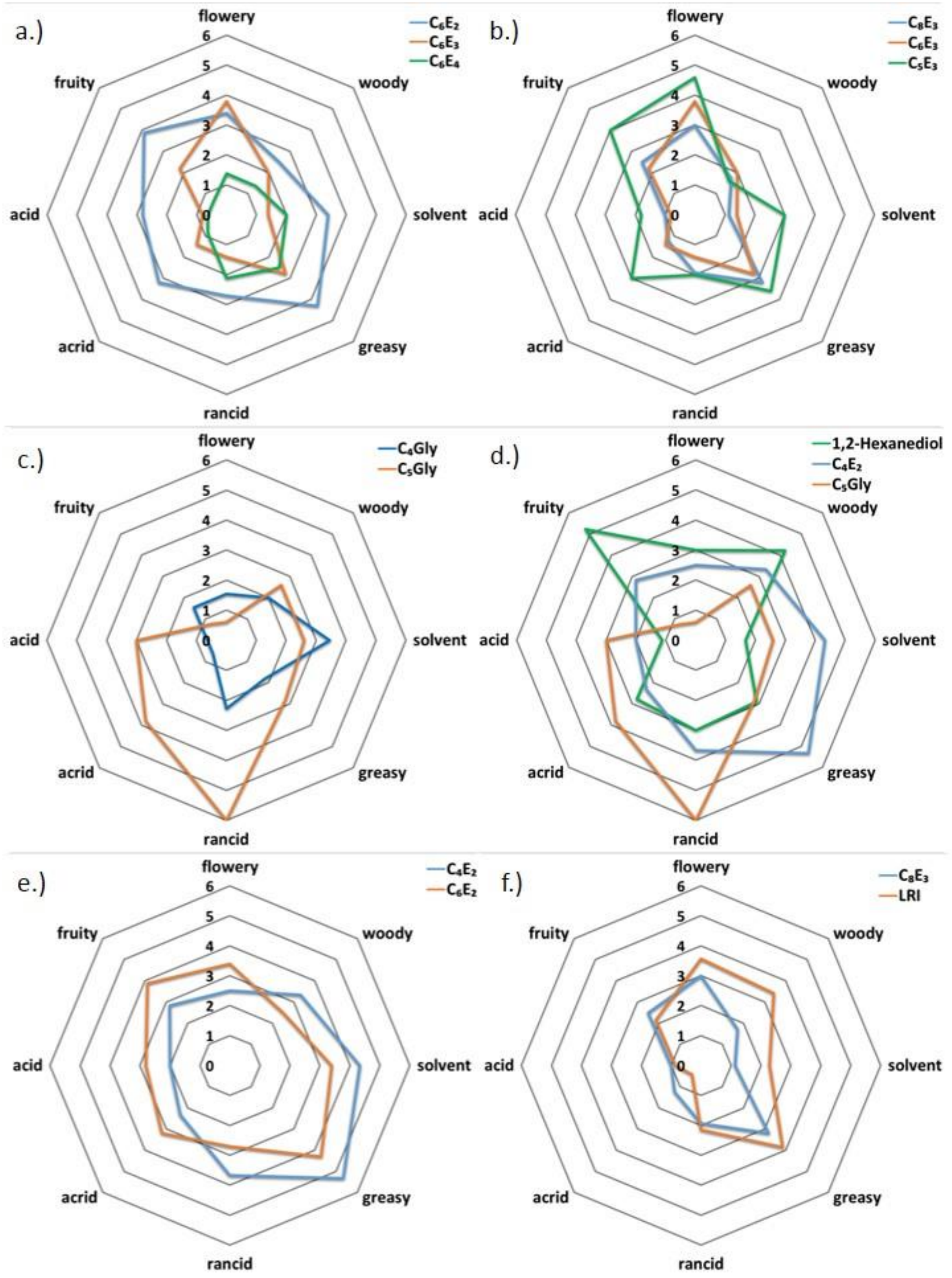

Figure 54 Star diagram of olfactory descriptors for several solvo-surfactants and LRI. The bigger the enclosed area, the stronger the perception of the overall scent of the amphiphile.

its lower volatility with maximums towards greasy and especially flowery notes. C_6E_4 ($T_{50\%}$ = 180 °C) shows little odour intensity with all descriptors. It is located almost circular around the centre with a slight displacement towards rancid and greasy notes. In **Figure 54b** the compounds with 3 ethoxy units are represented. Here as well, the most volatile compound C_5E_3 with a $T_{50\%}$ value of 142 °C has the biggest expansion. Additionally to the striking notes of C_6E_3, its smaller homologue has also a very strong fruity note, as well as solvent and acrid notes. Surprisingly C_8E_3 resembles C_6E_3 in intensity and odour signature. Comparing the results with **Figure 52**, a smaller area as for C_8E_3 was expected, since it shows weaker odour intensity with simultaneously lower volatility. **Figure 54c** shows the results for C_4Gly and C_5Gly. The latter has a strong maximum towards the descriptor "rancid", which explains its unpleasant odour. The difference with C_4Gly is remarkable. Although C_4Gly is very volatile, it shows only a small expansion towards the different notes. The most distinctive notes are "rancid", as in the case of C_5Gly, and "solvent". Since C_4Gly was evaluated as the most pleasant odour, relatively strong fruity, flowery or woody notes were expected. Probably the solvent note was perceived as very pleasant by the panellists. **Figure 54d** shows the star diagram of 1,2-hexanediol, C_4E_2 and C_5Gly which have according to **Figure 52** approximately the same odour intensity. The enclosed areas are of comparable size which is in agreement with the perceived intensity by the panellists. Furthermore 1,2-hexanediol possess the strongest fruity and woody notes of all investigated amphiphiles. In **Figure 54e** C_4E_2 and C_6E_2 are shown. Their appearance is very close to each other, however C_6E_2 is displaced a bit towards pleasant notes. Although their volatility is different, their odour intensity is comparable. The reference system LRI is shown in **Figure 54f** with C_8E_3, since they have same pleasantness and odour intensity according to **Figure 52**. Their expansion resembles, though LRI possess a stronger woody note.

2.5. Conclusion

The surfactant and solvent characteristics of solvo-surfactants were investigated. Initially the aqueous phase behaviour of several short-chain amphiphiles was studied. The critical temperature T_β increases, with increasing ethoxy number and decreases with decreasing carbon chain length, which is in accordance with literature. By comparison with T_β of long-chain surfactants, it was shown that there exist a linear relationship between T_β and i/j. Only C_4E_j's do not follow this trend, which is probably due to their high monomeric solubility in water. The influence of ionic surfactants on T_β was also investigated and it was shown that it augments strongly for SDS, DTABr and DHS, and only moderately for sodium oleate. The increase is especially strong in the water rich region and thus very interesting for aqueous fragrance solubilisation, where it is desired to use as few amphiphile as possible in order to create an efficient and temperature stable dispersion. Furthermore it was illustrated that the effect is independent from the C_iE_j solvo-surfactant and consequently only the type of the ionic surfactant is important.

The aggregation behaviour of several solvo-surfactants was studied and it was shown that C_6E_3 and C_6E_4 have a CAC of 81 mM, respectively 84 mM, whereas C_5-amphiphiles have a CAC between 220 and 264 mM. The concentrations are thus very high, which can be explained with their relatively low amphiphility. However for a constant number of ethoxy groups, the magnitude of the logarithm of the CAC depends linearly from the carbon chain length and this is even valid for short-chain amphiphiles. The interaction parameter β between C_6E_4/SDS, C_6E_3/SDS and C_5Gly/SDS was determined by applying the non-ideal mixing theory. A strong interaction for each pair was found, which is expected to be favourable for the efficient and temperature stable solubilisation of fragrances.

The PIT-Slope method was used to determine the hydrophile-lipophile balance of the solvo-surfactants by measuring changes in the PIT of a reference system upon addition of small quantities of a second amphiphile. It was shown that short-chain amphiphiles have barely an effect on the interface, since they partition strongly into the oil and/or water phase. Consequently $dPIT/dx_2$ is concentration dependent. With increasing carbon chain length ($i \geq 6$), the monomeric solubility is decreasing and the amphiphile accumulates at the interface, which increases the curvature and thus the PIT for hydrophilic solvo-surfactants and decreases it for hydrophobic solvo-surfactants. Especially C_6E_4 is interesting, since it turned out to be the most hydrophilic solvo-surfactant and thus very useful for fragrance solubilisation.

In the following the solvent properties of solvo-surfactants were investigated. Initially the evaporation characteristics of 29 amphiphilic compounds were investigated and classified according to their volatility. It is known that DMI ($T_{50\%}$ = 140 °C) separates the VOCs from the Non-VOCs. Due to EU regulations, which desire to reduce the VOCs, compounds are interesting for the industry, which lie beyond – but close to - this border. Triethyl citrate was the least volatile compound, which we found and is used to a greater extent in applications, where residues are unwanted. Therefore we classify amphiphilic compounds whose $T_{50\%}$ lies between 140 – 180 °C as SVOCs. These compounds are particularly interesting for industry, since they possess the requirements of being enough volatile to leave no residues and are not touched by EU regulations. In this context a general order was found, which describes the volatility of homologues in dependence of the polar head group.

$$\mathbf{C_iE_0 < C_iE_1 \approx C_iP_1 < C_iE_2 \approx C_i\text{-diol} < C_iE_3 < C_iGly < C_iE_4Me < C_iE_4 < C_iIso}$$

The order follows roughly the molecular weight of the compounds and in general it can be stated, that the more oxygen atoms are present, the lower the volatility of the compound.

Since a possible application of solvo-surfactants is the creation of water-based perfumes, the olfactory properties of several particular interesting compounds were investigated. It can be stated that the intensity of the perceived odour is bigger, the higher the volatility of the amphiphile. However it was expected that C_4Gly will be more intensively perceived, since its volatility is relatively high. In contrast C_5Gly shows an inverse behaviour. Thus the perception of an odour depends on a more complex mechanism, which involves a combination of millions of receptors in the olfactory system. The odour pleasantness was as well investigated, and it was shown that besides C_5Gly, which has a strongly unpleasant odour, all amphiphiles have neither a very pleasant very nor unpleasant odour. Nevertheless it was able to identify C_5E_3, C_6E_3, C_6E_4 and C_8E_3 as particularly interesting solvo-surfactants, since their odour intensity is relatively low, and thus they do not perturb the scent of the fragrance composition. Furthermore they are classified as SVOCs, and therefore not touched by EU regulations.

2.6. Experimental part

2.6.1. Construction of the (pseudo)binary phase diagrams

Amphiphile and water, respectively aqueous ionic surfactant solution were given into thin glass tubes, sealed with a tight screw cap and put into a thermostated water bath. The phase borders were determined by visual observation of the phase behaviour under temperature increase. The heating rate was 0.2 °C/min.

2.6.2. Surface tension measurements

Surface tensions were measured with the tensiometer K11 (Krüss) using the Wilhelmy plate method. Aqueous concentrated solutions of the surfactant(s) were prepared and given step by step to the thermostated measurement vessel, which contained 10 mL Millipore water. The mixture was stirred and left alone for 5 minutes before the surface tension was measured. The precision of the force transducer of the surface tension apparatus was 0.1 mN/m and before each experiment, the platinum plate was cleaned in blue-coloured flame. The temperature was stabilized at 25.0 ± 0.1°C with the thermo-regulated bath Julaba F12.

2.6.3. PIT-Slope method

Initially the reference system $C_{10}E_4$/*n*-octane/0.01 M NaCl(aq) was prepared in a 20 mL glass vial with stirrer. Thereby 4.85 g of *n*-octane and NaCl(aq), $\delta = 0.01$ M were given to the vial, before 0.3 g of $C_{10}E_4$ was added. The system was shaken and left over night. If the mixture was prepared correctly a three phase system appeared at ambient temperature after equilibration. The sample was then given into the measurement device, where a conductivity sonde was immersed into the mixture. A temperature-regulating HUBER Ministat 125 was connected to the water bath, wherein the sample was located. It was then subjected to two heating–cooling cycles at a linear rate of 1°C/min and under stirring (1000 rpm). The temperature interval was from 15 – 45 °C. The conductivity and temperature were simultaneously measured by a Radiometer Analytical CDM 210 conductimeter fitted with a CDC741 T platinized platinum probe. The software used was custom written in a Labview 7.1 National Instruments platform. The program carries out real time acquisition at ca. 2 data points per second. The PIT represents the strong decline of the conductivity. It is determined by applying two parallel tangents to the curve. Upon addition of the second amphiphile, the change in PIT can be monitored. If the PIT approaches 15 °C or 45 °C for very hydrophobic, respectively hydrophilic amphiphiles, the temperature interval was adjusted.

2.6.4. Thermo gravimetric analaysis

The volatility of several compounds have been investigated by thermo gravimetric analysis (TGA) with a TA Instruments TGA Q50 apparatus. Thereby approximately 20 mg of each compound was given into a platinum crucible and a temperature ramp of 5 °C min^{-1} was applied from 20 °C to 300 °C under nitrogen atmosphere. The decrease of the mass was followed as a function of time and temperature.

2.6.5. Synthesis of (poly)ethylene glycol monoalkylether

The synthesis was performed according to known procedure and used for all C_iE_j's, which were not obtained from supplier.[107] 5.0 equivalents of poly(ethylene) glycol were given with into a round bottom flask, followed by 1.0 equivalent of sodium hydroxide (aq, 50 wt.%). The mixture was stirred at 80 °C for one hour and afterwards traces of potassium iodide were added, in order to catalyse the substitution reaction. 1.0 equivalent of 1-bromoalkane was then given drop wise into the mixture for the next 4 hours, and during this procedure the flask was heated under reflux up to 120 °C. Then the mixture was left over night at same conditions.

Table 9 Distillation temperature and pressure for several C_iE_j's, as well as their purity after distillation. The yield is indicted before distillation.

Amphiphile	T [°C]	P [mbar]	Purity [wt.%]	Yield [%]*
C_5E_2	101-108	0.23	≥ 98	44
C_5E_3	117-126	2.0-2.1	≥ 99	53
C_5E_4	138-145	1.7-2.3	≥ 97	55
C_6E_3	99-109	0.2-0.3	≥ 98	51-56
C_6E_4	112-117/106-111	0.1-0.3/0.06-0.10	≥ 99	39-57
C_8E_3	112-113	0.23	99	51
C_8E_4	127-132	0.08	97	58
$C_{10}E_4$	-	-	≥ 99	-

*before distillation

To purify the product, the mixture was extracted between a water and oil phase. For ~1,5 kg of crude product 1000 mL of water was added and the mixture was extracted in a separation funnel 3 times with 500 mL of toluene. Afterwards the organic phase was evaporated and charged with 250 mL of water and 750 mL of methanol and then extracted 3 times with 1000 mL of petroleum ether. The aqueous phase was evaporated partially to remove methanol, charged with 250 mL of water and then extracted 3 times with 500 mL of cyclohexane. The solvo-surfactant C_6E_4 and C_5E_4 were thereby to hydrophilic for the oil phase, so that the separation funnel had to be heated in order to obtain a migration of the amphiphile into the oil phase. After the solvent was removed, the crude product was distilled under vacuum, and its purity was determined via GC-FID. $C_{10}E_4$ was synthesized according to same procedure in laboratory. However the synthesis was not performed by the author of this thesis.

2.6.6. Synthesis of 1-O-alkylglycerol

The synthesis of monoalkylglycerol is a two-step procedure.[103,112] First 1.0 equivalent of alcohol is added to 1.0 equivalent of NaOH solution (aq, 50%) with 0.005 equivalent of the phase transfer catalyst tetrabutyl ammonium bromide. Then the mixture is stirred at slightly elevated temperature (40-50°C) until homogenisation. The resulting alcoholate serves as a strong electron donor in a substitution reaction with the bromide of epibromohydrine (1.0 equivalent), which is added drop wise during 1 hour.

Afterwards the mixture is left overnight under stirring and reflux at 40-50°C. Eventually it is extracted three times with hexane (100 mL per 100 g mixture). In the end the organic phase is evaporated and the crude product is distilled under vacuum.

Table 10 Distillation temperature and pressure for pentylglycidyl ether and two C_iGly's, as well as their purity after distillation. The yield is indicted before distillation.

Compound	T [°C]	P [mbar]	Purity [wt.%]	Yield [%]
C_5Glycidyl ether	115-121	0.05	≥ 99	54-67
C_4Gly	-	-	≥ 98	95-96
C_5Gly	-	-	≥ 99	≥ 97

The pure alkyl glycidyl ether is then added into water (500 mL per 25 g) and the solution is left 48 hours under stirring and reflux at 100 °C. The reactant is hydrolysed, which results in an opening of the triangle. The water is evaporated and in order to guarantee the complete removal of water, the product is lyophilised overnight. No distillation was performed. C_4Gly was directly hydrolysed from commercially available butyl glycidyl ether.

2.6.7. Materials

Table 11 Summary of all relevant materials used in this chapter. They were either bought from industrial supplier, or synthesized. Some compounds were left-overs from former Ph.D. students.

Compound	Abbreviation	Supplier	Purity
Amphiphiles			
Ethylene glycol monobutylether	C_4E_1	Sigma Aldrich	≥ 99%
Ethylene glycol monopentylether	C_5E_1	Fluka	≥ 99%
Diethylene glycol monobutylether	C_4E_2	Sigma Aldrich	≥ 99%
Diethylene glycol monopentylether	C_5E_2	Synthesized	≥ 98%
Diethylene glycol monohexylether	C_6E_2	Sigma Aldrich	95%
Diethylene glycol monooctylether	C_8E_2	Laboratory	-
Triethylene glycol monopentylether	C_5E_3	Synthesized	≥ 99%
Triethylene glycol monohexylether	C_6E_3	Synthesized	≥ 98%
Triethylene glycol monooctylether	C_8E_3	Synthesized	99%
Tetraethylene glycol monopentylether	C_5E_4	Synthesized	≥ 97%
Tetraethylene glycol monohexylether	C_6E_4	Synthesized	≥ 99%
Tetraethylene glycol monooctylether	C_8E_4	Synthesized	97%
Tetraethylene glycol monodecylether	$C_{10}E_4$	Laboratory	≥ 99%
3,6,9,12-Tetraoxaoctadecan-1-methylether	C_6E_4Me	Laboratory	-
3,6,9,12-Tetraoxaicosan-1-methylether	C_8E_4Me	Laboratory	-
1-O-Butylglycerol	C_4Gly	Synthesized	≥ 98%
1-O-Pentylglycerol	C_5Gly	Synthesized	≥ 99%
1-O-Ethylhexylglycerol	iC_8Gly	Laboratory	-
Propylene glycol monopropylether	C_3P_1	Sigma Aldrich	≥ 99%

Butylene glycol monopropylether	C_4P_1	Sigma Aldrich	≥ 99%
5-O-Propylisosorbide	C_3Iso	Laboratory	95%
5-O-Pentylisosorbide	C_5Iso	Laboratory	97%
1,2-Hexanediol	1,2-C_6-diol	Sigma Aldrich	98%
1,2-Octanediol	1,2-C_8-diol	Sigma Aldrich	98%
Solubiliser LRI	LRI	Sensient	-
Sodium Dodecyl Sulfate	SDS	Acros	≥ 99%
Dihexyl sulfosuccinate	DHS	Fluka	80% (aq)
Sodium Oleate	-	TCI	≥ 97%
Dodecyl trimethylammonium bromide	DTABr	Alfa Aesar	99%
1-Alcohols			
1-Butanol	C_4E_0	Alfa Aesar	99%
1-Pentanol	C_5E_0	Alfa Aesar	≥ 98%
1-Hexanol	C_6E_0	Alfa Aesar	99%
1-Heptanol	C_7E_0	Alfa Aesar	99%
1-Octanol	C_8E_0	Alfa Aesar	99%
1-Decanol	$C_{10}E_0$	Alfa Aesar	≥ 98%
1-Dodecanol	$C_{12}E_0$	Alfa Aesar	98%
Precursors			
1-Bromopentane	C_5Br	Sigma Aldrich	98%
1-Bromohexane	C_6Br	Sigma Aldrich	98%
1-Bromooctane	C_8Br	Sigma Aldrich	99%
Triethylene glycol	E_3	Alfa Aesar	99%
Tetraethylene glycol	E_4	Alfa Aesar	99%
Epibromohydrine	-	Sigma Aldrich	98%
Butyl glycidyl ether	-	TCI	≥ 98%
Divers			
Eucalyptol	-	Firmenich	≥ 99%
n-octane	C_8	Sigma Aldrich	≥ 99%
Triethylcitrate	-	Sigma Aldrich	99 %

Chapter 3

The Equivalent Alkane Carbon Number of polar oils

3.1. Classification of oils according to their hydrophobicity

As for surfactants, a classification of the hydrophobicity of polar hydrocarbon oils is required. The required HLB value is a method, which was established to classify an oil according to its hydrophobicity.[11,12] As the HLB-value, it is obtained by observing the stability of a series of emulsions. However in this case, two emulsifiers with known HLB-value are mixed in different ratios, so that their mixed HLB values enclose the whole range between the two emulsifiers. Afterwards the same volume of oil and water is given to the sample and the mixture is stirred and left for 24 hours. The required HLB-value is then obtained by visual interpretation of the most stable emulsion, thus the one which has dephased the least.[11,161] Unfortunately the required HLB has several drawbacks, which make the interpretation of the results difficult. If the formed emulsions are too stable, the evaluation is imprecise since there is no significant difference in phase separation between the samples. Thus the destabilising time has to be increased, which may result in a very time consuming procedure. On the other hand, emulsions which destabilise rapidly, leave no time to note any changes in their stability. Unlike the HLB-value for surfactants, which is still widely used, the required HLB-value is rarely used in industry and in research. Mostly it is used to classify complex oils, e.g. essential and vegetable oils.[162–164] By keyword search with Google Scholar, one obtain 15500 results for "HLB-value" but only 214 results for "required HLB-value".

In 1964 Shinoda *et al.* introduced a method to classify surfactants and oils by determining the phase inversion temperature (PIT) of a non-ionic surfactant/oil/water (SOW) system[6]. This method, which is less empirical than the HLB, gave values, which were in good agreement with those of the required HLB.[7] The PIT can be determined visually or by conductivity. However the first may be inaccurate, depending on the system and the latter requires the addition of small quantities of salt, which may have an influence on the PIT itself. Cash *et al.* introduced 1977 the concept of the equivalent alkane carbon number (EACN)[165], a dimensionless number which characterizes the hydrophobicity of an oil. Furthermore it is independent of temperature and considers penetration effects. The EACN concept enables to classify the hydrophobicity of any hydrocarbon compound which is liquid and non-miscible with water. Since the introduction of this concept several EACN values for various types of oils such as triglycerides and esters[166], aliphatic, aromatic and chlorinated hydrocarbons[107,167], as well as terpenes[168] have been determined. Furthermore it has been used to explain oil segregation of a less hydrophobic oil into the interfacial layer[169] and Tchakalova *et al.* used the concept to determine the surface activity of fragrances in an oil mixture[170]. It is known that the structure of the compound, unsaturated bonds and the introduction of heteroatoms have a distinct effect on the EACN value of an oil. As a rule of thumb any modification decreases this value in comparison to its linear hydrocarbon homologue. While branching has a relatively weak influence, cyclisation or the addition of a double bond results already in a pronounced decrease, whereas functional groups as esters or ethers severely reduce the EACN value.[107,166,168] Additionally it was shown before, that the hydrophobicity depends also strongly on the location of the functional group in the molecule[166], e.g. the ester ethyl myristate and octyl octanoate are constitutional isomers with an EACN of 5.3 and 8.1 respectively. However, the determination of the EACN can be a time consuming process. First a calibration curve with several linear alkanes has to be constructed and then the phase behaviour of the desired oil has to be determined.[107] Especially for long chain surfactants, this procedure is very time consuming, since the adjustment of the equilibrium can take up to several days, even weeks. A more rapid possibility to obtain the EACN values is the use of chemoinformatics, and particularly quantitative structure-property relationships (QSPR). Bouton *et al.* already used a QSPR model to estimate the EACN of terpenes.[171] Unfortunately the resulting parameters – namely Kier A3, and average negative softness – are far from having a trivial physicochemical meaning and the quality of the model is strongly dependent on the chemical structures in the training set. Another popular method to classify an oil according to its hydrophobicity is the determination of the logarithmic partition coefficient Log P[172] of a solute between 1-octanol and water. This method is frequently used in pharmacy *etc*. Unfortunately the Log P is not very well adapted for SOW systems, which appear particularly in cosmetics or in enhanced oil recovery, since it is strongly dependent on the temperature and due to the absence of micelles, it does not consider penetration effects of polar oils into the interfacial layer between water and oil, which is commonly observed in these systems.

The EACN concept exist already for a while. Yet its use in industry and research is moderate. According to Google Scholar only 432 hits were obtained for the keyword research using "equivalent alkane carbon number". However 46 of them since 2014, arguing for an increasing use of this concept in research.

3.2. The fish cut – Tracing the phase borders

The EACN of a polar oil is obtained experimentally by determining the fish tail temperature T* in a SOW system and comparing it with a calibration curve. T* was predominantly determined by investigation of the phase behaviour of C_6E_4/Oil/Water systems at a constant WOR (α = 0.5, w/w) as a function of temperature T (ordinate) and amphiphile mass fraction γ (abscissa). Since C_6E_4 is a short-chain amphiphile, it equilibrates rapidly. Thus more oils can be investigated in less time. However for some oils, $C_{10}E_4$, $C_{12}E_6$ or $C_{12}E_8$ were used, in order to compare the obtained results with different amphiphiles, or since the hydrophobic characteristics of the oil made it necessary to use one of the latter. The fish tail is characterized by the temperature T* at which the phase behaviour inverts from a Winsor I phase to a Winsor II phase, and $\gamma*$, which implies the efficiency of the system, that is the minimum surfactant mass fraction necessary to obtain a Winsor IV phase (**Figure 55**). It represents the intersection, where all the Winsor phases meet. Furthermore the fish tail temperature T* represents a system of zero curvature, and thus the optimal formulation. T* was determined by tracing the phase borders of the SOW system.

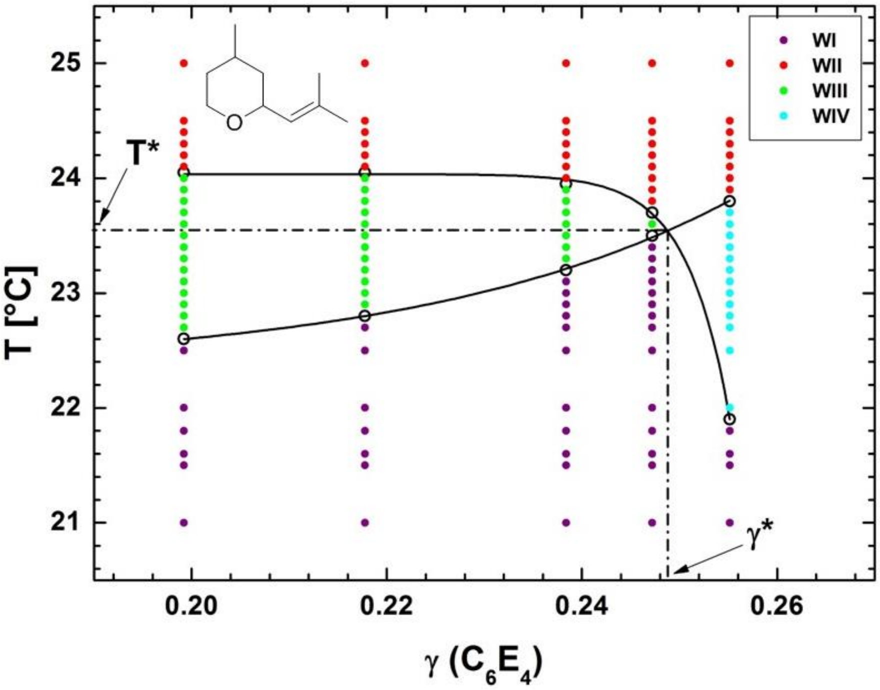

Figure 55 The fish tail of the ternary system C_6E_4/rose oxide/water. Each point represents an observation of the phase behaviour, which was assigned to its corresponding Winsor phase (WI,WII,WIII or WIV). The intersection of the curves indicates the fish tail temperature T* and the efficiency γ*.

The phase borders were roughly determined, in order to know their locations. Then the temperature was altered in 0.1°C steps, in order to determine precisely the alterations in the phase behaviour of the SOW system. The EACN of a hydrophobic compound is then determined by comparing its fish tail temperature T* with a calibration curve. These curves are obtained by measuring T* of several linear alkanes with a well-defined poly(ethylene) glycol monoalkylether. In this work we rely on the calibration curves made by Bouton[168] *et al.* and Queste[107]*et al.* Furthermore the calibration curve of $C_{12}E_6$ was constructed in order to verify the coherence of the EACN concept with several different C_iE_j's.

3.3. EACN determination via salinity scan

Another method to determine the EACN of an oil is the salinity scan with an ionic surfactant. Thereby the optimum salinity S* is determined, which represents the weight concentration of salt in aqueous solution, necessary to obtain the optimum formulation. During this method, the equilibrated phase behaviour of a SOW system with WOR =1 (v/v) is observed as a function of increasing salt concentration. If the excess oil and water phase have the same volume, the optimum salinity S* is found, which represents a system with zero curvature. With a calibration curve made of *n*-alkanes and their corresponding S*-values, the EACN of an unknown polar oil can be determined.

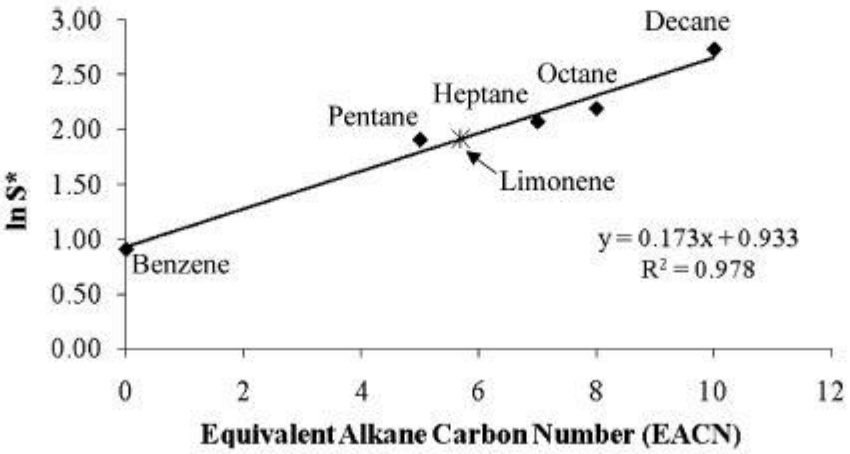

Figure 56 **The salinity scan performed in a SOW system (WOR = 1, v/v) with 2.6 wt.% dihexyl sulfosuccinate (DHS) as ionic surfactant and NaCl as salt. The calibration curve consists of the *n*-alkanes and benzene. Limonene was assigned an EACN of 5.7 according to this method.**[27]

Witthayapanyanon et al. used this method to determine the EACN of limonene (**Figure 56**). [27] Thereby limonene shows a similar phase behaviour as it is expected from hexane, with an EACN of 5.7. Elsewhere a value of 8.5 was found for limonene.[173] The EACN determined with C_6E_4 and C_8E_4 by the fish-tail method is 2.0 and 1.6. Thus there is already an incoherence within the EACN determination according to the salinity scan and moreover, there is also a huge difference between the two methods. This indicates that the EACN might not be a universal value for all surfactant types. However Ontiveros *et al.* found with $C_{10}E_4$ for ethyl oleate an EACN of 7.3, which is in good accordance with the EACN of 7 found by Minana-Perez *et al.* using an extended surfactant of the type alkyl polypropylene oxide ether sulphate.[166,174]

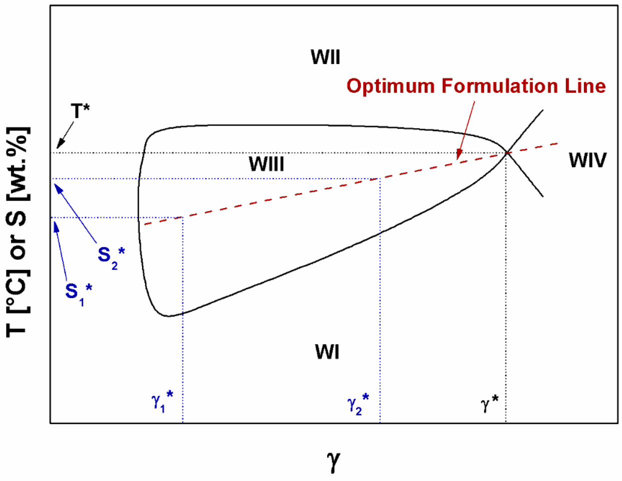

Figure 57 **Schematic representation of a fish cut in a non-ionic and ionic SOW system. The optimum formulation line does not proceed linearly for polar oils, which in turn imposes a surfactant concentration dependency onto the optimum formulation S* of the system. However T* is characterised by the intersection where all the Winsor phases meet and thus independent of the surfactant concentration.**

It is thus not yet clear, if both types of EACN determination give coherent values. Nevertheless the determination with extremely pure (poly)ethylene glycol ethers was proved to be valid for different C_iE_j's and is independent of the amphiphile concentration.[168,171] In contrast the EACN determination according to a salinity scan, is not yet verified upon validity with different ionic surfactants. Furthermore the results may vary with varying surfactant concentration, since the optimal formulation line is usually not parallel to the x-axis (**Figure 57**).[25] Since there is no standardised protocol for the salinity scan, surfactant concentrations between 1 – 10 wt.%, as well as WOR =1 – 4, can be found in literature, which may result in imprecise EACN values.[23,174,175] Furthermore it can be seen that EACN values of polar oils were determined, and then used as an absolute value in calibration curves, *e.g.* benzene. Its EACN was determined with a technical surfactant and was found to be equal to zero.[176] However Salager *et al.* stated that the result for benzene might be erroneous, since this polar oil induces the fractionation of different species contained in the technical surfactant.[177] Nonetheless benzene, as well as other polar oils, such as toluene or *p*-xylene are found in calibration curves, imposing a questionable slope on the curve.[27,175] As a rule of thumb, an oil's phase behaviour should be verified with several different surfactants, using only *n*-alkanes in the calibration curve, before allocating a final absolute EACN value. Thus in this work only well-defined poly(ethylene) glycol monoalkylethers were used, since they have – as shown in **Chapter 2** – coherent properties with respect to each other and they give according to their correlation curves same results in the determination of the EACN of polar oils.

3.4. The application of the HLD equation to the calculation of the EACN

The HLD equation introduced in **Chapter 1** can be used to calculate the EACN of polar oils. For SOW system without salt and co-surfactant, the equation can be simplified:

$$HLD = Ccn - k \cdot ACN + c_t(T^* - 25) \qquad \textbf{(22)}$$

In the case of optimum formulation, the HLD value is set to zero. At this reference point, the surfactant has same affinity for the water and oil, so that the spontaneous curvature of the system is zero. The equation can then be solved for ACN:

$$ACN = \frac{Ccn - 25c_t}{k} + \frac{c_t}{k}T^* \qquad \textbf{(23)}$$

A linear equation is obtained, where the first term signifies the intercept and the second term describes the slope multiplied with T*. These coefficients can be determined experimentally, by measuring *T** of several *n*-alkanes. The linear fitting gives then an intercept *a* and slope *b*, which corresponds to those of **Equation 23**. Thus for each non-ionic surfactant a calibration curve can be obtained, which corresponds to the following type:

$$EACN = a + b \cdot T^*_{C_iE_j} \qquad \textbf{(24)}$$

ACN was replaced with EACN, since it shall be used to calculate the EACN of polar oils and not *n*-alkanes. In this work the calibration curves of Bouton and Queste were used for the calculation of the

EACN, determined with C_iE_4 (i = 6,8,10).[107,171] Furthermore the calibration curve of $C_{12}E_6$ was newly determined and the one of $C_{12}E_8$ was constructed according to experimental data from Kunieda. However the latter implies polar oils in its calibration curve, which is due to previously stated reason a questionable approach. Nevertheless it was used to give an approximate image of the extremely low EACN of linalool. In **Table 12**, a summary of all in this work relevant equations are given.

Table 12 Correlation equations for the calculation of the EACN of polar oils for several non-ionic surfactants, as well as the range, wherein an oils EACN's can be determined. The EACN range represents approximate values, since the determination of the exact values is extremely difficult.

Amphiphile	Intercept *a*	Slope *b*	EACN Range
C_6E_4	-6.0	0.182	-4 to 11
C_8E_4	-3.5	0.247	-2 to 20
$C_{10}E_4$	-1.0	0.359	1 to 33
$C_{12}E_6$	-7.8	0.320	-7 to 23
$C_{12}E_8$	-14.5	0.320	-14 to 16

The fish tail temperatures of several $C_{12}E_6$/*n*-alkane/water systems were determined, according to the procedure described in **Section 3.2**, in order to create a calibration curve. The results are given in **Figure 58** (left). With increasing carbon chain length of the oil, T* and γ* are increasing. Moreover the expansion of the three-phase region is augmenting, which is due to the less favourable interaction of $C_{12}E_6$ with the oil phase. T* can then be used to create a calibration curve, which is shown together with those made by Bouton and Queste in **Figure 58** (right).

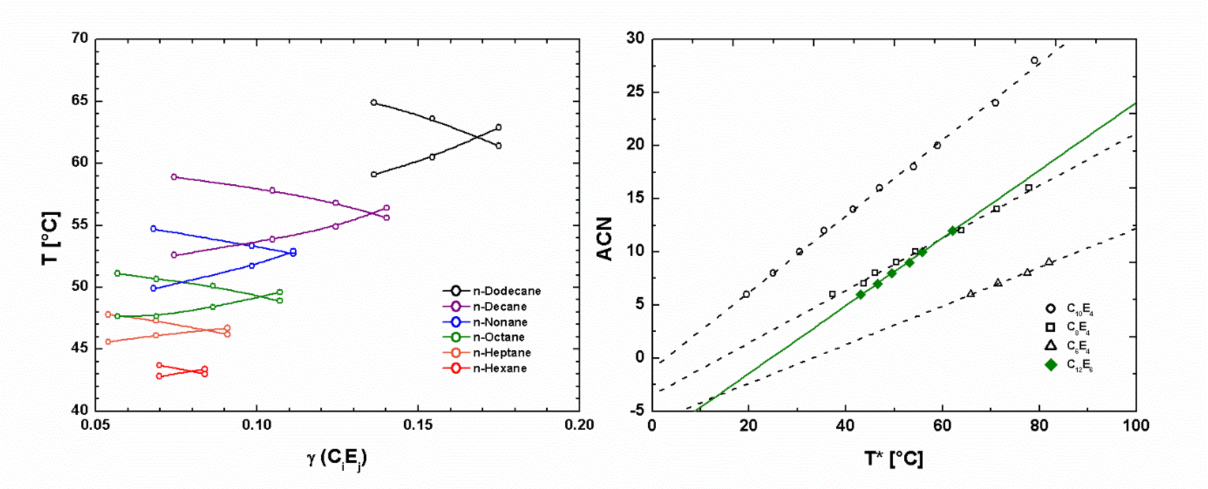

Figure 58 Left: Fish tails of several $C_{12}E_6$/*n*-alkane/water systems. With increasing ACN of the oil, T* and γ* are increasing. Right: Calibration curve of $C_{12}E_6$ (green) in comparison with those made of C_iE_4 (i = 6,8,10).

The slope is comparable with the one of $C_{10}E_4$. However the intercept is much smaller, which makes it possible for $C_{12}E_6$ to measure the fish cut of polar oils with much lower EACN. With decreasing EACN, the T*-value of $C_{12}E_6$ and C_6E_4 are approaching until they intersect at an EACN equal to -3.6. Thus at this value, the phase behaviour of both amphiphiles should be similar according to their affinity to oil and water. Unfortunately there is yet no oil known with such an EACN value. Thus it could not be verified. Furthermore the tricritical point may have been passed with C_6E_4, since polar oils tend to decrease the three-phase region, until it disappears at the tricritical point. In this work it was possible to obtain EACN values of -3.3 with C_6E_4. However the three-phase region was extremely narrow. Furthermore it was not possible to determine the EACN of toluene with same amphiphile, since no three-phase region appeared. In contrast $C_{12}E_6$ can be used to determine the EACN of oils with a higher polarity. Theoretically they can be investigated by the latter, if their EACN is between -7 to 23. The expansion of the three-phase regions with $C_{12}E_6$ are relatively large, which indicates that the tricritical point is attained later and thus lower EACN values are possible. However the exact location of the tricritical point is not known, which may result in a limitation well before the theoretical lower boundary of -7.

3.5. The EACN of several polar oils measured with different non-ionic surfactants

Many polar oil exhibit an EACN which is well outside the range, which is determinable with *n*-alkanes. Due to its low boiling point, the lower limit is mostly achieved with hexane. Thus it has to be extrapolated in order to calculate the EACN of very polar oils. This bears the possibility of an error, which increases with decreasing EACN. Therefore it is important to compare result, which were obtained with different amphiphiles, in order to validate the correctness of the correlation function and minimize the error.

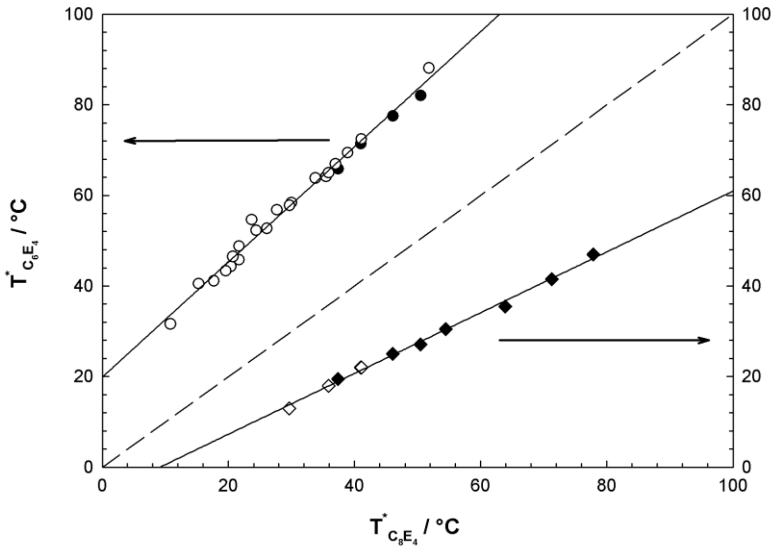

Figure 59 Fish tail temperatures T* for several SOW systems. Full circles and diamonds represent the *n*-alkanes, whereas empty symbols stand for polar oils, e.g. terpenes.

In a publication from 2010, Bouton *et al.* compared T* of several polar oils, measured with C_iE_4 (i = 6,8,10), which resulted in a linear behaviour between their fish tail temperatures (**Figure 59**).[171] The curves show this behaviour between the T*-values of C_6E_4 and C_8E_4, as well as C_8E_4 and $C_{10}E_4$. The relationship is not only linear for *n*-alkanes, but also for polar oil i.e. terpenes. Even for very polar compounds the extrapolated curves maintain its overall linearity, arguing for reliable correlation equations.

The findings shall be verified for a surfactant with different quantity of ethoxy groups and carbon chain length. $C_{12}E_6$ was chosen, since its strong amphiphilicity permits the measurement of T* values over a long range. The fish tail temperatures of the polar oils 1-octyne and ethyl decanoate were constructed, in order to compare their results with those of C_6E_4 and $C_{10}E_4$. In **Figure 60** the fish cut of $C_{12}E_6$/ethyl decanoate/water, as well as several fish tails are shown. Regarding the ester, the γ* value increases in this order $C_{12}E_6 > C_{10}E_4 > C_6E_4$. Burauer *et al.* found same order for the oil *n*-octane.[56] Concerning the critical mass fraction γ*, it can be stated that the higher the amphiphilicity of the amphiphile, the lower it is. The same behaviour is observed for 1-octyne, which was measured with $C_{12}E_6$ and C_6E_4. With $C_{10}E_4$ its T* value is below 0 °C. The fish tail temperature is decreasing following the order $C_6E_4 > C_{12}E_6 > C_{10}E_4$. According to the location of ethyl decanoate with respect to 1-octyne, it can be stated that the latter has in both cases – with C_6E_4 and $C_{12}E_6$ – a smaller EACN than the ester, since their T*-value is lower.

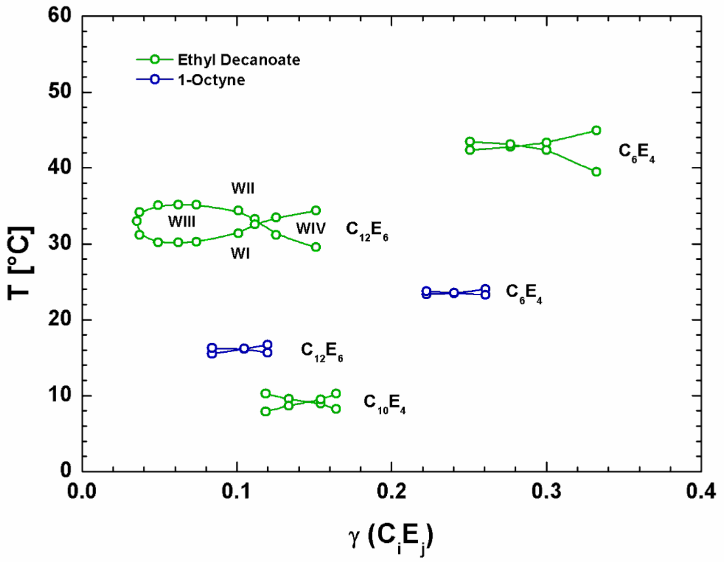

Figure 60 Fish tails of ethyl decanoate and 1-octyne, determined with C_6E_4, $C_{10}E_4$ and $C_{12}E_6$.

The fish tail temperatures of the *n*-alkanes, ethyl decanoate and 1-octyne are gathered in **Figure 61**. Therein the T*-values between C_6E_4 and $C_{12}E_6$, as well as $C_{10}E_4$ and $C_{12}E_6$ are compared. The *n*-alkanes follow a linear relationship and even the polar oils ethyl decanoate ($\overline{EACN}$ = 2.2) and 1-octyne ($\overline{EACN}$ = -2.2) can be found on or very close to the linear curve. Thus it can be assumed that the correlation equations are also quite accurate under extrapolation. Furthermore the determination of the EACN is independent of the (poly)ethylene glycolether and can be done with any of them. Concerning the procedure of the measurement, the solvo-surfactant C_6E_4 may be the most preferred, since it can be used for a huge variety of interesting oils (*e.g.* terpenes, fragrances) with an EACN between -4 and 11, at simultaneously rapid equilibration. Oils with a higher EACN can be investigated with C_8E_4 or $C_{10}E_4$, with the drawback of longer equilibration time. An alternative could be the not here investigated C_6E_3, since it is less hydrophilic than C_6E_4, but equilibrates as well very fast. For very polar oils with EACN values below the tricritical temperature of C_6E_4, very hydrophilic surfactants have to be used, such as $C_{12}E_j$ (j = 6,7,8) or $C_{10}E_j$ (j = 6,7,8).

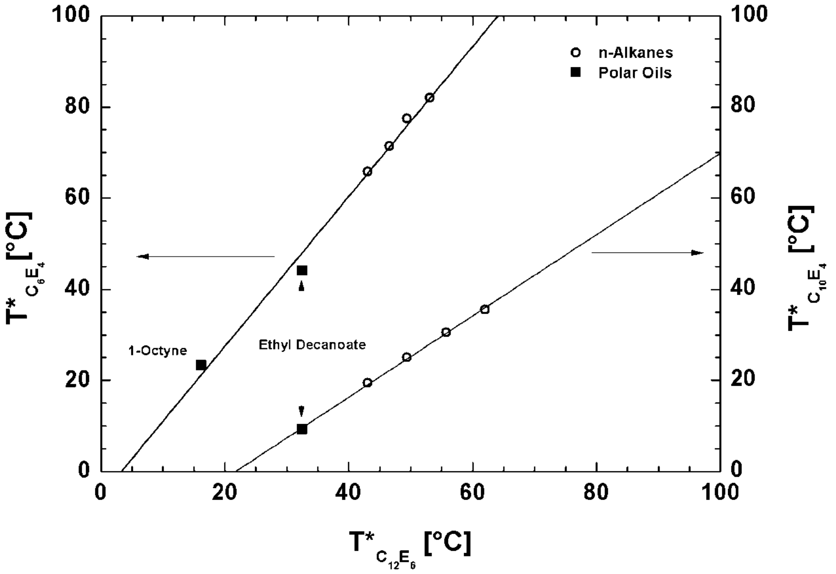

Figure 61 The Fish tail temperature T* of several SOW systems, compared between C_6E_4 and $C_{12}E_6$, as well as $C_{12}E_6$ and $C_{10}E_4$. A linear relationship is observed, arguing for the independency of the EACN from the used poly(ethylene) glycolether.

3.6. Result, trends and particularities of the determined EACN values

It this work, the EACN of 46 compounds was determined, ranging from simple molecules, such as cyclodecane, to complex multi-functionalised fragrances, such as α-damascone. 43 of them were determined with C_6E_4 as amphiphile, thereof two as well with $C_{12}E_6$. Two polar oils were investigated with $C_{10}E_4$ and one with $C_{12}E_8$. Furthermore various series of functionalised hydrocarbon oils were investigated, in order to demonstrate the influence of the functional group on the EACN of the oil. The results are completed with those obtained from previous work.[107,166,167,171]

3.6.1. Summary of all measured T*-values and their corresponding EACN's

All results obtained with C_6E_4, C_8E_4 and $C_{10}E_4$ are shown in **Table 13**. The structure of the compound, the EACN as well as T* and γ* are indicated. The EACN of several oils was investigated with two or three amphiphiles. In these cases the indicated EACN represents the average value.

Table 13 Summary of all investigated oils with C_6E_4, C_8E_4 and $C_{10}E_4$. The structure of the molecule is indicated, as well as its EACN, T* and γ*. Newly determined oils are indicated with an "*a*". The remaining compounds were summarized from literature.[107,166,167,171]

Compound	Structure	EACN	T*[°C]			γ*		
			C_6E_4	C_8E_4	$C_{10}E_4$	C_6E_4	C_8E_4	$C_{10}E_4$
			***n*-Alkanes**					
Octacosane	$C_{28}H_{58}$	28.0	-	-	79.0	-	-	0.590
Tetracosane	$C_{24}H_{50}$	24.0	-	-	71.0	-	-	0.460
Eicosane	$C_{20}H_{42}$	20.0	-	-	59.0	-	-	0.318
Octadecane	$C_{18}H_{38}$	18.0	-	-	54.0	-	-	0.278
Hexadecane	$C_{16}H_{34}$	16.0	-	77.9	47.0	-	0.550	0.245
Tetradecane	$C_{14}H_{30}$	14.0	-	71.3	41.5	-	0.491	0.217
Dodecane	$C_{12}H_{26}$	12.0	-	63.9	35.5	-	0.441	0.170
Decane	$C_{10}H_{22}$	10.0	-	54.5	30.5	-	0.357	0.141
Nonane	C_9H_{20}	9.0	82.0	50.5	-	0.609	0.329	-
Octane	C_8H_{18}	8.0	77.5	46.1	25.0	0.567	0.293	0.105
Heptane	C_7H_{16}	7.0	71.4	43.8	-	0.516		-
Hexane	C_6H_{14}	6.0	65.8	37.4	19.5	0.470	0.257	0.080
			Branched & Cyclic Alkanes					
Squalane	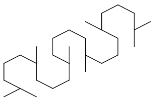	24.4	-	-	71.0	-	-	0.390
Dodecylcyclohexane	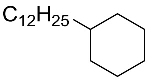	17.3	-	-	51.5	-	-	0.257
Decylcyclohexane	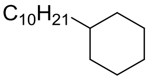	14.4	-	-	43.0	-	-	0.228
Butylcyclohexane	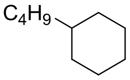	7.0	72.4	41.1	22.0	0.522	-	0.110
Propylcyclohexane	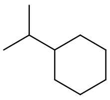	5.7	65.0	35.9	18.0	0.474	-	0.097
Cyclodecane[a]	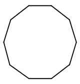	5.5	63.0	-	-	0.381	-	-
***cis*-Decalin**[a]	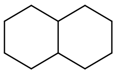	5.3	62.3	-	-	0.398	-	-
Isopropylcyclohexane	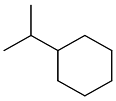	5.3	63.8	33.8	15.2	0.467	-	-
1.4-Dimethylcyclohexane	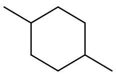	4.4	58.4	30.0	-	0.410	-	-
Ethylcyclohexane	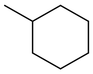	4.2	57.8	29.7	13.0	0.404	-	0.058
Cyclooctane[a]	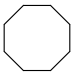	4.1	55.5	-	-	0.336	-	-

1.2-Dimethylcyclohexane	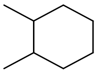	3.3	54.6	23.7	-	0.388	-	-
Methylcyclohexane	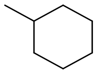	3.2	52.3	24.4	-	0.378	-	-
Cyclohexane	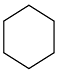	2.2	46.5	20.7	-	0.329	-	-
Halogenated Alkanes								
1-Chlorohexadecane	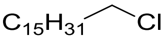	9.8	-	-	30.0	-	-	0.230
1-Chlorotetradecane	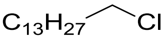	8.0	-	-	25.0	-	-	0.175
1-Chlorododecane	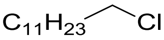	5.6	-	-	18.5	-	-	0.140
1-Chlorodecane	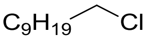	3.5	-	-	12.5	-	-	0.100
1-Bromo-3-methylpropan[a]	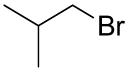	-3.3	14.8	-	-	0.226	-	-
Unsaturated Alkanes								
Squalene[a]	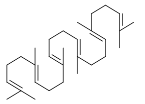	13.8	-	-	41.3	-	-	0.319
1-Octadecene[a]	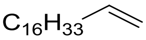	14.2	-	-	42.4	-	-	0.369
1-Dodecene[a]	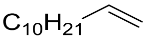	8.1	77.7	-	-	0.550	-	-
1-Decene[a]	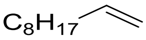	5.5	63.2	-	-	0.441	-	-
1-Octene[a]	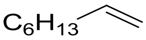	3.9	54.6	-	-	0.420	-	-
***cis*-Cyclooctene**[a]	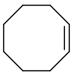	1.6	41.6	-	-	0.263	-	-
1-Methyl-1-cyclohexene	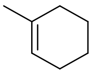	0.4	37.4	12.4	-	0.310	-	-
4-Methyl-1-cyclohexene	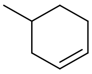	0.4	36.3	13.2	-	0.300	-	-
3-Methyl-1-cyclohexene	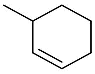	-0.1	35.3	10.5	-	0.282	-	-

Cyclohexene	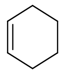	-1.2	26.5	-	-	0.222	-	-
1-Tetradecyne[a]	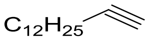	3.9	54.3	-	-	0.345	-	-
1-Dodecyne[a]	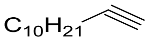	2.0	44	-	-	0.296	-	-
1-Decyne[a]	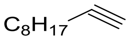	0.1	33.8	-	-	0.250	-	-
1-Octyne[a]	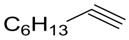	-1.8	23.3	-	-	0.240	-	-
Dodecylbenzene	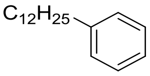	7.9	-	-	24.5	-	-	0.192
Decylbenzene	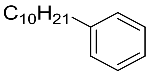	6.2	-	-	19.5	-	-	0.162
Octylbenzene	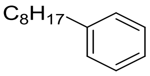	4.3	-	-	14.0	-	-	0.118
Butylbenzene[a]	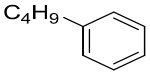	0.4	35.2	-	-	0.274	-	-
***p*-Xylene**[a]	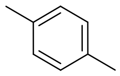	-2.3	20.2	-	-	0.244	-	-
Phenyl-1-butyne[a]	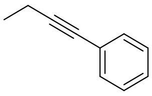	-3.3	15.1	-	-	0.281	-	-
		Terpenes						
Longifolene	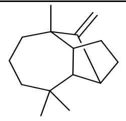	6.5	69.5	38.9	-	-	0.262	-
***p*-Menthane**	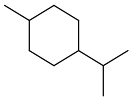	6.0	66.9	37.0	15.6	0.469	0.234	-
Caryophyllene	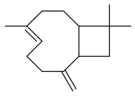	5.6	64.1	35.5	-	0.435	0.238	-
Pinane	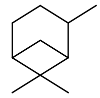	4.0	56.8	27.7	-	0.373	0.183	-
α-Pinene	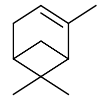	3.4	52.7	26.1	-	0.353	0.181	-
***p*-Menth-2-ene**	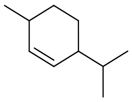	3.3	50	26.9	-	-	0.172	-

Δ-3-Carene	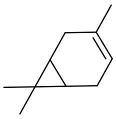	2.5	48.8	21.7	-	0.339	0.184	-
β-Pinene	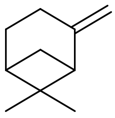	2.2	45.8	21.7	-	0.315	0.180	-
Limonene	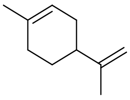	2.0	44.3	20.4	-	0.284	0.162	-
γ-Terpinene	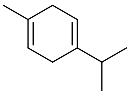	1.8	43.3	19.6	-	0.287	0.178	-
α-Terpinene	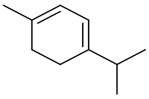	1.3	41.1	17.7	-	0.289	0.183	-
Terpinolene	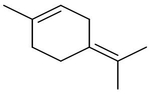	1.0	40.5	15.3	-	0.297	0.177	-
***p*-Cymene**	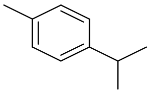	-0.4	31.6	10.8	-	0.259	0.174	-
Esters								
Ethyl decanoate	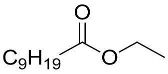	2.2	43.0	-	9.2	0.283	-	0.143
Ethyl dodecanoate	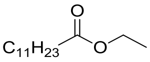	3.8	-	-	13.4	-	-	0.150
Decyl butyrate	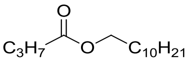	5.0	-	-	16.8	-	-	0.161
Ethyl myristate	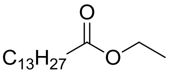	5.3	-	-	17.4	-	-	0.164
Hexyl octanoate	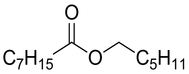	6.2	-	-	20.1	-	-	0.177
Myristyl propanoate	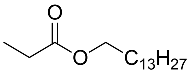	6.8	-	-	21.6	-	-	0.169
Ethyl palmitate	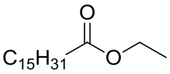	6.8	-	-	21.6	-	-	0.176
Butyl dodecanoate	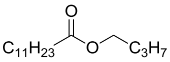	7.2	-	-	22.8	-	-	0.175
Isopropyl myristate	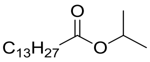	7.3	-	-	22.9	-	-	0.219
Ethyl oleate	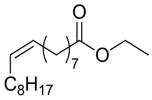	7.3	-	-	23.0	-	-	0.166
Octyloctanoate	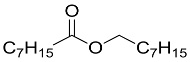	8.1	-	-	25.2	-	-	0.178
Hexyl dodecanoate	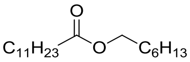	9.4	-	-	28.8	-	-	0.193
Diethers								
Dibutylether[a]	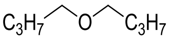	2.4	46.3	-	-	0.310	-	-
Dipentylether[a]	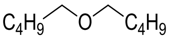	4.2	56.3	-	-	0.392	-	-
Dihexylether[a]	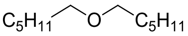	6.2	67.3	-	-	0.468	-	-

Diheptylether[a]	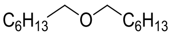	8.0	76.9	-	-	0.543	-	-
Dioctylether[a]	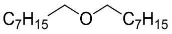	10.3	89.5	-	-	0.581	-	-
2-Alkanones								
2-Octanone[a]	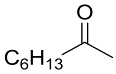	-3.4	14.6	-	-	0.220	-	-
2-Decanone[a]	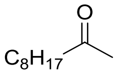	-2.1	21.8	-	-	0.222	-	-
2-Undecanone[a]	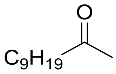	-1.3	25.8	-	-	0.231	-	-
2-Dodecanone[a]	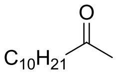	-0.6	29.8	-	-	0.235	-	-
Alkanenitriles								
Octanenitrile[a]	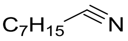	-1.7	23.7	-	-	0.301	-	-
Decanenitrile[a]	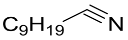	-0.5	30.1	-	-	0.301	-	-
Dodecanenitrile[a]	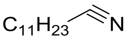	0.4	35.0	-	-	0.306	-	-
Fragrances								
Methyl cedrylether[a]	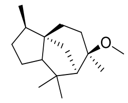	3.5	52.1	-	-	0.332	-	-
ω-Hexadecenlactonate[a]	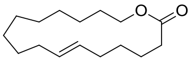	1.0	38.6	-	-	0.276	-	-
Menthyl acetate[a]	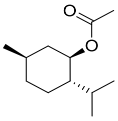	-0.1	32.5	-	-	0.244	-	-
Citronellyl acetate[a]	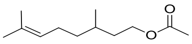	-0.2	31.9	-	-	0.252	-	-
Geranyl acetate[a]	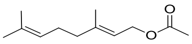	-0.6	29.9	-	-	0.255	-	-
Linalyl acetate[a]	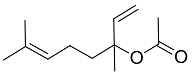	-0.8	28.4	-	-	0.248	-	-
Ethylene brassylate[a]	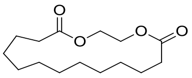	-1.0	27.4	-	-	0.264	-	-
α-Damascone[a]	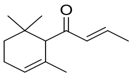	-1.2	26.3	-	-	0.264	-	-
Menthone[a]	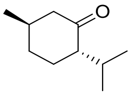	-1.5	24.8	-	-	0.277	-	-
Eucalyptol[a]	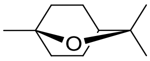	-1.6	24.4	-	-	0.213	-	-
Methyl dihydrojasmonate[a]	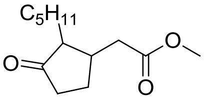	-1.7	23.8	-	-	0.258	-	-

Rose oxide[a]	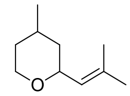	-1.7	23.6	-	-	0.249	-	-
β-Ionone[a]	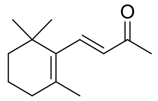	-1.8	23	-	-	0.248	-	-
***D*-Carvone**[a]	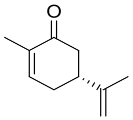	-3.1	16	-	-	0.249	-	-

[a] our work

Ethyl decanoate and 1-octyne were also investigated with $C_{12}E_6$ and linalool with $C_{12}E_8$. Their results are summarized in **Table 14**.

Table 14 Oils investigated with $C_{12}E_6$ and $C_{12}E_8$. The structure of the molecule is indicated, as well as its EACN, T* and γ*.

Compound	Structure	EACN	T*[°C]		γ*	
			$C_{12}E_6$	$C_{12}E_8$	$C_{12}E_6$	$C_{12}E_8$
Ethyl decanoate	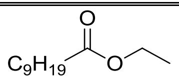	2.2	32.5	-	0.116	-
1-Octyne[a]	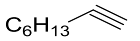	-2.6	16.2	-	0.118	-
Linalool[a]	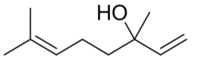	-11.4	-	9.5	-	0.256

[a] our work

3.6.2. Dependency of T* from functional groups, revised according to the effective packing parameter concept

The effective packing parameter offers a possibility to rationalize T* of a SOW system according to the influence of the oil on the interfacial film of surfactants. The beginning of this concept was in 1976 when Israelachvili *et al.* introduced an equation, which characterises the type of surfactant assemblies formed in aqueous solutions as a function of the surfactant structure.[33] The packing parameter P of a binary SW system is defined as $P = \nu_s/(\sigma_s l_s)$ where ν_s is the volume of the hydrophobic tail of the amphiphile and l_s is its length. σ_s is the equilibrium area per surfactant molecule at the interface of the micelle. For more complex SOW ternary systems, additional parameters, such as the nature of the oil or the presence of a co-surfactant, also influence the packing parameter of the surfactants.[171] Tchakalova *et al.* published a simplified form of the Constant Interfacial Thickness (CIT) model[43], the so called effective packing parameter $\bar{P}$:

$$\bar{P} = \frac{\nu_s + \tau\nu_o}{(\sigma_s + \tau\sigma_o)l_s} \qquad \textbf{(25)}$$

..where ν_0 is the molecular volume of the oil, σ_0 the area occupied per oil molecule at the micellar interface and $\tau = N_o^I/N_s^I$ is the number of oil molecules per surfactant molecule in the palisade layer. If $\bar{P} < 1$, an o/w microemulsion is formed, whereas for $\bar{P} > 1$ a w/o microemulsion appears. $\bar{P} = 1$ represents a bicontinuous microemulsion at the optimum formulation (T = T*). In **Figure 62** a schematic representation of the dependency of oil penetration and temperature on the effective packing parameter is shown. The dashed line represents thereby the optimum formulation at T*.

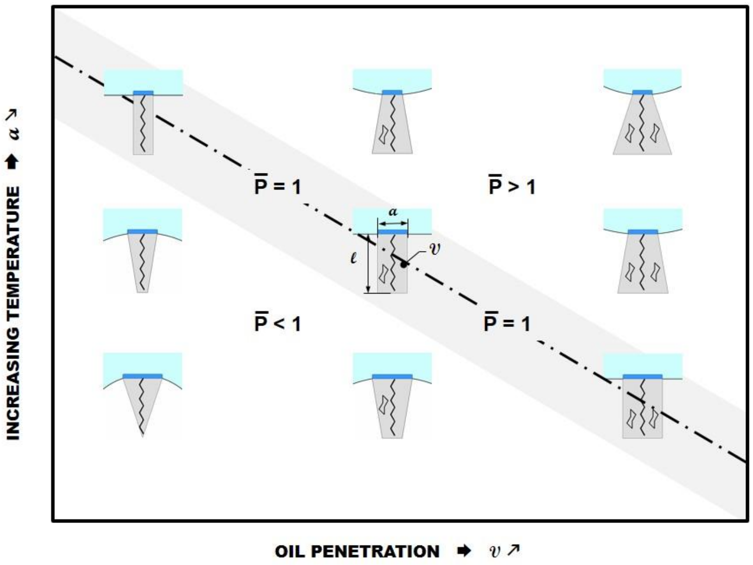

Figure 62 Schematic representation of the influence of oil penetration and temperature on the effective packing parameter. The dashed line indicates the optimum formulation at T*.[171]

According to **Equation 25**, the effect of a polar oil on T* can be explained. Oils - non-polar or polar - have the tendency to adsorb within the interfacial layer. Its affinity for the latter depends particularly on their structure and functional groups. Even *n*-alkanes are capable to penetrate between the hydrophobic surfactant tails, increasing the effective volume of them.[178] In fact the solubilisation behaviour of polar oils can occur in different ways. It may be predominantly solubilised in the micellar core or rather like a co-surfactant in the interfacial layer.[61] The affinity of the polar oil for the interfacial film determines τ in **Equation 25**. The bigger it is, the more oil can be found at the interface, and thus the stronger the influence of the oil on $\bar{P}$. Consequently an oil, which has high affinity to the interface, due to its structure and/or polarity, can be found more frequently in the palisade layer, which in turn will increase the effective volume of the hydrophobic tail ($\nu_s + \tau\nu_o$). This cannot be compensated by the oil contribution to the effective equilibrium area of the surfactant ($\sigma_s + \tau\sigma_o$), since σ_o is very small for oils and co-surfactants. On the other hand, oils with a low affinity for the interface, contribute only slightly to $\bar{P}$. Consequently the effective packing parameter can explain the evolution of the fish tail temperature, upon alteration of the hydrophobicity of the oil. T* is obtained at the optimum formulation, where the mean curvature is said to be zero and the packing parameter unity.[179]

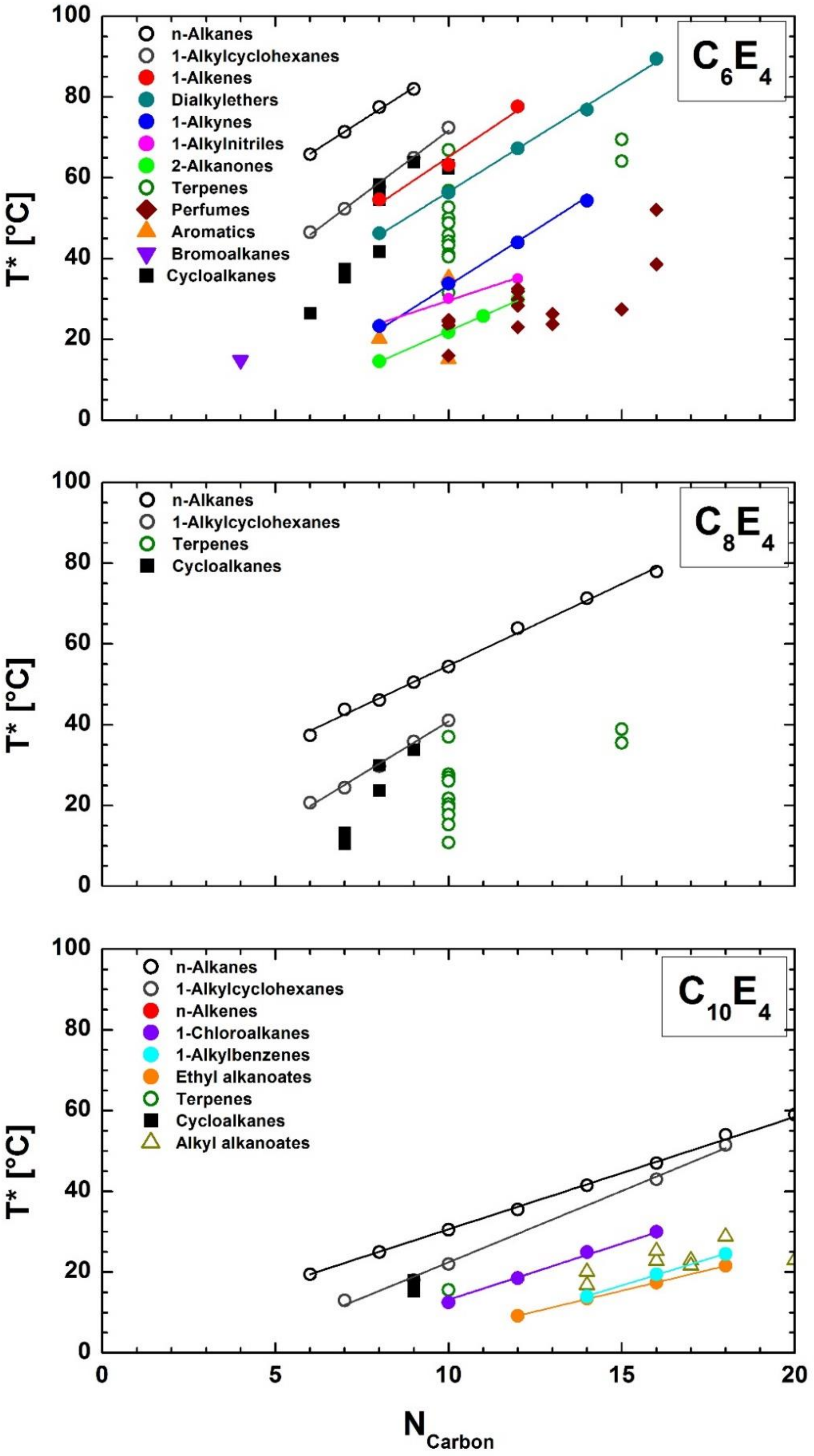

Figure 63 The fish tail temperature T* of various oils in dependence of their carbon number. The diagrams are shown for C_6E_4 (top), C_8E_4 (middle) and $C_{10}E_4$ (bottom).

With increasing oil penetration, the effective volume of the hydrophobic surfactant tail increases, while σ stays nearly unchanged. The system is thus inverting from an o/w microemulsion ($\bar{P} < 1$) to a w/o microemulsion ($\bar{P} > 1$). Same inversion can be obtained by increasing the temperature, which practically does not affect ν, but dehydrates the ethoxy head groups, making them less hydrophilic and thus decreasing σ. Consequently in a SOW system at T*, replacing the oil with a more polar oil, results in the formation of a w/o microemulsion. In order to return to the optimum formulation, one has to decrease the temperature.

The fish tail temperature T* is already determined for a huge variety of different polar oils, such as terpenes, 1-alkylbenzenes, 1-alkylcyclohexanes, 1-chloroalkanes or esters. In this work many further functionalised compounds as well as fragrances were investigated according to its phase behaviour and their EACN was determined. New EACN values were obtained for series of 1-alkenes, 1-alkynes, dialkylethers, 2-alkanones, alkanenitrils and various perfume molecules which are frequently used in perfumery, as well as several other halogenated, cyclic or aromatic compounds.

The fish tail temperature of all polar oils as well as *n*-alkanes is shown in **Figure 63** as a function of their carbon number. Series of homologues are connected by linear fits, as it is the case for *n*-alkanes, 1-alkylcyclohexanes, 1-alkenes, 1-alkynes, dialkylethers, ethyl alkanoates, 2-alkanones and alkanesnitriles. Striking is the distribution of the (sesqui-)terpenes, which consists of 10 respectively 15 carbon atoms. Their T*-value is distributed over a temperature interval of 40°C in the case of C_6E_4. Though they are rather small molecules with comparable size, their phase behaviour differs strongly, which can be attributed to their varying polarity, caused by branching, cyclisation or unsaturation. The heteroatom-containing perfume molecules seem to be distributed randomly. However the presence of an ether, ester or ketone group in connection with cyclisation, branching or unsaturation, results in a strong decrease of T*, which positions all of them below the curve of the 1-alkynes. In general every functionalization of an oil decreases T* in comparison to its *n*-alkane homologue. The magnitude of this decrease depends thereby strongly on its size, the functionalisations in the molecule, as well as on the amphiphile. Comparing the three surfactants, it can be seen, that there exist a trend towards lower *T**-values, with increasing hydrophobic chain, which is due to the decreasing hydrophilicity of the surfactant.

3.6.3. The EACN of polar oils and their dependency from the functionalization

All measured T*-values were used to calculate the EACN of the corresponding oil, using one of the correlation equations. The results are summarised for all series in **Figure 64**. It is assumed that the EACN augments linearly with increasing number of carbons. The intercept and slope of their fits is given in **Table 15**. There is a strong parallel correlation between several compound series. However 1-alkylcyclohexanes, ethyl alkanoates, alkanenitrils and 2-alkanones show a clearly visible deviation from the parallelism.

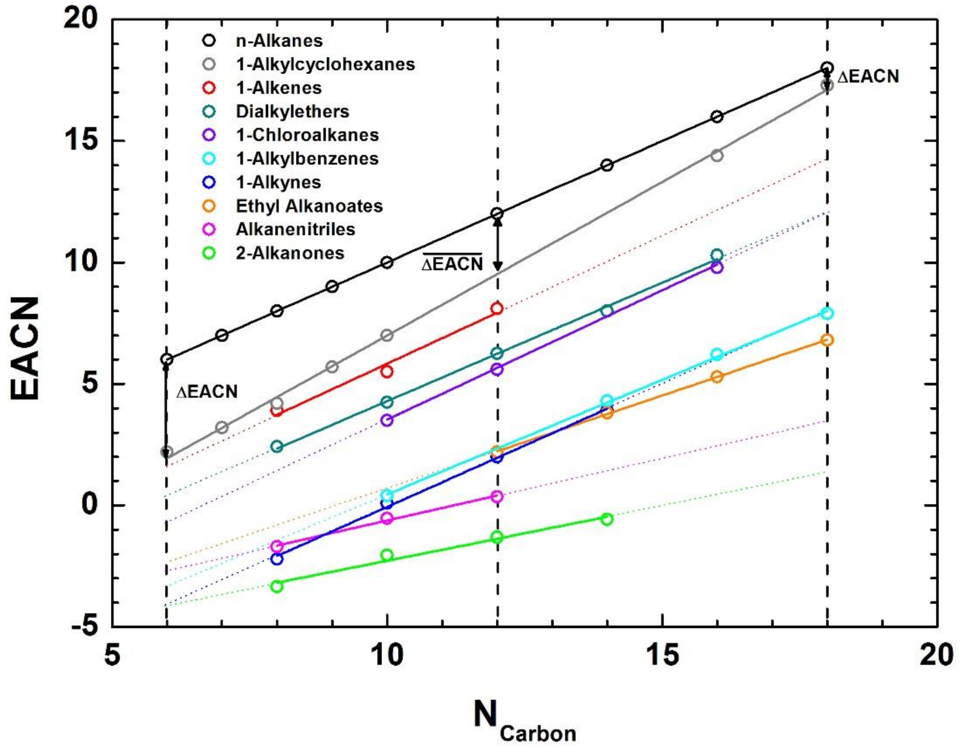

Figure 64 The EACN of *n*-alkanes and several series of functionalised oils in dependence of N_{Carbon}. The influence of the functional group on the EACN was determined by calculating ΔEACN for each N_{Carbon} between 6 – 18.

The data points were fitted linearly and in order to obtain a measure for the decrease in EACN upon functionalization, the EACN of all oils with a carbon number between 6 and 18 were calculated according to their fitting equation. Thereby $\overline{\Delta EACN^X}$ indicates the averaged EACN difference from its *n*-alkane homologue. It was obtained according to **Equation 26**.

$$\overline{\Delta EACN^X} = \frac{\sum_{N=6}^{18}\left(N - \left(a^X + m^X N_{carbon}\right)\right)}{13} \qquad \textbf{(26)}$$

..*where* a^X and m^X is the intercept and slope of the fit of compound type X. N_{carbon} signifies the number of carbon atoms of the observed polar oil, whereas N is the carbon number of the homologue *n*-alkane oil. The number 13 describes the quantity of oils, which were used for the calculation of $\overline{\Delta EACN^X}$. The latter can thus be used to classify the effect of the functionalization on the hydrophobicity of an oil with a carbon number between 6 and 18. The higher it is, the bigger is the effect of the functional group on its EACN. In **Table 15**, the effect of the different functionalization's on the EACN is shown. According to that, cyclisation has a rather small influence on the EACN, whereas the addition of a ketone group decreases the EACN strongly. The influence on the EACN follows this order: 1-Alkylcyclohexanes < 1-alkenes < dialkylethers ≈ 1-chloroalkanes <1-alkylbenzenes ≈ ethyl alkanoates ≈ 1-alkynes < alkanenitriles < 2-alkanones. However, as already seen in **Figure 64**, several types of compounds do not correlate parallel with *n*-alkanes. Since the data correlate very well linearly and do not scatter around the best fit, it is appropriate to use the standard deviation of $\overline{\Delta EACN^X}$ as an indication for the deviation from parallelism. Theoretical considerations with regards to the effective packing parameter may explain the obtained results.

Table 15 Summary of the intercept a^X, the slope m^X and $\overline{\Delta EACN^X}$ of the compound series, shown in Figure 64. $\overline{\Delta EACN^X}$ is a mesure for the decrease in EACN upon functionalization. Its standard deviation indicates thereby the parallel deviation from the *n*-alkane line.

Type of compound X	Intercept a^X	Slope m^X	$\overline{\Delta EACN^X}$	Standard Deviation
1-Alkylcyclohexanes	-5.7	1.3	2.5	1.0
1-Alkenes	-4.7	1.1	4.1	0.2
Dialkylethers	-5.5	1.0	5.8	0.1
1-Chloroalkanes	-7.1	1.1	6.3	0.3
1-Alkylbenzenes	-9.0	0.9	9.7	0.2
Ethyl Alkanoates	-7.0	0.8	9.7	0.9
1-Alkynes	-10.2	1.0	10.0	0.0
Alkanenitrils	-5.8	0.5	11.7	1.9
2-Alkanones	-6.8	0.5	13.4	2.1

a. 1-Alkylcyclohexanes

$\overline{\Delta EACN^X}$ is 2.5 for 1-alkylcyclohexanes with a standard deviation of 1.0. Thus the influence of cyclisation on the EACN is rather poor and decreases even with increasing alkyl chain length. The cycle is smaller than its linear homologue, which in turn results in an easier penetration into the surfactant layer. Thus τ is bigger, and the oil contribution to v_s is higher than for linear alkanes. However with increasing alkyl chain length, the probability of the cycle to be at the interface decreases, since there is no reason that the cycle is more polar than its linear homologue. Thus for long chain alkylcyclohexanes, their EACN is approaching those of linear alkanes. Furthermore it can be concluded that cyclisation – and branching as well – results in a lower EACN only because of the smaller size of the molecule.

b. 1-Alkenes

The 1-alkenes contain with their double bond in terminal position a π-electron cloud, which is responsible for their increased interfacial affinity. Their $\overline{\Delta EACN^X}$ is 4.1 ± 0.2. Thus it can be considered to proceed parallel to the *n*-alkanes. The volume of 1-alkenes is close to those of *n*-alkanes, so that the alteration in EACN is predominantly due to their stronger affinity for the interface, and thus the higher τ value.

c. Dialkylethers

Dialkylethers contain an oxygen in their centre, with two lone pair electrons, which have a high affinity for the interface. However due to its central position it is sterically hindered, which is assumed to result in a lower τ value, compared to ethyl alkanoates and 2-alkanones, where the functional group is close to the terminal position. Its $\overline{\Delta EACN^X}$ is thus equal to 5.8 ± 0.1 and consequently even smaller than the values of homo-atomic hydrocarbon oils, such as 1-alkylbenzenes or 1-alkynes.

d. 1-Chloroalkanes

1-Chloroalkanes have a similar effect as the dialkylethers on the EACN. Their $\overline{\Delta EACN^X}$ is equal to 6.3 ± 0.3. Due to their halogen atom, these molecules are slightly bigger than their alkane homologue, and due to their free electron pair they are also more affine for the interface. However the size of the chloride atom is very huge and thus the free electrons are distributed over a bigger space. Thus their affinity for the interface is smaller than it is for oxygen or nitrogen molecules.

e. 1-Alkylbenzenes

The $\overline{\Delta EACN^X}$ of 1-alkylbenzenes is 9.7 ± 0.2. Due to its aromatic cycle it has a strong affinity for the interface, and in contrast to 1-alkylcyclohexanes, it can be considered that the cycle is the part of the molecule, which enters the palisade layer, since there is a strong difference between the polarity of it and the alkyl chain. Appel *et al.* investigated via phase observation and scattering experiments, the influence of the alkyl chain on the ternary phase behaviour. He figured out, that the monophasic region is increasing with augmenting alkyl chain.[180] Furthermore Fletcher *et al.* showed that alkylbenzenes behave in diiodomethane like a surfactant, with a CMC and aggregation number.[181] Thus 1-alkylbenzenes can be considered as a weak co-surfactants in SOW systems.

f. Ethyl alkanoates

Ethyl alkanoates have a $\overline{\Delta EACN^X}$ of 9.7 with a standard deviation of 0.9. The difference in EACN is thus slightly increasing with augmenting carbon chain length, with respect to *n*-alkanes. Consequently the ester function has a bigger effect on the EACN for longer compounds, than for smaller, which is quite surprising. A possible explanation is given in **Section 3.5.4**.

g. 1-Alkynes

1-Alkynes contain a slightly acidic proton with a pK_a around 25. Together with the π-system, it is responsible for strong penetration into the interface, which results in a $\overline{\Delta EACN^X}$ = 10.0. It proceeds parallel to the *n*-alkanes, so that the length of the alkyne has no influence on σ_o. The addition of a triple bond has quite the same results on the EACN as the aromatisation or esterification.

h. Alkanenitriles

Alkanenitriles are very affine for the interfacial layer. Thus their $\overline{\Delta EACN^X}$ = 11.7 ± 1.9. Like 1-alkynes they exhibit an electron-rich π-system. Furthermore they contain a free electron pair, which is predestined for favourable interactions with water in the interface. As in the case of ethyl alkanoates, their $\Delta\overline{EACN^X}$ depend from the length of the alkyl chain. A possible explanation is given in **Section 3.5.4**.

i. 2-Alkanones

The group of molecules, which bear the strongest effect on the EACN are the 2-alkanones. The $\overline{\Delta EACN^X}$ is equal to 13.4 with a strong standard deviation of 2.1. Thus their EACN depend as well on the length of the hydrocarbon chain. It is interesting that ketones have a lower EACN than their homologue esters, although the latter consists of two oxygen atoms, and thus more free electron pairs, which may interact with the interface. However it can be also considered that their effective equilibrium area σ_o is smaller than in the case of esters, which in turn results in a weaker contribution to σ_s.

3.6.4. Positioning of polar oils at the interface in dependence of the alkane carbon chain.

In **Section 3.6.3**., it was shown that ethyl alkanoates, alkanenitriles and 2-alkanones have a non-parallel evolution of their EACN with increasing N_{Carbon} with regards to *n*-alkanes. Same was observed for 1-alkylcyclohexanes, with the difference that it approaches the reference curve of *n*-alkanes with increasing N_{Carbon}. This development was explained with the non-existing difference in polarity between the cyclohexane head group and the alkyl chain. However in the case of highly polar oils the head group has a strong affinity for the interfacial layer, which is with regard to **Figure 64** dependent from the alkyl chain length. In this section an attempt is made to explain this deviation from parallelism, by referring to the effective packing parameter. In **Figure 65** a demonstrative representation of the location of the polar head group of several alkanenitrils and 1-alkynes in the interfacial layer is shown.

Considering the results from **Table 15**, alkanenitriles decrease strongly the EACN, which can be attributed to their strong affinity for the interface. Same is valid for 1-alkynes, which has approximately the same influence on the interface as alkanenitriles for $N_{Carbon} = 8$. However for increasing N_{Carbon} the evolution of the EACN deviates. The EACN of 1-alkynes augments parallel to *n*-alkanes, whereas alkanenitrils have a lower EACN than expected with increasing N_{Carbon}. It can be assumed that 1-alkynes behave similar to *n*-alkanes, with the difference of being closer to the interface. With increasing carbon chain length, the polar head group of the oil moves towards the interior of the aggregate. Consequently τ decreases, since the affinity of the oil for the interface decreases. It is assumed that the decrease in τ happens proportional with increasing N_{Carbon} between all series which are parallel to *n*-alkanes. In the case of alkanenitrils, the hydrophilic head group has a stronger affinity for the interface and thus the alteration of the head group position in the interfacial layer is less affected by the carbon chain length. Hence the decrease in τ is weaker compared to 1-alkynes, which in turn results in a smaller EACN than expected and thus a deviation from parallelism with the reference curve of *n*-alkanes.

It is striking that the deviation from parallelism is only obtained for hetero-atomic hydrocarbons with strong hydrogen bond acceptors. It can thus be concluded that the difference in polarity between the polar head group and the alkyl chain imposes a relatively strong amphiphilicity to the molecule, which in turn results in strong co-surfactant characteristics. The only exception is found for dialkylethers, where the hydrogen bond acceptor is located in central position and thus sterically hindered. It is thus assumed that τ is already from the beginning small.

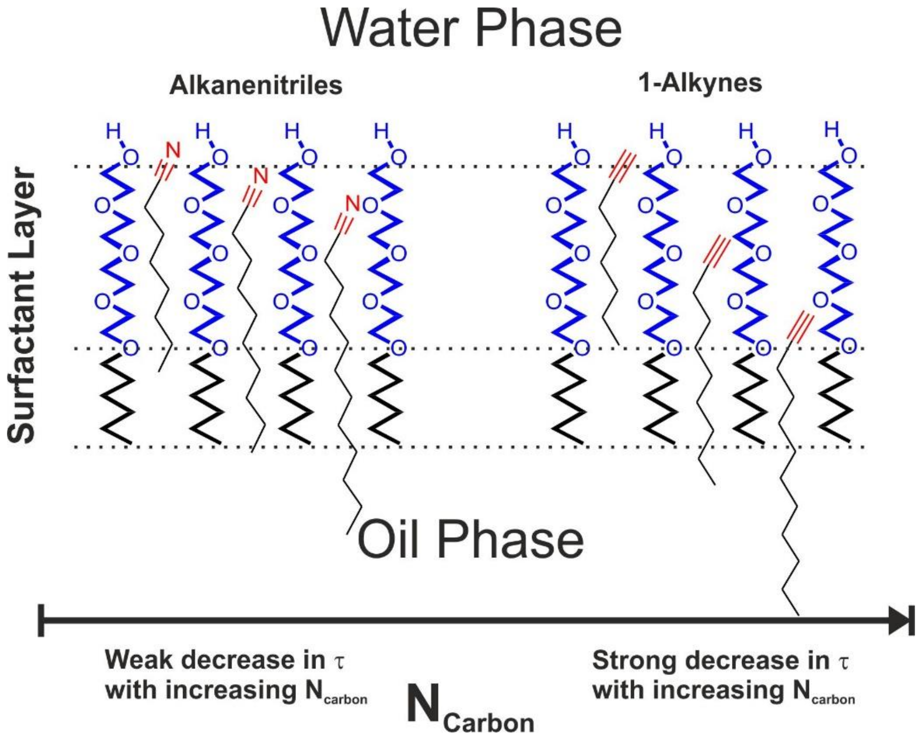

Figure 65 Schematic representation of the positioning of alkanenitriles and 1-alkynes in the C_6E_4 surfactant layer, in dependence of N_{Carbon}.

3.6.5. The influence of functional groups on the EACN of complex molecules.

The influences of functional groups on the EACN of simple oils, was also studied for complex oils. *p*-Menthane is a terpene molecule with a cycle. It can be used as a base molecule to identify the effects of further functionalization, such as unsaturation, esterification etc. These complex molecules are compared to linear homologues with same carbon number and same functionalization, as shown in **Figure 64**. Due to cyclisation and branching *p*-menthane has an EACN, which is four units lower compared to *n*-decane. Unsaturation decreases the EACN of *p*-menthane by 2.7 and of *n*-decane by 4.5. Thus it has not the same influence on the polarity of the molecule. However if we compare the EACN decrease upon several different forms of functionalization *i.e.* addition of an ester group, aromatisation etc. it can be seen, that the decrease is linear with respect to each other (**Figure 66**).

Ethyl decanoate deviates a bit stronger than the other compounds. It is expected that methyl undecanoate – which would be the real analogue to menthyl acetate - would lie closer to the curve, since Ontiveros *et al.* showed that the farther outside the functional groups, the lower the EACN.[166] Unfortunately the EACN value of this compound is not available yet. Nevertheless it can be clearly seen, that there are similarities between simple and complex molecules, regarding the relative decrease of the EACN upon functionalization.

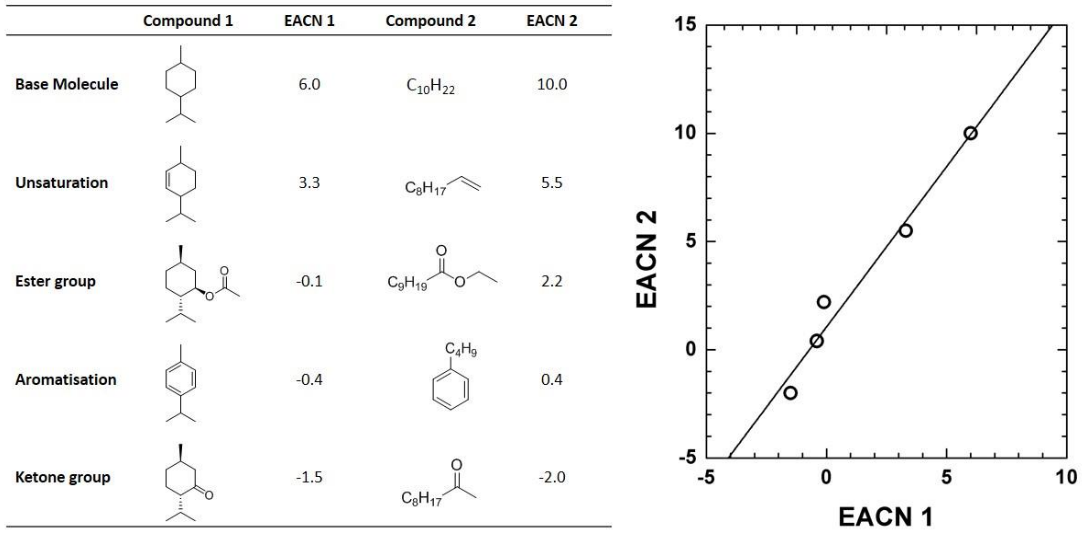

	Compound 1	EACN 1	Compound 2	EACN 2
Base Molecule		6.0	$C_{10}H_{22}$	10.0
Unsaturation		3.3	C_8H_{17}	5.5
Ester group		-0.1	C_9H_{19}	2.2
Aromatisation		-0.4	C_4H_9	0.4
Ketone group		-1.5	C_8H_{17}	-2.0

Figure 66 The influence of functionalising a complex molecule, compared to its linear homologue. Left: Compounds and type of functionalization, as well as their corresponding EACN values. Right: Linear correlation between the EACN of complex and linear oils.

3.6.6. The EACN of polar perfume molecules

Perfume molecules are complex oils, which exist in several different kinds of structures with various functionalizations. In this work the EACN of 14 hetero-atomic perfumes was determined. These compounds are characterised by their complex structure, which implements several functional groups simultaneously. In **Figure 67** a summary of all measured fragrances in combination with their location on an EACN scale is shown. First of all, it can be stated that all measured molecules can be found between 3.5 and -3.1, with a strong density between 0 and -2. The highest EACN value was obtained for methyl cedrylether, which consists of 15 carbon atoms and an ether group. The tricyclic structure with a methoxy groups is much more polar than for example diheptylether, which has an EACN of 8.0. Unlike the latter, the methyl cedrylether can penetrate stronger into the interface due to its terminal functional group. Thus the oil contribution to the effective volume of the amphiphile ($+\tau\nu_o$) is higher. The acetates are located very close together, between 0 and -1, although the structure of methyl acetate is very different of the other three acetates. Citronellyl acetate has one double bond less than geranyl acetate, but an EACN, which is only 0.4 higher. However the addition of a double bond to decane results in a decrease of 4 units. Considering that, it can be concluded that the influence of a functional group on the EACN is not additive, and depend strongly on the groups already present in the molecule. Same was already observed in the previous section. Another example can be found by comparing limonene with *D*-carvone, as well as *p*-menthane with menthone. Addition of a ketone group results in a diminution of the EACN by 5.1, whereas the addition of one to *p*-menthane decreases it by 7.5. Another

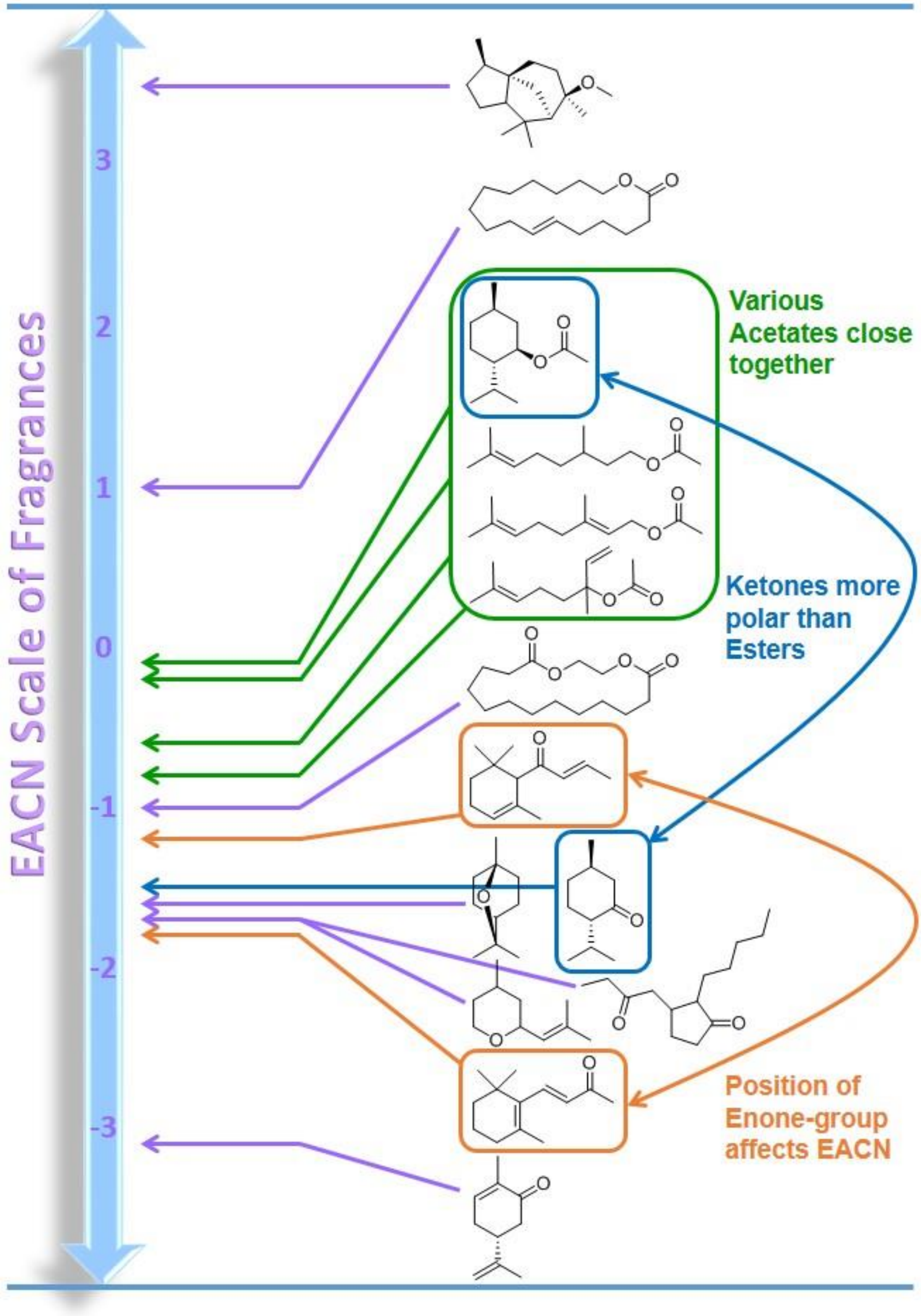

Figure 67 EACN scale of fragrances. Values were obtained between -3.1 for *D*-carvone and 3.5 for methyl cedrylether. The EACN values of perfume molecules are concentrated between 0 and -2, although their structures vary strongly.

remarkability is the difference in EACN between *β*-ionone and *α*-damascone. These molecules are isomers, which contain an enone group. The connection to the cycle is inverse, which results in a difference of -0.6 units. It was already stated elsewhere[135], that the location of the functional group affects the EACN, since the penetration may be hindered by a too central position in the molecule. Furthermore the same tendencies are observed as in the case of simple molecules. An ester imposes more polarity to a molecule than a double-bond, which can be seen by comparing ω-hexadecenlactone and ethylene brassylate. Furthermore menthyl acetate is less polar, than menthone. Thus it confirms the results from **Section 3.5.3.**, which has shown that the ketone group has a stronger influence on the polarity of a molecule, than an ester. It can be concluded that the smaller the molecule, the higher the quantity of functionalisations and the stronger the influence of those functional groups on the polarity of the compound, the lower is the EACN of the oil. Thus it is not surprising that *D*-carvone shows the lowest EACN of all fragrances, since it is small due to cyclisation and branching and is functionalised with two unsaturations and a ketone group. The latter has thereby the strongest effect on the EACN of all here investigated groups.

3.6.7. The System $C_{12}E_8$/linalool/water

Polar oils with a strong hydrogen bond donor, such as alcohols, were not considered so far, since they tend to penetrate strongly into the interface. Thus they show co-surfactant characteristics, which decrease strongly T*. For the non-ionic surfactants which were frequently used in this thesis it would decrease T* below 0°C, making it impossible to determine the fish tail of the SOW system. However a surfactant which is able to determine the fish tail temperature of certain alcohols is $C_{12}E_8$. It was already used to determine the phase behaviour of linalool and geraniol in an aqueous $C_{12}E_8$ solution.[61] Thereby it was found that geraniol decreases stronger T* than linalool. It is believed that geraniol penetrates deeper into the interfacial film due to its primary alcohol group, whereas linalool is sterical hindered due to its tertiary hydroxyl group.

In this part a fish cut of $C_{12}E_8$/linalool/water with WOR = 1 (w/w) was constructed. The optimal formulation line, as well as the monomeric solubility γ_{mon} and γ^* were determined by measuring the relative volume V/V_0 of the bicontinuous microemulsion in the three phase region.[56] Thereby V signifies the volume of the middle phase, and V_0 the volume of all phases together. The relative Volume increases linearly with increasing surfactant mass fraction. By measuring the volume of the middle phase for several surfactant contents, it can be extrapolated to a phase volume of 0 and 1, which represent γ_{mon} respectively γ^*. Knowing the latter two, the monomeric solubility of the surfactant in linalool $\gamma_{mon,linalool}$, as well as the weight fraction of surfactant at the interface $\gamma_{interface}$ can be calculated. $\gamma_{interface}$ and $\gamma_{mon,linalool}$ can be obtained from the following equations:

$$\gamma_{interface} = \gamma^* - \frac{\gamma_{mon}}{(1-\gamma_{mon})} \cdot (1-\gamma^*) \qquad \textbf{(27)}$$

$$\gamma_{mon,linalool} = \frac{\gamma_{mon} + \gamma_{mon,water}[\alpha(1-\gamma_{mon}) - 1]}{\gamma_{mon} + \alpha(1-\gamma_{mon}) - \gamma_{mon,water}} \quad \textbf{(28)}$$

$\gamma_{mon,water}$ can be neglected for $C_{12}E_8$, since its critical micelle concentration is with 0.004 wt.% very low. α signifies the weight fraction of linalool in water and linalool, which is here 0.5. Just one tube was prepared with equal masses of water and linalool, in order to save the very expensive surfactant. Then small amounts of $C_{12}E_8$ were added to the sample. Between each addition the phase borders were determined and if a three-phase region was present, the relative volume of the bicontinuous microemulsion was measured for each temperature step (0.5°C). Equilibration time was surprisingly fast with several hours up to one day.

In **Figure 68** (left) the relative volume is shown in dependency of the weight fraction of $C_{12}E_8$ in the mixture. By extrapolating to 0 and 1, γ_{mon} as well as γ^* can be determined. The temperature at which the relative volume of the bicontinuous microemulsion was measured is shown in **Figure 68** (right). In a system with same volume of water and oil, the optimum formulation is determined, when the excess phases have the same volume. In this case, same masses of linalool and water were used, so that the optimum formulation cannot be determined this way. However it turned out that the expansion of the three-phase region shows a maximum in dependence of the temperature (see **Experimental part**). It is not known if this maximum can be interpreted as the optimum formulation or if it appears due to alterations in the density of the middle phase, according to changes in its composition. However these maximums can serve as a support to find T* and T_{mon} (temperature at which the minimum amount of surfactant is solubilised monomerically). Since this line does not proceed straight and parallel to the x-axis, T* and T_{mon}, is obtained by exponential extrapolation to γ_{mon} and γ^***.**

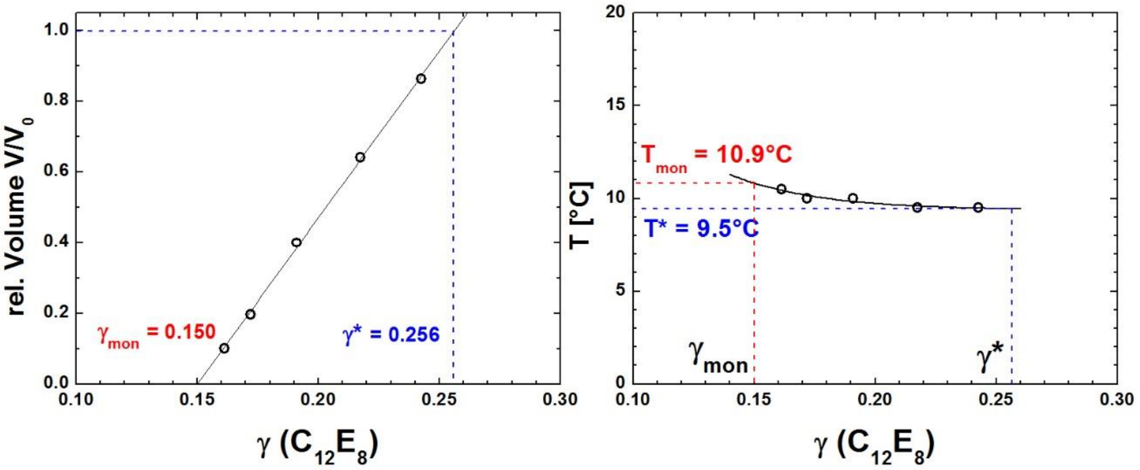

Figure 68 Left: The relative volume of the middle phase in dependence of the surfactant mass fraction. By fitting and extrapolating to 0 and 1, γ_{mon} and γ^* are obtained. Right: In order to obtain T* and T_{mon}, the curve was exponentially extrapolated to γ_{mon} and γ^*.

The previously obtained results can then be used to construct the complete fish diagram of $C_{12}E_8$/linalool/water, which can be seen in **Figure 69**. It is slightly distorted, which is caused by the partition of the constituents between the phases. Augmenting the weight fraction of $C_{12}E_8$ in the mixture results in a higher solubilisation of linalool and water in the bicontinuous microemulsion. The fragrance is due to its alcohol group very surface affine, which in turn results in a more hydrophobic interface. Thus the curvature increases and the optimum formulation decreases, imposing a distorted form onto the fish cut. It is striking that the monomeric solubility of the surfactant $C_{12}E_8$ in water and oil is extremely high, with a value of 0.15. Burauer *et al.* investigated the monomeric solubility of several C_iE_j's in octane and he found for $C_{12}E_j$ (j = 4-7) values between 0.004 and 0.007.[56] $C_{12}E_8$ is expected to be close to them, which in turn shows the huge influence of the oil polarity on the monomeric solubility of even big non-ionic surfactants. Consequently the efficiency of the system is rather poor for a long chain (poly)ethylene glycolether. A surfactant mass fraction of 0.256 is needed to obtain a monophasic microemulsion and only 0.125 can be found at the interface. These are values which lie in the region of C_6E_4 and polar oils with an EACN around 0. This indicates the problematic in efficiently solubilising weakly hydrophobic oils, with a co-surfactant character, such as linalool.

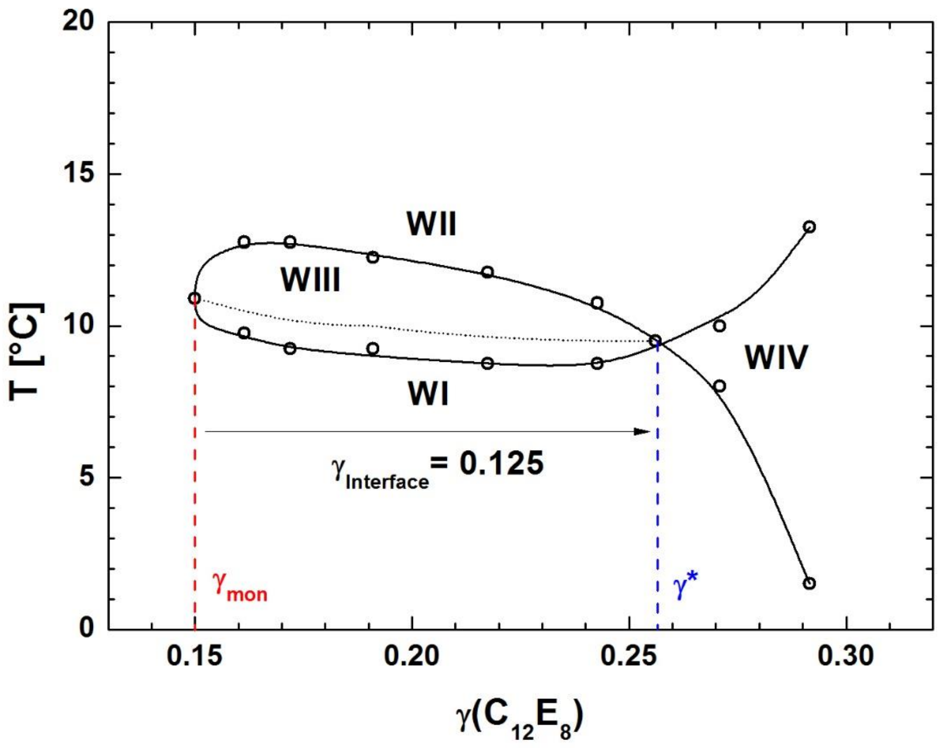

Figure 69 **Complete fish diagram of $C_{12}E_8$/linalool/water. It is slightly distorted and its three-phase body is relatively narrow. Due to the high monomeric solubility of $C_{12}E_8$ in linalool, only approximately 50% of the surfactant is located at the interface.**

Figure 70 The system $C_{12}E_8$/linalool/water at γ = 0.172. Left: 8 °C. Centre: 10 °C. Right: 14 °C.

The high monomeric solubility of $C_{12}E_8$ in linalool is demonstrated in an image in **Figure 70**. The WI system on the left possess a huge excess oil phase, arguing for a high content of the surfactant. In the WIII system in the centre, the excess oil phase stays nearly unchanged, while a middle phase appears. On the right the WII system is shown, where the upper phase increases only slightly in volume, arguing for a relatively small quantity of linalool in the WIII middle phase.

The three phase body of the SOW system can be displayed in a ternary phase diagram (**Figure 71**). Since $\gamma_{mon,water}$ is very small it can be neglected, which enables the calculation of $\gamma_{mon.linalool}$ according to **Equation 28**. The green striped triangle represents the three phase region. It has an uncommon form with γ^* and $\gamma_{mon,linalool}$ on the same height of the ternary diagram. The WI and WII phases are represented schematically and not measured in detail. The expansion of the WII region is probably much bigger than for the WI, since the excess oil phase contains a lot of $C_{12}E_8$. However this is just speculation and was not verified within this work.

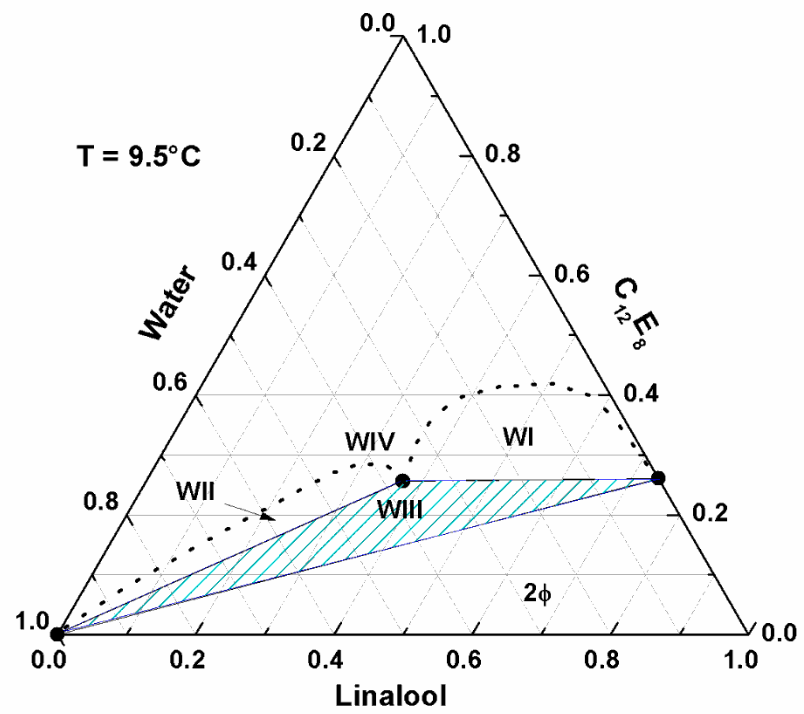

Figure 71 The ternary phase diagram of the $C_{12}E_8$/linalool/water system. The striped triangle represents the three phase body. The WI and WII phases are shown schematically.

The EACN of linalool can be determined according to the correlation curve of $C_{12}E_8$, which was built up from experimental data of Kunieda *et al.*[18,19], in combination with EACN values obtained from Bouton *et al.* and Ontiveros *et al.* In **Section 3.4** it was shown that the EACN is independent of the chosen (poly)ethylene glycol ether. Thus an EACN of 2.2 and 7.3 was allocated to cyclohexane, respectively isopropyl myristate to build up the correlation curve. Normally a calibration curve shall only be made of *n*-alkanes. Unfortunately there was not enough reliable experimental data to establish one, which consists only of *n*-alkanes, so that it was resorted to the experimental results isopropyl myristate and cyclohexane. The correlation curve is shown in **Figure 72** and possess a very low intercept. Consequently it is possible to assign an EACN of -11.4 to linalool, which represents the lowest ever measured EACN according to this method. Kunieda investigated as well the system $C_{12}E_8$/2-ethylhexanol/water and obtained a *T**-value of 18°C. An EACN value of -8.7 can thus be allocated. 2-Ethylhexanol is used as a fragrance in perfume composition. Furthermore it can be used as a starting material to prepare the solvo-surfactant ethylhexylglycerol, which is an approved amphiphile in cosmetics.[20.21]

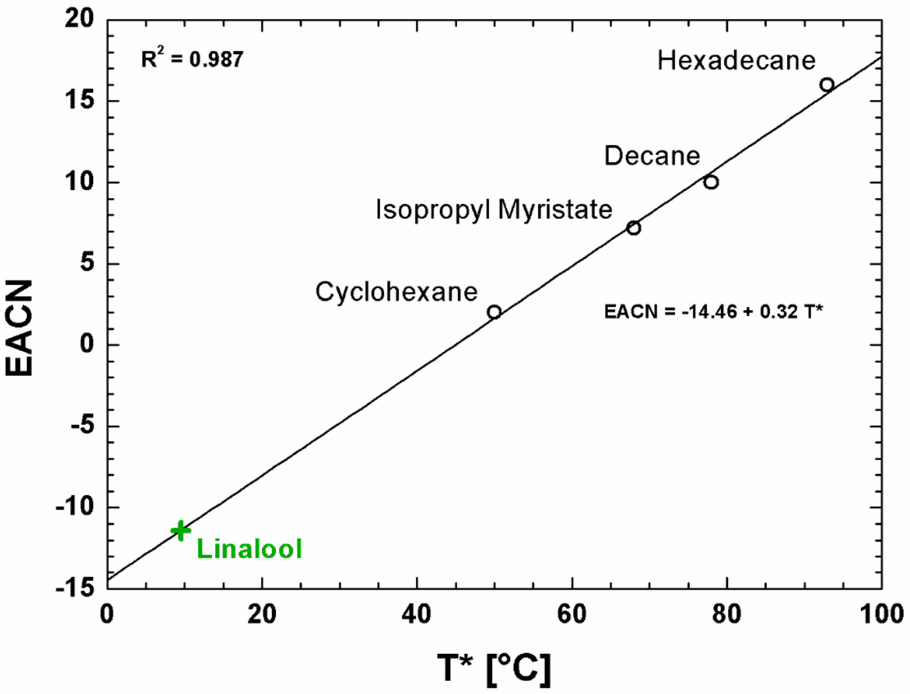

Figure 72 The calibration curve for $C_{12}E_8$. According to this curve, linalool possess an EACN value of -11.4.

3.6.8. The critical surfactant mass fraction γ* as a function of the EACN

With the determination of the fish tail temperature T*, the minimum surfactant mass fraction γ*, which is needed to obtain a Winsor IV phase, is also known. γ* is a measure for the efficiency of the system. The smaller it is, the more efficient is the surfactant, since less is needed to solubilise same amounts of water and oil. Kahlweit and Strey already investigated the influence of various surfactants on γ* and concluded that an increase in the hydrophobic chain of a C_iE_j surfactant, results in a strong diminution of γ*, whereas an increase in the number of ethoxy groups leads to a slight augmentation.[56,133] Based on these findings, it can be concluded that the more hydrophobic a surfactant, the higher its efficiency. The results previously obtained by Ontiveros[166], Bouton[171] and Queste[107] were united with the results obtained in this work, in order to investigate the influence of a decreasing EACN on γ^*. In **Figure 73** the γ^*-values of all measured oils with C_6E_4. C_8E_4 and $C_{10}E_4$ are shown in dependence of their EACN. The filled circles represent thereby the *n*-alkanes, whereas the hollow circles represent the polar oils. Each data set was fitted with an exponential fit, in order to highlight their trend. All curves show a non-linear behaviour. Initially the decrease in γ^* resembles a linear curve, but with decreasing EACN, they tend towards a plateau. However the data is extremely scattered around the fit, which indicates that γ^* does not only depends on the hydrophobicity of the oil. The data points obtained with C_6E_4 are particularly scattered for an EACN below 0, with γ^* between 0.2 and 0.3. For C_8E_4, the data points between -1 and 4 have almost constant γ^* values (0.18), whereas the oils measured with $C_{10}E_4$ are extremely scattered with γ^* values from 0.05 to 0.32 between an EACN of 2 and 15.

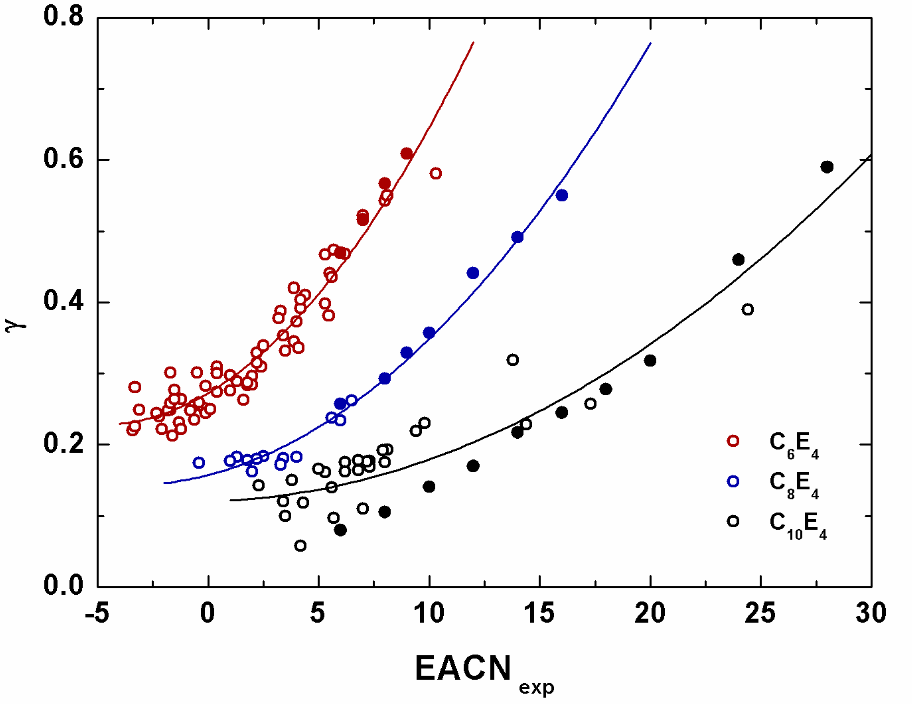

Figure 73 The critical mass fraction γ^* of C_6E_4, C_8E_4 and $C_{10}E_4$ with various polar oils (hollow circles) and *n*-alkanes (filled circles) in dependence of the EACN. The fit describe the overall trend of γ^* with decreasing EACN.

Despite the scattering of the data points, the general trend of the curve is observable. With decreasing EACN, the critical amphiphile mass fraction γ^* decreases as well, until the plateau is attained, at which γ^* stays nearly constant. Thus another effect than the decreasing hydrophobicity of the oil, influences the progress of the curve. In a ternary mixture the amphiphile partitions between oil and water. Considering a Winsor III system at the optimum formulation, most surfactant can be found at the interface, which is represented by the bicontinuous microemulsion. However some surfactant is also solubilised monomerically in the excess water and oil phase. Often in literature these excess concentrations are referred to as the critical aggregation concentrations in water, respectively oil.[56] The CAC's and CMC's of several C_iE_j's are shown in **Chapter 2**. For long chain surfactants ($i \geq 10$) the monomeric solubility in water can be neglected. C_8E_4 and C_6E_4 show higher CAC's with 0.23 wt.%, respectively 2.2 wt.%. However the loss of amphiphile is bigger in the excess oil phase. In literature it can be found that an excess octane phase consists of 4.9 wt.% C_6E_4, 3.6 wt.% C_8E_4 or 1.8 wt.% $C_{10}E_4$ at the optimum formulation.[56] Thus it can be considered that much amphiphile is lost in the excess oil phase and it may even increase with increasing polarity of the oil, since the interactions between the oil and the ethoxy groups of the surfactant become more favourable. The reason for the scattering, which is extremely high in the case of $C_{10}E_4$, can probably be attributed to the packing of the oils between and within the surfactant layers. An ester with a sterical hindered functional group in the centre of its molecule may take more space within the surfactant layer, as well as in the oily interior, than an ester with its functionalization in terminal position.

3.6.9. The monomeric solubility of C_6E_4 in fragrances

In the previous section, the dependence of γ* from the EACN of the oil was shown. It was concluded that the lower the EACN, the higher the monomeric solubility of the amphiphile in the oil phase. In this part the monomeric solubility γ_{mon}, as well as the amphiphile concentration at the interface $\gamma_{interface}$ were determined for several fragrances according to the procedure described in **Section 3.6.7**. However the optimum formulation line was not determined. Consequently γ_{mon} was interpreted by a parallel shift with respect to γ*, and not by the beginning of the optimum formulation line. Since previous studies have shown that the fish-head is flat blunted[166,168], it is assumed that γ_{mon} is not gravely affected by this approximation. The fish tail and thus T* were determined according to the procedure described in **Section 3.2**. The relative volume of the middle phase was then determined after equilibration at the given temperature. The fragrances methyl cedrylether, ω-hexadecenlactone, menthyl acetate, citronellyl acetate, menthone and *D*-carvone were used for the determination of γ_{mon}, $\gamma_{interface}$ and γ*.

In **Figure 74** the relative volume V/V_0 is shown in dependence of γ. The intersection with the x-axis at $V/V_0 = 0$ represents the monomeric solubility of the surfactant γ_{mon} in water and oil, whereas the intersection at $V/V_0 = 1$ represents γ*. Methyl cedrylether shows the biggest difference between γ_{mon} and γ*. The lowest difference is obtained for *D*-carvone, where the curve is almost parallel to the y-axis. According to **Equation 27** $\gamma_{interface}$ can be calculated. In **Figure 75** it is shown together with γ_{mon} and γ* in dependence of the EACN of the oil. Furthermore the values from literature for octane and hexyl methacrylate are added.[56,58] As shown previously, γ* is reducing with decreasing EACN, until the plateau is attained, from whereon it can be considered approximately constant. In contrast $\gamma_{interface}$ decreases constantly, whereas γ_{mon} increases. At high EACN values γ* and $\gamma_{interface}$ are very close together, whereas for low values a huge difference between these two concentrations appears. The difference can be found monomerically dissolved in the water and oil phase. γ_{mon} is steadily increasing and essentially intersects the $\gamma_{interface}$-curve at EACN $\approx$ 0. Thus from thereon more amphilphile exists monomerically dissolved than aggregated.

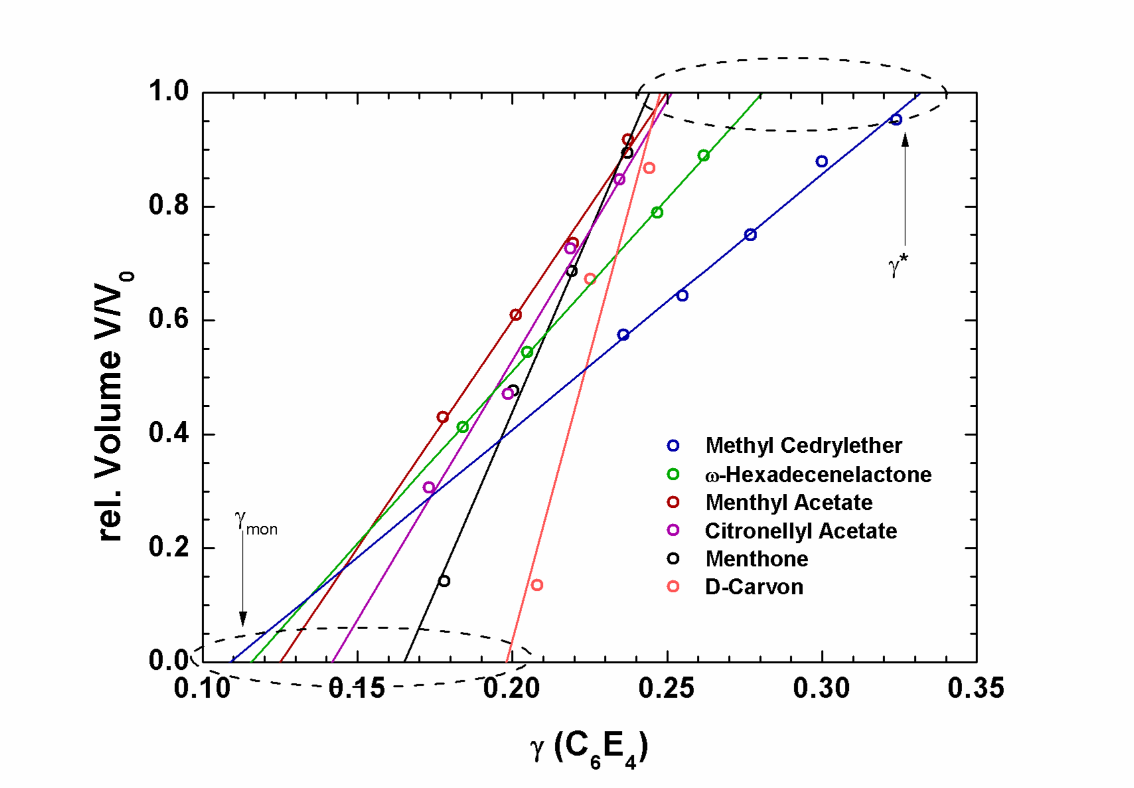

Figure 74 **The relative volume of the middle phase in dependence of the C_6E_4 mass fraction γ. By extrapolation, γ_{mon} and γ*can be determined. Metyl cedrylether has the lowest monomeric solubility of all here investigated fragrances, whereas *D*-carvone the highest.**

The results are summarized is **Table 16**. The reason for the higher monomeric solubility of C_6E_4 in polar oils, lies in the interaction of the oil with the ethoxy groups of the amphiphile. The addition of polar groups to the molecule, such as a double bond, ether, etc. results in a less unfavourable or even favourable interaction with the ether or hydroxyl functionalization of C_6E_4. Thus the latter can be more easily dissolved like a solute in a solvent.

Table 16 Summary of all critical mass fractions γ*, the amphiphile mass fractions at the interface $\gamma_{interface}$ and monomeric solubilities γ_{mon} for C_6E_4 in several polar oils.

Compound	EACN	γ*	γ_{mon}	$\gamma_{interface}$
Octane	8.0	0.474	0.049	0.447
Methyl cedrylether	3.5	0.332	0.109	0.250
Hexyl methacrylate	1.1	0.251	0.123	0.187
ω-Hexadecenelactone	1.0	0.281	0.116	0.143
Menthyl acetate	-0.1	0.250	0.125	0.146
Citronellyl acetate	-0.2	0.252	0.142	0.128
Menthone	-1.5	0.244	0.165	0.095
D-Carvone	-3.1	0.248	0.198	0.062

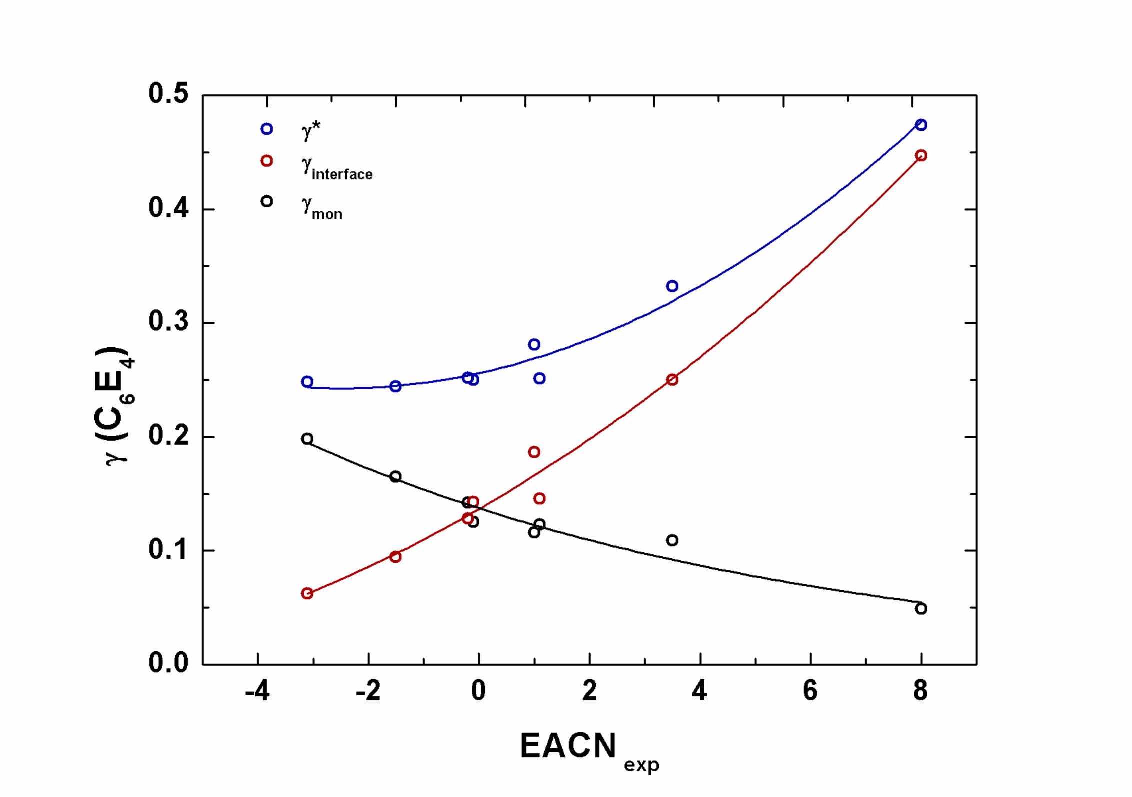

Figure 75 The critical mass fraction γ^*, the amphiphile (C_6E_4) mass fraction at the interface $\gamma_{interface}$ and the monomeric solubility γ_{mon} are shown in dependence of the oil's EACN. With decreasing EACN, γ^* attains a plateau because γ_{mon} increases. Thus less amphiphile can be found at the interface.

Knowing γ_{mon} and γ^*, as well as the phase borders from T* determination, the complete fish diagram can be constructed. In **Figure 76** they are shown for methyl cedrylether, ω-hexadecenelactone. citronellyl acetate, menthone and *D*-carvone. In terms of clarity, the fish cut for menthyl acetate was not shown. However it resembles strongly to the one made with citronellyl acetate. With decreasing EACN the three-phase region of the fish cut is decreasing in size. This region is thereby shrinking in width and height. The fish cut of *D*-carvone shows only a mini three-phase region. Its biggest expansion in temperature represents 0.3°C. Thus it is very close to the tricritical point, at which the three-phase region disappears.

According to **Equation 28**, $\gamma_{mon,oil}$ can be calculated. It was assumed that $\gamma_{mon,water}$ represents the critical aggregation concentration of C_6E_4, which is 0.023. Together with γ^*, the three phase triangle in the ternary SOW phase diagram can be constructed. In **Figure 77** they are shown for methyl cedrylether, citronellyl acetate and *D*-carvone. The ether shows the biggest expansion, which can be attributed to the high amount of amphiphile in the interface, as well as the relatively low solubility of C_6E_4 in the oil. In the case of citronellyl acetate, the triangle shrinks, since the amphiphile is more efficient in solubilising this oil. However the loss of monomerical dissolved amphiphile is as well bigger. The triangle resembles strongly to the three phase triangle of $C_{12}E_8$/linalool/water in **Figure 71**, as well as their fish cut's do. Long chain surfactant have the ability to form liquid crystalline phases, which may be unwanted in certain application. Thus their phase behaviour can be imitated with a short-chain amphiphile and another oil. If the oil is changed to *D*-carvone, the triangle shrinks further, but only because the

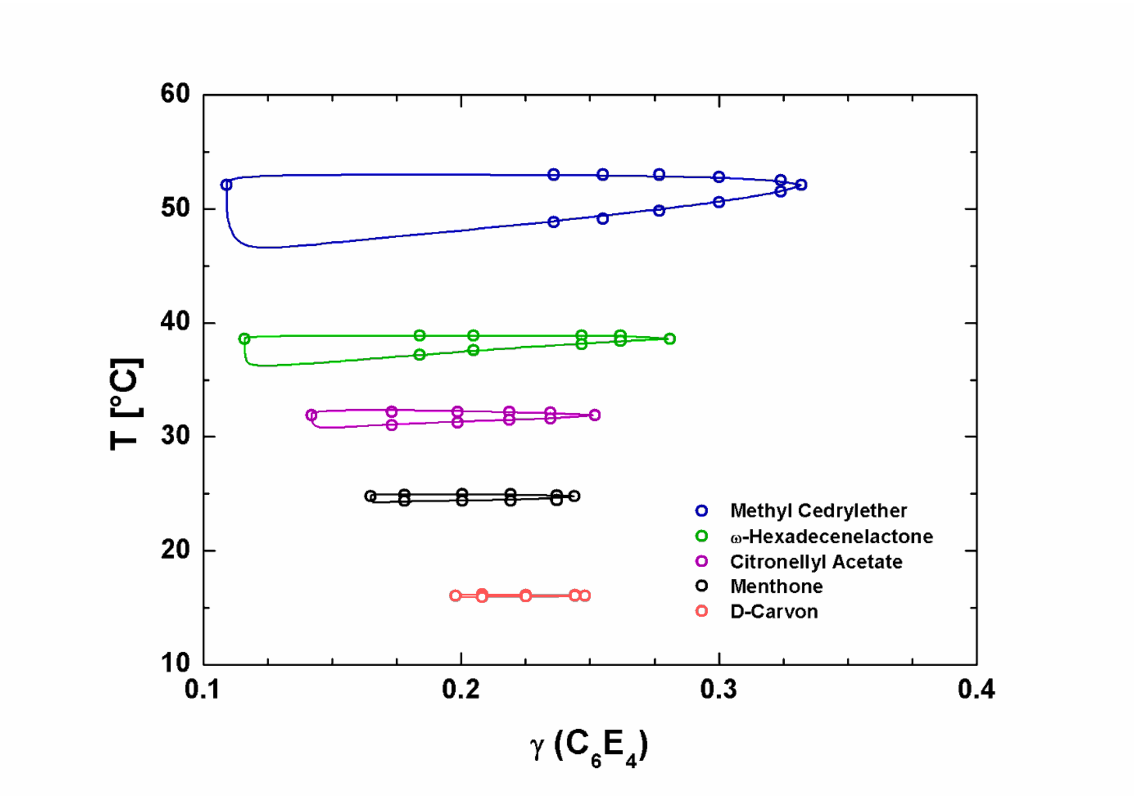

Figure 76 The three phase bodies of the fish diagrams for the C_6E_4/fragrance/water systems. With decreasing T* the expansion of the three phase body narrows. For *D*-carvone the largest expansion is 0.3°C.

monomeric solubility of the amphiphile increases. The efficiency stays the same. In conclusion to the previously obtained results, it can be stated that the polarity of an oil greatly affects the monomeric solubility of the amphiphile, as well as the expansion of the three-phase region. With increasing polarity of the oil, more and more amphiphile is dissolved monomerically in water and oil.

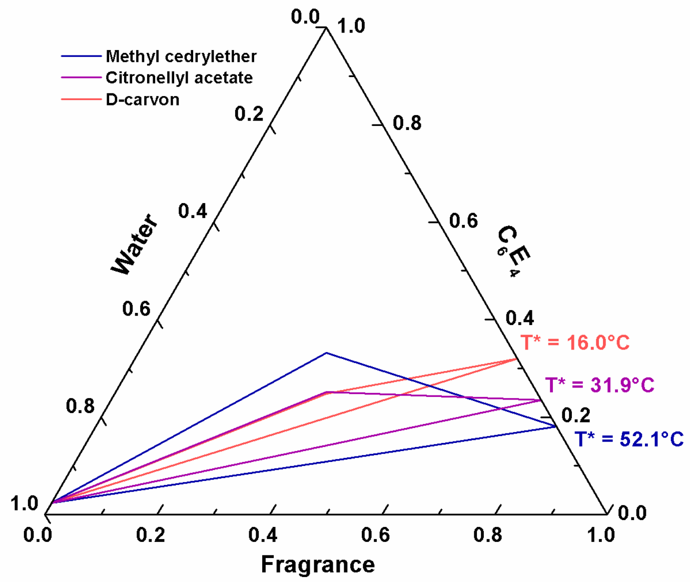

Figure 77 The location of the three phase region of several C_6E_4/fragrance/water systems in a ternary phase diagram. In terms of clarity only the triangles for methyl cedrylether, citronellyl acetate and *D*-carvone were displayed.

3.7. EACN predictions with COSMO-RS

In the last decades theoretical models have been established to predict properties of gaseous and liquid systems. In gas phase the interactions between molecules can be neglected, which is not the case for liquids. These types of systems are much more complicated, for which reason big efforts have been dedicated into the development of modelling software, which handle complex liquids. Four models have been used particularly, in order to compute these systems: Molecular Dynamics[186,187] (MD) and Monte Carlo[188] (MC) Simulation, group contribution methods (UNIversal Functional Activity Coefficient[189,190],UNIFAC) and dielectric continuum methods (Conductor-like Screening Model[191] (for Real Solvents[192]), COSMO(-RS)). Group contribution methods need the description of all functional groups and the interactions between each other, which is not always the case. MD and MC calculations need a complex parameterisation and the calculations are in general very time consuming. In contrast COSMO-RS is a rapid method, which allows the calculation of the chemical potential of all organic solute-solvent systems. Once the molecule is constructed, it is stored in the data base and can be reused again. In general the construction of a molecule takes some hours up to several weeks depending on the complexity of the molecule. The molecules used in this work took several hours up to 3 days calculation time, whereas huge complex molecules e.g. polymers. polycyclic compounds need weeks.

The dielectric continuum solvation model COSMO was invented by Klamt in 1991.[191] It gives acceptable results for solutes in non-polar solvents, but it is not adapted to solutes in polar solvents. Therefore the extension COSMO-RS was established in 1995. The COnductor like Screening MOdel for Real Solvents[192,193] combines quantum chemical calculations with statistical thermodynamics in order to compute the chemical potentials of molecules in solvents and mixtures. Solvent, as well as the solute are considered by COSMO-RS as an ensemble of molecules of different kind. For each type of molecule *X* a DFT calculation with the COSMO model is performed, which in turn gives the total energy E_i^{COSMO} and the screening charge density σ on the molecular surface. The molecules are then considered as an ensemble of pairwise interacting molecules in a virtual conductor. After a statistical and thermodynamic treatment, the specific interactions between the molecular surfaces are obtained.

Electrostatic interaction energy:

$$E_{es}(\sigma.\sigma') = \frac{\alpha'}{2}(\sigma + \sigma')^2 \quad \textbf{(29)}$$

Hydrogen bond interaction energy:

$$E_{hb}(\sigma.\sigma') = c_{hb} min\{0.\sigma\sigma' + \sigma_{hb}^2\} \quad \textbf{(30)}$$

E_{es} is also known as the misfit energy, which results from the fact that at perfect fit of the two screening charge densities σ and σ', the electrostatic contact energy is zero. The three parameters α', c_{hb} and σ_{hb} have been adjusted to a large number of thermodynamic data.[194] For the following considerations the interacting molecules are replaced by the pair-wise interactions of the molecule surfaces. The composition of this surface ensemble can then be described by the distribution function $p^X(\sigma)$ since every interaction depends on σ. This so-called σ-profiles are histograms, which translate the information from the 3-dimensional σ-surface into a 2-dimensional representation. Thus it describes the distribution of the screening charge density (SCD) on a molecular surface. If the solute is considered in contact with a piece of surface of an ensemble *S* (solvent), the chemical potential of the compound can be calculated. First the σ-potential $\mu_S(\sigma)$ of the solvent has to be obtained by an iterative solution of the following equation:

$$\mu_S(\sigma) = -\frac{RT}{a_{eff}} ln\left\{\int d\sigma'\, p_S(\sigma') exp\left(\frac{a_{eff}}{RT}\left(\mu_S(\sigma') - E(\sigma.\sigma')\right)\right)\right\} \qquad \textbf{(31)}$$

Thereby a_{eff} denotes an effective, statistically independent piece of contact area and $\mu_S(\sigma')$ describes the distribution function of the solvent. The σ-potential gives a detailed description about the preferences of a solvent *S* with surface of polarity σ. On a standard personnel computer it can be solved within milliseconds. By integration over the surface of each compound *X*, the chemical potential of *X* in a solvent *S* is obtained:

$$\mu_S^X = \int p^X(\sigma)\mu_S(\sigma)d\sigma + \mu_{comb,S}^X \qquad \textbf{(32)}$$

The combinatorial contribution $\mu_{comb,S}^X$ is a correctional parameter, which considers size and shape effects of the solute and solvent and normally it is very small. In can be summarized that COSMO-RS takes the σ-profile of a solute and the σ-potential of a solvent in order to obtain the chemical potential μ_S^X of a compound *X* in a solvent *S*, which in turn can be used to predict several solution properties, *i.e.* partition coefficient, vapour pressure, solubility etc. During the last years, this model gained increasing importance in scientific research, with the evidence of its relevant treatment of a wide range of solubility phenomena ranging from true solubility of molecular solutes – *i.e.* an organic UV filters in cosmetic oils[195] – to complex partition coefficients in micellar systems[196] – *i.e.* log P of various polycyclic aromatic hydrocarbons between water and micelles of TritonX-100.[197] Recently Smirnova *et al.* used COSMOmic, an extension of COSMO-RS, in combination with molecular dynamics to predict the partition coefficient of solutes in multiple self-assembled micelles of sodium dodecyl sulfate and cetyltrimethylammoniumbromide.[198] These kinds of highly sophisticated approaches are required for such complex systems but are only recommendable for the characterization of pure compounds.[194] In the case of complex mixtures, poorly-defined fluids or complex properties, alternative practical approaches have to be found, such as quantitative structure-property relationship (QSPR) models.

3.7.1. The σ-surface, σ-profile and σ-potential

COSMO-RS is able to generate the σ-profiles and potentials of various compounds and it ends up with the calculation of the chemical potential of a solute in a solvent, which in turn enables the prediction of physical properties e.g. partition coefficient etc.

The σ-profile gives a detailed image of the polarity and hydrogen bonding features of solutes, whereas the σ-potential provides a description of the solvent behaviour regarding electrostatics, hydrogen bonding and hydrophobicity.[199] The σ-surface is a three-dimensional representation of the van der Waals size of the molecule. Thereby, red coloured surface indicate the location of surface with hydrogen bond donor affinity and blue describes surface, which has an affinity for hydrogen bond acceptors. Green surface is hydrophobic surface and prefers surface with same polarity. (**Figure 78**).

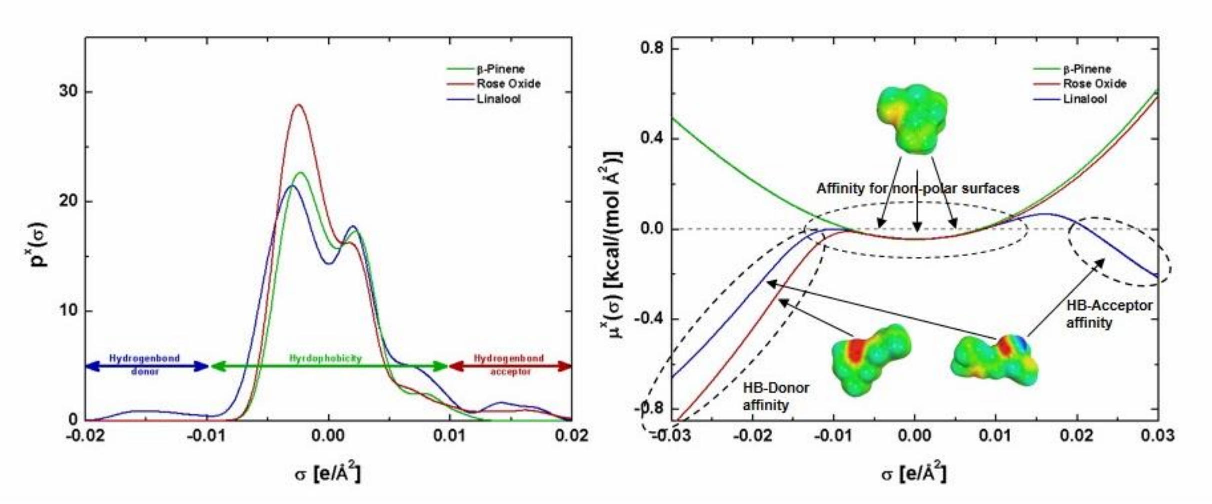

Figure 78 Left: σ-profile of β-pinene, rose oxide and linalool. The central peak indicates the non-polar part of a molecule, whereas the small peaks on the outside describe the hydrogen bond acceptor and donor capabilities. Right: The σ-potential of β-pinene, rose oxide and linalool. Only the latter has affinity for hydrogen bond donor and acceptors, whereas rose oxide is only affine for hydrogen bond donors. β-Pinene likes only to get in contact with non-polar surface.

The σ-profile is in its origin a histogram, which represents the distribution of surface with varying polarity on a molecule's surface. The higher the peak, the bigger the expansion of this kind of polarity on the molecular surface. By definition σ < -0.01 e/Å^2 describes a surface with hydrogen bond donor capabilities, whereas σ > 0.01 e/Å^2 defines a surface with hydrogen bond acceptor capability. In between the hydrophobic part of a molecule is given, whose size is proportional to the non-polar surface area. In **Figure 78** (left) β-pinene, rose oxide and linalool show a strong peak around $\sigma = 0$, which describes the hydrophobic part of the molecule. Rose oxide contains an ether function, which results in a flat peak for σ > 0.01 e/Å^2. Linalool contains additionally a hydrogen bond donor capability because of its alcohol group, which results in a small peak for σ < -0.01 e/Å^2. The differences, which can be already seen by observing the σ-surface, are also remarkable in the σ-potential (**Figure 78** (right**)**). β-Pinene shows a parabolic behaviour, which is characteristic for molecules without a strong acceptor or donor capability. Its potential is negative for screening charge densities close to zero. Thus it prefers solvents or solutes, which have a strong negative potential for their hydrophobic surface. This is the case for rose oxide and linalool. However they have also a strong affinity for hydrogen bond donors. Linalool even for hydrogen bond acceptors. The σ-potential is a good tool to identify a molecules affinities. In this work, it is used to classify an oil in three types. Oils without acceptor or donor capability are denominated as "non-acceptors", whereas oils with an acceptor capability are denominated as "acceptors". All the other oils which contain a hydrogen bond donor capability, with or without an acceptor, are denominated as "donors". The latter is not used in the following considerations, since there are few EACN's known of donors.

3.7.2. The σ-moment approach

QSPR models based on specific descriptors of COSMO-RS, the σ-moments, have already been successfully applied to several problems, such as blood-brain partitioning[194] or the estimation of the surface tensions of molecular liquids.[200] In this work the σ-moment approach was used to estimate the EACN of polar hydrocarbon oils. Thereby the EACN of several polar hydrocarbon oils was experimentally obtained and a multilinear regression analysis using COSMO-RS σ-moments was performed, in order to create a correlation equation which is able to estimate the EACN of a large variety of hydrophobic compounds.

For the prediction of molecule properties, the σ-profile of the solute, as well as the σ-potential of the solvent are needed. Unfortunately COSMO-RS is not able to generate the σ-profile and -potential of an interface composition in structurally sophisticated systems like amphiphile films, which makes it up to this day impossible to predict directly properties which are linked to interfacial penetration. However COSMO-RS offers a possibility to predict these complex properties indirectly, by using σ-moments. The σ-moments $M_i^X$are linear descriptors which can be used to build quantitative structure property relationship (QSPR) models. They are very well described by a Taylor-like expansion of the σ-potentials.[201]

$$\mu_S(\sigma) \approx \sum_{i=-2}^{6} c^i M_i^X \tag{33}$$

In **Equation 33** c^i representsthe σ-moment coefficient, which can be derived by multilinear regression analysis with sufficient data. They describe the solvent, which shall here represent the structured interface, whereas $M_i^X$is the *i*-th σ-moment of the solute *X*. They describe the various oils, which were used in this approach. The σ-moments i = [0,…,6] are obtained by integration according to following relationship:

$$M_i^X = \int_{-\infty}^{+\infty} p^X(\sigma)\sigma^i d\sigma \tag{34}$$

If a compound contains hydrogen bond acceptors or donors, hydrogen bonding moments $M_{acc/don}^X$ can be defined. There exist four sets of hydrogen bond descriptors and the first is obtained according to following considerations:

$$M_{-1}^X = M_{acc}^X = \int_{+\sigma_{hb}}^{+\infty} p^X(\sigma)(\sigma - \sigma_{hb})d\sigma \tag{35}$$

$$M_{-2}^X = M_{don}^X = \int_{-\infty}^{-\sigma_{hb}} p^X(\sigma)(-\sigma - \sigma_{hb})d\sigma \tag{36}$$

This replaces the screening charge density σ in **Equation 34**, by a simple function $f_{l,acc/don}(\sigma)$, which introduces a hydrogen bonding threshold σ_{hb}. If $\pm\sigma$ of a certain part of the molecular surface is higher than the threshold, it is considered as a hydrogen bond donor, respectively acceptor. σ_{hb} is an adjustable parameter obtained from **Equation 30**. There are in total four hydrogen bonding descriptor sets (l = [1,…,4]), and the second to fourth pairs are obtained by using fixed threshold values, as well as absolute values.

$$M_{l,acc/don}^{X} = \int p^{X}(\sigma) f_{l,acc/don}(\sigma) d\sigma \qquad \text{with}$$
$$f_{l.acc/don}(\sigma) = Abs\left[\begin{cases} 0 & if \quad \pm\sigma \leq (0.006 + 0.002l) \\ \pm\sigma - (0.006 + 0.002l) & if \quad \pm\sigma > (0.006 + 0.002l) \end{cases}\right] \tag{37}$$

The fixed thresholds have no physical meaning and were chosen by the developer of COSMO-RS. For a QSPR model only one set of hydrogen bonding moments shall be considered, since all 4 sets carry basically the same information. The only difference is the location of threshold, beyond which the descriptor is considered as a hydrogen bond acceptor or donor. In this work the second hydrogen bond donor and acceptor descriptors are taken for all considerations and linear regression analysis.

3.7.3. The σ-moments and their dependencies from EACN

There exist nine σ-moments, with partly well-defined physical meaning. M_0^X describes the surface area of a molecule. M_1^X the total charge, which is equal to zero for all the oils investigated in this thesis, since they carry no charge. M_2^X the total polarity of a molecule (not equal to the electric dipole moment) and M_3^X is a measure for the asymmetry of the σ-profile. M_{4-6}^X have no simple physical meaning, whereas M_{acc}^X and M_{don}^X describe the hydrogen bond acceptor, respectively donor capacities of a molecule.

The dependencies of the 8 relevant σ-moments from the measured EACN are shown in **Figure 79**. They are separated in three categories. First there are the linear alkanes, which serve as reference molecules. Then there are the polar oils, which contain no strong hydrogen bond acceptor and donor, referred to as non-acceptors in this thesis. At last there are the compounds, which contain a strong hydrogen bond acceptor but no donor, referred to as acceptors. No hydrogen bond donor containing molecules were investigated in this part here. The σ-moments of each oil can be found in the appendix.

Looking at the 0th descriptor M_0^X, it can be seen that it is increasing linearly with increasing EACN for *n*-alkanes, which is not surprisingly, since the addition of -CH_2-segments results in a constant increase of the surface area. However there is also a scattered but linear trend recognisable for non-acceptors and acceptors. They tend to have as well a higher EACN with increasing surface area. The acceptors lie thereby above the non-acceptors, which signifies the importance of their functional group. Comparing an acceptor oil with a non-acceptor oil with same surface area, the EACN of the first is smaller than of the latter, because of his functionalization. There are some exceptions, but the general trend is unquestionable. The influence of the acceptor on the EACN can be seen by looking at the 2nd descriptor. The *n*-alkanes mimic the base line. Lower polarity is hardly possible and only observed for

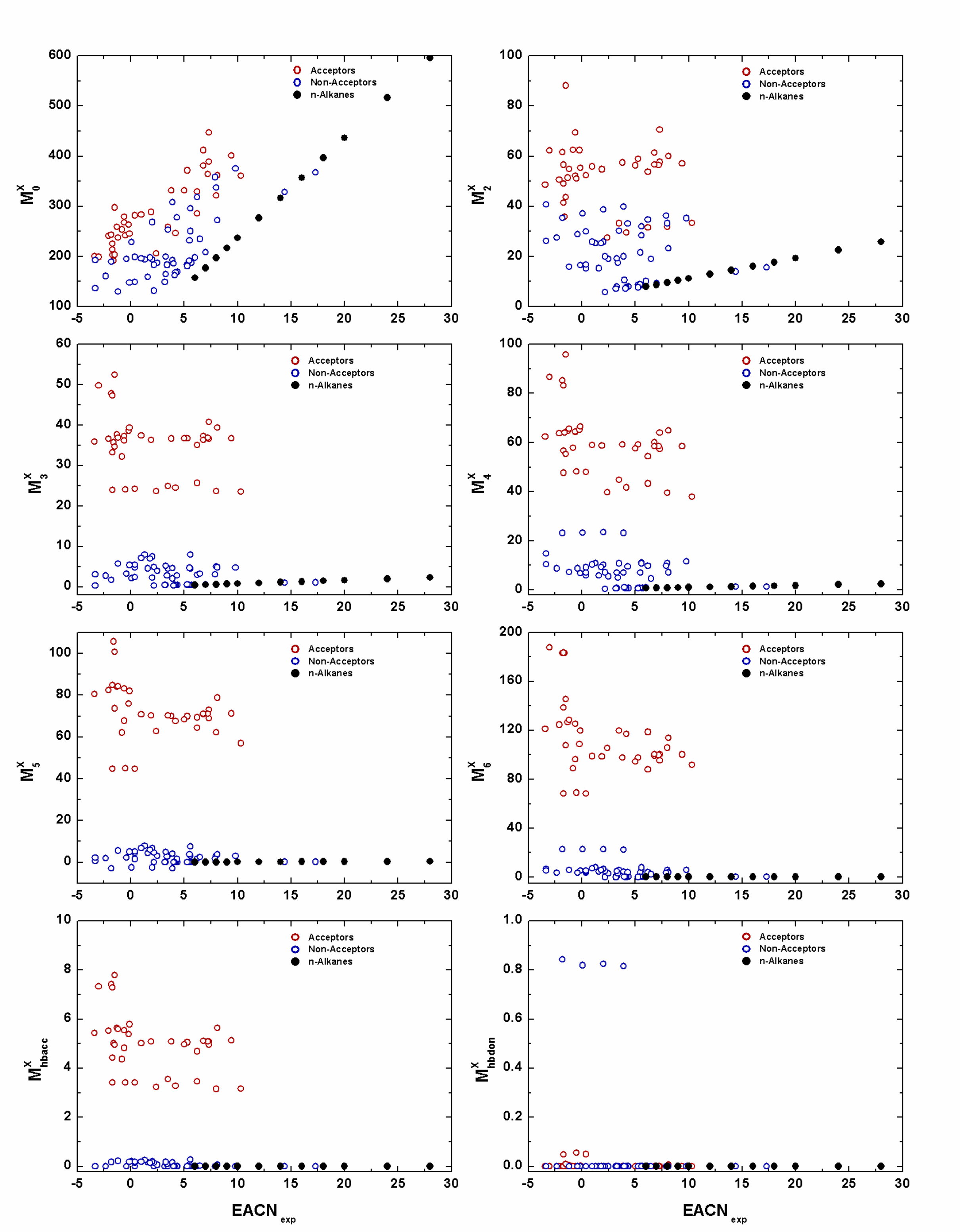

Figure 79 Scatter plot of the various σ-moments from the experimental EACN of polar oils. Due to their different penetration characteristics, the oils were separated in non-acceptors and acceptors. Furthermore the *n*-alkanes were highlighted in terms of having a reference.

long chain 1-alkylcyclohexanes. Acceptors and non-acceptors are apparently scattered randomly. However they are clearly separated around a value of 40, with few exceptions. Thus the lower EACN of acceptors at higher surface area can be explained by a higher polarity of the molecule, with regards to non-acceptors and *n*-alkanes. It is evident that the σ-moments M_0^X and M_2^X are crucial descriptors, since the EACN of an oil depends on its influence on the interface. Thus a bigger size hinders the molecule to penetrate the interface and increases the EACN, whereas a higher polarity of the molecule stands for a higher surface affinity, which in turn decreases the EACN. The 3rd descriptor is the first parameter, which cannot be assigned to a clear physical meaning. It describes the asymmetry of the σ-potential, which is given for the acceptors, whereas the non-acceptors and *n*-alkanes show rather symmetric σ-potentials. Thus it may serve as a descriptor, which separates the acceptors or donors from the compounds, which contain none of them. However compounds with both, acceptor and donor capabilities may have values over the whole range, e.g. linalool with 19, geraniol with 40 or even negative values for phenol (-23), since its donor capability is much stronger than its acceptor capability. Therefore the 3rd σ-moment seems to be rather a mathematical descriptor, which is also the case for M_{4-6}^X. In general only the M_0^X shows a correlation with the EACN. The rest - even M_2^X - is scattered rather randomly around two groups, acceptors and non-acceptors with *n*-alkanes. M_{acc}^X shows also same distribution, but with the difference that the non-acceptors have extremely low values, with a maximum of 0.3. These acceptor capabilities appear when a molecule is unsaturated or possess a halogen atom. The last descriptor is M_{don}^X and with some exceptions zero. The four lone standing non-acceptors are 1-octyne, 1-decyne, 1-dodecyne and 1-tetradecyne. Their hydrogen atom in terminal position is acidic, even though rather weak. Decanoic acid for example has a value of 5.3.

It can be concluded that the σ-moment approach offers 8 descriptors which may be interesting for the built up of QSPR models. Four of them are particularly interesting, because they have an easy understandable physical meaning (M_0^X,M_2^X,M_{acc}^X,M_{don}^X). The remaining descriptors have thus a rather mathematical function in a QSPR model.

3.7.4. Multi-linear regression and statistical validation of the selected descriptors

Multi-linear regression is a mathematical approach, for modelling the relationship between two or more independent (explanatory) variables and a dependent (explained) variable by correlating a linear prediction function to the set of the measured data.[202] The best fitted line is thereby obtained by minimizing the deviations from that line. The σ-moments were used to perform a multi-linear regression analysis, in order to obtain a model for the prediction of the EACN. M_0^X(i = -2 – 6) can be obtained from COSMO-RS calculations for each oil and has been used as independent variables in the regression, whereas the experimentally determined EACN values served as the dependent variable. Following expression was obtained for the prediction of the EACN.

$$EACN_{pred}^X = c_k + \sum_{i=-2}^{6} c_i M_i^X \qquad \textbf{(38)}$$

In **Equation 37** the coefficients c_k,c_i are estimated during the regression analysis. The coefficients are thereby adjusted in order to minimise the error between experimental and predicted EACN values. Together with the calculated σ-moments, $EACN_{pred}^{X}$ can be predicted. The goodness of the regression can be determined by calculation of the coefficient of determination R^2. In the case of just one explanatory variable, R^2 is calculated as follows.

$$R^2 = 1 - \frac{\sum_{i=1}^{x}\left(EACN_{exp}^{X} - EACN_{calc}^{X}\right)^2}{\sum_{i}^{x}\left(EACN_{exp}^{X} - \overline{EACN}\right)^2} = 1 - \frac{SSE}{SST} \tag{39}$$

$EACN_{exp}^{X}$ is the measured EACN value of compound X, whereas $EACN_{calc}^{X}$ stands for the calculated value according to the best fit. $\overline{EACN}$ is the mathematical mean of all experimental EACN values. The numerator includes the sum of squared errors of prediction (*SSE*) and it measures the deviation of the observation from the calculated values. The bigger it is, the worse is the model. The total sum of squares (SST) measures the deviation of the observations from the mean and is always higher than SSE. In **Figure 80** a demonstrative representation of *SSE* and *SST* can be seen. R^2 is a value between 0 and 1 and indicates the quality of prediction of the model.

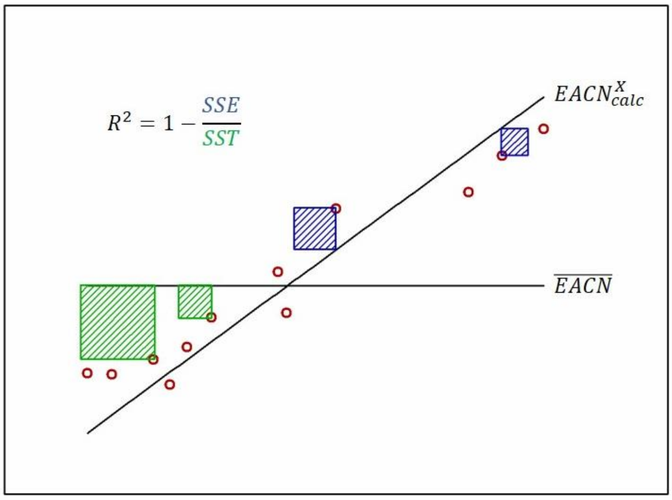

Figure 80 Demonstrative representation between the sum of squared errors (SSE) and the total sum of squares (SST). The lower SSE and the higher SST, the better the coefficient of determination R^2.

Another important error which measures the accuracy of the prediction is the standard error of the estimate *SEE*. It can be obtained by

$$SEE = \sqrt{\frac{\sum_{i=1}^{x}(EACN_{exp}^{X} - EACN_{calc}^{X})^2}{N-2}} = \sqrt{\frac{SSE}{N-2}} \tag{40}$$

Where *N* signifies the number of compounds in the regression. R^2 and *SEE* are two values, which permit to validate the quality of the regression analysis. While R^2 describes the overall correctness of the prediction, *SEE* gives an absolute value, which indicates the average deviation of the predicted values from the regression line.

Since R^2 and SEE give no information if the chosen regression represents the best fit according to the number of descriptors, the optimal number of parameters d_{opt} has to be determined, using the fitness function defined by Kubinyi[203]:

$$FIT = \frac{R^2 \cdot (N - d - 1)}{(N + d^2) \cdot (1 - R^2)} \quad \mathbf{(41)}$$

..where d represents the number of descriptors used in the regression. The variables R^2 and d are obtained from the multilinear regression. The higher *FIT* the better the fit. After each analysis, the most insignificant descriptor is removed and the regression is repeated. The significance of a descriptor is obtained by application of the t-test.[204] This test estimates if the null hypothesis H_0 or the alternative hypothesis H_1 is true. H_0 implies that there is no significant difference between two averaged data sets. Demonstrated in an example, it would mean that a certain descriptor in a regression analysis has no significant result on the outcome, and removing it would have basically no effect on the predicted value. H_1 signifies exactly the contrary. That is the descriptor is significant for the outcome of the regression. Whether H_0 or H_1 is applicable or not, is validated by the result of the *p*-value, which is obtained during the t-test. It indicates a probability between 0 and 1, and thus refers to the likelihood, whether or not the null hypothesis is true. The t-test can be performed automatically with a huge variety of software, such as SPSS Statistics or MS Excel.

$$\begin{array}{lll} p > 0.05 & H_0 = true & Parameter\ insignificant \\ p \leq 0.05 & H_0 = false & Parameter\ significant \end{array}$$

The border at 0.05 is historically fixed and in this work it was used for all t-tests. However there exist also borders of 0.01 or 0.10 etc. The t-test is no prove for the significance of a parameter, but it is highly unlikely that the null hypothesis is true for a *p*-value smaller than 0.05. **Figure 81** gives a schematic representation of the whole procedure. It can be summarized in 4 steps, which are necessary to obtain the best fit between experimental and predicted values.

1.) First the σ-moments M_i^X are obtained for each oil via COSMO-RS calculations. The EACN of an oil is experimentally determined by comparing the phase behaviour of a SOW system with a correlation curve.
2.) The independent variables M_i^X and the dependent variable $EACN_{exp}$ are used in a multilinear regression analysis. The coefficients c_k and c_i of the σ-moments are obtained, as well as R^2 and the SEE of the correlation.
3.) The t-test is applied to the descriptors in order to determine their significance for the correlation. The σ-moment with the highest *p*-value is thus the least significant and can be rejected. Step 2.) and 3.) is repeated until only one descriptor is left.

4.) The fitness of the correlation is calculated for each d, with the corresponding R^2. The highest FIT describes the best fit with the optimal number of descriptors d_{opt}.

It is important to have a sufficient number of experimental data to obtain a statistically relevant and stable model (N > 20). The Fitness Function works very well for independent descriptors. However it might not give the actual best fit, if some descriptors are dependent of each other. In the case of few descriptors the obtained best fit can be checked upon manual selection of those, in order to verify if other combination give better results.

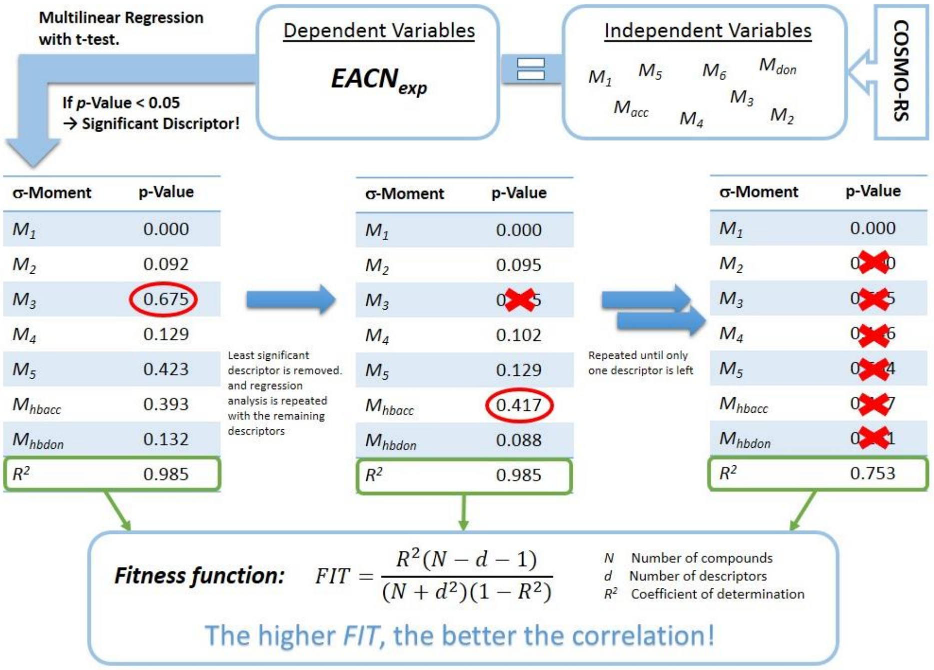

Figure 81 Schematic representation of the procedure to obtain the best fit. After the multi-linear regression with independent and dependent variables, a t-test is executed and the least significant descriptor is rejected. The best fit with the optimal number of descriptors d_{opt} is obtained for the maximum FIT value.

3.7.5. EACN prediction of polar oils

Several multi-linear regression analysis were performed in order to obtain a QSPR model for the prediction of the EACN of several oils. The non-acceptor and acceptor oils were used separated and together in the regression, in order to highlight the strengths and limitations of the models. The accuracy of the models was verified with a validation set. 8 non-acceptors were chosen, consisting of squalane, squalene, 1-octadecene, cyclodecane, decalin, *cis*-cyclooctene, 1-phenyl-butyne, 1-bromo-3-methylpropane. For the acceptors, molecules were chosen, which were already investigated by other groups in literature. Three diethers were chosen, namely dipropoxybutane, dibutoxyethane and dipropoxyethane.[205] Furthermore hexyl methacrylate was used in the validation set.[58]

a. EACN Prediction of Polar Oils without Acceptors

σ-Moments of 56 non-acceptor oils were generated with COSMO-RS. Their EACN values were determined experimentally. A multilinear regression analysis was performed and the best fit was obtained by application of **Equation 41**. In **Figure 82** the R^2 and *FIT* values in dependency of d can be seen. *FIT* has its maximum for two descriptors, which represents d_{opt}. R^2 is basically constant between 2 and 7, and decreases strongly if the number of descriptors is reduced to one. The two last descriptors are M_0^X and M_2^X, which represent the surface area and the polarity of the molecule. Following equation for the prediction of the EACN of non-acceptor oils was obtained:

$$EACN_{pred1}^{X} = -4.0 + 0.070M_0^X - 0.33M_2^X \quad \textbf{(42)}$$

This equation makes also physically sense, since the surface area term is linked to a positive coefficient, which indicates that the EACN is augmenting with increasing size. In contrast the coefficient linked to the polarity is negative, which implies a reduction of the EACN with increasing polarity. This is the case for all types of functionalization, e.g. aromatisation, unsaturation.

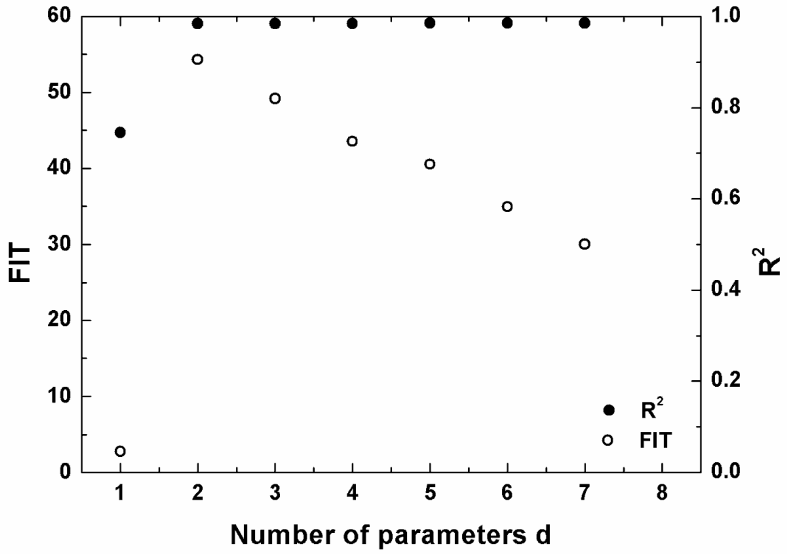

Figure 82 The dependence of *FIT* and R^2 from the number of descriptors *d*. The maximum *FIT* indicates the best fit.

Figure 83 shows the correlation between predicted and measured EACN. The training set represents the 56 oils, which were used in the multi-linear regression. Based on these results, the confidence and prediction bands were calculated. The confidence bands signifies a 95% probability that the best fit between experimental and predicted values lies within these bands. The interval is very narrow and symmetrical aligned around the best fit, which is represented by definition as $EACN_{pred} = EACN_{exp}$. An unsymmetrical behaviour can thus be an indication for a systematically error in the calculation of the model. The prediction bands indicates the 95% probability of the EACN values to be within this interval around the linear regression line. Consequently it can serve as a border to verify the correctness of the model. This was made by predicting the EACN of a validation set consisting of eight oils with **Equation 42**. These polar oils were not implemented in the initial regression analysis. Six oils were predicted well within the prediction bands. However two oils of the validation set did not fell into the interval. Squalane has a measured EACN of 24.4 and a predicted of 27.5. Its unsaturated homologue squalene has a measured EACN of 13.8 and a predicted of 10.4. Both oils exist in several conformers, which give different values in a range of approximately 2 EACN units. Unfortunately it is not known which conformation represents the real conformer in the micelle, so that the average is taken for each oil. A solution for this problem may be a conformational analysis via molecular dynamics simulation.[206] Furthermore COSMO-RS generates the σ-moments for the whole molecule. This may result in a problem for molecules, which have their polar functionalizations distributed uniformly over the whole molecule, such as in the case of squalene, where the unsaturation is not concentrated on one side of the molecule. It can be assumed that the polar double bonds of squalene are not all at the same time penetrated into the interface, since it is geometrically impossible. Thus M_2^X is overestimated by COSMO-RS for squalene, which in turn results in a considerable lower EACN than expected.

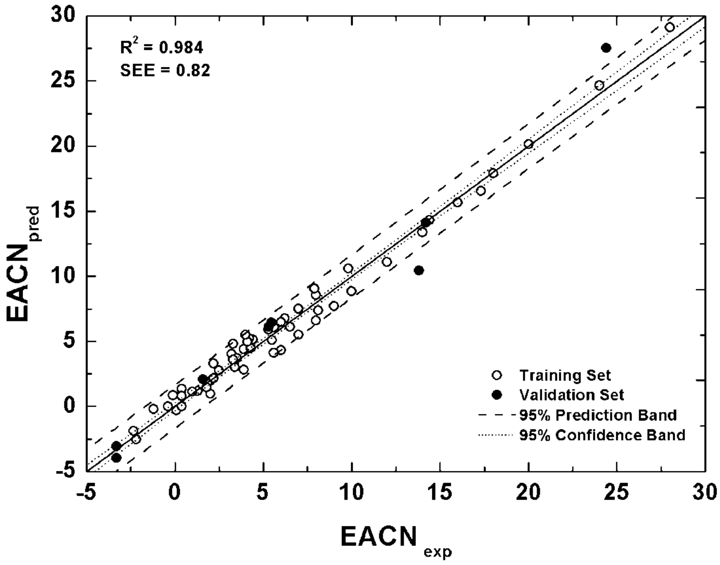

Figure 83 Experimental EACN versus predicted EACN for non-acceptor oils. The correlation is very good with R^2 = 0.984 and SEE = 0.82. However two of the eight oils of the validation set are not predicted correctly (Squalane and squalene).

Squalane on the other hand lies in a region, where few data was available and thus the process of error minimization during the regression analysis has a small statistical importance on the creation of the equation. Nevertheless polar oils, which are smaller, with less conformers are very well predicted by the model. With an R^2 value of 0.982 and an SEE of 0.82 the model shows also its statistical relevance according to accuracy.

b. EACN Prediction of polar oils with acceptors

Polar oils, which contain a hydrogen bond acceptor, such as esters, ethers etc. are more complex molecules. Due to the increased surface affinity, they tend to penetrate stronger into the interface, which is not only influenced by the type of functional group, but also by its location.[61,166,170] Therefore the acceptors are observed separated from the non-acceptor oils. 38 acceptors were used in a training set for the multi-linear regression. The validation set consists of 4 oils, whose T* values were obtained from literature.[58,205]

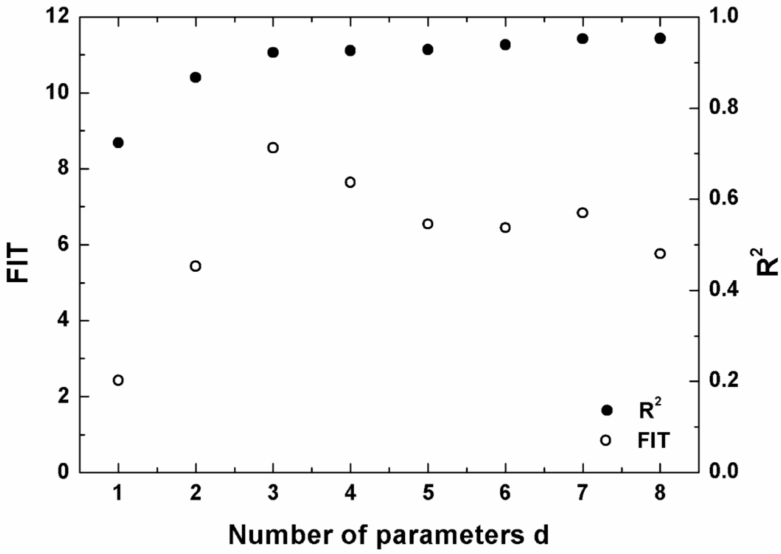

Figure 84 The dependence of *FIT* and R^2 from the number of descriptors *d*. Maximums are obtained at *d* = 3 and 7.

The fitness of the regression was determined and it can be seen in **Figure 84**, that there are two maximums obtained. The first appears at *d* equal to 7, whereas the second appears at d equal to *3*. The predictive equations are as follows:

$$\begin{aligned} EACN_{pred2}^{X} = {} & -8.1 + 0.030M_0^X + 0.64M_2^X + 1.33M_3^X \\ & -1.99M_4^X - 2.01M_5^X + 1.11M_6^X + 13.17M_{acc}^X \end{aligned} \quad \textbf{(43)}$$

$$EACN_{pred3}^{X} = -7.8 + 0.060M_0^X - 0.19M_4^X + 0.05M_6^X \quad \textbf{(44)}$$

Equation 43 depends on all σ-moments, except the donor descriptor, which is not surprising, since there are barely hydrogen donor capabilities present in the used compounds. Furthermore the equation has rather a mathematical sense, than a physical. The descriptors M_{3-6}^X have no physical meaning and the coefficient allocated to M_2^X is positive, which would signify an increase in EACN with increasing polarity. This is not consistent with common sense. **Equation 44** consists of three descriptors, whereof two have only a mathematical meaning. The correlations between experimental and predictive EACN values are shown in **Figure 85** and **Figure 86**.

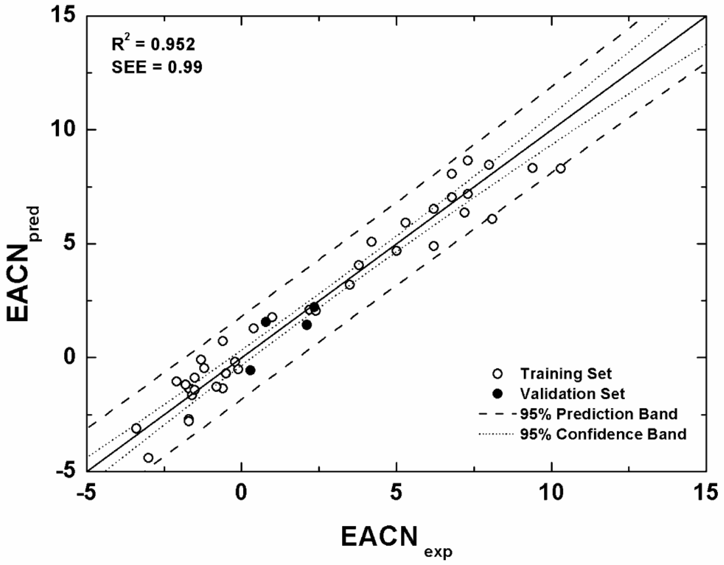

Figure 85 Experimental vs. predicted EACN for acceptor oils. The correlation was obtained with an equation consisting of 7 descriptors (Equation 43). The validation set is correctly predicted.

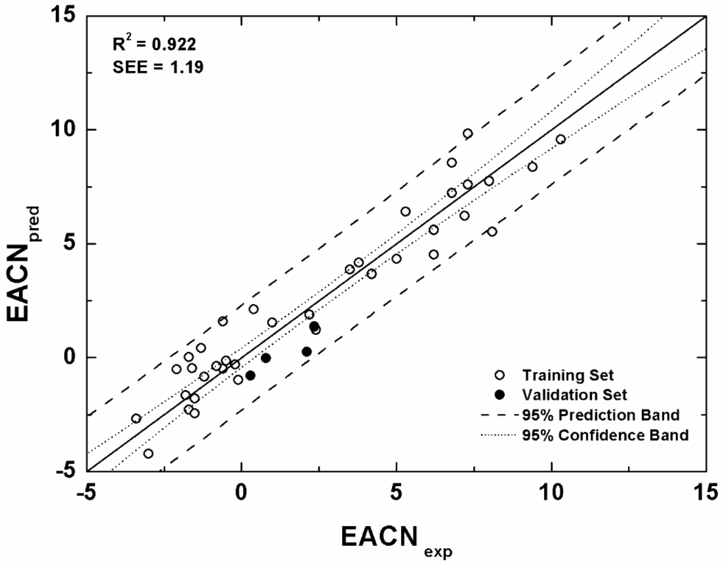

Figure 86 Experimental vs. predicted EACN for acceptor oils. The correlation was obtained with an equation consisting of 3 descriptors (Equation 44). The validation set is correctly predicted.

The 7-descriptor equation results in a good prediction with R^2 = 0.952 and SEE = 0.99, whereas the 3-descriptor equation has a worse prediction with R^2 = 0.922 and SEE = 1.19. However the latter shows a higher fitness, which in turn indicates, that only 3 parameters are necessary for a decent prediction of the EACN. On the one hand many descriptors may improve the prediction for compounds which lie in between the training set, but on the other hand it worsen the predictions for compounds which lie outside of the observed interval. In contrast a fit with few descriptors keeps also outside the data interval a relatively strong predictive power. For both models, the validation set was predicted within the prediction bands. It can be seen, that the confidence bands are moving apart for very low and high EACN values, indicating the uncertainty, due to small number of data.

As already stated above, the fitness function may not give the best fit, if descriptors depend of each other. In this case the best fit can only be obtained by try and error. Since the non-acceptors show a strong correlation with M_0^X and M_2^X, they were kept until the end during the multilinear regression analysis. **Figure 87** shows the calculated fitness of the correlation. Until the first maximum at $d = 7$ the points show same procedure as in **Figure 84**. In the following not the descriptor with the highest *p*-value is removed, since it is M_2^X, but the descriptor with the second highest probability for a true null hypothesis. Thus *FIT* is decreasing stronger compared to the removing of M_2^X. However continuing the procedure, the analysis results in a model with only two descriptors and even a higher fitness than in the case of $EACN_{pred3}^X$. This is an example for an interaction between two or more descriptors, which can be considered possible, concerning the proportional distribution of M_{-2}^X and M_{3-6}^X in dependence of the EACN.

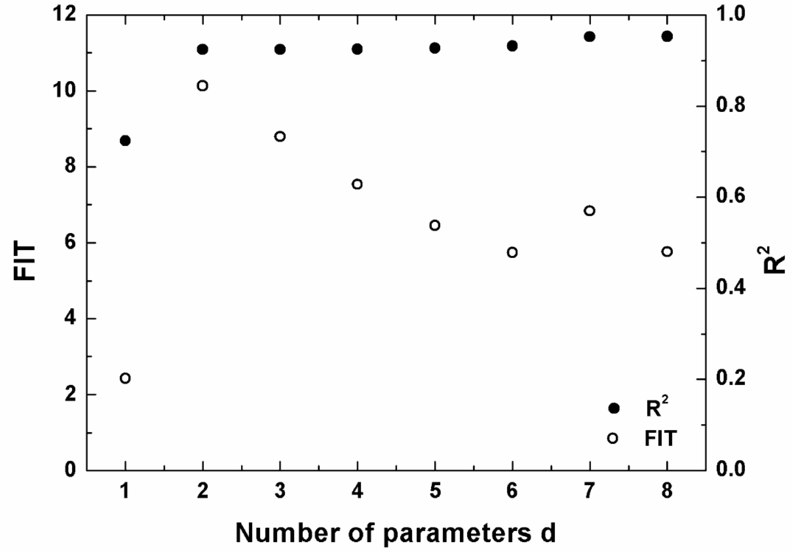

Figure 87 Dependence of *FIT* and R^2 from the number of descriptors *d*. M_0^X and M_2^X were kept in the regression analysis, which resulted in a maximum at *d* = 2, with a higher FIT than in Figure 84.

The obtained correlation function in **Figure 88** is slightly more accurate than in **Figure 86** with $R^2 = 0.924$ and SEE = 1.16. However it does not achieve the accuracy given by $EACN_{pred2}^X$ within the observed interval. Nevertheless only two descriptors are needed to obtain a decent prediction.

$$EACN_{pred4}^X = -6.8 + 0.060M_0^X - 0.15M_2^X \qquad \textbf{(45)}$$

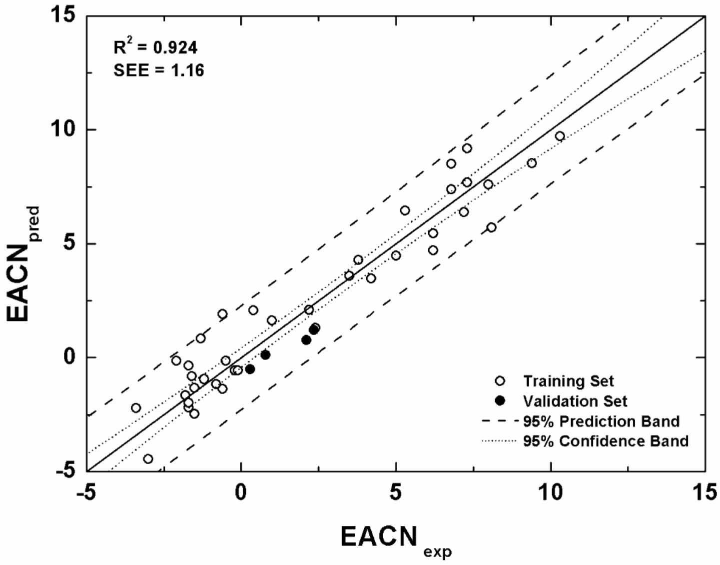

Figure 88 Experimental vs. predicted EACN for acceptor oils. The correlation was obtained with an equation consisting of 2 descriptors (Equation 45). The validation set is correctly predicted.

The equation has the same structure as $EACN^X_{pred1}$, but with different coefficients. The constant is approximately 3 units smaller, which indicates an overall smaller hydrophobicity of the used compounds. The influence of the surface area is slightly smaller, what makes on average 2.6 EACN units difference. The polarity coefficient is more than halved. Indeed M^X_2 is for acceptors on average 60% bigger than for non-acceptors. Thus the equation is very close to $EACN^X_{pred1}$, which gives rise to the assumption that the whole set of oils might be predicted acceptable with these two parameters.

c. EACN Prediction of all Hydrocarbon and Polar Oils together

Since **Equation 42** and **Equation 45** turned out to be very close in their structure, a multi-linear regression analysis was performed with all oils together. It is preferred to have a model, which is valid for all hydrocarbon oils, since the distinguishing in acceptor and non-acceptor oils, is only based on their σ-potentials, where a non-acceptor shows only affinity for hydrophobic surface, whereas acceptors as well for hydrogen bond donors. However there might exist exceptions for big molecules with several functionalisations, such as squalene. The latter is not correctly predicted by $EACN^X_{pred1}$, but $EACN^X_{pred4}$ predicts a value of 14.5, which is close to the experimental value of 13.8. Consequently all 94 oils were used in the training set, and all 12 oils were used in the validation set. The procedure was the same as in the previous regression analysis. The fitness was determined in dependency of the number of descriptors and gave a maximum at *d* = 4 (**Figure 89**).

$$EACN^X_{pred5} = -4.1 + 0.066M^X_0 - 0.29M^X_2 - 0.04M^X_6 + 1.37M^X_{acc} \quad \textbf{(46)}$$

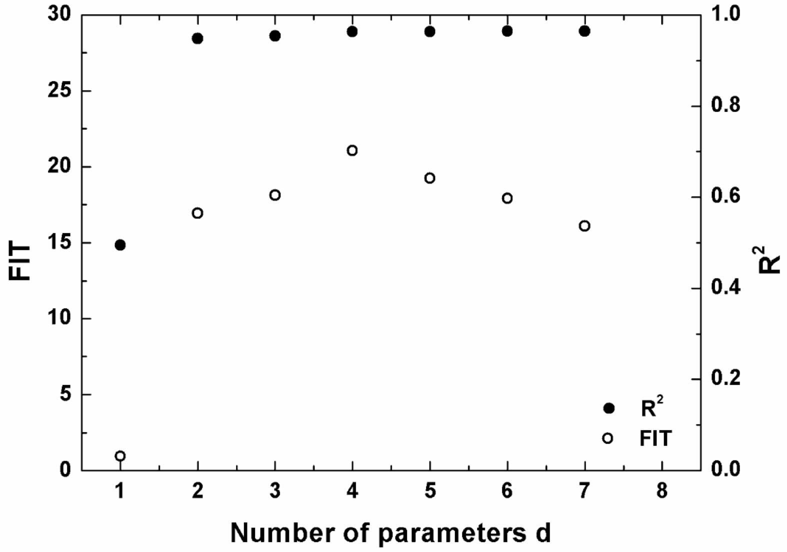

Figure 89 The dependence of *FIT* and $R^2$from the number of descriptors *d*. All non-acceptor and acceptor oils were used together in the regression analysis, which resulted in a maximum at *d* = 4.

As $EACN^X_{pred1}$ and $EACN^X_{pred2}$, the equation depends positively on the M^X_0 term and negatively on the M^X_2 term. M^X_{acc} is linked to a positive coefficient, which makes no sense, since an oil with a strong hydrogen bond acceptor shall have a stronger surface affinity, thus a lower EACN. Consequently M^X_{acc} has rather a mathematical meaning, which performs a correction to the predicted EACN**,** depending on whether it is an acceptor or non-acceptor. Furthermore M^X_6 was identified as a relevant descriptor, which has no physical meaning.

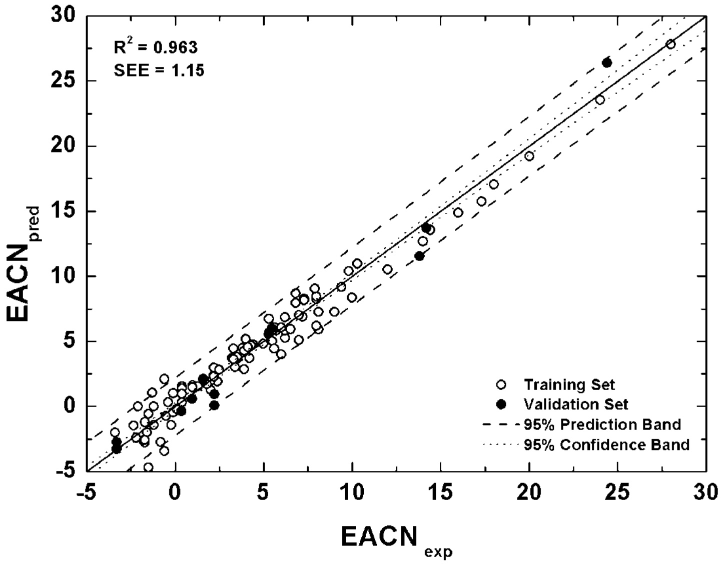

Figure 90 Experimental vs. predicted EACN for acceptor oils. The correlation was obtained with an equation consisting of 4 descriptors (Equation 46). The validation set is correctly predicted.

The correlation between experimental and predicted EACN values can be seen in **Figure 90**. The R^2 value is 0.963 and SEE is 1.15. The complete validation set lies within the prediction bands, including squalene and squalane, which indicates a higher robustness of the correlation compared to sources of error.

The quantity of descriptors was reduced to two, consisting of M_0^X and M_2^X, in order to compare the results with the previous models. Although their fitness is according to **Figure 89** lower compared to the 4 descriptor correlation, the result which can be seen in **Figure 91**, gave a decent correlation with $R^2 = 0.948$ and SEE = 1.35. Furthermore the whole validation set is predicted within the bands.

$$EACN_{pred6}^{X} = -5.1 + 0.065M_0^X - 0.22M_2^X \qquad \textbf{(47)}$$

The equation is a sort of averaged equation between $EACN_{pred1}^{X}$ and $EACN_{pred4}^{X}$ with relatively high scattering around the regression line. Thus the standard error of the estimate is relatively high. Nevertheless, the equation is able to predict the EACN of acceptor and non-acceptor oil properly with only two physical parameters.

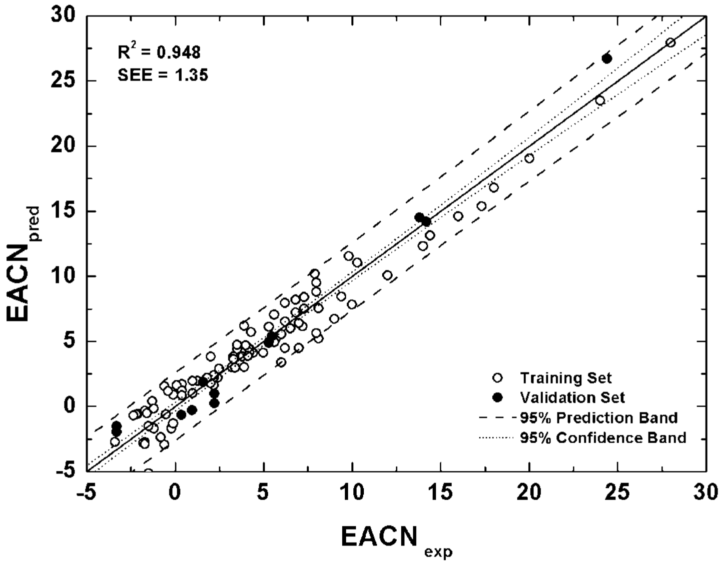

Figure 91 Experimental vs. predicted EACN for acceptor oils. The correlation was obtained with an equation consisting of 2 descriptors (Equation 47). The validation set is correctly predicted.

d. A pragmatic approach to a better EACN prediction

Consisting only of 8 relevant descriptors ($M_1^X = 0$), the σ-moments invite to try out different mathematical operations between them, in order to verify if there exist dependencies and differences, which may result in a better regression for the use in industry, where application is more important than explanation. After experimenting with multiplication, division, logarithmic calculus etc. a descriptor combination turned out to be particularly interesting. M_0^X divided by M_2^X showed surprising differences between acceptor, non-acceptor and alkane molecules. This pseudo-descriptor has no easy physical meaning, but it can be described as the occupied surface area per one unit of polarity. It is further referred to as normalised surface area $M_{0/2}^{X}$. Thus a high value stands for a big molecule with few or weak functionalizations. In **Figure 92** the experimental EACN is shown against the normalised surface area. There are two groups clearly distinguishable. Encircled in violet, a group of molecules can be seen, which consists of *n*-alkanes, as well as branched and cycled hydrocarbons. Although the latter are referred to as polar oils in terms of simplicity, their decrease in EACN is caused by their decreasing size upon branching and cyclisation. Only after a functionalization, which introduces a higher local density of electrons, the decrease in EACN is also caused by the increasing polarity. The green circle includes only molecules which contain one or more unsaturations or heteroatoms. Furthermore it can be clearly seen, that acceptor molecules have rather lower $M_{0/2}^{X}$ values than the non-acceptors. Squalene with an EACN of 13.8 and a normalised surface area of 7.6 behaves like an outlier. Probably it should rather be treated as an acceptor, since it has a very high M_2^X descriptor due to its six double bonds.

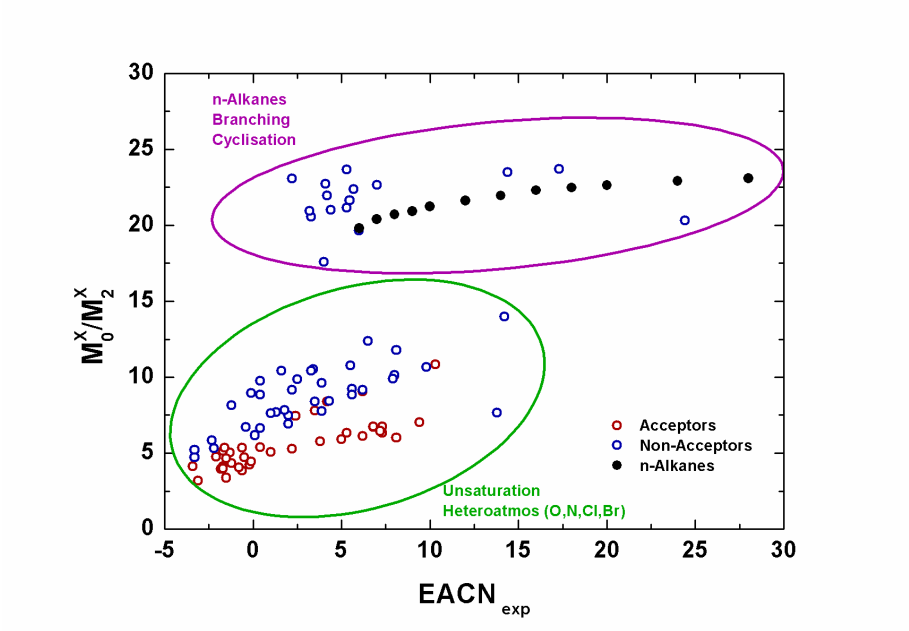

Figure 92 The normalized surface area $M_{0/2}^{X}$ in dependence of the experimental EACN. Two groups appear, consisting of linear, branched and cyclic alkanes (violet), and of unsaturated, hetero-atomic hydrocarbons (green). Within the latter, a clear distinction between non-acceptors and acceptor is visible.

The normalised surface area was thus used as an additional descriptor in the multilinear regression analysis with 94 oils. According to the fitness equation d_{opt} = 3 was obtained.

$$EACN_{pred7}^{X} = -8.6 + 0.057 M_0^X - 0.14 M_2^X + 0.25 M_{0/2}^X \quad \text{with} \quad M_{0/2}^X = \frac{M_0^X}{M_2^X} \qquad \textbf{(48)}$$

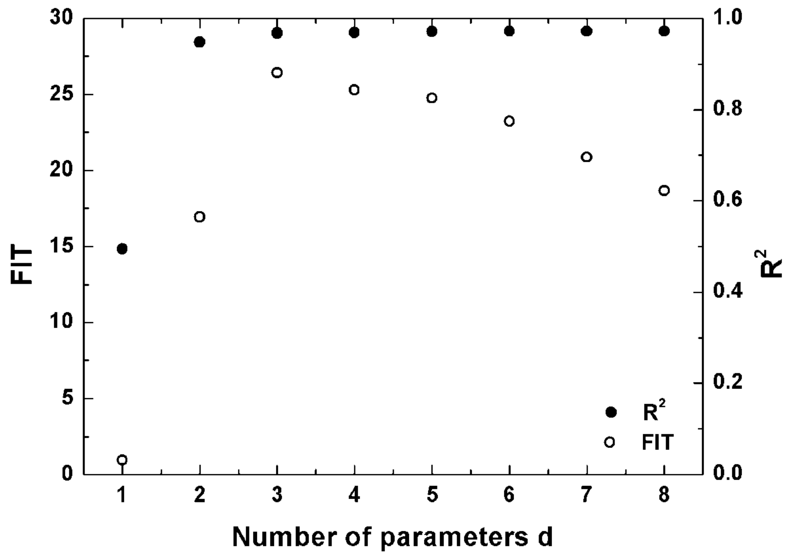

Figure 93 The dependence of *FIT* and $R^2$from the number of descriptors *d*. All non-acceptor and acceptor oils were used together in the regression analysis, which resulted in a maximum at *d* = 3.

The structure of the equation is similar to $EACN^{X}_{pred1}$ and $EACN^{X}_{pred4}$, with the difference of having an additional descriptor. The surface area is connected to a positive coefficient and the polarity is connected to a negative coefficient, which is in accordance with common sense. $M^{X}_{0/2}$serves thereby as a correctional descriptor, which permits to differentiate branched and cyclic from unsaturated hydrocarbons and acceptor containing oils. The fitness of the correlation is with a value of 26.4 the highest of all regressions, which include acceptors and non-acceptors (**Figure 93**).

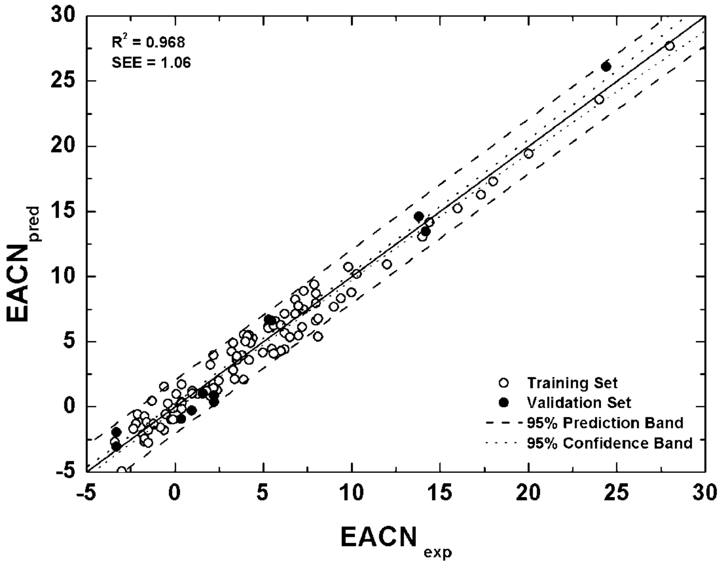

Figure 94 Experimental vs. predicted EACN for acceptor oils. The correlation was obtained with an equation consisting of 3 descriptors, thereof one pseudo-descriptor (Equation 48). The validation set is correctly predicted.

In **Figure 94**, the correlation consisting of the training and validation set can be seen. The R^2 value is with 0.968 slightly better than for $EACN_{pred5}^{X}$, as well as SEE with 1.01. Furthermore all polar oils of the validation set were estimated within the prediction bands.

e. A summary of all multi-linear regressions

The multi-linear regression analysis resulted in seven equations, which can be used to predict the EACN of non-acceptors, acceptors or both. In **Table 17** they are summarized under their abbreviation *P1-P7*, which stands for the number of prediction. Their constants are shown as well as the coefficients for the corresponding σ-moments. M_0^X is indicated with three digits after the decimal point, since the third digit is very relevant for the outcome of the EACN calculation, which is usually indicated with one digit after the decimal point. The remaining σ-moments are indicated with two digits, since depending on the equation, one or two digits after the decimal point are relevant.

In **Table 18** the number of descriptors for each equation, as well as their use for acceptors, non-acceptors or both is indicated. Furthermore the outcome of the statistical validation is listed, with the coefficient of determination R^2, the standard error of the estimate SEE and the fitness of the correlation *FIT*. At last the score of the validation set is given. *P1* results in the best correlation with the smallest SEE. Its FIT is also very high, arguing for the quality of the correlation. However 2 oils of the validation set – squalane and squalene - were not correctly predicted. The first is located in a region where few experimental data is available, resulting in a correlation equation with little statistical weight for relatively high EACN values. The latter has a M_2^X descriptor, whose value lies in the region of acceptor molecules. Thus non-acceptor molecules with $M_2^X > 50$ shall be considered as acceptor-like molecules. *P2* to *P4* is used only for the prediction of acceptor EACN's. Their fitness is in general very low, with its lowest value for *P2*. Though it has the smallest SEE, its prediction ability for compounds, which lie outside the observed data is highly questionable. *P4* is a better fit according to the FIT and shows also an acceptable SEE. *P5* to *P7* can be used for both, acceptor and non-acceptor prediction. Best results are obtained with *P7*, which consists of two descriptor and a pseudo-descriptor, which is built up of the first two σ-moments in the equation.

Table 17 Summary of all equations, which were used for the prediction of the EACN of non-acceptor, acceptors or both, as well as their abbreviation.

	Abb.	Const.	M_0^X	M_2^X	M_3^X	M_4^X	M_5^X	M_6^X	M_{hbacc}^X	$M_{0/2}^X$
$EACN_{pred1}^X$	*P1*	-4.0	0.070	-0.33						
$EACN_{pred2}^X$	*P2*	-8.1	0.027	0.64	1.33	-1.99	-2.01	1.11	13.17	
$EACN_{pred3}^X$	*P3*	-7.8	0.056			0.19		0.05		
$EACN_{pred4}^X$	*P4*	-6.8	0.060	-0.15						
$EACN_{pred5}^X$	*P5*	-4.1	0.066	-0.29				-0.04	1.37	
$EACN_{pred6}^X$	*P6*	-5.1	0.065	-0.22						
$EACN_{pred7}^X$	*P7*	-8.6	0.057	-0.14						0.25

The results for the prediction of the EACN's of polar oils and *n*-alkanes are shown in **Table 19**. The obtained values are compared to the experimental EACN, and the best prediction is marked in green, whereas the worst is marked in red. It can be seen that *P1* is good for the prediction of the *n*-alkanes, which is kind of useless, since their EACN is given by definition. Furthermore they can be predicted perfectly with an R^2 = 0.999 by correlating them only to M_0^X. However *P1* is particularly good for the prediction of halogenated alkanes, aromatics and (with exceptions) terpenes.

Table 18 Summary of the statistical results from the multi-linear regression analysis. The number of descriptors is given as well as their use for acceptors and/or non-acceptors is indicated. Furthermore R^2, *SEE* and *FIT*, as well as the score of the validation set is shown. Note that the *FIT* can only be compared between correlations, which use the same data set.

	Descriptors	Acceptors	Non-Acceptors	R^2	SEE	FIT	Validation Set
P1	2		x	0.984	0.82	54.3	6 of 8
P2	7	x		0.952	0.99	6.8	4 of 4
P3	3	x		0.922	1.19	8.6	4 of 4
P4	2	x		0.924	1.16	10.1	4 of 4
P5	4	x	x	0.963	1.15	21.1	12 of 12
P6	2	x	x	0.948	1.35	16.9	12 of 12
P7	3*	x	x	0.968	1.06	26.4	12 of 12

*including pseudo-descriptor

P2 shows the best results for ester type molecules. They have different steric properties due to the location of their ester group in the molecule. Thus their EACN prediction is rather difficult and more descriptors have an improving effect. The acceptor fragrances can be decently predicted by *P3*. *P4* is neither especially bad, nor good for any type of oil. The predictions done by P5 turned out to be very good for the non-acceptor molecules, except for cyclohexenes. However it has a poor prediction quality for ketones, as well as nitriles. *P6* is surprisingly good for cyclic compounds, with and without double bond, linear alkenes and several terpenes with an EACN higher than 2. Worst results are though obtained for halogenated alkanes, aromatics and alkynes. With *P7* poor results are obtained for various non-acceptor types of molecules, such as cyclic alkanes, linear alkenes and terpenes. The prediction of acceptors is neither very good, nor very bad.

Table 19 All results from the prediction of the EACN with the equations *P1* to *P7*. The best prediction is highlighted in green. The worst in red. Oils of the validation set are written in bold.

Name	$EACN_{exp}$	*P1*	*P2*	*P3*	*P4*	*P5*	*P6*	*P7*
Octacosane	28.0	29.1				27.8	27.9	27.7
Tetracosane	24.0	24.7				23.5	23.5	23.6
Eicosane	20.0	20.1				19.2	19.0	19.4
Octadecane	18.0	17.9				17.0	16.8	17.3
Hexadecane	16.0	15.7				14.9	14.6	15.2
Tetradecane	14.0	13.4				12.7	12.3	13.1
Dodecane	12.0	11.1				10.5	10.1	10.9

Decane	10.0	8.9	8.4	7.8	8.8
Nonane	9.0	7.7	7.3	6.7	7.7
Octane	8.0	6.6	6.2	5.6	6.6
Heptane	7.0	5.5	5.1	4.5	5.5
Hexane	6.0	4.3	4.0	3.4	4.3
Squalane	24.4	27.5	26.4	26.7	26.1
Dodecylcyclohexane	17.3	16.6	15.7	15.4	16.3
Decylcyclohexane	14.4	14.3	13.6	13.1	14.1
Butylcyclohexane	7.0	7.5	7.0	6.4	7.8
Propylcyclohexane	5.7	6.3	5.8	5.2	6.6
Cyclodecane	5.5	6.4	6.0	5.4	6.6
***cis*-Decalin**	5.3	6.1	5.7	5.0	6.7
Isopropylcyclohexane	5.3	5.9	5.5	4.9	6.0
1.4-Dimethylcyclohexane	4.4	5.1	4.8	4.1	5.3
Ethylcyclohexane	4.2	5.2	4.8	4.2	5.5
Cyclooctane	4.1	5.0	4.6	3.9	5.4
1.2-Dimethylcyclohexane	3.3	4.8	4.5	3.8	4.9
Methylcyclohexane	3.2	4.0	3.7	3.0	4.2
Cyclohexane	2.2	3.3	3.0	2.2	4.0
1-Chlorohexadecane	9.8	10.6	10.4	11.5	10.7
1-Chlorotetradecane	8.0	8.6	8.5	9.5	8.7
1-Chlorododecane	5.6	6.1	6.1	7.1	6.2
1-Chlorodecane	3.5	3.7	3.8	4.7	3.9
1-Bromo-3-methylpropan	-3.3	-3.1	-2.8	-2.0	-3.0
Squalene	13.8	10.4	11.5	14.5	14.6
1-Octadecene	14.2	14.1	13.7	14.2	13.5
1-Dodecene	8.1	7.4	7.2	7.5	6.8
1-Decene	5.5	5.1	5.0	5.3	4.4
1-Octene	3.9	2.8	2.9	3.0	2.1
***cis*-Cyclooctene**	1.6	2.0	2.1	1.9	1.0
1-Methyl-1-cyclohexene	0.4	1.3	1.4	1.2	0.3
4-Methyl-1-cyclohexene	0.4	0.8	1.0	0.9	-0.2
3-Methyl-1-cyclohexene	-0.1	0.9	1.0	0.9	-0.1
Cyclohexene	-1.2	-0.2	0.0	-0.2	-1.3
1-Tetradecyne	3.9	4.4	4.3	6.2	5.5
1-Dodecyne	2.0	1.9	2.0	3.8	3.2
1-Decyne	0.1	-0.3	-0.2	1.6	1.0
1-Octyne	-2.2	-2.5	-2.4	-0.6	-1.3
Dodecylbenzene	7.9	9.0	9.0	10.2	9.4
Decylbenzene	6.2	6.8	6.8	7.9	7.1
Octylbenzene	4.3	4.5	4.7	5.7	4.9
Butylbenzene	0.4	0.0	0.3	1.2	0.3
p-Xylene	-2.3	-1.9	-1.5	-0.7	-1.7
Phenyl-1-butyne	-3.3	-4.0	-3.3	-1.5	-1.9
Longifolene	6.5	6.1	5.9	6.0	5.3
p-Menthane	6.0	6.5	6.1	5.5	6.3
Caryophyllene	5.6	4.1	4.4	4.9	4.1

Pinane	4.0	5.5				5.2	4.7	5.0
α-Pinene	3.4	3.0				3.0	3.0	2.1
p-Menth-2-ene	3.3	3.6				3.6	3.6	2.8
Δ-3-Carene	2.5	2.8				2.8	2.9	2.0
β-Pinene	2.2	2.2				2.3	2.4	1.4
Limonene	2.0	1.0				1.3	1.8	0.8
γ-Terpinene	1.8	1.5				1.7	2.2	1.2
α-Terpinene	1.3	1.2				1.6	2.0	1.0
Terpinolene	1.0	1.2				1.5	2.0	1.0
p-Cymene	-0.4	0.0				0.3	1.2	0.3
Ethyl decanoate	2.2		2.1	1.9	2.1	2.4	1.6	1.7
Ethyl dodecanoate	3.8		4.0	4.2	4.3	4.5	3.8	4.0
Decyl butyrate	5.0		4.7	4.3	4.5	4.8	4.1	4.2
Ethyl myristate	5.3		5.9	6.4	6.5	6.7	6.1	6.2
Hexyl octanoate	6.2		4.9	4.5	4.7	5.2	4.5	4.4
Myristyl propanoate	6.8		7.0	7.2	7.4	7.9	7.2	7.1
Ethyl palmitate	6.8		8.1	8.6	8.5	8.7	8.2	8.2
Butyl dodecanoate	7.2		6.4	6.2	6.4	6.9	6.1	6.1
Isopropyl myristate	7.3		7.2	7.6	7.7	8.2	7.5	7.4
Ethyl oleate	7.3		8.7	9.8	9.2	8.3	8.4	8.9
Octyloctanoate	8.1		6.1	5.5	5.7	5.9	5.2	5.4
Hexyl dodecanoate	9.4		8.3	8.4	8.5	9.2	8.4	8.3
Dibutylether	2.4		2.1	1.2	1.3	1.9	2.2	1.3
Dipentylether	4.2		5.1	3.7	3.5	3.7	4.5	3.6
Dihexylether	6.2		6.5	5.6	5.5	5.8	6.5	5.7
Diheptylether	8.0		8.5	7.8	7.6	8.2	8.8	8.0
Dioctylether	10.3		8.3	9.6	9.7	11.0	11.0	10.2
2-Octanone	-3.4		-3.1	-2.7	-2.2	-2.0	-2.7	-2.7
2-Decanone	-2.1		-1.0	-0.5	-0.1	0.0	-0.6	-0.6
2-Undecanone	-1.3		-0.1	0.4	0.8	1.1	0.4	0.4
2-Dodecanone	-0.6		0.7	1.6	1.9	2.1	1.6	1.6
Octanenitril	-1.7		-2.7	-2.3	-2.2	-2.8	-2.7	-2.7
Decanenitrile	-0.5		-0.7	-0.1	-0.1	-0.8	-0.6	-0.6
Dodecanenitril	0.4		1.3	2.1	2.1	1.5	1.7	1.7
Rose oxide	-1.7		-1.4	0.0	-0.3	-1.2	-0.3	-0.7
Geranyl acetate	-0.6		-1.4	-0.5	-1.4	-3.4	-3.0	-1.8
Linalyl acetate	-0.8		-1.3	-0.4	-1.2	-2.7	-2.4	-1.6
Citronellyl acetate	-0.2		-0.2	-0.3	-0.6	-1.4	-1.7	-1.0
Menthyl acetate	-0.1		-0.5	-1.0	-0.6	-0.5	-1.3	-1.0
Eucalyptol	-1.6		-1.7	-0.5	-0.8	-2.0	-0.5	-1.2
D-Carvone	-3.1		-4.4	-4.2	-4.4	-6.1	-5.9	-4.9
Damascone	-1.2		-0.5	-0.8	-0.9	-1.4	-1.7	-1.4
β-Ionone	-1.8		-1.2	-1.7	-1.7	-2.6	-2.8	-2.1
ω-Hexadecenlactonate	1.0		1.8	1.5	1.6	1.6	1.0	1.2
Menthone	-1.5		-0.9	-1.8	-1.3	-0.6	-1.5	-1.8
Methyl Cedryl Ether	3.5		3.2	3.9	3.6	3.7	4.4	3.6
Methyl Dihydrojasmonate	-1.7		-2.8	-2.3	-2.0	-2.6	-2.9	-2.4

Ethylene Brassylate	-1.5	-1.4	-2.4	-2.5	-4.7	-5.2	-2.8
Dipropoxybutane	2.2	2.2	1.4	1.2	0.1	1.0	0.8
Dibutoxyethane	2.2	1.4	0.3	0.8	0.9	0.2	0.4
Dipropoxyethane	0.4	-0.6	-0.8	-0.5	-0.4	-0.6	-0.9
Hexylmethacrylate	1.1	1.6	0.0	0.1	0.6	-0.3	-0.3

This summary permits to see which equation works well for which types of molecules. However the quantity of best predictions (green) and worst predictions (red) is no measure for the overall quality of the correlation equation. Only R^2,*SEE* and *FIT* are able to give a statistical relevant measure for the quality of the prediction. Thus *P7* is the best equation for the prediction of the EACN of acceptor and non-acceptor oils.

3.7.6. Influence of surface area and polarity on the EACN.

There has been so far no quantitative interpretation of structural parameters influencing EACNs of oils. To shed some light to this issue with the COSMO-RS model, 11 oils with 10 carbons were selected and positioned in **Figure 95** as a function of their van der Waals surface M_0^X and their overall polarity M_2^X. The 4 inclined straight lines correspond to the iso-EACN curves calculated from **Equation 42** for EACN values equal to -5, 0, +5 and +10 respectively. *n*-Decane is used as a reference oil for identifying oils having a smaller or larger area than it, depending on whether they are located to the left or right of the dotted vertical line. Here, only the 1-chlorodecane has a greater area than *n*-decane due to the fact that the chlorine atom is much larger than the hydrogen atom. On the other side, 1-decene and 1-decyne have a slightly smaller area then *n*-decane while cyclic oils have a much smaller one. The dashed horizontal line separates, saturated (cyclo)alkanes from unsaturated and chlorinated oils that are significantly more polar than *n*-decane.

Comparing experimental EACNs of alkanes and cycloalkanes in **Figure 95**, one notes that they vary substantially from 5.3 (*cis*-decalin) to 10.0 (*n*-decane) while they have approximately the same polarity (M_2^X) as *n*-decane. Note that *n*-alkanes are not very well predicted by **Equation 42**. Actually M_0^X alone would be sufficient for a perfect correlation. Consequently M_2^X imposes a slight polarity dependence, which comes from the tetrahedral arrangement of the -CH$_2$- segments and is increasing with augmenting N$_{\text{Carbon}}$. The lower EACN values of cyclic oils do not come from a higher polarity as it may be assumed. It is simply due to a smaller van der Waals surface which decreases their interactions with surrounding oil molecules and increases its partition coefficient towards the interfacial film of surfactants. In the same way, it is worth comparing the EACN of *p*-menthane with that of the three unsaturated and aromatic derivatives (*p*-menthene, α-terpinene and *p*-cymene) located just above it. Actually, these four molecules have virtually identical surfaces but differ markedly with regard to their polarity as well as their EACNs that follow the same trend starting from *p*-menthane (EACN = + 6.0) to *p*-cymene (EACN = -0.4). The same argument can be applied to *n*-decane, 1-decene and 1-

chlorodecane that exhibit fairly similar M_0^X but their EACNs greatly diminish as a result of increasing M_2^X.

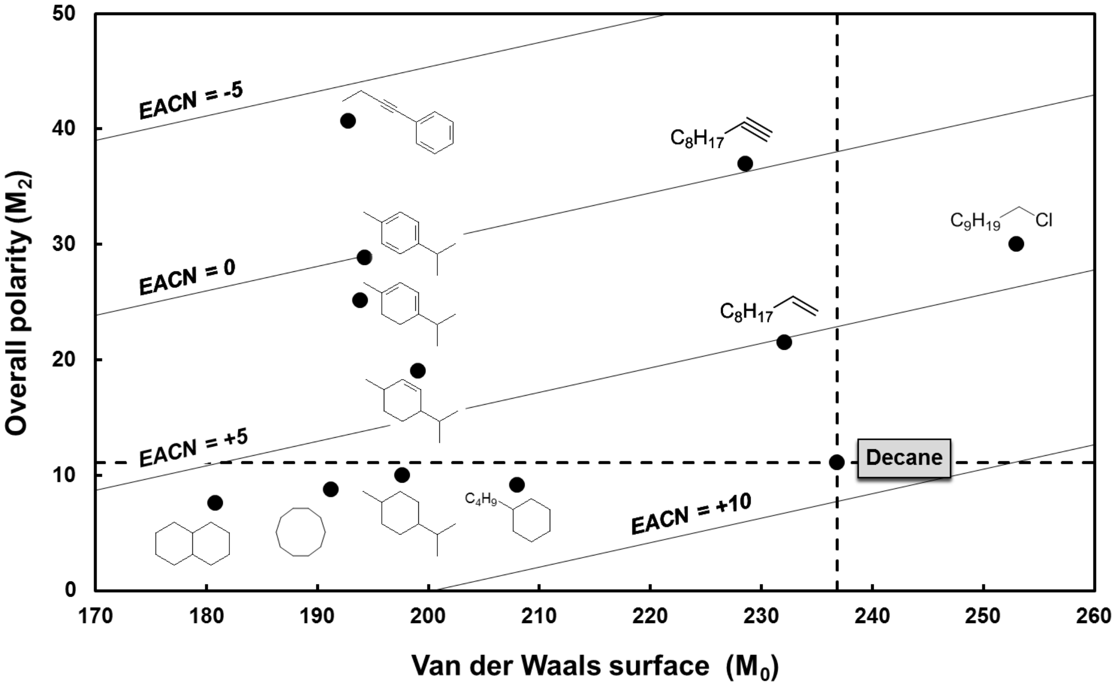

Figure 95 Position of a selection of various oil molecules with 10 carbons as a function of their van der Waals surface (M_0^X) and their overall polarity (M_2^X). Inclined straight lines correspond to the iso-EACN curves calculated from Equation 42.

3.7.7. The application of the EACN prediction to fragrances

The prediction of the EACN of fragrances can be of particular interest in the cosmetic and perfume industry. Fragrances are used in almost every personal care product and many of them are based on a SOW system. A shampoo consists of several surfactants in water, as well as co-surfactants, salts, thickeners, antioxidants etc. In order to obtain a pleasant odour, fragrances are added, which may lead to a destabilisation of the emulsion, if their hydrophobicity is not adapted. Considering the vast amounts of fragrances with various structures and functional groups, a reliable prediction of their EACN facilitates the process of finding suitable odorants, which do not destabilize the (micro-)emulsion, or suitable amphiphiles, which are able to form stable (micro-)emulsions. Furthermore if the molecule exists in the database of COSMO-RS, the whole process is time-saving, as well as inexpensive.

The predictions *P5*, *P6* and *P7* were used to verify their statistical relevance for the EACN prediction of fragrances. Thereby only the terpenes studied by Bouton[171] *et al.* and the acceptor containing fragrances of this work (**see Figure 67**) were used, in order to calculate R^2 and *SEE*, as well as the confidence and predictions bands.

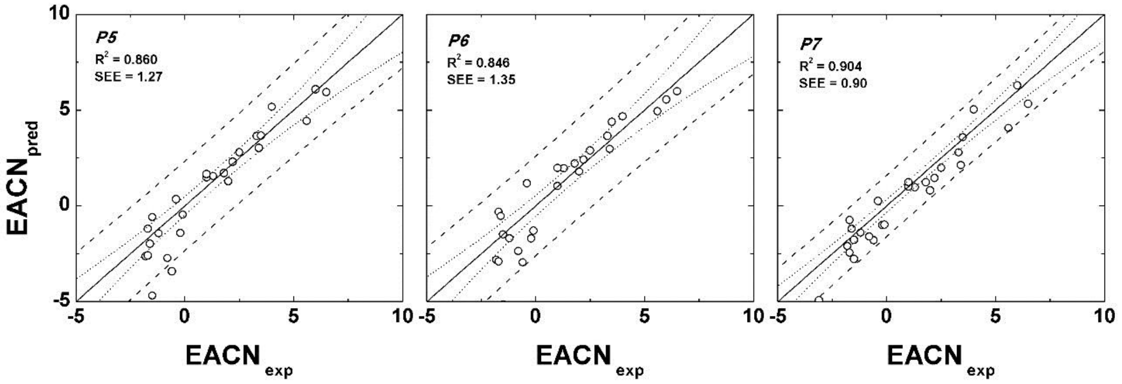

Figure 96 The application of the prediction equations *P5*, *P6* and *P7* to the estimation of the EACN of perfume molecules. Best results are obtained for *P7* with R^2 = 0.904 and *SEE* = 0.90.

In **Figure 96**, the predictions done with *P5*, *P6* and *P7* can be seen. Their coefficient of determination is lower than for the predictions made in **Section 3.7.5**. However another set of molecules is used here, which in turn allows only the comparison with each other. In contrast the standard error of estimate can be compared with all correlations throughout this work, since it indicates the average deviation from the regression line. Thus *P7* is a very good equation for the prediction of the EACN of acceptor and non-acceptor fragrances. With a SEE = 0.90 it is clearly better than *P5* and *P6* with 1.27, respectively 1.35. Confidence and prediction bands are clearly tighter for *P7* than for the other two predictions, arguing for a better prediction of the EACN.

3.7.8. Prediction of the EACN by correlation with calculated surfactant/oil phase diagrams

Another approach for the prediction of the EACN was tried by calculating the SO binary phase diagrams of several oils with COSMO-RS and correlating T_α to the EACN of the oil. The phase behaviour of a SOW system is given by the superposition of the phase behaviour of its binary systems. Since the water can be seen as a constant and the surfactant is predefined, the only composition variable of the ternary system is the oil. The latter is not present in SW binary system and uninfluential in the WO system. However in the SO system it is crucial.

There are not many examples of binary SO phase diagrams in literature. Kahlweit *et al.* determined the upper critical temperature T_α for the system C_6E_5/*n*-alkane.[207] For *n*-decane he found approximately 18 °C. A more hydrophobic surfactant decreases this temperature, as well as an oil with a lower EACN. Thus it can be considered that C_6E_4 and polar oils give a T_α below 0°C. Since these values are experimentally not easily accessible, another approach was tried by using COSMO-RS. For this approach only the EACN's of the oils measured by Bouton *et al.* were considered.[171] As surfactant C_6E_4 was used for the calculation of the phase behaviour. In **Figure 97** an example of the binary phase diagram of C_6E_4 in longifolene can be seen, which consists of a two-phase region for low temperatures. By increasing the temperature the mixture becomes a monophasic reverse micellar solution. However the phase diagram does not correspond to the actual phase behaviour of this system, since it was experimentally verified that C_6E_4 and longifolene are completely miscible between 0-100°C.

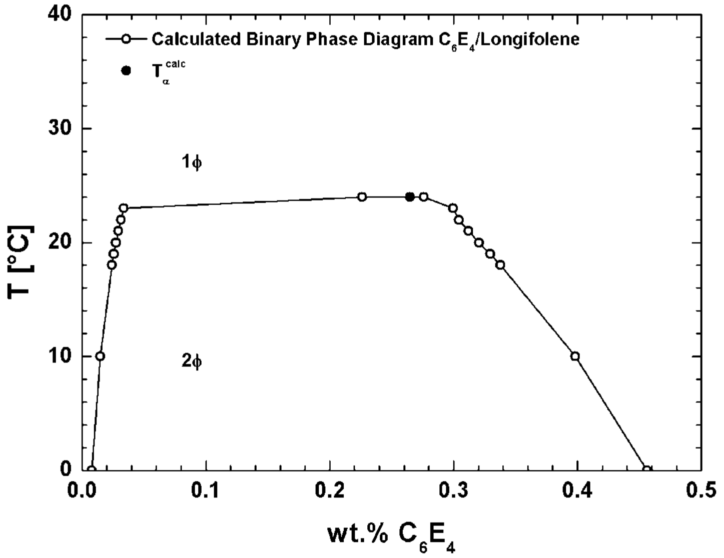

Figure 97 Calculated binary phase diagram of C_6E_4/longifolene. The experimentally determined miscibility gap lies in reality below 0°C.

COSMO-RS is not able to consider aggregation phenomena, as it is the case in such SO systems. Thus it regards the solubility phenomena as a simple solute in solvent problem. However even without the aggregation, T_α^{calc} is based on the interaction of the solvo-surfactant with the oil, and thus dependent of the hydrophobicity of the latter. Therefore T_α^{calc} represents a hypothetical critical temperature of a SO mixture, if aggregation does not occur. It was calculated for a series of *n*-alkanes from methane to eicosane. Then their alkane carbon number was displayed in dependence of T_α^{calc}, in order to obtain an exponential fit, which permits the calculation of the EACN of polar oils (**Figure 98**).

$$EACN_{pred8}^{X} = 3.92 \cdot e^{0.02 \cdot T_\alpha^{calc}} \qquad \textbf{(49)}$$

Since COSMO-RS is a computational program, it is even possible to calculate a hypothetical T_α of gaseous *n*-alkanes, such as methane, ethane etc.

The EACN of polar oils can then be calculated with **Equation 49**. In a last step the experimental EACN values are set up against the predicted EACN values and their confidence and prediction bands are determined, as well as R^2 and *SEE* (**Figure 99**). The correlation is rather disappointing ($R^2 = 0.739$). Also the standard error of the estimate is with 1.68 relatively high. However it is clearly visible that there is a relationship between the calculated hypothetical T_α^{calc} and the experimental EACN value. It is not known if the correlation would be better if the real T_α^{calc} value can be calculated. Also the fact, that the correlation curve in **Figure 98** is of an exponential nature, limits its use for oils with an EACN bigger than 0.

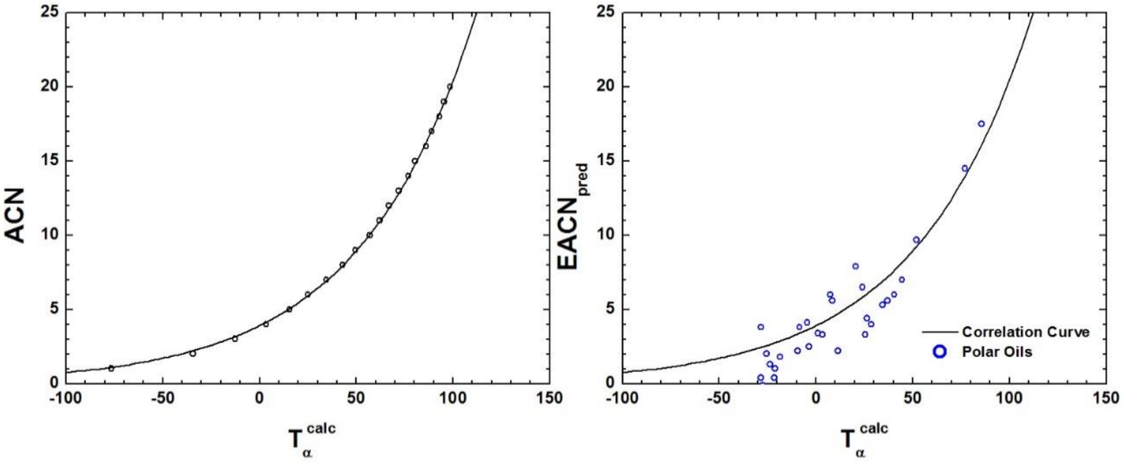

Figure 98 Left: The dependence of ACN from T_α^{calc}. The exponential fit gives an equation, which is able to predict the EACN of polar oils. Right: The predicted EACN of several polar oils. The T_α^{calc}values were obtained from the calculated SO binary diagrams.

The prediction with this approach is clearly less convincing than with the σ-moments. Furthermore its use for very polar oils is limited. Nevertheless the correlation of an oils EACN with its T_α value in combination with a known surfactant, has its eligibility. It shall be noted that Shinoda *et al.* showed that the critical temperature T_β of a C_iE_j/water system correlates well with the phase inversion temperature of same surfactant in water and octane (WOR = 1).[6] Unfortunately T_α is not easy accessible by experiment and COSMO-RS is not yet able to consider aggregation.

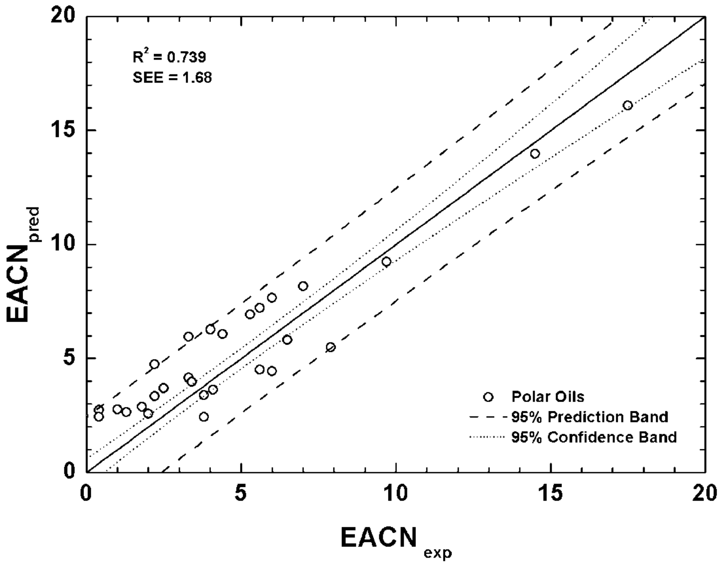

Figure 99 Experimental EACN versus predicted EACN. The correlation is modest and the SEE is relatively high.

3.8. Conclusion

This chapter threats the hydrophobic characteristics of polar oils. In this context their EACN was determined, as well as the monomeric solubility of amphiphile in a SOW system. Furthermore COSMO-RS σ-moments were used to establish QSPR models, which are able to predict the EACN of various hydrophobic compounds.

Initially it was shown that the determination of the EACN is independent of the chosen C_iE_j. It was already reported by Bouton *et al.* that C_iE_4 (i = 6, 8, 10) gave convenient EACNs for several investigated oils. Here it was shown, that same is valid for $C_{12}E_6$, which gave quite equivalent results for 1-octyne and ethyl decanoate in comparison with C_6E_4, respectively $C_{10}E_4$. It is surprising that amphiphiles, which differ in carbon chain length and ethoxy group number give equivalent results in EACN, since the latter is a value which is based on the penetration of the oil into the surfactant layer. Probably the interfacial layer is that flexible, that the penetration is barely hindered by the carbon chain length and ethoxy group number. In this context ionic surfactants might be less flexible, preventing the easy penetration of moderate polar molecules, such as limonene and thus resulting in a different EACN.

Finally C_6E_4 was used to determine the EACN of 46 oils, consisting of series of 1-alkenes, 1-alkynes, 2-alkanones, etc. as well as several complex fragrances, such as α-damascone, rose oxide, linalyl acetate etc. Together with the EACNs from literature the dependency of the EACN from the functionalization was investigated and following order was found:

***n*-Alkanes < 1-alkylcyclohexanes < 1-alkenes < dialkylethers ≈ 1-chloroalkanes < 1-alkylbenzenes ≈ ethyl alkanoates ≈ 1-alkynes < alkanenitriles < 2-alkanones**

Same ranking can be applied for fragrances. However the decrease in EACN upon functionalization is not the same, as in the case of linear oils. Consequently the presence of several functional groups in a complex molecule has no additive influence on the decrease in EACN.

The effect of the functional group on the EACN was theoretically explained with the effective packing parameter $\bar{P}$ (**Equation 25**). In general it can be stated that the bigger the polarity, and thus the surface affinity of the oil, the higher is the contribution of the oil to the effective volume of the amphiphile. Since σ_o is considered very small for oils, $\bar{P}$ is increasing, which in turn decreases T* and thus the EACN of the compound. On the other hand the increase in carbon chain length, decreases τ and $\bar{P}$ augments in relation to smaller carbon chain lengths. It was found that the EACN of 1-alkylcyclohexanes approximates those of *n*-alkanes with increasing EACN, which can be attributed to statistics. Since there is virtually no difference in polarity – and thus in surface affinity - between an alkyl chain and the cyclohexane group, the probability that the latter penetrates between the surfactant tails is decreasing with increasing N_{Carbon}. On the other hand, polar oils, such as ethyl alkanoates, alkanenitriles or 2-alkanoates, with a strong polarity due to their functional group, and thus a high affinity for the interface, show a lower EACN than expected with increasing N_{Carbon}, which can be attributed to a weaker decrease in τ and consequently to a stronger oil contribution to the effective volume of the amphiphile ($+\tau\nu_o$).

In this context the influence of the EACN on the monomeric solubility of C_6E_4 in the SOW system was investigated with various fragrances of varying polarity. Thereby it was found that γ^* decreases with decreasing EACN, which is in accordance with literature. However for very polar oils, γ^* evolves towards a plateau and remains virtually constant. Consequently the monomeric solubility of C_6E_4 in fragrance and water was investigated and it was found that it is steadily increasing, which in turn results in less amphiphile at the interface. *D*-Carvone, menthone and citronellyl acetate have even less amphiphile at the interface than monomerically dissolved. The latter system can also be compared to $C_{12}E_8$/linalool/water. $C_{12}E_8$ is a long chain surfactant with a small CMC and monomeric solubility in alkane/water systems. However in linalool, whose EACN was determined as -11.4, only a mass fraction of 0.125 of $C_{12}E_8$ is found at the interface, whereas 0.150 is present monomerically dissolved in principally linalool. These values lie in the magnitude of the system C_6E_4/citronellyl acetate/water. It is thus evident that the EACN of an oil affects strongly the efficiency of a surfactant and that the beneficial effect of a less unfavourable contact area between the amphiphile and the oil is counteracted by the loss of high monomeric solubility in the oil.

It is thus important to know the EACN of the oil, in order to anticipate the phase behaviour in a SOW system. In this regard, COSMO-RS σ-moments were used in order to build up QSPR models, which are able to predict the EACN of any hydrocarbon oil, which consists no strong hydrogen bond donors. σ-Moments are descriptors, which relate molecular properties to physico-chemical descriptors, such as surface area, polarity, etc. Seven models were generated via multi-linear regression analysis, which predict either non-acceptor, or acceptor or both type of oils. The correctness of the model was verified with a validation set. The best results were obtained for prediction model *P7*, with *FIT* = 26.4. This model consists of the physico-chemical descriptors M_0^X and M_2^X, as well as of the pseudo-descriptor $M_{0/2}^X$. The latter turned out to distinguish very well branched and cycled oils, from unsaturated and halogenated oils, as well as from oils with a strong acceptor. It is thus very useful as a corrective descriptor. Eventually it was found that model *P7* is especially good for the prediction of small fragrance molecules.

In almost all models, two descriptors were particularly important. The surface area M_0^X and the overall polarity M_2^X. It was shown that branching and cyclisation results in a decrease in surface area, and thus their lower EACN compared to linear alkanes is only due to the smaller size of the molecule, which enables a stronger penetration into the surfactant layer. On the other hand, unsaturation or any other functionalisation which increases the electron density imposes a strong polarity to the molecule, which manifests itself in an augmentation of the M_2^X descriptor. The latter and M_0^X are thus two structural descriptors, which are able to explain the hydrophobicity/EACN of an oil. In this context model P6 is particularly interesting, since it is able to predict adequately the EACN of all hydrocarbon oils, without hydrogen bond donors. Thereby M_0^X is linked to a positive coefficient, indicating the increase in EACN with augmenting size, and M_2^X is linked to a negative coefficient, indicating the decrease in EACN, with augmenting polarity. Hence the model makes also physically sense.

3.9. Experimental part

3.9.1. Sample preparation for the determination of the fish tail temperature T*

The fish-tail temperature T* was determined by investigating the phase behaviour of the C_iE_4/oil/water (i = 6, 10) and $C_{12}E_j$/oil/water (j = 6, 8) systems at a constant Water-to-Oil Ratio (WOR = 1, w/w) as a function of temperature (ordinate) and surfactant mass fraction γ (abscissa). T* was determined by observing the alterations of the phase behaviour with decreasing temperature at different mass fractions of surfactant. Thereby water, oil and surfactant were introduced in a thin glass tube and closed with a screw cap. The samples were gently shaken and placed into a thermostatic water bath. Temperature was altered in 0.1 °C steps for C_iE_4's, respectively 0.5 °C steps for $C_{12}E_j$'s and equilibration time was from 30 min to 5 days depending on the surfactant and the adjustment of the equilibrium. Tubes were weighted from time to time to verify that no mass loss occurred. Oils with a high T* (> 50 °C) were added to tubes which were sealed by flame after freezing in liquid nitrogen to avoid any mass loss.

3.9.2. Temperature dependent determination of the relative volume of the bicontinuous microemulsion in the $C_{12}E_8$/linalool/water system

After each temperature step (0.5 °C) the samples were left for equilibration and the relative volume of the bicontinuous microemulsion was determined by measuring the phase heights. The procedure was repeated for each surfactant mass fraction γ and temperature step. **Figure 100** illustrates the relative volume as a function of temperature for each γ.

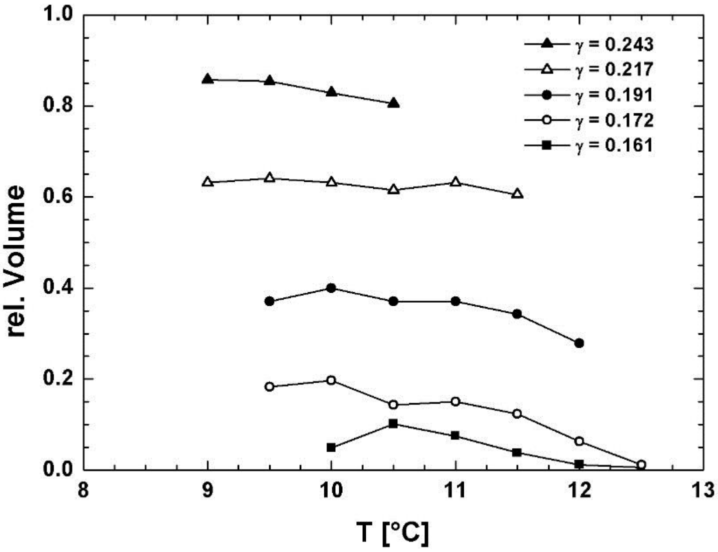

Figure 100 The relative volume of the bicontinuous microemulsion as a function of T for each mass fraction γ.

3.9.3. COSMO-RS calculation

The modelling program ArgusLab (v. 4.0.1. Planaria Software LLC, Seattle, USA) was used to draw the molecules. Molecular geometries were optimized by DFT/COSMO calculations, carried out with the quantum chemical program TURBOMOLE (TURBOMOLE GmbH, Karlsruhe, Germany) using a triple zeta valence polarization basis set and the B88-PW86 exchange-correlation functions. COSMOtherm (C30_1301 version, COSMOlogic, Leverkusen, Germany) was then used for the generation of the σ-profiles and σ–potentials, as well as for the σ-moments.

3.9.4. Materials

Compound	Supplier	Purity
Amphiphiles		
Tetraethylene glycol monohexylether	Synthesized	≥ 98%
Tetraethylene glycol monodecylether	Laboratory	≥ 99%
Hexaethylene glycol monododecylether	TCI	≥ 97%
Octaethylene glycol monododecylether	TCI	≥ 97%
Oils		
n-Hexane	Sigma Aldrich	≥ 97%
n-Heptane	Sigma Aldrich	99%
n-Octane	Sigma Aldrich	≥ 99%
n-Nonane	Sigma Aldrich	≥ 99%
n-Decane	Alfa Aesar	≥ 99%
n-Dodecane	Alfa Aesar	≥ 99%
Cyclodecane	Sigma Aldrich	95%
cis-Decalin	Sigma Aldrich	99%
Cyclooctane	Sigma Aldrich	99%
1-Bromo-3-methylpropane	Sigma Aldrich	99%
Squalene	Sigma Aldrich	≥ 98%
1-Octadecene	Sigma Aldrich	≥ 95%
1-Dodecene	Sigma Aldrich	≥ 99%
1-Decene	Sigma Aldrich	97%
1-Octene	Sigma Aldrich	98%
cis-Cyclooctene	Sigma Aldrich	95%
1-Tetradecyne	Sigma Aldrich	≥ 97%
1-Dodecyne	Alfa Aesar	97%
1-Decyne	Alfa Aesar	98%
1-Octyne	Alfa Aesar	96%
Butylbenzene	Sigma Aldrich	≥ 99%
p-Xylene	Acros	99%
Phenyl-1-butyne	Alfa Aesar	98%
Dibutylether	Sigma Aldrich	99%
Dipentylether	TCI	98%
Dihexylether	TCI	98%
Diheptylether	Alfa Aesar	98%

Dioctylether	Sigma Aldrich	99%
2-Octanone	Fluka	97%
2-Decanone	Sigma Aldrich	≥ 98%
2-Undecanone	Alfa Aesar	98%
2-Dodecanone	Sigma Aldrich	≥ 97%
Octanenitrile	Alfa Aesar	98%
Decanenitrile	Alfa Aesar	98%
Dodecanenitrile	Sigma Aldrich	99%
Ethyl decanoate	Sigma Aldrich	≥ 98%
Fragrances		
Methyl cedryl ether	Sigma Aldrich	> 96%
ω-Hexadecenelactone	Sigma Aldrich	≥ 98%
Menthyl acetate	TCI	> 98%
Citronellyl acetate	TCI	> 95%
Geranyl acetate	Alfa Aesar	98%
Linalyl acetate	Sigma Aldrich	≥ 97%
Ethylene brassylate	Sigma Aldrich	≥ 95%
α-Damascone	Firmenich	> 97%
Menthone	Firmenich	> 98%
Eucalyptol	Firmenich	≥ 99%
Methyl dihydrojasmonate	Sigma Aldrich	≥ 96%
Rose oxide	Sigma Aldrich	> 98%
β-Ionone	Sigma Aldrich	96%
D-Carvone	TCI	> 99%
p-Menthane	Givaudan	> 99%
α-Pinene	Acros	98%
β-Pinene	Acros	98%
p-Cymene	Acros	> 99%
Linalool	Alfa Aesar	97%

Chapter 4

Fragrance solubilisation in water-rich microemulsions

4.1. Background[3,208]

Fragrances were already used 4000 B.C. in Egypt, China, Mesopotania. These cultures used herbs and incenses to burn them in a religious offering ceremony. Hence originates also the word "perfume", since the Latin *per fume* signifies "through smoke". The knowledge to create perfumes arrived in Europe between the 11th and 12th century when crusaders brought it with them from the Islamic world. In the 16th and 17th century perfumes became more and more popular in Europe, but it was reserved to the nobility and rich tradesman. By the end of the 19th century the first synthetic scents were made and compositions became more complicated. In 1882 Paul Parquet created *Fougére Royale*, which introduced a new era in perfumery. The following years were marked with major achievements in the discovery and synthesis of new fragrances, which provided the creation of several milestones in the perfume industry. In 1917 *Chypre* was created by Francois Coty. A perfume, which became a typical representative for a whole family of related fragrances. Ernest Beaux developed in 1921 the perfume *Chanel N°5* for Coco Chanel. It is today the most known and sold perfume world-wide. By the time perfumes became cheaper and thus affordable for most of the people. Nowadays the odorants used in perfumes can be found in quite every personnel and home care product, such as detergents, shampoos or cleansers etc.

The mixing of fragrances can be described as the artistic part of the creation of a perfume. There are a lot of different scents which can be combined in a perfume, and the perfumer needs a lot of experience to create a product which meets the demands of the customer. Basically a perfume composition can be classified in three notes. The head note, heart note and base note. The head note – also known as top note – consist of rather small molecules, which are very volatile, so that they evaporate quickly. They are perceived as the very first after application of the perfume and thus they are responsible for a person's initial impression. In general they last only several minutes on the skin. The heart note – also known as middle note –follows the head note. Together with the base note, it represents the main theme of the perfume. They can last several minutes to hours on the skin. The base note consists usually of large molecules, which evaporate slowly. Thus they are not perceived in the first minutes, but on the other hand they can be perceived several hours.

In former days the discovery of new odorants was based on extraction techniques, which were applied on natural materials, such as fruits, plants or animals. Basically these methods can be classified in expression, distillation and solvent extraction methods. The first is the simplest methods, which is particularly used for citrus oils. The fruit peel is thereby pressed, until the oil is obtained. Such compounds are called expressed oils. Another possibility to obtain fragrances is by steam distillation, which is usually performed with plants, such as herbs, flowers, wood, etc. They are placed into a still and hot water steam is blown over them, which in turn results in the release of the small fragrance molecules. The oils obtained with this method are known as essential oils. For example the steam distillation of leaves of pine, results in the essential oil of pine. The most important method to obtain fragrance oils is by solvent extraction, with petroleum ether, acetone, ethyl acetate, etc. A concrete is obtained, which can be distilled in order to obtain an essential oil. An interesting method is the extraction of fragrance compounds with supercritical carbon dioxide, since at atmosphere pressure, the "solvent" evaporates and thus leaves an oil of high quality without solvent residues.[209–211] However the pressure, which is needed to fluidise carbon dioxide is huge. Thus expensive equipment is needed, as well as huge amounts of energy, which in turn results in a more expensive product.

Perfumes as they can be found in the mass market, are usually a mixture of a fragrance composition dissolved in one or more solvents, such as ethanol, glycerol or dipropylene glycol, and often also water. Since fragrance and water do not mix, the phase behaviour of a ternary solvent/fragrance/water system depends strongly on the composition of its constituents. In **Figure 101**, the ternary phase diagram of ethanol/citronellol/water can be seen, which exhibit a big two-phase region for an ethanol mass fraction below 0.4.[212] Furthermore several zones are indicated, which classify a fragrance tincture in different types. According to this scheme, a real perfume contains 15 – 40 wt.% of fragrances, whereas an *Eau de Parfum* has between 10 – 20 wt.%. An *Eau de Toilette* contains 5 – 15 wt.% of perfume compound and an *Eau de Cologne* consists of 3 – 8 wt.% fragrances. Finally an aftershave has only 1 – 3 wt.% of odorant in its composition.

Figure 101 Ternary phase diagram of ethanol/citronellol/water. The dark region represents the two phase region, whereas the white region represents the monophasic region. Furthermore the various possible tinctures are indicated.

Besides the solubilisation of fragrances with simple solvents, other methods exist, in order to obtain a monophasic mixture. Cyclodextrin has been used to solubilise fragrances in water. These compounds represent cyclic oligosaccharides, with various different fictionalisations. In their cavity, they are able to incorporate guest molecules, such as fragrances.[213] Furthermore cyclodextrins have been successfully applied to aroma therapeutic textiles.[214,215] With the inclusion of fragrances, the guest-host complex can be anchored to fibres. While trapped in the cavity, the physical properties of the guest molecule are changed. Thus the volatility of the fragrance is reduced, which in turn results in an evaporation over a longer period. Another possibility is the encapsulation of fragrances with polymers.[216–219] Thereby exist two principal methods. On the one hand, there is the preparation of polymer nanoparticles, which are formed by crosslinking of the polymer chains. The fragrance solubilises then inside the porous structure. On the other hand there exist vesicles, which form an outer polymer layer around the fragrance droplets. Furthermore polymers, as well as surfactants are used to solubilise fragrances in lamellar liquid crystals.[220–222] The zero curvature of the aggregates enables the solubilisation of higher amounts of fragrance between the layers. Surfactants are also used to solubilise fragrances in a monophasic microemulsion.[61,69,70,220,223]

However the previously discussed systems contain compounds which are not volatile and would leave residues on the skin. Thus they are rather applicable in shampoos, crèmes, textiles etc. For the use in perfumery, the amphiphilic compounds have to be volatile. Recently patents have been published, which claim the invention of water-based perfumes, with volatile solvo-surfactants, such as 1-O-alkylglycerols or 1,2-alkanediols.[72,73] Nevertheless few research is done on the solubilisation of fragrances with hydrotropes or solvo-surfactants.[65,66] Therefore in this chapter, the phase behaviour of solvo-surfactant/fragrance/water systems is investigated. Thereby it was studied how to achieve a temperature stable microemulsion, which is able to solubilise as much fragrance as possible.

4.2. Solubilisation of β-pinene in ethanol and water

Traditionally ethanol is the most used solvent in perfumery. It is able to dissolve almost every fragrance and it leaves no traces due to its high volatility. In our group, we investigated the ternary phase diagram of ethanol/fragrance/water, which can be seen in **Figure 102**. As fragrances, β-pinene, methyl cedryl ether, β-ionone and linalool was chosen. It can be seen that almost 75 wt.% of ethanol is needed to dissolve same amount of water and β-pinene, whereas only approximately 40 wt.% is needed to solubilise same amounts of water and linalool. The two-phase region is bigger in the case of β-pinene, which can be explained with its stronger hydrophobicity compared to linalool. On the other hand linalool behaves as citronellol (**see Figure 101**), since both are comparable in structure and polarity. This may not be the case in a SOW system. Kanei *et al.* showed that linalool and geraniol, which are isomers, behaves very different in the system $C_{12}E_8$/fragrance/water. This can be explained with the tertiary alcohol of linalool, which is satirically hindered concerning the penetration into the interfacial layer. Considering the result from **Chapter 3**, where it was found that the EACN of an oil depends mainly on its size and polarity, it can be also explained why methyl cedrylether (EACN = 3.5) is easier to solubilse than β-pinene (EACN = 2.2), and β-ionone (EACN = -1.8) as easy as linalool (EACN = -11.4). Since there exist no interface, the solubilisation of these compounds is determined by the interactions of the constituents with each other in the bulk. Thus favourable interactions between polar parts of the fragrance and water are also counteracted by unfavourable interactions. In this context, methyl cedryl ether can be solubilised easier, due to the hydrogen bond interactions between water and its ether group, despite its bigger size compared to β-pinene. Thus the order does not follow the EACN, since in a SOW system an interface exists, which permits small and/or surface active molecules, to penetrate easier between the surfactant tails, and thus arrange their hydrophilic parts toward the water interface, and the hydrophobic part towards the hydrocarbon core. Hence minimizing the unfavourable contact area with water.

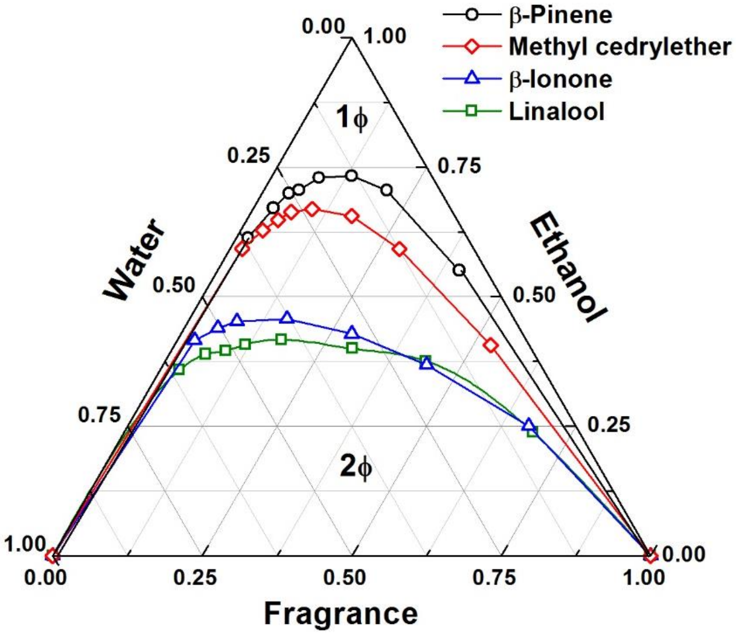

Figure 102 Ternary phase diagram of ethanol/fragrance/water. Ethanol is much more efficient in solubilising the alcohol linalool, than the bicyclic terpene β-pinene.

Due to reasons, which were already described in **Section 2.4.1.**, it is desired to replace ethanol. Many different alcohol-based solvents, such as long-chain alcohols, benzyl alcohol, etc. are used to solubilise hydrophobic substances in water.[224] Morgan *et al.* used the green solvent dimethyl isosorbide to solubilise hydrophobic compounds in water.[225] There exist many more possibilities to replace ethanol. Nevertheless these system are not very efficient and high quantities of solvent are needed to solubilise the fragrance in water. Therefore more efficient and still volatile compounds have to be found.

4.3. Solubilisation of fragrances with amphiphiles

An alternative for solvents are short-chain amphiphiles, such as C_6E_4, C_6E_3 or C_5Gly, etc. These compounds were classified by us as solvo-surfactants, since they exhibit solvent properties, such as volatility and surfactant properties, such as aggregation. In the following the phase behaviour of several solvo-surfactants was investigated, in order to figure out their usefulness for aqueous fragrance solubilisation.

4.3.1. The ternary system C_6E_3/β-pinene/water

The phase behaviour of C_6E_3/β-pinene/water is investigated, in order to determine the efficiency of a solvo-surfactant to solubilise a fragrance in the water-rich corner of the ternary phase prism. The influence of the solvo-surfactant to water ratio (SWR) on the maximum solubilisation of fragrances *x** and the optimal temperature T* is verified. The SWR and the quantity of solubilised fragrance are defined as follows…

$$w = \frac{m(Solvo - surfactant)}{m(Solvo - surfactant) + m(water)} \tag{50}$$

$$x = \frac{m(Fragrance)}{m(total)} \tag{51}$$

..where *m(total)* signifies the total mass of the mixture. In **Figure 103** three lund cut's at varying *w* can be seen. Each ternary system shows a large mono-phasic region (WIV) for lower contents of β-pinene. With increasing amount of the fragrance, the monophasic interval is shrinking, until it arrives at the intersection *x**,T*. The efficiency *x** indicates the maximum solubilisation of the hydrophobic compound by the amphiphilic solution. This points represents the optimum formulation at which all the Winsor phases are in equilibrium. The optimal temperature T* is always lower in the water-rich corner, than at WOR = 1. Further increase in β-pinene content, results in the appearance of a WIII phase, which is very narrow. Analogue to the fish cut, a WII region appears for higher temperatures and a WI region for lower temperatures. Increasing the C_6E_3 to water ratio results in an increase in efficiency of the system. Thus the maximum mass fraction of solubilised β-pinene *x** is strongly increasing. In contrast T* is only increasing slightly.

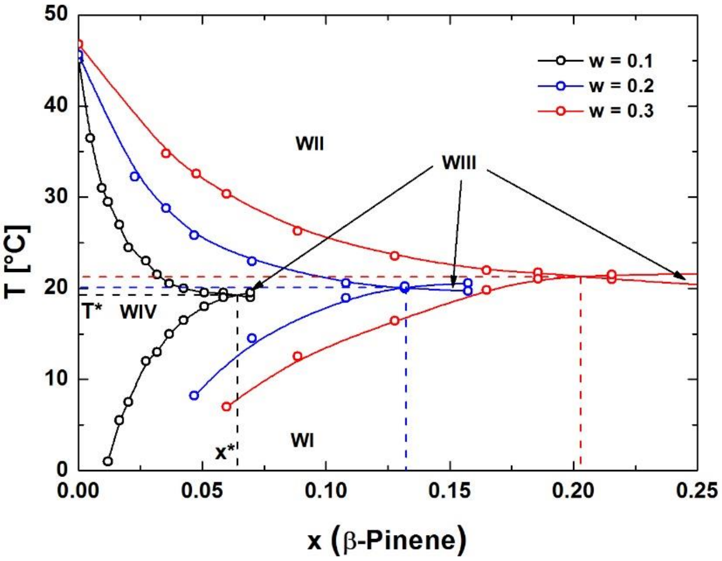

Figure 103 The lund cut of C_6E_3/β-pinene/water at different *w*. The efficiency increases with augmenting *w*, whereas T* stays almost the same.

In order to obtain a complete image of the phase behaviour in the water rich corner of the ternary system C_6E_3/β-pinene/water, its fish cut at WOR = 1 is investigated in **Figure 104**. T* is here 22.5 °C and thus not very different from the optimal temperatures in **Figure 103**, which lie between 19.4 and 21.0 °C.

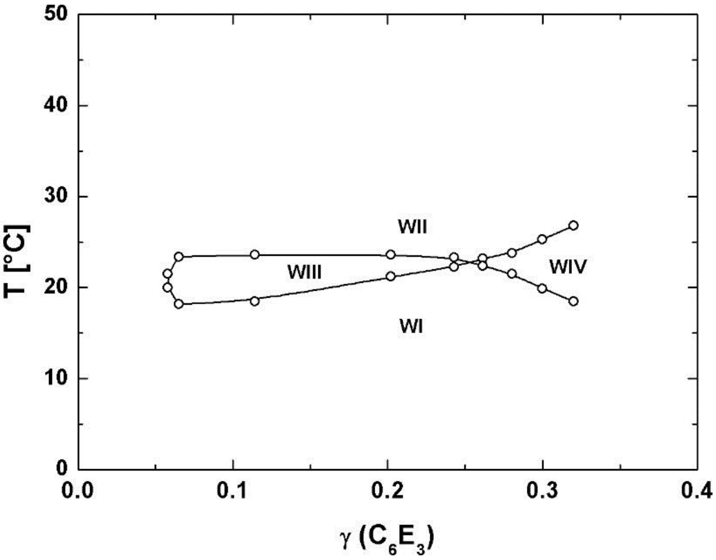

Figure 104 Fish cut of the ternary system C_6E_3/β-pinene/water. The three-phase region is relatively narrow. The fish tail temperature T* is 22.5 °C, whereas γ* is 0.25.

The optimal temperature T* of the three lund cut's and the fish cut can be summarized in a ternary phase diagram (**Figure 105**), in order to see the evolution of the optimum formulation of the system. The curve is not linear and the temperature is with a change of approximately 3 °C very moderate.

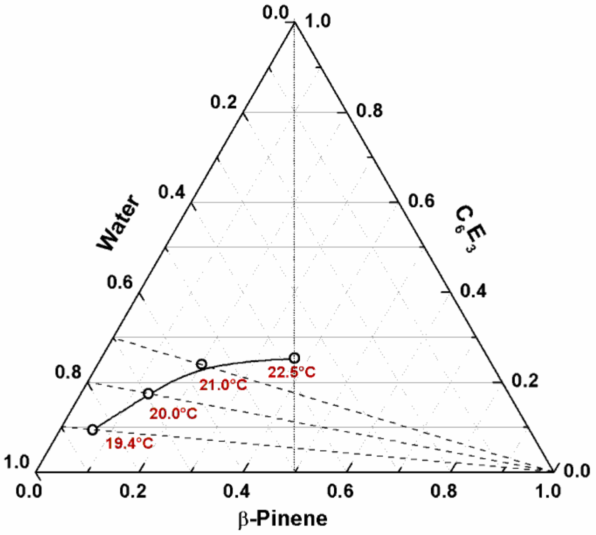

Figure 105 Temperature dependence of the optimum formulation at various SWR and WOR =1.

Kahlweit *et al.* traced the temperature interval of several C_iE_j's with *n*-alkanes.[226,227] Thereby he showed how the three-phase region becomes more and more narrow with decreasing hydrophobicity of the oil, until the three-phase body disappears at the tricritical point. Fragrances are mostly very polar oils, which will consequently diminish the three-phase region. In **Section 3.6.9.**, it could be seen that for the system C_6E_4/fragrance/water, the tricritcal point was almost attained for *D*-carvone.

Considering the results from **Figure 105**, it can be stated that T* is only changing marginally with decreasing SWR. Furthermore an efficient solubilisation is attained, if the quantity of amphiphile is increased to $w = 0.2$ or even $w = 0.3$. However these quantities are relatively high for an aqueous fragrance solubilisation, where a low viscosity of the mixture has to be maintained. Consequently it was concentrated at $w = 0.1$ in the following, if not stated otherwise.

4.3.2. Influence of the amphiphile and oil on the lund cut

In the following the influence of the amphiphile and oil on the phase behaviour of the SOW system is investigated. Thereby the lund cut was traced for several solvo-surfactants and different fragrances. In **Figure 106** the diagrams for C_5E_j (j = 2 – 4), C_6E_j (j = 2 – 4) and C_8E_j (j = 3, 4) with β-pinene as fragrance are shown. SWR is in all cases 0.1. For all C_iE_j's, T* is augmenting with increasing number of ethoxy units, which is in accordance with literature.[56,207] The C_5E_j's are all miscible with water over a big temperature range, particularly C_5E_3 and C_5E_4. However already small quantities of β-pinene decrease the temperature interval strongly, until the critical point x*,T* is attained. The efficiency of (poly)ethylene glycol monopentylethers is very small with x* between 0.02 and 0.025. For C_5E_2 the tricritcal point was already passed. Thus it can be concluded that the amphiphile is too soluble in the water and oil phase, to build up a three phase region. In the case of (poly)ethylene glycol monohexyl ethers, x* increases strongly to values of 0.06 and 0.065 for C_6E_4, respectively C_6E_3. The characteristic point for C_6E_2 is below 0 °C, which is due to its rather hydrophobic character. Same is valid for C_8E_3, which is in contrary to C_8E_4 a solvo-surfactant. The latter was anyways investigated in order to form an enlarged overview of the phase behaviour of solvo-surfactants. C_8E_4 is thus classified as a surfactant by us, and shows the highest efficiency with $x^* = 0.089$ in comparison to the solvo-surfactants. The big difference between C_5- and C_6-glycols, can be attributed to the high monomeric solubility of the first in water and oil. According to their CAC values, a C_5E_j mass fraction of approximately 0.06 is solubilised monomerically in water. Additionally it can be supposed that even more is lost in the oil phase. Thus there is few amphiphile left over to form the amphiphilic film between water and oil. Ergo the (poly)ethylene glycol monopentylethers are only poorly efficient solvo-surfactants and thus we concentrate in our studies rather on C_6- and C_8-amphiphiles.

In Figure **107** the lund cut of $C_{12}E_6$/β-pinene/water is shown. It was made in order to highlight the differences in the phase behaviour in comparison to the short-chain glycol ethers. As expected, the efficiency of this system is much higher with $x^* \approx 0.27$. However the monophasic region is very narrow and there is a huge liquid crystalline phase, which is separated from the monophasic region by a narrow two-phase region. The overall form of thel cut is comparable to those made with solvo-surfactants. The big difference is the liquid crystalline phase, which counteracts the good efficiency of the system, and thus cancels out $C_{12}E_6$ as a potential candidate for aqueous fragrance solubilisation. Additionally it is non-volatile, which in turn is another reason for its inapplicability to our purpose.

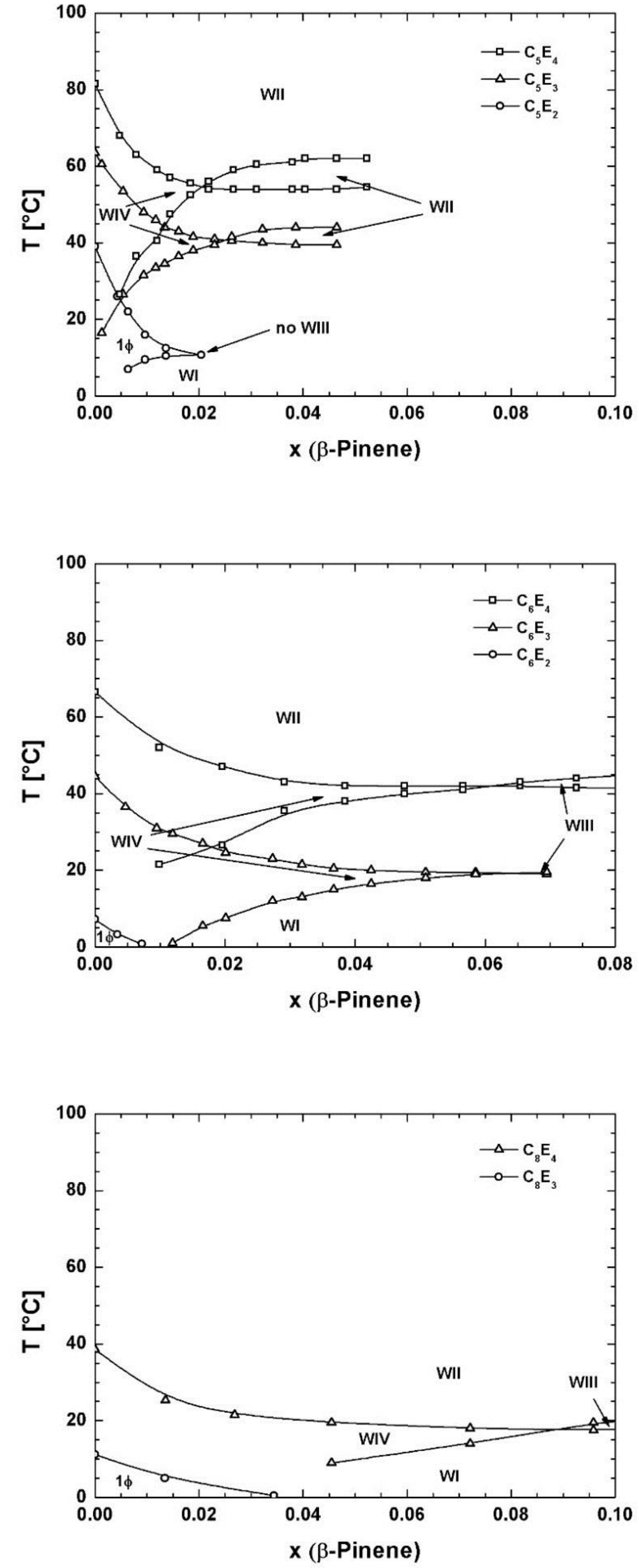

Figure 106 Lund cuts of several C_iE_j/β-pinene/water systems. Top: C_5E_j (j = 2,…,4). The tricirtical point is passed for C_5E_2. Centre: C_6E_j (j = 2,…,4). The optimum formulation lies below 0 °C for C_6E_2. Bottom: C_8E_j (j = 3,4). The optimum formulation lies as well below 0 °C for C_8E_3.

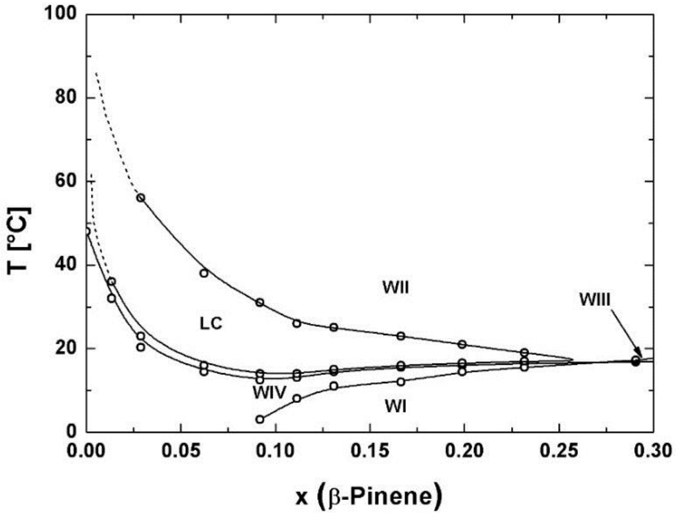

Figure 107 The lund cut of the system $C_{12}E_6$/β-pinene/water. A huge liquid crystalline phase appears right above the monophasic region.

Another compound which influences strongly the phase behaviour of a SOW system is the oil itself. In **Figure 108** the lund cut for several fragrances in aqueous C_6E_4 solution can be seen. C_6E_4 was chosen, since it is the most hydrophilic solvo-surfactant (see **Section 2.3.3.d.**), and thus it is able to determine the optimum formulation of very polar fragrances.

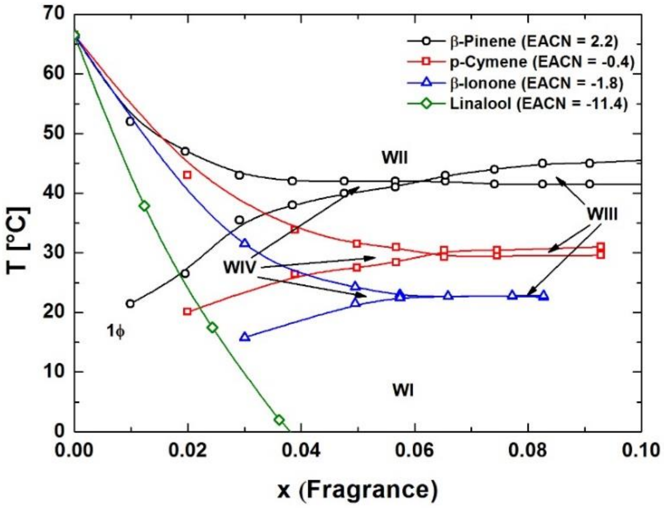

Figure 108 Lund cuts of the systems C_6E_4/fragrance/water. With decreasing EACN of the fragrance, the phase diagram shifts to lower temperatures. Furthermore the three-phase region narrows.

T* decreases with lowering EACN, since due to the higher polarity of the fragrance, it penetrates stronger into the interfacial layer. Hence resulting in a decrease of the curvature of the aggregates. Thereby the efficiency increases slightly, while the three-phase region decreases in size. For β-ionone the three phase region is almost disappeared. Linalool is that polar, that the optimum formulation lies below 0 °C. Considering the previous results, it is evident that the solubilisation of fragrances is complex, since the phase behaviour depends strongly on the hydrophilic-lipophilic nature of the amphiphile and the hydrophobicity of the oil. Furthermore these systems are highly sensitive to temperature alterations.

4.3.3. The effect of linalool on the phase behaviour of C_6E_4/β-pinene/water

In several studies in literature it was shown that polar compounds, such as alcohols are able to penetrate into the interface.[61,222] Kanei *et al.* showed thereby that perfume compounds may solubilise in the interfacial layer or in the hydrophobic core, depending on their polarity. He investigated the system $C_{12}E_8$/fragrance/water and stated that limonene is rather solubilised in the core, whereas alcohols, such as linalool, geraniol or eugenol penetrate strongly into the interface.

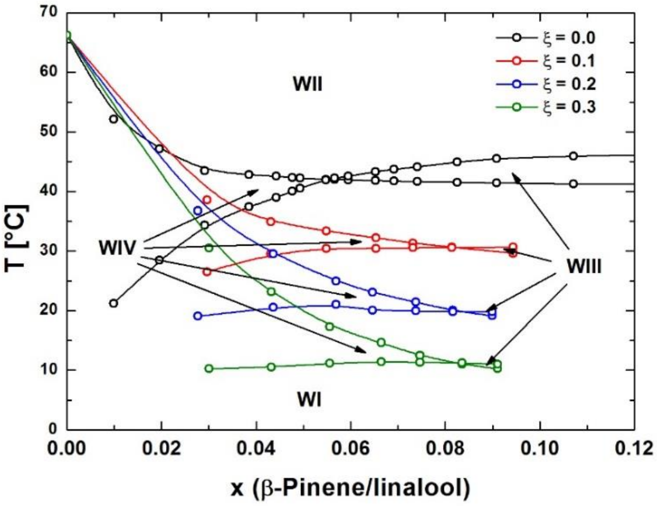

Figure 109 The evolution of the lund cut with increasing ξ, in the C_6E_4/β-pinene+linalool/water system. The intersection where all Winsor phases meet, represents the maximum solubilisation x*. In terms of clarity, ξ = 0.05 and 0.35 were not shown.

In this part the phase behaviour of C_6E_4/β-pinene+linalool/water systems is investigated. Thereby the oil phase composition is defined by:

$$\xi = \frac{m(linalool)}{m(linalool) + m(\beta - pinene)} \qquad \textbf{(52)}$$

The lund cuts for ξ = 0.00, 0.05, 0.10, 0.20, 0.30, 0.35 are investigated. The amphiphile mass fraction in water is in all cases 0.1. **Figure 109** summarizes the results for four of them. The lund cuts for ξ = 0.05 and 0.35 are not shown in terms of clarity. The initial lund cut with only β-pinene as oil is shown in black. With increasing linalool mass fraction ξ, the cut shifts towards lower temperatures. While the lund cut is quite symmetric in the beginning, it becomes more and more asymmetric with a lower phase border almost parallel to the abscissa for ξ = 0.3. This results furthermore in an increase of the temperature interval, wherein a monophasic WIV phase is obtained.

The composition of the microemulsion at *x** for each ξ, is summarised in **Figure 110**. With increasing linalool content, the mass fraction of β-pinene (+linalool) and C_6E_4 is changing in a non-linear way. The solubilised amount of β-pinene is increasing until a maximum is attained for $\xi = 0.10$. Further addition of linalool, results in a decrease of β-pinene in the mixture. The total oil mass fraction – β-pinene and linalool – increases also until a maximum at $\xi = 0.15$ is attained and afterwards it decreases only slightly. The mass fraction of C_6E_4 is nearly constant all over the observed interval, with a slight minimum at $\xi = 0.15$. In can be concluded that linalool acts as a co-surfactant until $\xi = 0.10$, by increasing the amount of β-pinene solubilised in the microemulsion. In the following the micellar interface is saturated with linalool and it migrates into the hydrophobic core, where it replaces β-pinene. The latter is thus decreasing in quantity. The overall solubilisation of fragrances is still increasing a bit until $\xi = 0.15$, which represents the optimal mass fraction of linalool ξ_{opt} in the system, at which the highest possible amount of fragrance mixture is solubilised (x^*_{opt}). Linalool may enter into the hydrophobic core between the amphiphile alkyl-chains and β-pinene, which results probably in a denser packing. Thus the amount of solubilised fragrance is still slightly increasing, even after the interface is saturated with linalool. However in the end x^* is decreasing slightly, probably also due to the fact, that the increasing polarity of the oil mixture, augments the monomeric solubilisation of C_6E_4. Consequently less amphiphile is present at the interface.

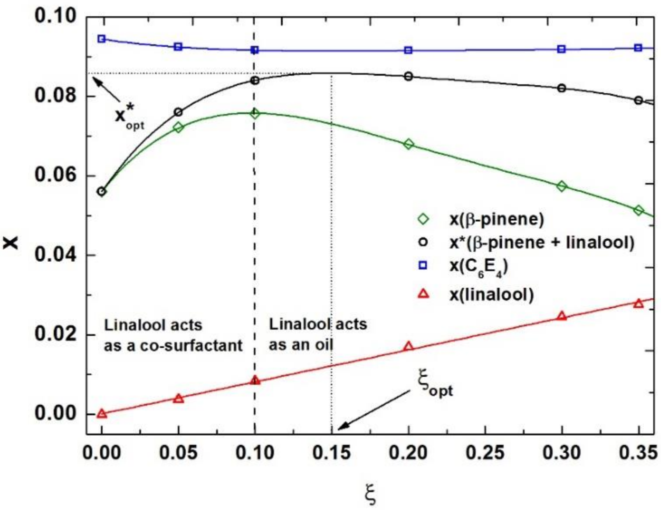

Figure 110 The composition of the bicontinuous microemulsion at the optimum formulation. Linalool acts as a co-surfactant until the interface is saturated. Afterwards it solubilises in the micellar core.

This experiment shows that there are different solubilisation sites for an oil. Thus the mixing of a very polar fragrance, with a high affinity for the interface, and a fragrance, which is clearly less polar, can increase the efficiency of the system. Thereby an optimal ratio between the two fragrances have to be found.

4.3.4. Prediction of the optimum formulation of aqueous fragrance formulations

The mixing of oils with different EACN, results in an alteration of T*. As already shown in **Section 4.3.2.**, a more polar fragrance tend to decrease T* stronger than a rather non-polar fragrance. In **Figure 111** the evolution of T* with increasing weight percentage of linalool is shown. The results originate from **Figure 109**. The experimental T*-values show a slight deviation from linearity, which is also observed in literature in similar systems.[23,62] Since it was shown, that the three-phase region is relatively narrow for short-chain amphiphiles with polar oils, the HLD equation can be applied to estimate T* of the mixture. Treating linalool as a co-surfactant results in an additional term in the HLD equation, with regards to a ternary SOW system.

$$HLD = Ccn - k \cdot EACN - aA + c_T(T^* - 25) \tag{53}$$

In order to estimate T*, the equation can be changed as follows..

$$T^* = \frac{-Ccn + k \cdot EACN + a \cdot A}{c_T} + 25 \tag{54}$$

..where *A* represents the alcohol mass concentration (wt.%) in the mixture and *a* is an alcohol specific coefficient, which can be determined with the PIT-Slope method of Ontiveros *et al.*[135] For linalool *a* is equal to 0.37. The coefficient *k* is usually 0.15 for C_iE_j's[25] and c_T and *Ccn* can be obtained by comparing the coefficients of **Equation 23** in **Section 3.3.** with the coefficients of the linear fit of ACN/T* data for C_6E_4. They are 0.03 and -0.22 respectively. Knowing all the coefficients, as well as the EACN of the oil, T* can be calculated in dependence of the alcohol concentration *A*. It can be seen that the calculated T* values are very close to the experimental value. Since **Equation 54** shows a linear relationship between alcohol concentration and T*, the slight non-linear trend of the experimental curve cannot be imitated. Nevertheless the calculated value approximate very well the experimental data and only for high alcohol concentration, the deviation is more pronounced.

The HLD equation offers thus a possibility to estimate the T* of SOW systems in the water-rich corner of the Gibb's diagram. Thereby even mixtures of two fragrances can be used, when one compound behaves as a co-surfactant. Mixtures with more than two fragrances complicate the situation. However for those compounds, whose EACN is not too different, an averaged EACN of the composition can be attributed. Thereby following relationship is valid..

$$\overline{EACN} = \sum x_i EACN_i \tag{55}$$

The averaged EACN can then be applied in **Equation 53**. The estimation quality of T* was verified for three mixtures of fragrances with linalool. The latter was not treated as an oil, so that it was not considered in **Equation 55**. In contrast it was used in the co-surfactant term "*aA*". The total mass fraction of fragrances, including linalool, is 0.008, which was then given into an aqueous C_6E_4 solution ($x = 0.1$). The expansion of the three phase region was measured, whose average was used to approximate the T* value of the system. It is referred to as $\bar{T}$, and it was compared to the calculated value T^*_{calc}. The results, as well as the used systems are summarized in **Table 20**.

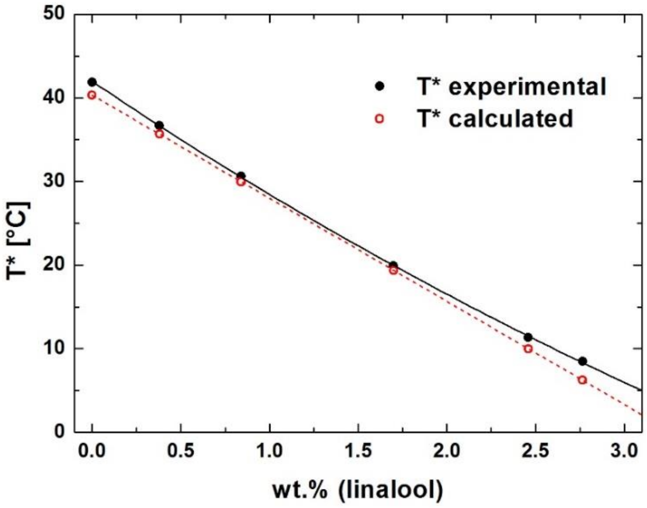

Figure 111 Evolution of T* with increasing linalool content. The progression is slightly non-linear. However the prediction via HLD is still quite accurate.

The composition of each sample was chosen so that T^*_{calc} is close to 20 °C. Sample 1 describes a fragrance mixture, which consists of very polar compounds. Thus their averaged EACN value is negative, with a value of -1.2. Such a mixture has already a low T* value, so that according to the objective to attain an optimal temperature around 20 °C, only small quantities of linalool were given into the mixture. The measured $\bar{T}$-value is equal to 23.3 °C, which is quite close to the calculated value of 20.2 °C. The second sample contained β-pinene, *p*-cymene and β-ionone with $\overline{EACN}$ = 0.0. The amount of added linalool is higher in this case, than in the previous one. T^*_{calc} is 19.9 °C and the experimental determined value is with 20.9 °C very close. In this case, the estimation turned out to be very precise. Sample 3 consists of rather weakly polar fragrances. *p*-Menthane is a cycled and branched hydrocarbon without any polar functionalisations and methyl cedrylether is a big C_{15}-ether. Their $\overline{EACN}$ is 3.9. Since their T* value is expected to be rather elevated (*i.e.* pinane, EACN = 4.0, T* = 56.8 °C), a relatively high amount of linalool has to be added. It is supposed that the elevated amount of linalool is responsible for the rather moderate accordance of the measured and calculated T*-value (15.4 °C to 19.6 °C respectively), since alcohols have no linear effect on the alterations of the interfacial curvature. Indeed the HLD equation is a linear relationship between the curvature and several formulation variables. This is valid for small concentrations of alcohols, but deviates for higher amounts. Nevertheless the HLD equation is quite useful for the estimation of the optimal temperature T* in water-rich systems, even with fragrance mixtures. Especially for the creation of water based perfumes, it can help the formulator in choosing the right surfactant for a given fragrance composition.

Table 20 Application of the HLD equation for the estimation of the optimal temperature for three fragrance mixtures in C_6E_4 with linalool as co-surfactant. The weight fraction *fw* of each compound in the fragrance mixture, as well as in the aqueous formulation are indicated. Based on *fw*, $\overline{EACN}$ was calculated according to Equation 55. T^*_{calc} was then determined according to Equation 54.

Sample 1							
Fragrance mixture 1 (FM1) with $\overline{\boldsymbol{EACN}} - \mathbf{1.2}$				SOW system			
	citronellyl acetate	α-damascone	β-ionone		FM1	linalool	C_6E_4 (aq)
fw	0.201	0.399	0.401	*fw*	0.075	0.005	0.920
EACN	-0.1	-1.2	-1.8				
Measured and calculated temperatures							
$\boldsymbol{T_1}$	22.9	$\boldsymbol{T_2}$	23.7	$\boldsymbol{\overline{T}}$	23.3	$\boldsymbol{T^*_{calc}}$	20.2
Sample 2							
Fragrance mixture 2 (FM2) with $\overline{\boldsymbol{EACN}} = \mathbf{0.0}$				SOW system			
	α-pinene	p-cymene	β-ionone		FM2	linalool	C_6E_4 (aq)
fw	0.333	0.332	0.335	*fw*	0.070	0.010	0.920
EACN	2.2	-0.4	-1.8				
Measured and calculated temperatures							
$\boldsymbol{T_1}$	20.7	$\boldsymbol{T_2}$	21.1	$\boldsymbol{\overline{T}}$	20.9	$\boldsymbol{T^*_{calc}}$	19.9
Sample 3							
Fragrance mixture 3 (FM3) with $\overline{\boldsymbol{EACN}} = \mathbf{3.9}$				SOW system			
	p-menthane	methyl cedrylether	α-pinene		FM3	linalool	C_6E_4 (aq)
fw	0.334	0.329	0.336	*fw*	0.054	0.026	0.920
EACN	6.0	3.5	2.2				
Measured and calculated temperatures							
$\boldsymbol{T_1}$	15.4	$\boldsymbol{T_2}$	16.0	$\boldsymbol{\overline{T}}$	15.7	$\boldsymbol{T^*_{calc}}$	19.6

4.3.5. The influence of ionic surfactants on the solubilisation of fragrances

a. The influence of DHS on the phase behaviour of C_6E_3/β-pinene/water at WOR = 1

Ionic surfactants are less temperature sensitive compared to non-ionic surfactant. Mixtures with both types of surfactants may form temperature-insensitive microemulsions. Kahlweit *et al.* showed that the 5-component system C_4E_1+AOT/*n*-decane/NaCl(aq) is able to form a temperature insensitive microemulsion between 30 – 80 °C at an amphiphile concentration of approximately 25 wt.%.[74] Better results are obtained in the system $C_{12}E_4$+AOT/*n*-decane/NaCl(aq), where a temperature insensitive monophasic region is obtained between 0 – 60 °C for a total surfactant concentration of only 7 wt.%.[228] The latter system is very efficient but contains unfortunately non-volatile surfactants. Also the first system with the volatile C_4E_1, contains 30 wt.% of AOT in the surfactant mixture. However both system showed that there exist a synergy in solubilisation and temperature stability, which is potentially applicable for fragrance solubilisation in water.

The synergy between ionic and non-ionic amphiphiles was already demonstrated in the pseudo-binary systems in **Chapter 2**. Though ionic surfactants are not volatile, small amounts (≤ 1 wt.%) can be considered as acceptable in a water-based perfume formulation. In this part, the effect of traces of DHS on the phase behaviour of C_6E_3/β-pinene/water is investigated, in order to verify if a synergy in solubilisation is obtained. Thereby aqueous DHS solutions were prepared, with either $\varepsilon = 0.9*10^{-4}$ (0.2 wt.%) or $\varepsilon = 2.8*10^{-4}$ (0.6 wt.%). The results can be seen in **Figure 112**. The fish cut of C_6E_3/β-pinene/water serves as reference system. The addition of 0.2 wt.% DHS to the water phase results in a bizarre distorted fish cut. Thereby a mono-phasic region appears as a twisted fish head of the diagram. The Winsor III phase is extremely shrunk with regards to the phase diagram without DHS. It has to be noted that the isolated mono-phasic region is quite turbid with a touch of opalescence and stays monophasic even after three weeks of equilibration time. Thus it is considered that the aggregates are extremely huge in this zone and consequently interact with the surrounding light. A similar phase behaviour was obsevered by Kahlweit *et al.* for the quaternary system C_6E_2/*n*-decane/sodium decyl sulfate (aq).[229]

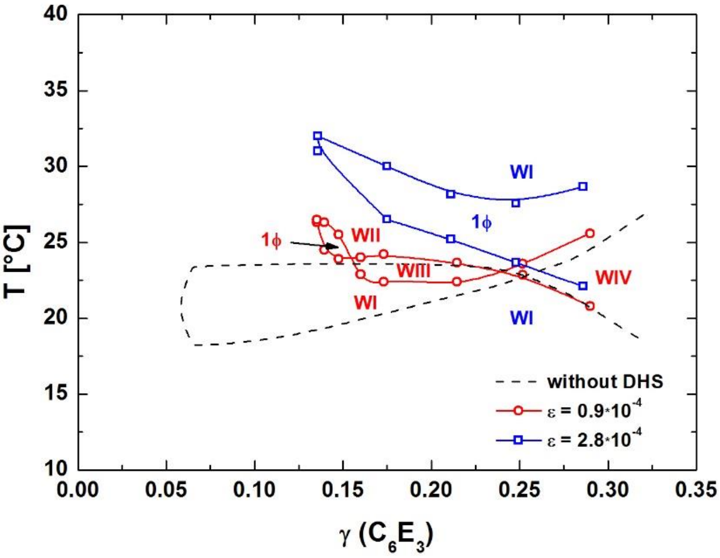

Figure 112 Influence of the ionic surfactant DHS on the fish cut of the ternary system C_6E_3/β-pinene/water. ε signifies the molar fraction of DHS in the water phase.

By adding 0.6 wt. % DHS to the aqueous phase, the WIII phase disappears completely, leaving a long drawn-out and relatively narrow monophasic region. In its upper top, the microemulsion showed as in the case before a turbid opalescent appearance, but stayed monophasic even after long equilibration. The region is displaced towards higher temperatures, which can be explained with the more hydrophilic pseudo-surfactant. Furthermore the system do not inverse anymore. The WII phase do not appear at higher temperatures. Instead a WI phase shows up, as it is the case for low temperatures. With increasing temperature the excess oil phase is solubilised, resulting in the WIV phase. Further increase in temperature dehydrates C_6E_3, which in turn becomes hydrophobic. However DHS is temperature insensitive in a system without salt. Thus the non-ionic amphiphile solubilises in the micellar core of DHS and β-pinene is squeezed out as excess phase, resulting in another WI-phase.

The addition of small quantities of DHS results in a synergy in solubilisation of β-pinene, as well as in an increase in temperature stability of the WIV phase. Nevertheless the monophasic region stays relatively narrow and is far away from the 60 °C temperature interval, which is obtained by Kahlweit. However he used *n*-decane as an oil, which shows a big three-phase body in the fish cut. Its expansion might be related to the extent of the monophasic region with ionic surfactant.

In **Figure 113** an attempt in explaining the phase behaviour in **Figure 112** is shown by using semi-schematic ternary phase diagrams. Thereby the phase diagrams consider the previous findings at a given temperature and DHS mass fraction. In **Figure 113.a** the ternary phase diagram of C_6E_3/β-pinene/water at 22.5 °C is shown. In order to facilitate the following explanations, the corners of the three phase region are denominated with **A**, **B** and **C**. In the following considerations **B** does not change, since it is assumed that ionic surfactants have little influence on the SO binary phase diagram. With addition of 0.2 wt.% DHS to the aqueous phase, **A** moves towards **C**, revealing a monophasic region in the water rich corner of the Gibb's triangle (blue shaded, **Figure 113.b**). Thereby the WIII shrinks and consequently also the adjacent WII lope. T* increases only slightly to 22.8 °C. In the three phase triangle, **C** is moving towards **B**, as the temperature is increased to 25.0 °C, since the ethoxy groups of C_6E_3 dehydrate, which turns the pseudo-surfactant more lipophilic (**Figure 113.c**). Furthermore **A** is shifting towards higher oil content. A higher temperature dehydrates the ethoxy head groups, which in turn results in a smaller effective equilibrium area. Thus the effective packing parameter increases towards 1 (see **Equation 25**), which indicates a zero curvature and more β-pinene can be solubilised. Thereby a strong synergistic interaction between C_6E_3 and DHS must occur, since only 13 wt.% of C_6E_3 is able to solubilise same amount of oil and water, whereas in the case of pure C_6E_3, 25 wt.% is needed. With further addition of DHS to the aqueous phase, the three-phase region disappears, since **A** merges with **C** (**Figure 113.d**). The system is not able to inverse from an o/w microemulsion to a w/o microemulsion. This can be attributed to the strong hydrophilic characteristics of the ionic surfactant DHS.

In order to understand the influence of an ionic surfactant on the phase behaviour of a SOW system, its (pseudo-)ternary phase prism has to be observed. Inspired from Kahlweit's phase prism (see **Figure 8**), a simplified schematic representation of the SOW – Temperature phase prism with and without ionic surfactant was designed (**Figure 114**). In the case without ionic surfactant, the phase behaviour is principally determined by the miscibility gaps of the SW and SO binary phase diagrams. Each point of the critical points line represents a composition at given temperature, which is in equilibrium with two phases. Starting from T_β, the addition of an oil decreases the critical point cp_β until the critical endpoint cep_β is attained. Consequently at lower temperatures the amphiphile is too hydrophilic to form any WIII and WII phases. The inverse happens, if one starts from T_α, where the addition of water results in an

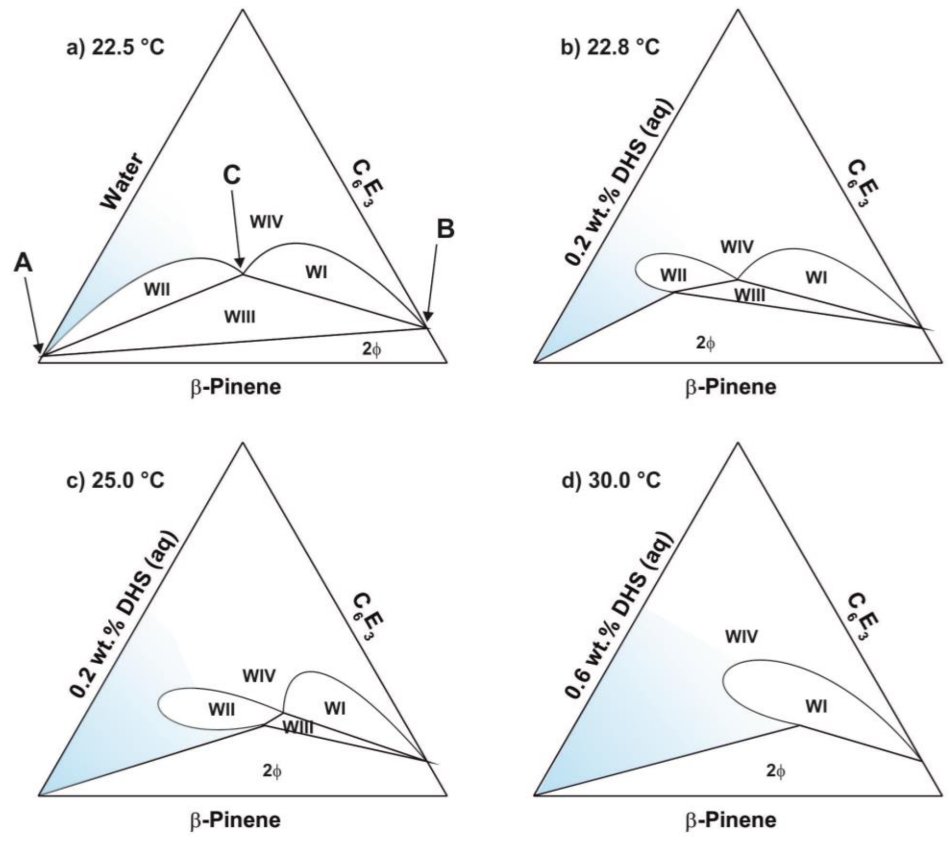

Figure 113 Semi-schematic representation of the ternary phase behaviour of C_6E_3/β-pinene/water upon addition of DHS to the water phase. The phase borders orientate themselves on the results from Figure 112. Their exact expansion is not known.

increase of the cp_α, until cep_α. There the WIII and WI phase disappear, since the amphiphile turns too hydrophobic. Thus the expansion of the three phase region is mainly determined by T_α and T_β, which is related to the solubility of the amphiphile in the water and oil phase.[207,226] On a molecularly level it can be explained with the amphiphile having high preferences for both the aqueous and oil phase. Consequently an amphiphile with a very high T_β and/or very low T_α, results in an approach of the critical endpoints, until there is no break in curve anymore. This point represents the tricritical point. From thereon, the system is not able to form any three-phase region and there is a continuous transformation of a WI to WII phase, or inverse. Kahlweit *et al.* showed in the system C_4E_2/*n*-alkanebenzene/water how the three-phase region is declining with decreasing alkane-chain of the oil.[230] While for *n*-heptylbenzene a narrow WIII phase could be observed, it disappeared for *n*-hexylbenzene. In addition it has to be stated that the SOW-T phase prism represents an idealised case. In reality the critical point of the SW binary phase diagram may increase in temperature upon addition of an oil. However this happens only if the temperature T_l of the cep_β lies above T_β. This may happen for hydrophobic oils and surfactants, and consequently lead to a paradox phase behaviour, where the addition of an oil to an immiscible SW mixture results in a monophasic region.[230] In this work all solvo-surfactant/fragrance/water mixtures behave according to **Figure 8/Figure 114**, with $T_\beta > T_l$.

The influence of an ionic surfactant on the phase behaviour of a SW system was already shown in **Chapter 2**. T_β and *w** increases, which strongly affects the critical points line in a temperature dependent pseudo-ternary phase prism. It is assumed that the ionic surfactant does barely affect the SO phase diagram. In **Figure 114** (right), the effect of an ionic surfactant on the critical points line and eventually on the phase behaviour of the SOW-T system can be seen. T_β increases and thus cep_β increases as well. Furthermore the three-phase region shrinks, since the superposition of the miscibility gaps in the binary phase diagrams SW and SO is reduced. The addition of ionic surfactant increases as well w^*, which in turn is responsible for the shrinking of the three-phase region towards T* and thus the shrinking of the WII lobe. Consequently a monophasic region is revealed in the water-rich corner.

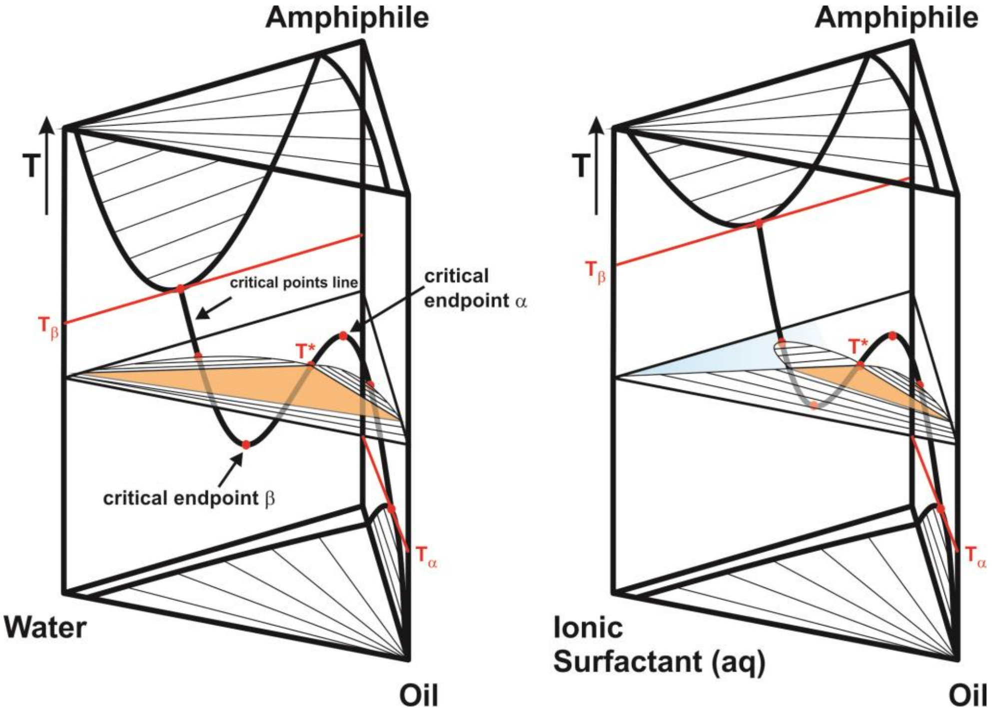

Figure 114 The influence of an ionic surfactant on the progression of the critical points line in the ternary phase prism. Left: The SOW-T system without ionic surfactant. The temperature dependent expansion of the three-phase region is enclosed by the critical endpoints cep_α and cep_β. Right: The SOW-T system with ionic surfactant. T_β augments, which in turn results in a shrinking of the three-phase region. Consequently a huge mono-phasic region appears in the water-rich corner of the prism.

Thus any alterations in the binary phase diagrams, affect the phase behaviour in a ternary diagram. According to the previous results and considerations, it can be concluded that the existence of a three-phase region is of great importance for an efficient solubilisation of fragrance in an aqueous amphiphile solution, since the shrinking of the WIII phase and the WII lobe, results in a monophasic region, which is close to a bicontinuous microemulsion. It is known that zero curvature represents the optimum formulation, at which a maximum of oil and water is solubilised.

b. The effect of salt on a quaternary mixture and its use for fragrance solubilisation

The effect of salt on the phase behaviour of C_6E_4/DHS/*p*-cymene/water is investigated, in order to verify its use for fragrance solubilisation. Kahlweit *et al.* described the influence of salts on the SOW phase behaviour.[48,50,134] Thereby he showed that salts can either increase or decrease T*. Since ionic surfactants tend to shift the monophasic region in a SOW system towards higher temperatures, electrolytes might be of interest for fragrance solubilisation, in order to decrease the temperature interval to ambient temperatures. Salts can either have a slating-in or salting-out effect.[231] The first effect describes the increased solubility of an amphiphilic compound in water, since they favour the hydration of the ethoxy groups, whereas the latter captures water, which in turn results in a dehydration of the head group of the amphiphile.[232,233] Thus the amphiphile becomes less soluble in water. In a ternary SOW the previously described effects are also valid. A salting-out electrolyte is thus able to decrease T* of the system, whereas a salting-in electrolyte increases it.

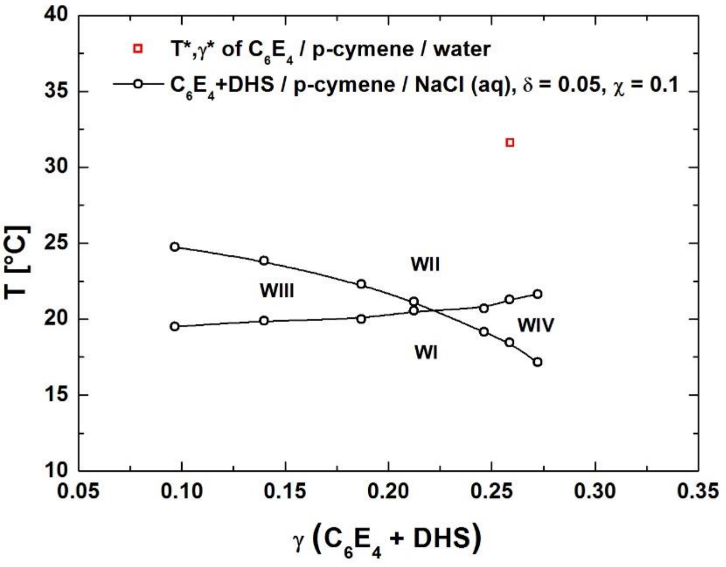

Figure 115 Fish cut of the 5-component system C_6E_4+DHS/*p*-cymene/ NaCl (aq) and fish tail of C_6E_4/*p*-cymene/water.

In this part, the fish and lund cuts of the SOW system C_6E_4/*p*-cymene/water were compared to those made with DHS and NaCl. The latter is known to be a salting out electrolyte. In the following considerations C_6E_4 and DHS were homogenised and utilized as a pseudo-surfactant.

$$\chi = \frac{m(DHS)}{m(DHS) + m(C_6E_4)} \tag{56}$$

χ describes the mass fraction of DHS in the amphiphile mixture. The mass fraction δ of NaCl in water was defined according to following relationship:

$$\delta = \frac{m(NaCl)}{m(NaCl) + m(H_2O)} \tag{57}$$

In **Figure 115**, the fish tail of C_6E_4/*p*-cymene/water, as well as the fish cut with DHS and NaCl can be seen. The data for the SOW system was obtained from literature.[171]

As it was shown in **Figure 112**, the addition of an ionic surfactant to a non-ionic SOW system results in an increase in efficiency of the system, as well as in a disappearance of the three-phase region. In contrast, the addition of an ionic surfactant and salt results in the reappearance of the WIII phase. The efficiency is slightly increasing. However the system returns also to a state with high temperature sensitivity.

Same behaviour can be observed for the lund cuts in **Figure 116**, where same systems were investigated. In this case the loss in temperature stability is even more pronounced than in the fish cut. With the addition of salt, the phase diagram returns to its original long drawn-out shape. Compared to **Figure 112**, where the addition of an ionic surfactant, results in a huge temperature stable monophasic region, the salt revert this effect. Though the here compared systems are not exactly the same, a comparison can be made, since the phenomenological influence of the salt stays the same. The electrolyte accumulates at the interface between water and oil, capturing water, which in turn is no longer available to hydrate the polar head groups of the amphiphiles. Even the ionic surfactant, which is usually temperature insensitive and prevents the system from inverting, as described previously, is screened by the salt and thus able to adopt a negative curvature. Consequently, the pseudo-surfactant is able to form a three phase region.

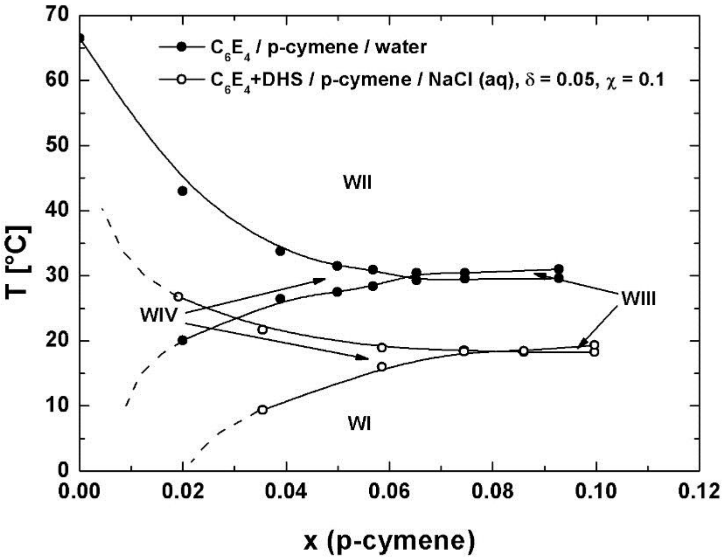

Figure 116 Lund cuts of the system C_6E_4/*p*-cymene/water and C_6E_4+DHS/*p*-cymene/NaCl (aq).

In conclusion the addition of salt has only little effect on the efficiency of the pseudo-surfactant to solubilise fragrances. Furthermore it reverts the temperature insensitivity of the system due to a screening effect, which in turn results in a diminution of the expansion of the mono-phasic region. The utile effect to adjust T* in dependence of the salt concentration, is thus less beneficial to fragrance solubilisation.

c. The effect of ionic surfactants on a water-rich microemulsion

In this part, the effect of small amounts of ionic surfactant on the phase behaviour of C_6E_3/β-pinene/water was investigated. Thereby a lund cut was performed at constant SWR (*w* = 0.1). As ionic surfactants, SDS and DHS were chosen, since according to the pseudo-binary phase diagrams in **Chapter 2**, they exhibit the strongest effect on the phase separation temperature at 10 wt.% solvo-surfactant content.

In **Figure 117**, the lund cuts for three different molar fractions of DHS were constructed. Thereby the lund cut without any ionic surfactant is shown as a reference system, in order to highlight the alterations, affected by DHS. In all three cases, it can be seen that the monophasic region is largely increasing with regards to the reference system. Thereby the lower phase separation border stays nearly constant. This indicates that the lower miscibility gap of the binary system C_6E_3/water is barely affected by the ionic surfactant. The lower miscibility gaps of all binary systems exist because of thermodynamic reasons. Consequently their appearance is not linked to the dehydration of polar head groups, such as in the case of the upper miscibility gap in the SW system. Eventually the upper phase border augments and reveals a huge monophasic region, which is increasing in size, with higher molar fractions of DHS. The highest efficiency in solubilisation of β-pinene was obtained for the lowest investigated molar fraction of DHS ($\varepsilon = 0.9{*}10^{-4}$). However with further increase of ionic surfactant content, the efficiency of the system reduces, whereas the temperature stability increases. The tapering monophasic region is thereby transforming to a flattened curve around the maximum solubilisation. Noticeable is the inexistent of the three-phase region. Instead a two-phase region is formed, with resembles in its appearance a WI phase. In its oil phase a white pseudo-phase is formed, which resembles a sort of crème and could be misinterpreted as a WIII phase. However there is no clearly defined interface between the pseudo-phase and the oil and water phase. It rather swims in the oil phase on top of the water phase. Probably it is precipitated amphiphile. Furthermore the system is – as described in **Section 4.3.5. -** not able to invert the phases. Thus instead of a WII phase, a WI phase is formed at elevated temperatures. Another difference to the phase behaviour of the reference system is the appearance of a liquid crystal phase directly above the monophasic region, which is increasing in size with augmenting DHS content. According to the phase rule, there should be a slight two-phase region between the liquid crystal phase and the mono-phasic region. However its expansion is so small, that it was not possible to determine. The appearance of a liquid crystal phase is somewhat surprising, since C_6-amphiphiles are not able to form those. Supposedly the interaction with the ionic surfactant, in combination with the polar oil, which is able to penetrate between the alkyl-chains, is responsible for this phenomena. Kunieda *et al.* showed in his work, how polar oils may induce the formation of hexagonal and lamellar phases.[234]

In **Figure 118**, the same type of diagrams as previously described, are seen, with the difference, that DHS was replaced by same molar fraction of SDS. The influence of SDS and DHS was already similar in the binary SW phase behaviour (see **Chapter 2**). Analogies are as well visible in the case of SOW systems. As DHS, the ionic surfactant SDS is able to increase the efficiency of the system, as well as the temperature stability. The expansion of the monophasic region corresponds thereby closely to those with DHS. Nevertheless, the latter turned out to be slightly more efficient in solubilising β-pinene, whereas the systems containing SDS are stable over a higher temperature interval. Furthermore SDS induces to a lower extent the formation of liquid crystalline phases. At $\varepsilon = 0.9{*}10^{-4}$, no liquid crystals were observed and those formed at higher mass fractions are still smaller in size compared to those obtained with DHS.

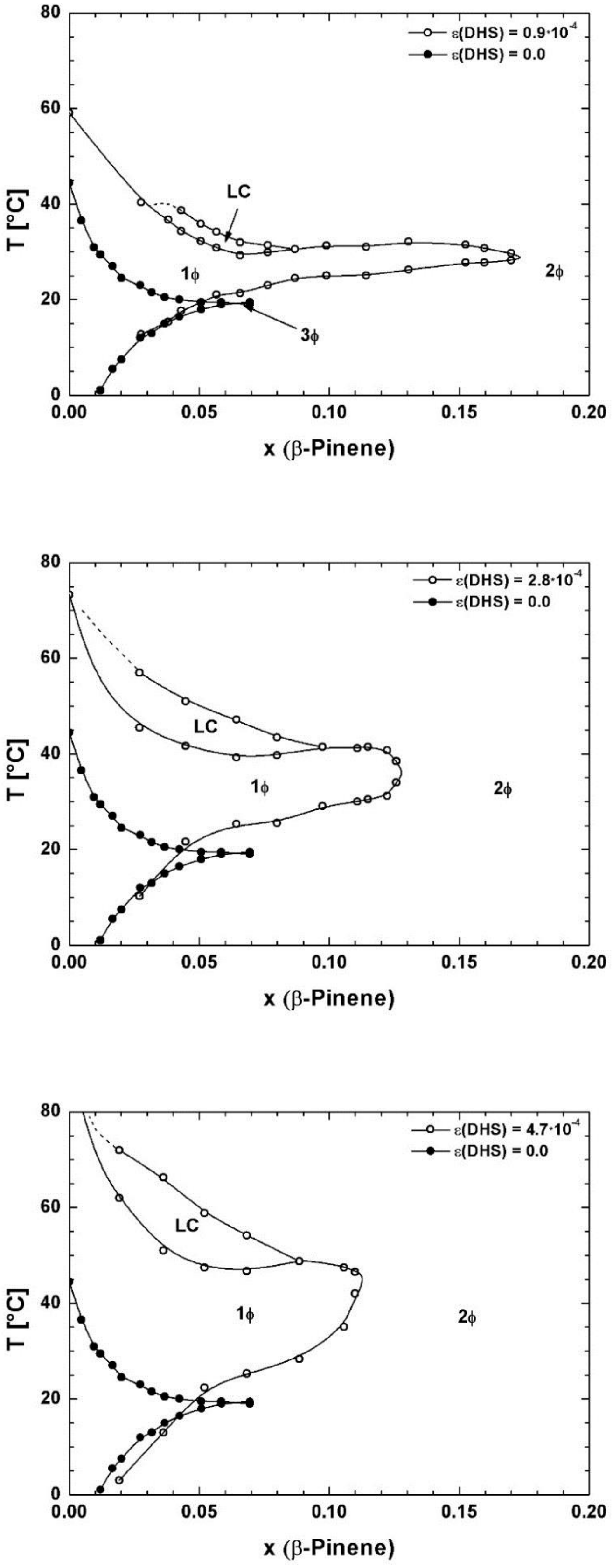

Figure 117 Influence of DHS on the ternary system C_6E_3/β-pinene/water. Upon addition of DHS, the three-phase region disappears, revealing a huge mono-phasic region. The efficiency of the mixed amphiphile to solubilise β-pinene, has its maximum for ε = 0.9*10^{-4}. Afterwards it is decreasing, while the temperature stability augments steadily.

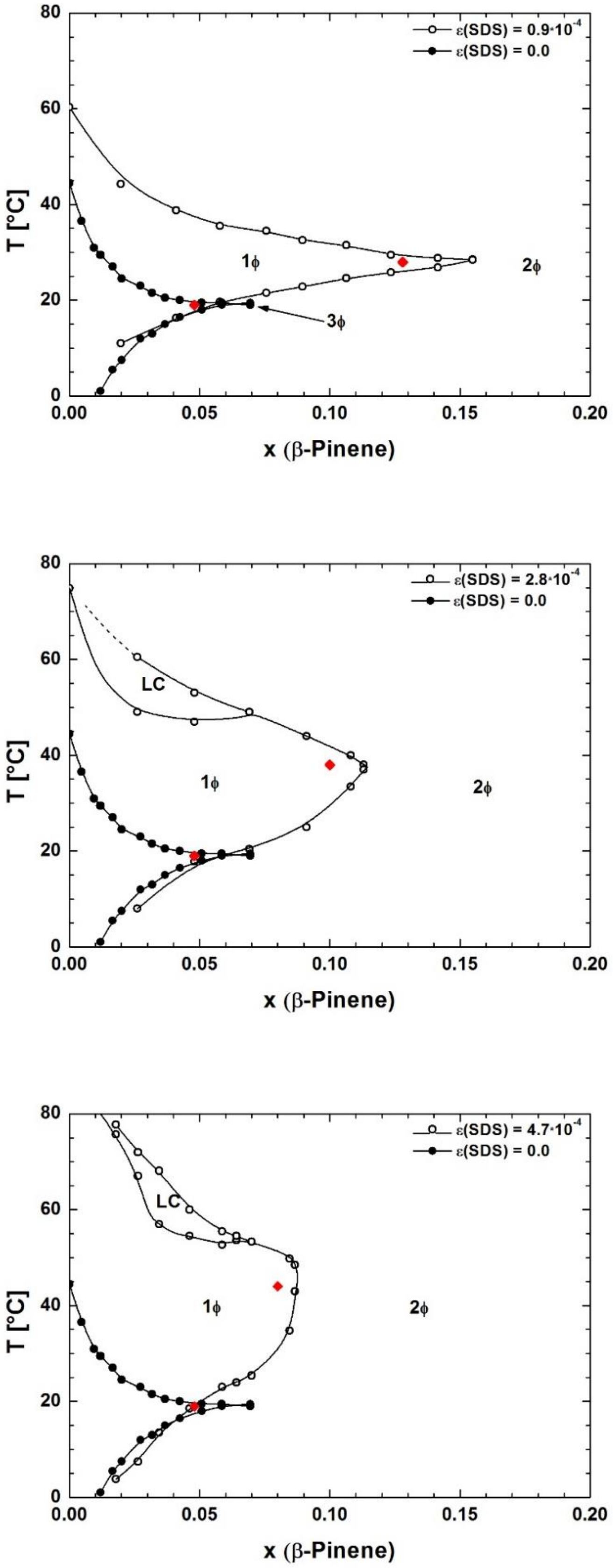

Figure 118 Influence of SDS on the ternary system C_6E_3/β-pinene/water. As in Figure 117, the three-phase region disappears upon addition of SDS and the mixed surfactant has a maximum in efficiency for $\varepsilon = 0.9*10^{-4}$. The red dots signify compositions, which are investigated by DLS in Section 4.3.6.

In both cases – with DHS or SDS - the increase in temperature stability can be attributed to the formation of charged mixed micelles. Thereby the interval within the mixture stays mono-phasic, augments continuously with increasing ε. It appears to be limited by the appearance of liquid crystalline phases. In contrast the magnitude of the solubilised amount of β-pinene is not increasing continuously and bears a maximum for a certain mass fraction of ionic surfactant. In **Figure 119** a schematic representation of the phase behaviour of the system solvo-surfactant/fragrance/water (SFW), respectively solvo-surfactant/fragrance/ionic surfactant(aq) is shown. The following considerations are of course also valid for other oils, and probably as well for surfactants. However the explanations are made with respect to the results in **Figure 117** and **Figure 118**.

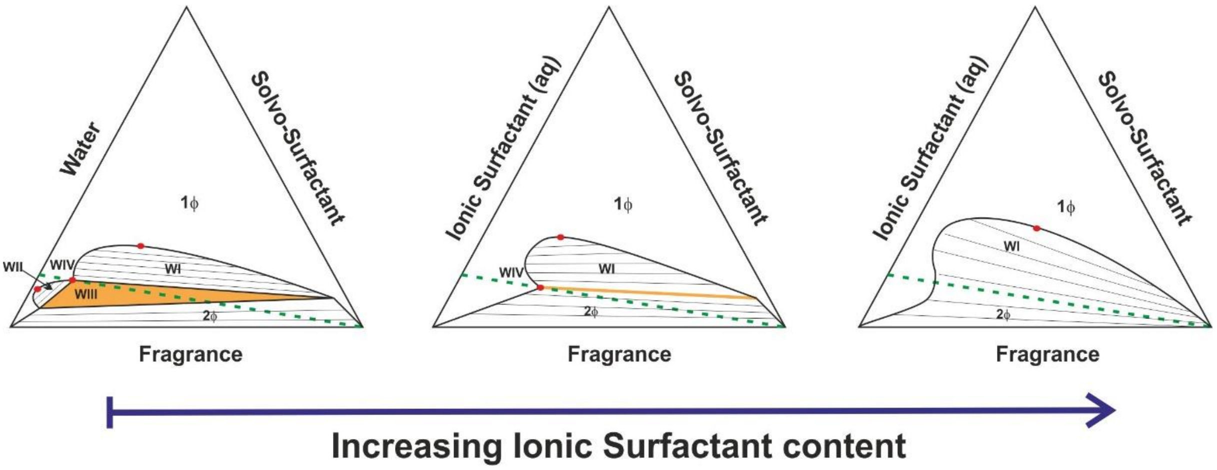

Figure 119 Schematic representation of the influence of ionic surfactant on the phase behaviour of a SFW system in the water-rich corner.

In the left diagram, the phase behaviour with no ionic surfactant can be seen. The WI – IV phases are present, as well as two critical and one characteristic points (red). The WIV phase is often used to signify a mono-phasic region. However more precisely it indicates a mono-phasic region, where the amphiphile has same affinity for the water and oil phase. This is the case in the vicinity of the characteristic point of the three-phase region. The temperature dependent lund cut is indicated as green dashed line. It traverses the monophasic region and the characteristic point, before entering the three-phase region. Increasing the temperature moves this point towards the right corner of the three-phase region, which in turn result in an expansion of the WII lobe. Thus at given temperature a WII phase is obtained in the lund cut. On the other hand, the decrease in temperature results in a movement of the characteristic point towards the left corner of the triangle. Consequently the WI lobe is increasing and a WI phase is obtained in the lund cut. With the addition of an ionic surfactant to the water phase, the three-phase region shrinks, until the critical and characteristic points of the WII and WIII phases are merging. It describes the optimal amount of added ionic surfactant, which is necessary to obtain the maximum expansion of the monophasic region towards higher oil content. It is the point at which the three-phase region disappears and for the given SOW system, it describes the most efficient binary surfactant system to solubilise the fragrance. The increase or decrease of ionic surfactant content, above or under the optimal ionic surfactant molar fraction, result in any case in less solubilisation of β-pinene. A molar fraction of $0.9*10^{-4}$ DHS or SDS, is very close to the optimal amount of ionic surfactant, since as it can be seen in **Figure 117** and **Figure 118**, the lund cut is long drawn-out, which indicates the recent disappearance of the three-phase region. On a molecular level, it can be imagined that the ionic surfactant forms mixed micelles with the solvo-surfactant, wherein the fragrance is solubilised. Due to the synergy between the two amphiphiles (see **Section 2.3.2.a.**), the solubilised quantity of fragrance increases, until at the optimal molar fraction of ionic surfactant the critical and characteristic points merge (**Figure 119**, centre). At this point the bicontinuous microemulsion is in equilibrium with excess oil and water. With further increase in ionic surfactant content, the pseudo-surfactant turns too hydrophilic and a balanced state with zero curvature cannot be formed anymore (**Figure 119**, right). There is neither a WIII phase, nor a WIV phase available. Consequently, after the disappearance of the three phase region, the curvature at the maximum solubilisation is not equal to zero. Starting from an o/w microemulsion at low temperature, the curvature is mainly determined by the solvo-surfactant (see **Figure 117** and **Figure 118**). With increasing temperature their polar head groups dehydrate and the curvature is approximating the optimal formulation. Thereby the excess fragrance oil is solubilised inside the micellar core and a mono-phasic region is formed. Without ionic surfactant the system would invert with increasing temperature. However the temperature insensitive ionic surfactant counteracts the inversion of the micelle. Consequently with further increasing temperature, the ionic surfactant content in the interfacial composition is increasing, since the dehydrated solvo-surfactant passes to the oil phase. Hence there are two consequences, which appear. First of all, the curvature is more and more determined by the ionic surfactant, which in turn results in a curvature, which is farther away from the optimum formulation. Secondly, less amphiphile is available at the interface to solubilise β-pinene, since the solvo-surfactant migrates to the oil phase. Consequently, the WIV phase shrinks. It can thus be concluded that the maximum solubilisation represents an aggregate with the closest curvature to zero. Furthermore a huge three-phase region in a SOW system may be favourable for the aqueous solubilisation of fragrances with traces of ionic surfactant, since bigger quantities of those are needed to merge the critical with the characteristic point. Unfortunately polar oils, such as fragrances tend to form small three-phase regions in short-chain C_iE_j's. In the next section dynamic light scattering measurements are performed in order to support the theoretical considerations, made in this section.

4.3.6. Dynamic light scattering investigation of the micelle size in the vicinity of the maximum solubilisation

In the previous section, it was shown that for a certain molar fraction of SDS in water, the efficiency to solubilize β-pinene has a maximum. Thereby it was possible to solubilize more than 15 wt.% of β-pinene with only 10 wt.% C_6E_3 in an aqueous SDS solution ($\varepsilon = 0.9*10^{-4}$). Same was observed in the case of DHS, where even 17 wt.% of β-pinene was solubilized.

In this part the micelle size in the vicinity of the maximum solubilisation was investigated by dynamic light scattering measurements with a LS spectrometer from LSinstruments at an angle of 90°. Thereby four mixtures were prepared, which are marked as red dots in **Figure 118**. The β-pinene content was chosen to be approximately 80 wt.% of the maximum solubilisation. The mixtures were measured at the temperature in the vicinity of the maximum solubilisation. Before the light scattering measurements were performed, the viscosity and refractive index of the monophasic mixtures at the desired temperature were determined. Relevant data is summerized in Table 21. The refractive index is nearly constant for all samples, whereas the dynamic viscosity changes extremely. However it is surprising that there is no continuous relationship between ε and η.

Table 21 Relevant data concerning the DLS measurements. The molar fraction ε of SDS in the aqueous phase, as well as the mass fraction *x* of β-pinene in the sample is indicated. Furthermore the dynamic viscosity η and the refractive index RI is shown. They are necessary to determine the hydrodynamic radius of the aggregate R_h. At last the maximum solubilisation *x of each system is shown.**

ε [$*10^{-4}$]	*x*(β-pinene)	η [mPa*s]	RI	R_h [nm]	*x**
0.0	0.048	2.88	1.361	4.1	0.064
0.9	0.128	1.93	1.358	8.3	0.155
2.8	0.100	8.86	1.353	5.8	0.113
4.7	0.080	5.71	1.351	5.4	0.088

In **Figure 120** the results from the scattering experiments can be seen. The left axis shows the hydrodynamic radius of the micelle in dependence of the molar fraction *x* of SDS, whereas the right axis shows the maximum solubilisation *x**. Without SDS the particle size is 4.1 nm and *x** is 0.064. With addition of SDS the maximum solubilisation and the micelle size increases to 0.155 and 8.3 nm. Further addition of SDS decreases *x** and R_h. Thereby the relation between R_h and *x** proceeds proportional to each other.

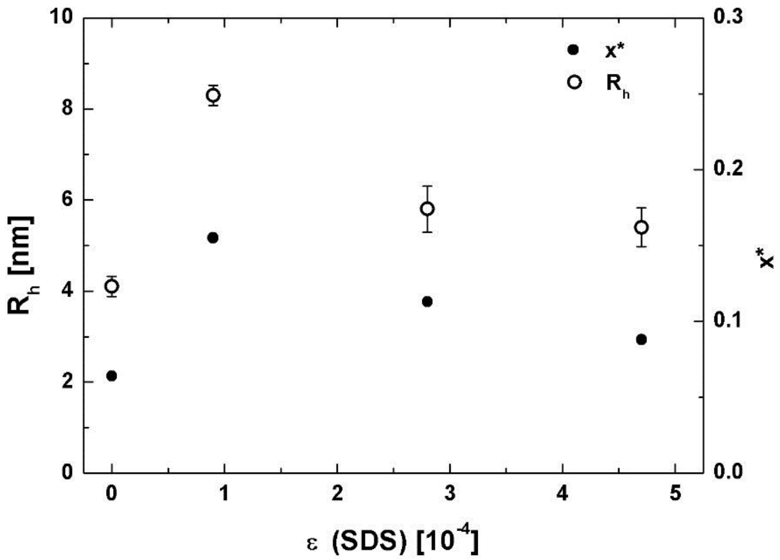

Figure 120 The hydrodynamic radius R_h of the aggregates as a function of the ionic surfactant molar fraction ε. The radius behaves proportional to the maximum solubilisation *x.**

It is striking that the micellar radius behaves similar to the amount of β-pinene solubilized in the mixed micellar aggregates. It has to be remembered that in the case without SDS, a three-phase region exists, whereas it disappears for already small amounts of SDS ($\varepsilon = 0.9*10^{-4}$). The characteristic point at which all the Winsor phases meet, represents a mixture with zero curvature, and consequently a bicontinuous microemulsion, which is known to solubilize huge quantities of oil and water. Between $\varepsilon = 0.0$ and $\varepsilon = 0.9*10^{-4}$, this point disappears. It can be assumed that R_h and x^* increases until the three-phase region disappears. Note that SDS is much less sensitive to temperature alterations. The polar head group is strongly hydrated, which in turn prevents the system to invert from WI to WII with increasing temperature and eventually the three phase region disappears. The molar fraction of SDS at which the three-phase region disappears can thus be considered as the optimal amount to obtain the highest solubilisation of the oil within the given SOW system. It is assumed that $\varepsilon = 0.9*10^{-4}$ is very close to this optimal amount, given the immense increase of x^* from 0.064 to 0.155. The following decrease in R_h and x^* can thus be explained with the increasing hydrophilicity of the interface. The higher the amount of SDS in the mixed micelle, the bigger the curvature of the aggregates and thus the farther is the system away from zero curvature. Roughly spoken, the system moves farther away from the possibility to form a bicontinuous microemulsion with increasing SDS content, beyond the optimal amount of SDS. This is especially indicated by the decreasing size of the aggregates.

The results from the DLS experiments, confirm the theoretical considerations in **Section 4.3.5.c**. Furthermore it is obvious now, that the boosting effect of an ionic surfactant has its limitations concerning the increase in efficiency to solubilize an oil in aqueous amphiphile solution. However the temperature stability of the system increases constantly. Regarding possible water based applications, it can be concluded that a compromise has to be made between temperature stability and amount of oil solubilized.

4.3.7. The 5-component system C_6E_4/β-pinene+linalool/SDS(aq) at various β-pinene to linalool ratios

In **Section 4.3.3.**, the phase behaviour of C_6E_4/β-pinene+linalool/water was investigated in dependence of varying ξ. Same is done in this section, with the difference of having SDS ($\varepsilon = 2.8*10^{-4}$) in the aqueous phase. It shall be verified it the co-surfactant characteristics of linalool persist in the presence of an ionic surfactant.

In **Figure 121** the phase diagrams are shown for ξ = [0.00, 0.08, 0.15, 0.35]. The efficiency of the system is only slightly increasing with augmenting linalool content. A maximum was obtained for ξ = 0.08 and consequently it is decreasing strongly. Thereby the tapering end of the phase borders are flattening, as it was observed in **Section 4.3.2.c.** for increasing ionic surfactant content. In the latter case, the flattening was explained with the increasing amount of ionic surfactant within the interfacial layer. Same is valid here, although the ratio between SDS and C_6E_4 is constant within the mixture. In **Chapter 3** it was shown that the monomeric solubility of the non-ionic amphiphile increases with decreasing

EACN. The two fragrances β-pinene and linalool can be seen as a pseudo-oil, whose EACN is decreasing with augmenting linalool content. Consequently the quantity of monomerically solubilsed C_6E_4 increases with augmenting ξ. Hence the ratio of SDS to C_6E_4 at the interface augments, which in turn results in a more hydrophilic and less temperature sensitive surfactant layer.

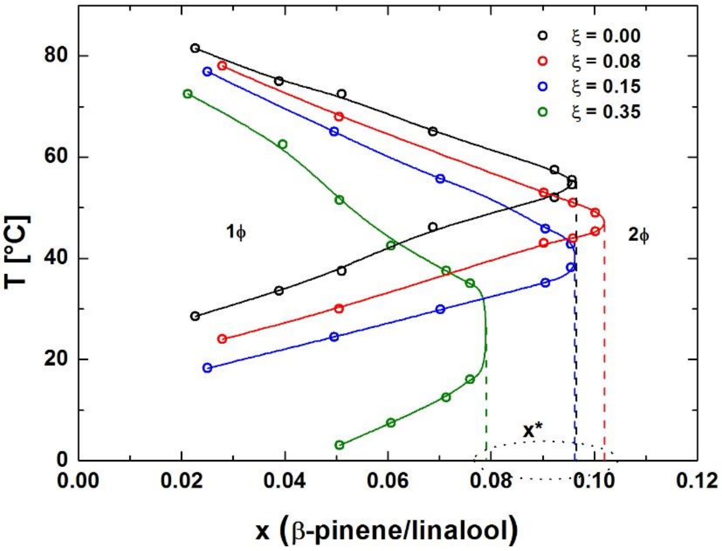

Figure 121 The 5-component system C_6E_4/β-pinene+linalool/SDS (aq). ξ signifies the mass fraction of linalool in the fragrance mixture. ε is $2.8*10^{-4}$ and *w* = 0.1. The maximum solubilisation x* is indicated with dashed lines.

It is thus possible to explain the evolution of x^* in dependance of ξ. Thereby it was compared to the results obtained without SDS (**Figure 122**). It can be seen that SDS increases strongly the efficiency of C_6E_4 to solubilise β-pinene (ξ = 0). With increasing linalool content, a maximum is obtained around ξ = 0.08. However there is only a slight increase in efficiency, compared to the system without SDS. Probably the penetration of linalool into the interfacial layer is hindered by the geometrical structure of SDS (big σ_0), which imposes a positive curvature onto the aggregate, whereas alcohols on the other hand are known to have a small σ_0. Consequently it is difficult for linalool to enter the interfacial layer. It can be imagined as a triangle, whose top represnts the alcohol group of linalool, which tries to enter a curved o/w micelle from the oil side. The close arrangement of the hydrophobic tails makes it difficult for a sterical hindered oil to enter within the layer. On the other hand, without SDS, the interface's curvature is highly sensitive to temperature effects, which in turn allows an easy penetration of linalool. Consequently stripped of from its potential of being a good co-surfactant, linalool behaves rather as an oil, which solubilises C_6E_4 monomerically with increasing ξ. Thus at ξ = 0.32, SDS has no more any superiour effect on the efficiency in solubilising the fragrance mixture, consisiting of β-pinene and linalool, in comparison to the system without SDS. Considering the previous results, an ionic surfactant is not able to boost the efficiency of any SOW system. It depends strongly on the used oil(s), and especially on the monomeric solubility of the solov-surfactant within this phase. However another important factor for aqueous solubilisation is the increase in temperature stability, which is induced by the formation of charged mixed micelles. In this context the temperature stability of the previously investigated systems at $x = 0.05$ is observed in dependence of ξ. Thereby the systems without SDS and with SDS are compared. Results are shown in **Figure 123**.

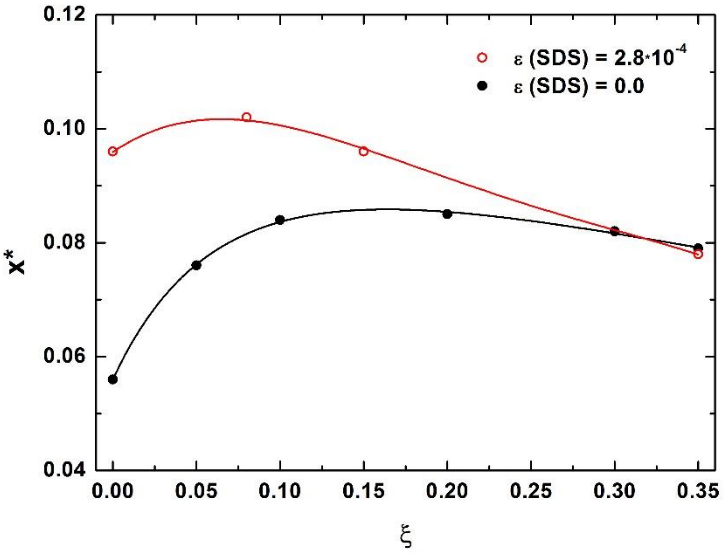

Figure 122 The maximum solubilisation *x as a function of ξ. SDS has a positive effect on *x** for low ξ, whereas it starts to have a negative effect around ξ = 0.3.**

It is obvious that SDS increases strongly the temperature stability of the here investigated systems. In the case without SDS, the monophasic region is very narrow and only slightly increasing in its expansion with augmenting ξ. On the other hand with SDS, the monophasic region is largely increased. Thereby the lower phase separation border remains almost unaffected, which was already observed in

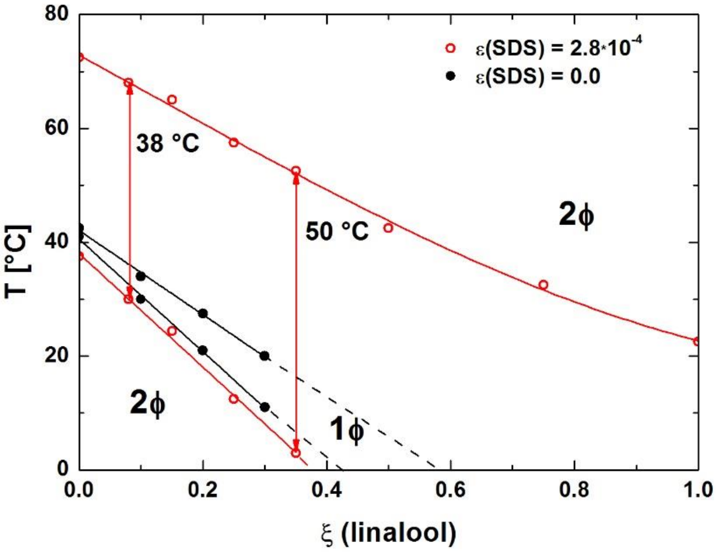

Figure 123 Temperature interval, within the mixture forms a monophasic microemulsion at $x = 0.05$. SDS increases strongly the temperature stability of the mixture and even an increase in ξ has a positive effect on the temperature stability.

Section **4.3.2.c**. In contrast, the upper border expands to high temperatures, which can be attributed to the increase of T_β in the pseudo-binary SW phase diagram (**Chapter 2**), and consequently the charging on the micelles. Furthermore the temperature interval, wherein a monophasic mixture is obtained, increases in size with augmenting ξ, since - as already described – the ratio of SDS to C_6E_4 at the interface augments due to the increased monomeric solubilisation of C_6E_4 in linalool.

Hence it can be concluded that an ionic surfactant will not always increase the efficiency of a non-ionic surfactant to solubilise an oil. However at any rate it will increase the temperature stability of the system to form a transparent, monophasic and stable mixture, which is highly desired for an application in fine perfumery or cosmetics.

4.3.8. Fragrance solubilisation in aqueous 1-O-pentylglycerol solution

a. The fish cut of C_5Gly/fragrance/water

Since poly(ethylene) glycol monoalkylethers are petro-sourced amphiphiles, it is desired to find bio-based and bio-compatible alternatives to replace C_iE_j's. Nowadays many alternatives have been found, such as sorbitane and sucrose ester or alkyl polyglycosides, which are sold commercially by huge global operating companies, such as BASF, Akzo Nobel, Henkel, etc.[235] However these surfactants are rather huge and thus do not possess the volatility, which is necessary for aqueous fragrance solubilisation. In the last years work was published, concerning short-chain alkylglycerols.[98,112] Thereby it was shown, that they may have the potential to replace C_iE_j's.

In this part, it was investigated if 1-O-pentylglycerol (C_5Gly) is able to solubilize efficiently fragrances in an aqueous solution. An efficient solubilisation is obtained at the optimal formulation (zero curvature). Consequently the EACN range had to be defined, wherein C_5Gly is able to form a three-phase region. Thereby the fish diagram of ω-hexadecenlactone (EACN = 1.0) and γ-terpinene (EACN = 1.8) was traced at WOR = 1 (**Figure 124**).

The fish diagram with ω-hexadecenelactone has its fish-tail temperature T* at 23.4 °C, and γ* at 0.36. Compared to the fish cut of C_5E_3/ω-hexadecenlactone/water, C_5E_3 is more hydrophilic, since its T* value is 38.0 °C. It is also slightly more efficient, with a γ* value of 0.35. However the three-phase region is much bigger in the case of C_5Gly. Indeed, the three-phase region of C_5E_3 is extremely narrow, which indicates the immediate proximity to the tricritical point. Given the negligible expansion of the three-phase region with C_5E_3, it can be assumed that the monomeric solubility of C_5E_3 in the oil and water phase is much higher than in the case of C_5Gly. The fish diagram of C_5Gly/γ-terpinene/water has an extremely enlarged three-phase region, compared to the system with ω-hexadecenelactone. The upper phase border is nearly constant, with the exception for γ = 0.15, where even at 99 °C a three-phase region was observed. The biggest expansion of the three-phase region is for the system with ω-hexadecenelactone approximately 20 °C, which is still quite huge compared to C_iE_j's with polar oils. In the case with γ-terpinene, the three-phase region expands over 60 – 70 °C, which is very different to the previous system, considering the slight difference in EACN between ω-hexadecenlactone (1.0) and γ-terpinene (1.8). A sample with the fragrance *p*-cymene (-0.4) and another one with β-pinene (2.2) were prepared in order to find a three-phase region with C_5Gly between 10 and 70 °C. However the first system was a WII phase, whereas the second system showed a WI phase all over the temperature range. The huge expansion of the three phase region is probably due to the strong increase of T_α in the binary C_5Gly/γ-terpinene diagram, compared to the one with ω-hexadecenelactone. Since C_5Gly consists of two hydroxyl groups, it can be assumed that its binary phase diagram SO is more sensitive to alterations in the polarity of the oil, than in the case of C_iE_j's.

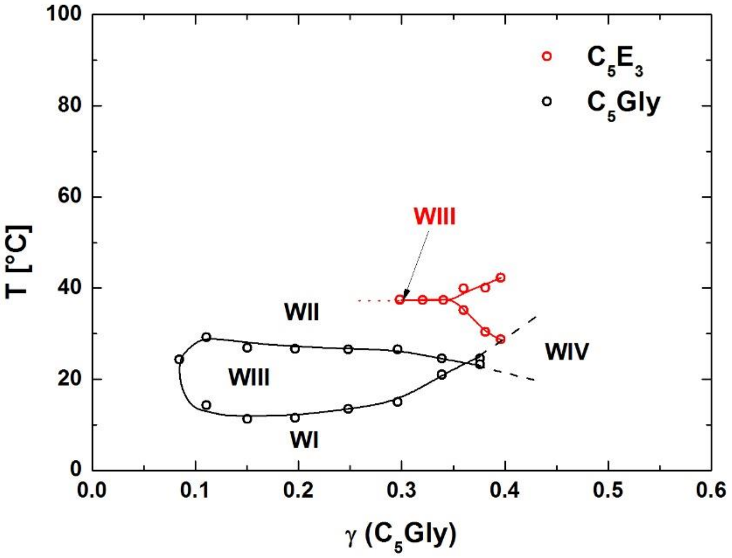

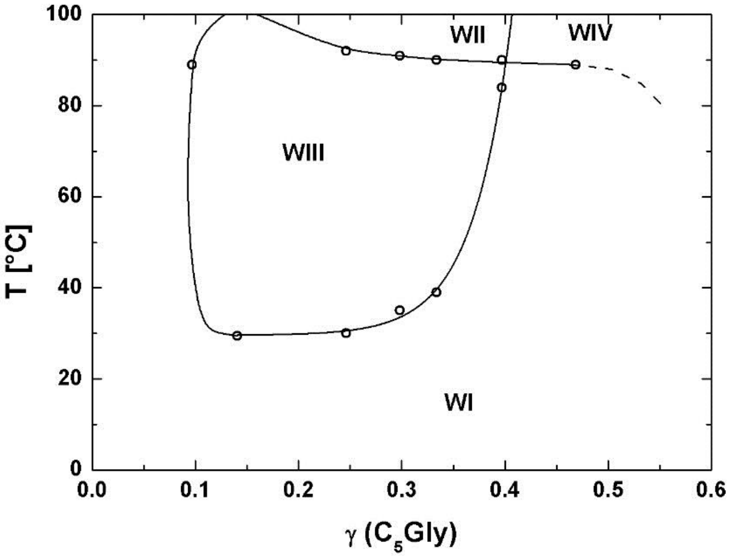

Figure 124 Top: Fish cut of C_5Gly/ω-hexadecenelactone/water and C_5E_3/ω-hexadecenelactone/water. Bottom: Fish cut of C_5Gly/γ-terpinene.

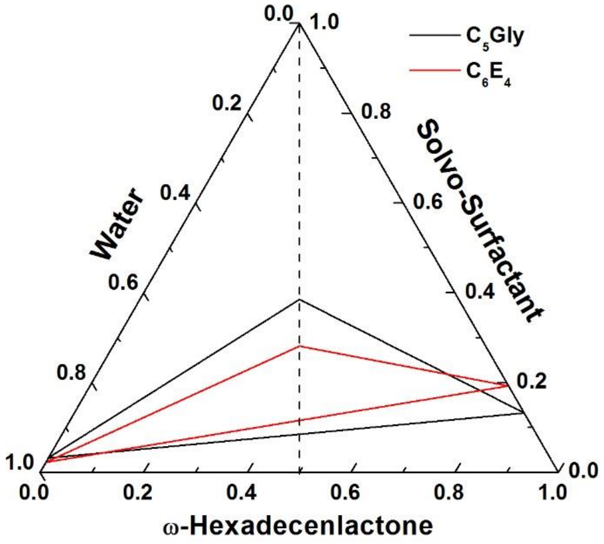

Figure 125 Three-phase triangle of C_5Gly/ω-hexadecenelactone/water and C_6E_4/ω-hexadecenelactone/water at 23.4 °C, respectively 38.6 °C. C_6E_4 is more efficient, however C_5Gly losses less amphiphile monomerically in ω-hexadecenelactone.

The monomeric solubility of C_5Gly in water and ω-hexadecenlactone was determined according to the procedure described in **Section 3.6.7**. Knowing the CAC of C_5Gly (**Section 2.3.2.a.)** it was possible to calculate $\gamma_{\text{mon},\gamma\text{-terpinene}}$ according to **Equation 28** and consequently to trace the three-phase triangle. Since it was not possible to determine γ_{mon} of C_5E_3, the triangle was compared to the one of C_6E_4/ω-hexadecenlactone/water in **Figure 125**. The results for the latter system are taken from **Section 3.6.9**.
It can be seen that C_6E_4 is more efficient in solubilising ω-hexadecenlactone. However less C_5Gly is solubilised monomerically. Due to its high CAC, slightly more C_5Gly is solubilised monomerically in water, than C_6E_4. In contrast much more C_6E_4 is lost in the ω-hexadecenlactone phase in comparison to C_5Gly. This can be attributed to the strong hydrophilic nature of the glycerol head group. The contact between the fragrance and the head group is highly unfavourable, which in turn results in a lower CAC in the oil phase. It can thus be assumed that the loss of C_5E_j amphiphiles in the oil-phase is even bigger. Consequently C_5Gly may be an alternative to them, since it show comparable efficiency in solubilising ω-hexadecenelactone.

b. Aqueous fragrance solubilisation with C_5Gly

It was shown that C_5Gly is able to solubilise ω-hexadecenelactone as good as C_5E_3 at a WOR = 1. Furthermore less C_5Gly is lost monomerically solubilised in the water and oil phase. However it was also shown that C_5Gly has an elevated CAC, which can be unfavourable for aqueous fragrance solubilisation, since less amphiphile can actively built up the interfacial layer between oil and water. Hence in **Figure 126** and **Figure 127** the lund cut of C_5Gly/ω-hexadecenlactone/water was constructed for w = 0.1 and w = 0.2. Furthermore the influence of SDS on the phase behaviour was investigated. Thereby same molar fractions ε were used as throughout the work.

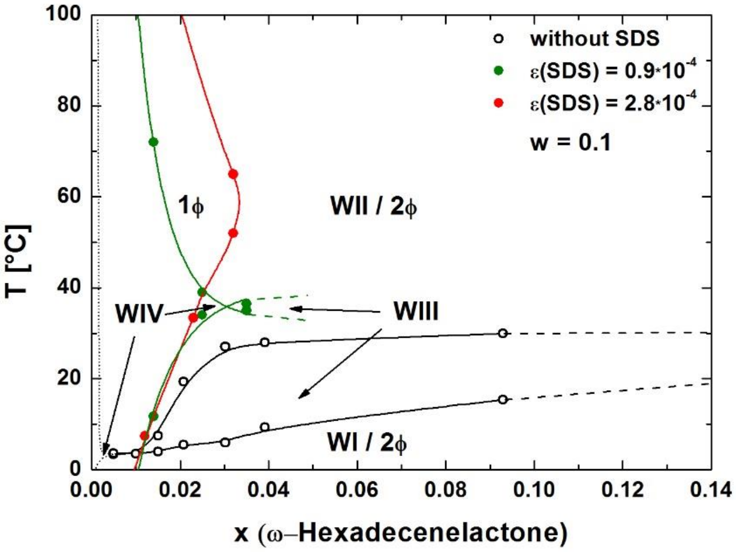

Figure 126 Lund cut of the system C_5Gly/ω-hexadecenelactone/SDS (aq). The SDS molar fraction ε is 0.0, $0.9{*}10^{-4}$ and $2.8{*}10^{-4}$. The amphiphile mass fraction in water is 0.1.

In **Figure 126** the lund cut for *w* = 0.1 can be seen. The monophasic region is very narrow and difficult to determine. However without any fragrance, the mixture is mono-phasic between 0 – 100 °C. Thus already small amounts of ω-hexadecenlactone are difficult to solubilise. The optimal temperature is ≈ 4 °C. In contrast the three-phase region is large, as in the case of the fish cut and expands over 20 °C. The addition of SDS (ε = $0.9{*}10^{-4}$) results in an augmentation of the optimal temperature to 36 °C. Thereby the three-phase region shrinks, but it does not disappear, as it was in **Section 4.3.5.c**. for C_6E_3/β-pinene/SDS (aq) for same ε. The efficiency of the system augments slightly to ~ 0.03. Further addition of SDS results in the disappearance of the three-phase region. The maximum solubilisation shifts to higher temperatures and is slightly increased. Thus C_5Gly is far from being efficient in the solubilisation of fragrances at *w* = 0.1. Even the addition of SDS cannot change the poor efficiency of C_5Gly to solubilise ω-hexadecenlactone.

Therefore same experiments were repeated at *w* = 0.2 (**Figure 127**). The lund cut without SDS shows a higher efficiency in solubilsing ω-hexadecenelactone, than any cut in **Figure 126**. T* is 5 °C and x_{max} is approximately 0.055. The three-phase region is also relatively big with an expansion of approximately 20 °C. The addition of SDS (ε = $0.9{*}10^{-4}$) augments T* as well as x_{max} to 38 °C and 0.09. As in **Figure 126**, the three-phase region is not disappeared, indicating that the system is able to solubilise even more fragrance, if ε is augmented. The red curve shows the lund cut at ε = $2.8{*}10^{-4}$ and an increase in x_{max} to approximately 0.13. Consequently a huge temperature stable monophasic region is obtained, which allows for example the solubilisation of 5 wt.% ω-hexadecenelactone between 15 to 100 °C.

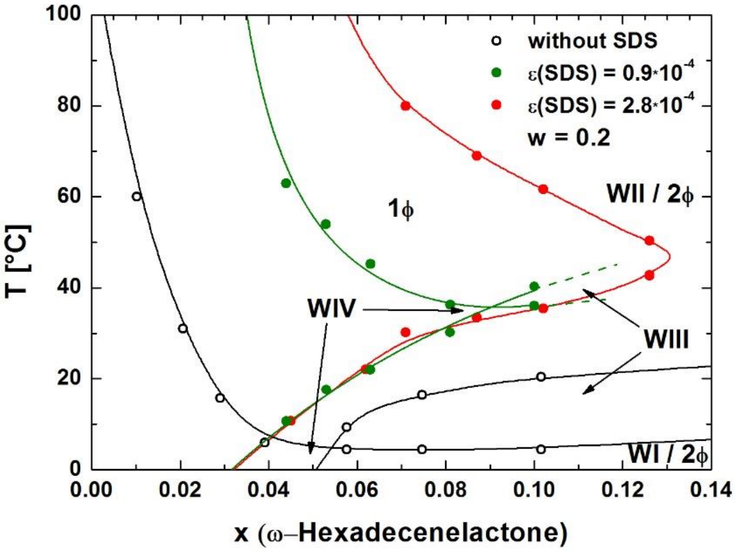

Figure 127 Lund cut of the system C_5Gly/ω-hexadecenelactone/SDS (aq). The SDS molar fraction ε is 0.0, $0.9*10^{-4}$ and $2.8*10^{-4}$. The amphiphile mass fraction in water is 0.2.

The huge difference in the phase diagrams between *w* = 0.1 and *w* = 0.2 can be explained with the huge CAC of C_5Gly in the water phase. Consequently less amphiphile is able to act at the interfacial layer. Still in both cases SDS has a very favourable effect on the temperature stability of the microemulsion. The disappearance of the three-phase region can be attributed to same reason as discussed in **Section 4.3.5**. Unlike in the case with C_6E_3/β-pinene/ionic surfactant (aq), the three-phase region still persists at $\varepsilon = 2.8*10^{-4}$. It can thus be assumed that a huge three-phase region is favourable for fragrance solubilisation, since more ionic surfactant can be added before the efficiency of the system is decreasing. Consequently temperature stability and efficiency increases simultaneously over a bigger ε–range. However compared to C_6E_j's, more C_5Gly is needed to achieve an acceptable solubilisation. Here only *w* = 0.1 and *w* = 0.2 was investigated. However mass fractions in between, may already give acceptable results. Another drawback of C_5Gly is the narrow EACN range (0.7 – 1.9), within it is able to form a three-phase region. Temperature is thus not a convenient formulation variable for glycerols and it is necessary to find an alternative, which is able to alter the interfacial curvature, as it is done for C_iE_j's with temperature. Sottmann *et al.* described in a publication the phase behaviour of alkyl glucoside/co-surfactant/*n*-alkane/water systems.[236] Alkyl glucosides are suger based surfactants, which are - as alkylglycerol - less sensitive to temperature alterations. Thus the formulation variable "temperature" was replaced by the weight fraction of a co-surfactant, *i.e.* 1-octanol. It was shown that with increasing alcohol content, the SOW system is able to invert from a WI phase to a WII phase at constant temperature. Consequently the alcohol enters the hydrophilic interface and alters the curvature of the film from positive to negative. Probably this method is also applicable to alkylglycerols, to tune the interface, so that fragrances with a higher EACN than of γ-terpinene can be efficiently solubilized. On the other hand this method cannot be applied for fragrances with a much lower EACN than ω-hexadecenelactone, since the addition of a co-surfactant results in a more hydrophobic interface and thus in a lower T*. However for very polar fragrances, the addition of an ionic surfactant may already be enough to raise the optimum formulation to ambient temperatures. At last it has to be noted, that unlike in the cases with C_6E_3, no liquid crystal phases were observed, which may be attributed to the shorter alkyl chain of C_5Gly.

4.4. Comparison between the well-defined C_8E_4 and its commercial counterpart Dehydol O4

In industry, rarely pure non-ionic surfactants are used, since their production is not cost- and eco-efficient. Furthermore poly-disperse surfactants turned out to be more efficient in oil solubilisation, surface wetting, etc. Therefore in this part the well-defined C_8E_4 was compared to the commercial surfactant Dehydol O4, which represents on average a C_8E_4 surfactant. Its composition was determined by GC-MS and GC-FID experiments and is shown in **Figure 128**. The arrangement of the peaks resembles a Poisson distribution with a maximum for C_8E_4.

It was investigated if a polydisperse mixture is superior to pure non-ionic surfactants in solubilising fragrances in an efficient and temperature stable microemulsion. Thereby single terpene oils were used, such as β-pinene and *p*-cymene, as well as complex oil mixtures, such as the essential oils, *pinus sylvestris* and *pinus pinaster*, or a fragrance mixture from a patent.[237] While the first essential oil was obtained from extraction of leaves and arms, the latter was composed of a mixture of synthetic terpenic compounds.

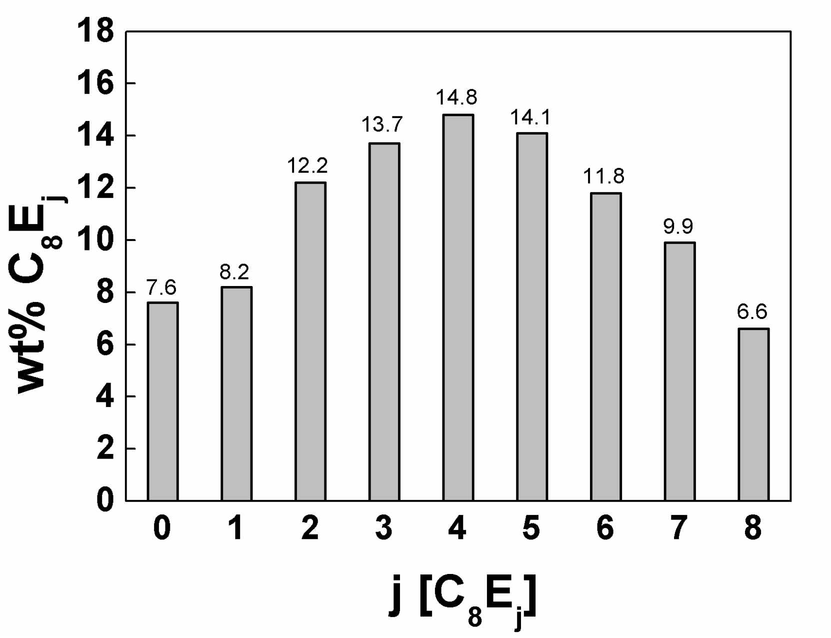

Figure 128 Composition of Dehydol O4. The distribution of the C_8E_j's follows a Poisson distribution. Above each bar the weight percentage of each compound in the surfactant mixture is indicated.

4.4.1. Mixed micellisation and interaction parameter β

Initially the synergy between C_8E_4 and SDS, as well as Dehydol O4 and SDS was investigated. Thereby the surface tensions of aqueous solutions containing different ratios of Dehydol O4 and SDS, as well as C_8E_4 and SDS, have been measured. The results are illustrated in **Figure 129**.

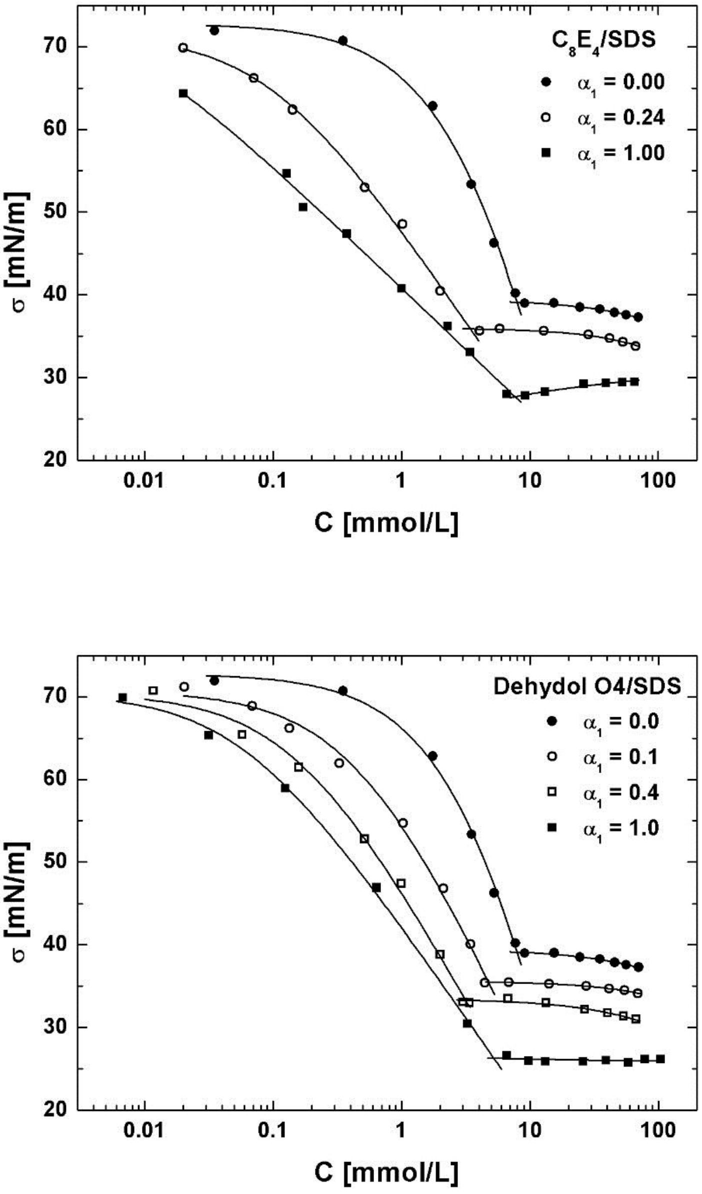

Figure 129 Surface tension σ in dependence of the amphiphile concentration C. In terms of clarity, not all measurements are displayed Top: Binary surfactant system C_8E_4/SDS. Bottom: Binary surfactant system Dehydol O4/SDS.

The CMC of single-component C_8E_4 is 7.7 mmol/L, while its poly-disperse counterpart Dehydol O4 has a value of 5.3 mmol/L. Addition of C_8E_4 or Dehydol O4 to aqueous solutions of SDS leads to a slight decrease of the CMCs, i.e. from 7.9 mmol/L for single-component SDS to 3.4 mmol/L for C_8E_4/SDS with $\alpha_1 = 0.24$ and from 7.9 mmol/L to 4.7 mmol/L and to 3.2 mmol/L for DehydolO4/SDS with $\alpha_1 = 0.1$ and 0.4 respectively, indicating a synergistic interaction between the amphiphiles. Furthermore, the surface tensions of surfactant mixtures are lower than the value obtained for single-component SDS in water and the curves approach the curve of single component non-ionic surfactant when its mole fraction increases. Ionic surfactants have usually higher surface tensions than non-ionic surfactants due to electrostatic interactions at the surface. However, added non-ionic surfactant molecules migrate to the water/air surface, resulting in a decrease of the electrostatic interactions. Hence, the surface tension diminishes, which is desirable for processes like emulsification, solubilisation, lubrication, etc. It is also noteworthy that the aqueous solution of Dehydol O4 separates in two phases just above the CMC and merges to one phase again with increasing concentration.

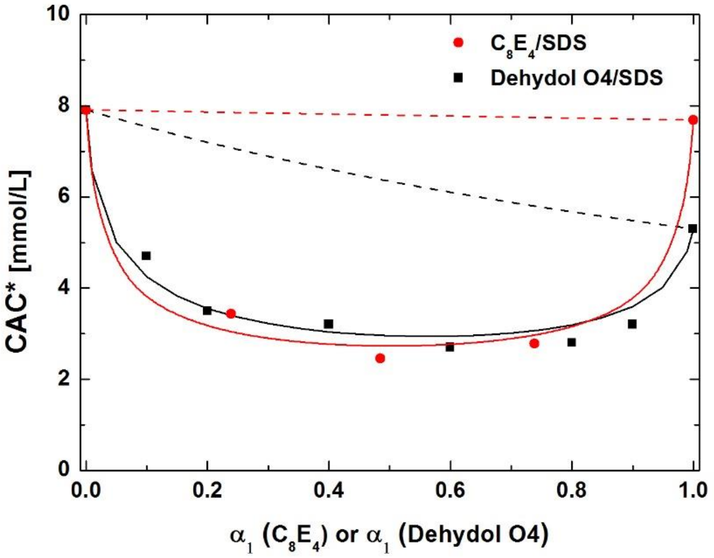

Figure 130 The mixed critical aggregation concentration CAC* as a function of α_1. The dashed lines represent the ideal case (β = 0). There is a strong interaction between the ionic and non-ionic surfactant, which result is an interaction parameter β of -4.2 for C_8E_4/SDS and -3.1 for Dehydol O4/SDS.

The experimental values of the mixed critical aggregation concentration CAC* for each molar ratio of the non-ionic/anionic surfactant mixture are displayed in **Figure 130**. The non-ideal curve fits were determined according to the model developed by Holland and Rubingh for mixed micelles (see **Chapter 2**) and compared with the ideal mixing curve. While the ideal curve fit results in a marginal decrease of CAC*, the nonideal curve fit of the experimental values shows a pronounced decrease. Its minimum of the mixed surfactant system C_8E_4/SDS is located at α_1 = 0.5 with a CMC of 2.7 mmol/L, compared to 7.8 mmol/L for the ideal curve fit. Dehydol O4/SDS has its minimum at α_1 = 0.55 at the CMC of 2.9 mmol/L, compared to 6.2 mmol/L for the ideal curve fit. The interaction parameter β calculated for the C_8E_4/SDS system is equal to -4.2. Lange and Beck have reported a value of -4.1 for C_8E_6/SDS; -3.9 for $C_{12}E_8$/SDS and -4.3 for $C_{10}E_6$/sodium pentadecylsulphate.[130] Rubingh and Holland found a β value of -3.6 for $C_{10}E_4$/SDS and -4.1 for C_8E_4/sodium decylsulphate respectively.[131] Although chain lengths and number of ethoxy units of the C_iE_j vary between 8-12 and 4-8 respectively, β changes only slightly and remains between -3.6 and -4.2. This indicates that the interaction between SDS and C_iE_j is more affected by the nature of the polar head group of the ionic surfactant rather than by the lengths of the hydrophilic and hydrophobic parts of C_iE_j. Indeed, the interaction parameter β of C_8E_4 with decyltrimethylammonium bromide is equal to -1.8 which is quite different from the above values.[9] So, the interaction parameter between Dehydol O4 and SDS is expected to be close to the value between C_8E_4 and SDS. However, the β value of -3.1 significantly differs from -4.2. Packing constraints in mixed micelle formation may have an influence on the interaction parameter since the different lengths of the polyethoxylated chains may produce unwanted antagonistic effects. Hence, the best fit for the mixture Dehydol O4/SDS does not fit well the measured values for high Dehydol O4 concentrations. Calculating the interaction parameter for $\alpha_1 = 0.8$ and 0.9 results in β values of -3.7 for both mole fractions, which in turn lies in the range of the above values. From the measurement of the β value, it is difficult to predict the influence of the interaction between SDS and C_8E_4 or Dehydol O4 on the solubilisation of oils.

4.4.2. Binary phase behaviour with and without ionic surfactant

The pseudo-binary phase diagrams of Dehydol and C_8E_4 in water and in an aqueous SDS solution are shown in **Figure 131**. *w* is the weight fraction of non-ionic surfactant in the mixture. The phase diagram of the C_8E_4/water system shows the expected miscibility gap around 40 °C. With increasing amounts of C_8E_4, the phase separation temperature increases accordingly, because a higher concentration results in an increase of ethoxy group concentration that has to be dehydrated. The addition of 1 wt.% SDS to the water phase charges the micelles and thus more energy in form of temperature increase has to be added to overcome – besides the dehydration of ethoxy groups - the electrostatic repulsion between micelles, until phase separation occurs.[238–240] Therefore, the critical temperature T_β, also known as cloud point evolves towards higher temperatures, as well as higher mass fractions of C_8E_4. Since at low non-ionic surfactant fractions, more SDS is available, and thus more ionic surfactant is distributed to each micelle, the increase is more pronounced in this region. With increasing amounts of C_8E_4, the curve passes through a minimum and eventually the dehydration of the ethoxy groups dominates again the curve slope change, as in the case without SDS. Roughly speaking, the same phenomena takes place for the Dehydol O4/water system, with and without SDS. However, a noticeable profound minimum in the curve of the binary system is observed at very low concentration, as well as a break in the curve of the pseudo-binary system at $w = 0.3$, T = 72 °C in the presence of SDS. Dehydol O4 is a surfactant mixture, consisting of C_8E_j with j ranging from 0 to 8. The low homologues (j = 0 to 2) are not miscible with water above 0 °C, so that they probably solubilise in the core of the micelles formed by the higher homologues. Since the minimum is located slightly above the CMC ($w = 0.0016$, T = 22°C), it can be assumed that the very first micelles are not able to solubilise all lower homologues. Then, at higher concentrations of Dehydol O4, the second phase disappears, because there are enough micelles of C_8E_j ($j > 3$) to solubilise the non-water soluble homologous C_8E_j ($j < 3$). In the presence of SDS, an anomaly is also visible. A break in the curve ($w = 0.3$, T = 72°C) occurs at higher temperatures, probably caused as well by the different solubilities of C_8E_j in water. As already shown, the interaction parameter β between C_8E_4 and SDS is higher than the one between Dehydol O4 and SDS. Hence, by increasing the concentration of Dehydol O4 – and at the same time by decreasing the concentration of

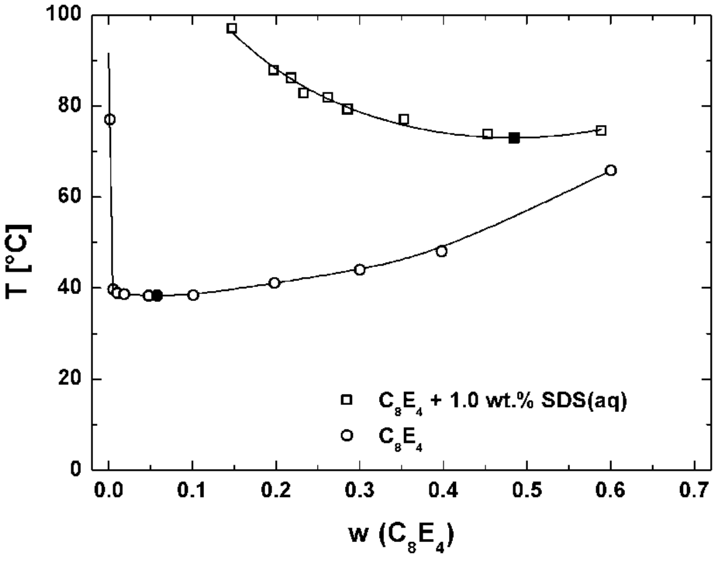

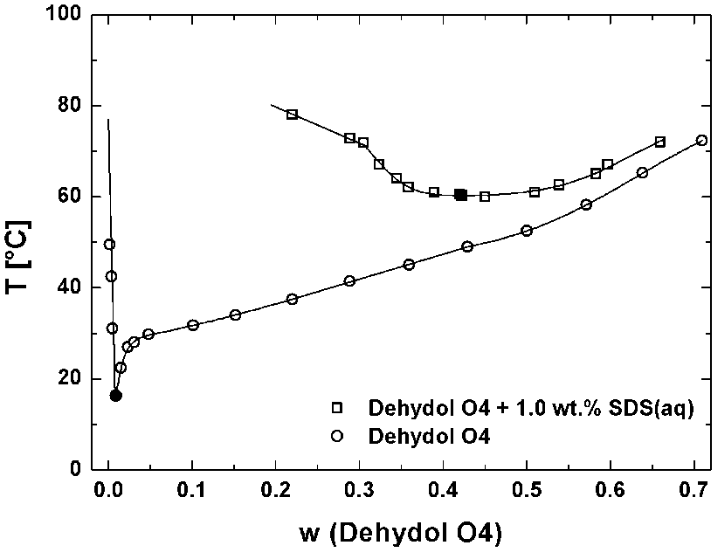

Figure 131 (Pseudo)-binary phase diagrams. Top: C_8E_4 in water and in aqueous SDS solution. Bottom: Dehydol O4 in water and in aqueous SDS solution.

SDS – the phase separation temperature diminishes. At the break point, probably one of the homologues in Dehydol O4 returns to the surfactant layer due to hydration of the ethoxy units and thus reduces the interaction parameter between Dehydol O4 and SDS due to unfavourable packing in the mixed micelle. Eventually the curve drops faster towards lower temperatures until the dehydration of the ethoxy units overcomes this effect. It is foreseeable that the differences between the pseudo-binary phase diagrams of C_8E_4 and Dehydol O4 will induce distinct effects on the solubilisation of fragrances. **Table 22** summarizes the critical temperature (T_β) and the critical compositions (w^*) obtained from the determination of the (pseudo-)binary phase diagrams.

Table 22 Critical temperature T_β and critical composition *w of C_8E_4 and Dehydol O4 in pure water and in aqueous SDS solution (1.0 wt.%).**

Compound(s)	*w**	T_β [°C]
C_8E_4	0.048	38.3
C_8E_4 + SDS	0.485	72.9
Dehydol O4	0.009	16.3
Dehydol O4 + SDS	0.423	60.2

The C_8E_4/SDS mixture has the highest critical temperature T_β of all investigated systems, followed by Dehydol O4/SDS. Pure Dehydol O4 has the lowest critical temperature and the lowest critical composition, owing to its poly-dispersity. The critical temperature and composition of a polyethoxylated glycol decrease with decreasing number of ethoxy units.[110]

4.4.3. Ternary phase behaviour with and without ionic surfactant

The solubilisation of β-pinene in the presence of different surfactant systems was investigated by constructing the T-β-pinene diagrams, i.e. the so-called lund cuts of the surfactant(s)/fragrance/water-temperature phase prism.[60] The lund cuts for the C_8E_4/β-pinene/water, C_8E_4+SDS/β-pinene/water, Dehydol O4/β-pinene/water and Dehydol O4+SDS/β-pinene/water systems are displayed in **Figure 132** and **Figure 133**.

C_8E_4 alone is capable of solubilizing β-pinene at low temperatures in a reduced monophasic region. At the optimal temperature T* (18.0 °C), a weight fraction of 0.089 of fragrance can be solubilised. Obviously the system is very temperature sensitive and no monophasic region is obtained above ≈ 20 °C since the increase of T gives a two-phase system. However, due to the relatively short alkyl chain length of C_8E_4, the system exhibits a very limited zone of liquid crystals. By replacing 1.0 wt.% non-ionic surfactant with SDS, the efficiency increases up to $w = 0.125$ of fragrance at T = 49.2 °C. Indeed, the ionic surfactant interacts with the non-ionic surfactant and thus, shifts the miscibility gap in the SW binary phase diagram to higher temperatures due to the presence of negative charges on the micelles. Since the phase behaviour in a surfactant/fragrance/water (SFW) Gibb's triangle is mainly determined by the superposition of the miscibility gaps of its SW, SF and FW binary phase diagrams, the increase of the cloud point in the SW binary system results in a shrinking of the three-phase region until it vanishes and hence, the monophasic region in the water rich corner expands.[229] This results in a higher efficiency of the mixed surfactant system in comparison with the single surfactant system. The higher temperature can be explained by the increase of the effective hydrophilicity of the surfactant system in the presence of SDS. Due to the anionic surfactant the amphiphilic film is stronger curved. Therefore, more energy in form of temperature increase has to be transmitted into the system, in order to approach zero curvature. However as already stated in **Section 4.3.5.c.**, the system is unable to achieve optimum formulation, since the ionic surfactant prevents the phase inversion. Consequently the non-ionic surfactant dehydrates and passes to the oil phase. Noticeable is the huge expanded area of the liquid crystalline phase after addition of SDS. Since strong interaction occurs between the ionic and nonionic surfactants, a more expanded rigid surfactant interface may form between the water and oil phase.

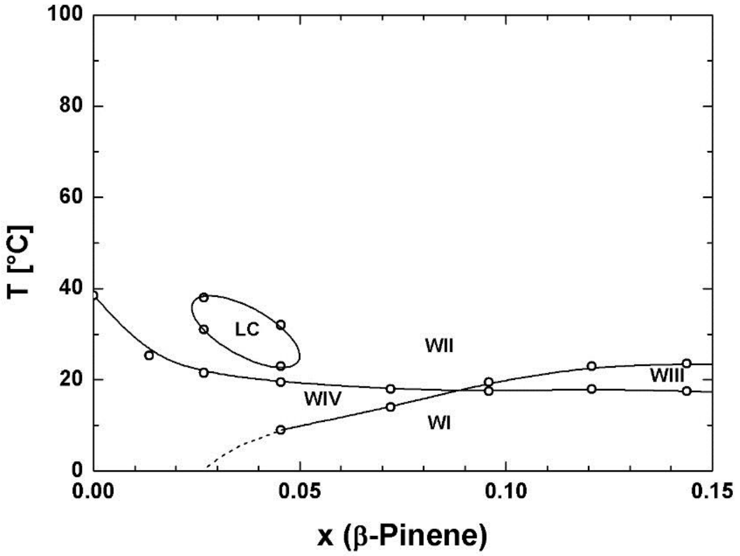

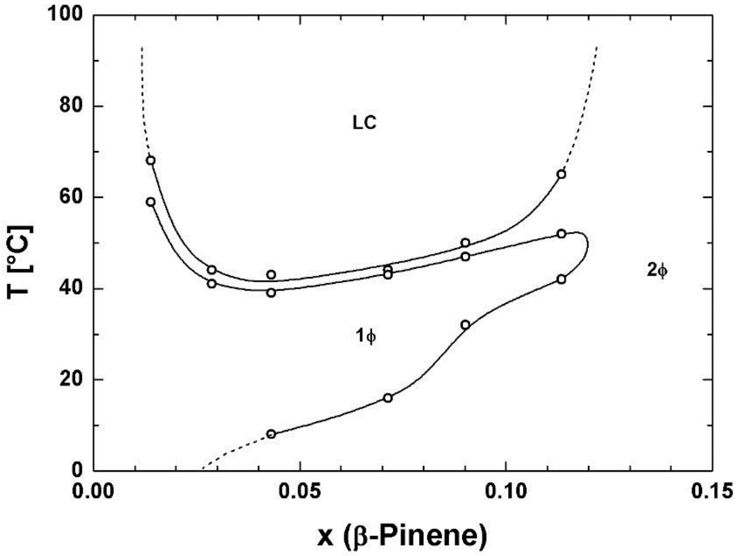

Figure 132 Lund cut through the SOW-T phase prism at constant surfactant-to-water ratio (w = 0.1). Top: The ternary system C_8E_4/β-pinene/water. Bottom: The pseudo-ternary system C_8E_4+SDS/β-pinene/water. The surfactant mixture contains90 wt.% C_8E_4 and 10 wt.% SDS.

In **Figure 133 (top)**, the ternary Dehydol O4/β-pinene/water system shows a more complicated phase behaviour. The binary phase diagram of Dehydol O4 in water has already set apart from the expected behaviour and obviously it affects fragrance solubilisation as well. In particular, the efficiency and T* increases to 0.125 and 26.4 °C respectively compared to 0.089 and 18.0 °C with C_8E_4.The liquid crystalline phase lies now at lower temperatures and lower fragrance content, surrounded by a monophasic region. Furthermore, another two-phase region is found at low temperatures (between 5 and

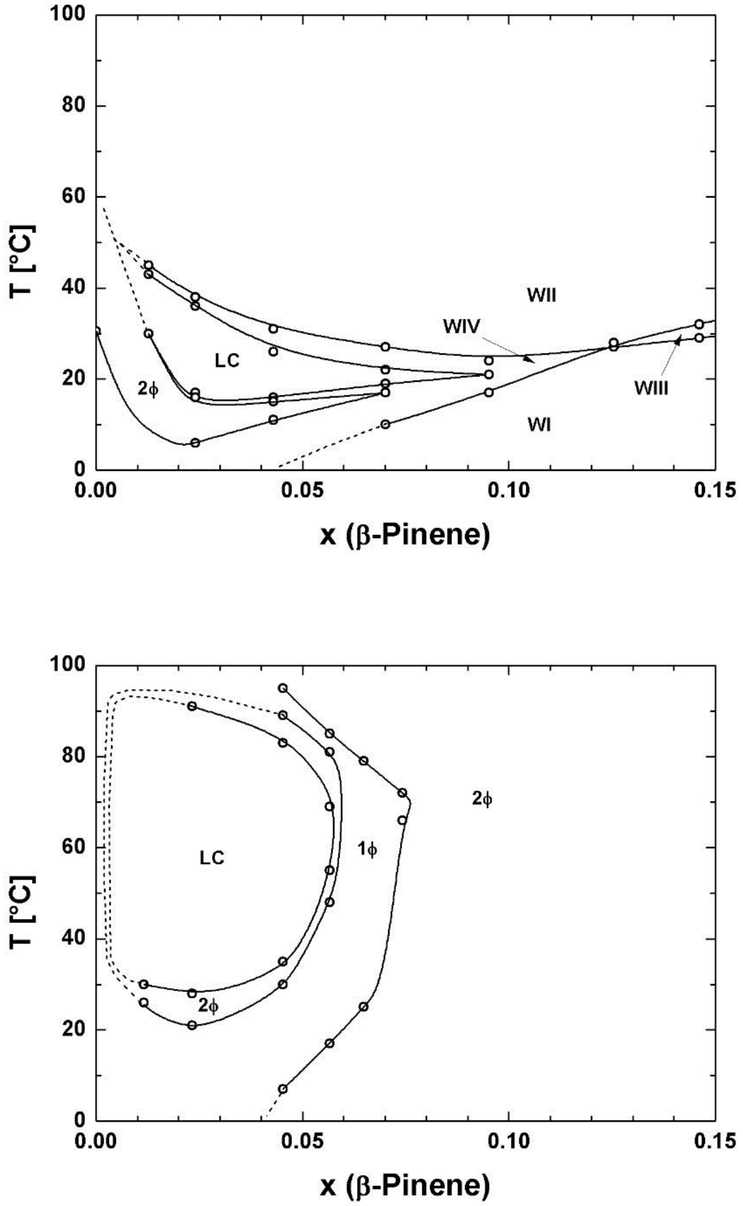

Figure 133 Lund cut through the SOW-T phase prism at constant surfactant-to-water ratio (*w* = 0.1). Top: The ternary system Dehydol O4/β-pinene/water. Bottom: The pseudo-ternary system Dehydol O4+SDS/β-pinene/water. The surfactant mixture contained 90 wt.% Dehydol O4 and 10 wt.% SDS.

20 °C) and low β-pinene concentrations (< 0.05), which is probably affected by the minimum in the binary phase diagram of Dehydol O4/water. By increasing temperature, a narrow one-phase region appears which results finally in a liquid crystalline phase. Further increase of the temperature leads to the melting of the liquid crystalline phase and above the narrow monophasic region, another two-phase region appears. Due to the poly-dispersity of Dehydol O4, the surfactants partition between the oil phase, water phase and interface.[241] With increasing temperature, the lower homologues become increasingly hydrophobic and migrate in the oil phase. The surfactants remaining at the interface have longer ethoxylated polar heads. This promotes the deformation of liquid crystalline phases, since a more

hydrophilic head group results in a more curved micelle. Therefore transitions from hexagonal or lamellar liquid crystalline phases to isotropic micellar phases are possible.[242]

In **Figure 133 (bottom)**, the liquid crystalline phase strongly expands as a function of T for *w* lower than 0.05, which is due to the same reason as in the case of C_8E_4 and SDS. Moreover, the efficiency dramatically decreases to 0.079 at T* = 69.0 °C. Actually, an increase in efficiency was expected, as it occurred for C_8E_4 in combination with SDS. As already brought up, the various glycols in Dehydol O4 partition differently between the phases. Thus, by increasing the temperature, the lower homologues migrate from the interface to the oil phase while the higher homologues migrate from the water phase to the interface. With the addition of SDS, a temperature-insensitive surfactant is introduced to the mixture. As in the pseudo-binary system, the ionic surfactant increases also the temperature stability of the non-ionic surfactant in the pseudo-ternary system. Therefore, the partition of the homologues surfactants occurs over a larger temperature range than in the case of Dehydol O4 alone, and thus less surfactant is available at the interface. Consequently, less fragrance can be solubilised with the Dehydol O4/SDS mixture compared to Dehydol O4 alone. However there is to some extent a constant amount of surfactant at the interface over the whole temperature interval, which results in the steep ascent of the phase boundary and thus an almost temperature insensitive microemulsion can be formed.

4.4.4. The temperature insensitive solubilisation of complex fragrance mixtures with synergistic mixtures of ionic and non-ionic surfactant

β-Pinene and *p*-cymene, as well as the essential oils *pinus sylvestris* and *pinus pinaster* were mixed with various aqueous solutions of surfactants. The phase diagrams were built as a function of temperature and weight fraction of terpene oil in the mixture, in order to determine the one-phase microemulsion region. The diagrams were investigated solely in the range between *w* = 0.05 to 0.07 of fragrance. As shown previously in **Figure 133**, the one-phase region obtained with 10 wt.% of Dehydol O4 alone is rather limited and fractionated in two parts by a LC zone whereas an aqueous surfactant mixture with 9 wt.% Dehydol O4 and 1 wt.% SDS is able to solubilize 6.5 wt.% of oil between 25 – 80 °C. Therefore, we studied here the solubilising properties of a binary surfactant mixture consisting of 9 wt.% of Dehydol O4 and 1 wt.% of SDS as solubilisation enhancers in order to solubilize terpenes, as well as more complex fragrant mixtures, by tracing their χ-cuts at 10 wt.% surfactant concentration. The monophasic regions obtained with the four terpene oils are shaded in blue in **Figures 134.**

The width of the monophasic regions depends on the hydrophobicity of the oil and the hydrophilicity of the ionic surfactant. It can be seen that *pinus sylvestris* behaves similarly to β-pinene, while *pinus pinaster* behaves similarly to *p*-cymene. This indicates that the apparent hydrophobicity of a multicomponent essential oil is related to the hydrophobicity and the ratio of each component in the mixture. Bouton *et al.* have assessed the EACN of β-pinene and *p*-cymene to 2.2 and -0.4 respectively, indicating that *p*-cymene is more polar than β-pinene.[171] It is possible to solubilize *p*-cymene within a larger temperature interval. Based on the oil composition (see **Appendix 2**) and on the hypothesis that

EACNs are roughly additive, an average EACN value to ≈ 3 can be calculated for *pinus sylvestris* and ≈ 0 for *pinus pinaster*. Therefore, it is understandable that *pinus sylvestris* and *pinus pinaster* behave similarly to β-pinene and *p*-cymene respectively.

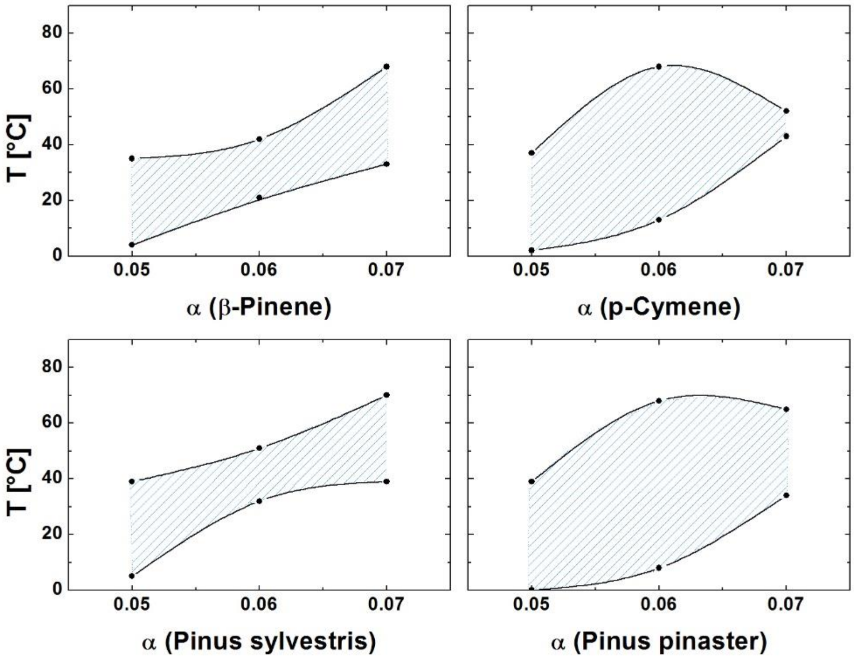

Figure 134 χ-cut at 10 wt.% surfactant content (9 wt.% Dehydol O4 + 1 wt.% SDS). The blue shaded region indicates the mono-phasic microemulsion. α is the mass fraction of oil in water and oil.

For practical application such as non-alcoholic perfumes, it is necessary to formulate aqueous solutions of complex fragrances which remain stable over a large temperature interval, i.e. 5 – 50 °C. As shown in **Figure 135**, a stable microemulsion containing 7 wt.% of a true fragrant composition (see **Appendix 2**) can be prepared with the binary Dehydol O4/SDS surfactant system.

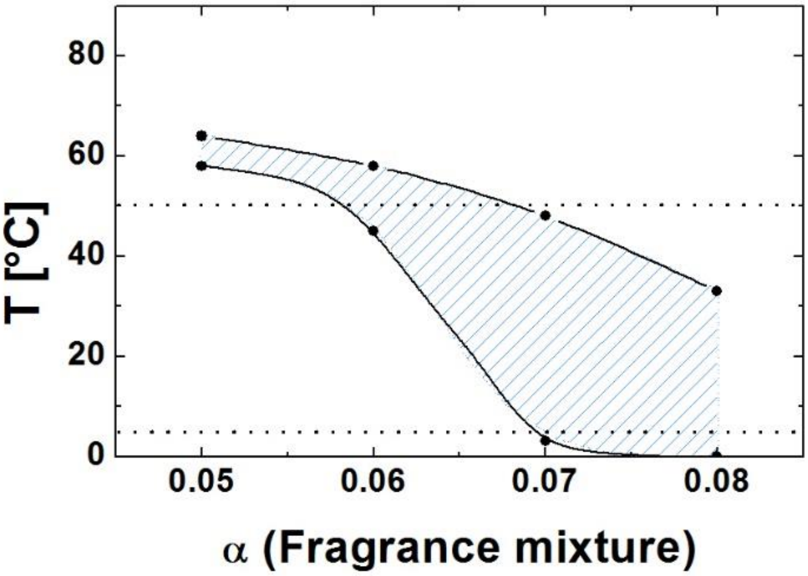

Figure 135 χ-cut at 10 wt.% surfactant content (9 wt.% Dehydol O4 + 1 wt.% SDS). The blue shaded region indicates the mono-phasic microemulsion. α is the mass fraction of oil in water and oil.

It is striking that in contrast to previous terpene oils, the temperature interval of stability of the microemulsion increases with the amount of oil. The one-phase region starts at high temperature (≈ 60 °C) and expands with higher amounts of oil to lower temperatures. The main difference between the fragrant composition and the terpene oils is the presence of large amounts of linalool (36.7 wt.%), a fragrant alcohol, and of the solvent dipropyleneglycol (19.2 wt.%). Depending on their chemical functionalities, terpene oils can solubilise in the interfacial surfactant monolayer between oil and water and alter the curvature.[170] Especially terpene alcohols, which can be used both as a co-solvent and as a co-surfactant in a microemulsion formulation, are good for solubilisation in the surfactant palisade. Garti *et al.* have shown that ethanol, propylene glycol and glycerol are able to increase the monophasic region in the water rich corner.[243] Stubenrauch *et al.* have already pointed out that the fragrance molecule geraniol is effective as a co-surfactant, which penetrates the interface and acts as a co-surfactant.[244,245] Tchakalova *et al.* stated that in the interface solubilised polar oils alter the curvature, thus leaving energetically unfavourable holes, which can be filled by co-extraction of more hydrophobic compounds of the oil mixture.[246] Therefore it can be concluded that linalool acts as a co-surfactant which solubilises in the interface and co-extracts more hydrophobic compounds closer to the palisade layer. Furthermore, dipropylene glycol acts as a co-solvent, which supports solubilisation as well. Thus it is possible to obtain an enlarged monophasic region with increasing amount of oil. Finally, it is noteworthy that in the absence of the ionic surfactant, the monophasic region, surrounded by liquid crystalline structures, is obtained only below 10 °C for 5 wt.% of the fragrant mixture. Linalool probably penetrates the interface and makes the non-ionic surfactant effectively more hydrophobic, which results in a shift of the whole monophasic region to lower temperatures. The effect of the ionic surfactant is thus remarkable, because it is able to shift the monophasic region to ambient temperatures by simultaneously increasing its expanded area.

4.5. Conclusion

Initially it was shown in this chapter, that ethanol is not very efficient for the solubilisation of fragrances in water. Consequently solvo-surfactants of the type C_iE_j, especially C_6E_3 and C_6E_4 were used to investigate their efficiency in fragrance solubilisation, with and without ionic surfactants or co-surfactants.

It was found that in water rich systems, same rules are applicable as in the case of WOR = 1. Basically it can be stated that the longer the alkyl-chain, the more efficient the amphiphile in solubilizing hydrophobic compounds. Thereby it was shown that C_5E_j systems are very inefficient, since their monomeric solubility is already very elevated. Consequently few amphiphile is available to be active at the interface. As expected, T* augments for more hydrophilic amphiphiles and decreases for fragrances, which possess a lower EACN. The latter was particularly investigated in the quaternary system C_6E_4/β-pinene+linalool/water, wherein the weight fraction of linalool in the oil mixture was augmented. The optimal temperature T* of the system decreases with increasing linalool content. This progression deviates slightly from linearity. However it was shown that the HLD equation can be applied successfully for these water rich systems, to predict the location of T* of a fragrance mixture. Furthermore linalool showed co-surfactant characteristics by increasing the efficiency of C_6E_4 to solubilize the fragrance mixture, with a maximum at $\xi = 0.15$. Afterwards the efficiency decreases, probably due to saturation of the interface with linalool and an increasing monomeric solubility of C_6E_4 in the fragrance mixture.

In the following the effect of traces of ionic surfactant on the phase behaviour of the C_6E_3/β-pinene/water system was investigated. Thereby it was shown that the temperature stability of the system augments as well as its efficiency to solubilize the oil. However the efficiency undergoes a maximum in dependence of the ionic surfactant molar fraction. This maximum represents the critical point at which the three-phase region, and thus the bicontinuous microemulsion, disappears. It is assumed to be close to $\varepsilon = 0.9*10^{-4}$ for both investigated ionic surfactants, DHS and SDS, where more than 15 wt.%, respectively 17 wt.% of β-pinene was solubilized. The system decreases in efficiency with further augmenting ionic surfactant content, since the latter prevents the system from inversion. Scattering experiments have shown that this decrease happens parallel to the evolution of the micelle size. Consequently a decrease in micelle size, can be attributed to a bigger curvature of the particle and thus less oil is solubilized in its interior. It is thus evident, that an applicable aqueous fragrance solubilisation consists of a compromise between efficiency and temperature stability, since at low ionic surfactant content, the system shows an extraordinary maximum solubilisation, whereas an acceptable temperature stability is usually only achieved at higher ionic surfactant content.

In this context, the solubilisation of the fragrance mixture β-pinene/linalool in aqueous C_6E_4 solution with traces of SDS was investigated. A molar fraction of $2.8*10^{-4}$ was chosen, since it appears to give a good compromise between efficiency and temperature stability. The increase in efficiency, compared to the system without SDS, is big for low ξ, marginal for medium ξ and even negative for higher ξ. Thus linalool acts barely as a co-surfactant in a SOW system with traces of ionic surfactant. The ionic surfactant imposes a strong curvature to the aggregates, which in turn prevents an easy penetration of linalool into the interface. Consequently it can be assumed that an ionic surfactant may even decrease the efficiency of an amphiphile to solubilize an oil, with a high surface affinity. Nevertheless the ionic surfactant is indispensable, since it augments strongly the temperature stability of the microemulsion, and it was shown that polar oils, such as linalool are even able to increase this stability, since it augments the monomeric solubilisation of C_6E_4 in the oil phase, and thus the SDS to C_6E_4 ratio in the interface.

Furthermore the applicability of C_5Gly for fragrance solubilisation was investigated. Thereby the EACN range, within the C_5Gly/fragrance/water shows a three-phase region, was determined by construction of fish diagrams. Two fragrances were found, which are able to form a WII phase, namely ω-hexadecenlactone (EACN = 1.0) and γ-terpinene (EACN = 1.8). The system C_5Gly/ω-hexadecenlactone/water shows a fish cut with a quite impressive three-phase region at T* = 23.4 °C, compared to C_5E_3, whose three-phase region is almost inexistent. By replacing ω-hexadecenlactone with the slightly more hydrophobic γ-terpinene, T* shift to 90.0 °C and the three-phase region augments extremely in size, which is probably due to a bigger sensibility of the hydrophilic head group to alterations in the polarity of the oil. Since it was also shown that the monomeric solubility C_5Gly in water and oil is lower compared to C_6E_4, the efficiency of C_5Gly to solubilize ω-hexadecenelactone was investigated by constructing the lund cut. It turned out that at a $w = 0.1$, C_5Gly solubilizes approximately only 1 wt.% of fragrance. Also with traces of SDS the efficiency augments only to 3 – 4 wt.% of ω-hexadecenelactone, which is very poor for an aqueous fragrance solubilisation. On the other hand with $w = 0.2$ the system showed an acceptable efficiency with 9 - 13 wt.% of solubilized fragrance. In both cases, the system contained a huge three-phase region, which decreases in size with augmenting molar fraction of SDS. However, compared to to C_iE_j systems, more SDS can be added, before the three-phase region disappears. It is thus also possible to obtain an efficient and temperature stable microemulsion, with the drawback of using more than just 10 wt.% of non-ionic amphiphile in the stock solution.

In the last part of the chapter, it was investigated if the technical surfactant Dehydol O4 is more efficient in solubilizing oils than the well-defined C_8E_4. Thereby their aqueous phase behaviour was investigated and it was shown that the binary phase diagram of Dehydol O4 possesses an unusual phase behaviour due to the partition of its different constituents between the phases. Furthermore a lower interaction parameter β was assigned to the system Dehydol O4/SDS (-3.1), compared to C_8E_4/SDS (-4.2), which indicates that the interaction is less favourable between the technical surfactant and SDS. In the ternary SOW system it was shown that Dehydol O4 is more efficient in solubilising β-pinene. Nevertheless in combination with SDS, Dehydol O4 is less efficient than C_8E_4/SDS. However Dehydol O4/SDS showed an elongated monophasic region, wherein it was possible to solubilise approximately 7 wt.% of β-pinene between 20 – 70 °C. This region appears due to the partition of the various constituents of Dehydol O4 between the phases. Additionally SDS charges the micelles, which in turn prevents the inversion of the phases. This region was thus investigated by solubilising essential oils and fragrance(s) (mixtures). Thereby it was found that it was easier to solubilise the more polar oils within a larger temperature interval. This confirms the findings from the C_6E_4/β-pinene+linalool/SDS (aq) system, where it was shown that oils with higher polarity, increase the SDS to C_6E_4 ratio at the interface.

4.6. Experimental section

4.6.1. Materials

Compound	Supplier	Purity
Essential oils		
Pinus sylvestris	Cooper	-
Pinus pinaster	Cooper	-
Fragrance mixture		
α-Pinene	Acros	98%
β-Pinene	Acros	98%
Limonene	Sigma Aldrich	97%
Camphene	Sigma Aldrich	95%
Camphor	Sigma Aldrich	98%
Cineole	Sigma Aldrich	≥ 95%
Ocimene	Sigma Aldrich	≥ 90%
Linalool	Alfa Aesar	97%
Linalyl acetate	Sigma Aldrich	≥ 97%
Dipropylene glycol	Sigma Aldrich	99%
Fragrances		
ω-Hexadecenelactone	Sigma Aldrich	≥ 98%
γ-Terpinene	Firmenich	≥ 97%
Amphiphiles		
Dehydol O4	Cognis	technical
1-O-Pentylglycerol	Synthesized	≥ 99%
Triethylene glycol monohexyl ether	Synthesized	≥ 98%
Tetraethylene glycol monohexyl ether	Synthesized	≥ 98%
Hexaethylene glycol monododecyl ether	TCI	≥ 97%

4.6.2. Determination of the ternary phase diagrams ethanol/fragrance/water

Several tubes with different ratios of fragrance to water were prepared. The total mass was 2 g. A small stirrer was added and the samples were weighted. Then they were given onto a stirring platform and 50 μL of ethanol were added in each vial, until the mixture turned monophasic. Consequently the samples were weighted again and the difference corresponds to the mass of ethanol, added to obtain a monophasic region. The experiment was performed at room temperature (≈ 25 °C).

4.6.3. Sample preparation for the lund cut

The lund cut's were traced by investigating the phase behaviour of the C_iE_j/fragrance/water or C_5Gly/fragrance/water systems a constant SWR as a function of temperature (ordinate) and fragrance mass fraction γ (abscissa). T* was determined by observing the alterations of the phase behaviour with decreasing temperature at different mass fractions of fragrance. Thereby a stock solution of non-ionic amphiphile in water was prepared, which was then distributed to several thin glass tubes. In the following rising quantities of fragrance were added and the tubes were closed with a screw cap. The samples were then shaken and placed into a thermostatic water bath. Temperature was altered in 0.1°C steps and equilibration time was from 10 min to 2 days depending on the amphiphile and the adjustment of the equilibrium. Same procedure was applied in the cases, where an ionic surfactant was used. Thereby the latter was solubilised in water, which was then used to prepare the non-ionic amphiphile stock solutions.

4.6.4. Micelle size determination via dynamic light scattering

The hydrodynamic radius R_h of micelles was determined via scattering experiments. However initially the refractive index, as well as the density and viscosity of the microemulsion had to be determined at the desired temperature.

a. Sample preparation

Stock solutions of each sample were prepared. Thereby each vial and test tube was rinsed several times with Millipore water to eliminate dust particles. The tubes were then enrolled into a weakly perforated aluminium foil and given into a drying chamber. The foil attracts dust particles, while the tubes are drying, and thus prevent them from contaminating again with dust. Eventually the stock solutions were prepared by applying the liquid constituents through a syringe, connected to a Millipore filter with a pore diameter of 0.1 μm. The samples were then closed with a screw cap and equilibrated at the desired temperature (19 °C, 28 °C, 38 °C and 44 °C).

b. Refractive index measurements

The refractive index was determined with a Novex Refrectometer, connected to the thermo-regulated water bath Alpha from Lauda. Thereby the samples were equilibrated at the desired temperature, before several drops very given between the thermostated refractors.

c. Density and viscosity measurements

The density and viscosity measurements were performed with one apparatus, which consists of the Density Meter DMS 4100M and the Microviscosymeter Lovis 200 ME from Antor Paar.

The density was measured by injecting approximately 2 mL of the sample in an integrated capillary. The density is then measured with a connected reference oscillator.

The obtained value was used for the determination of the viscosity of the mixture. The measurement follows the principles of a falling sphere viscosymeter. Thereby the monophasic mixture was given into a capillary ($\emptyset_{int} = 1.59\ mm$), followed by a small metal pellet. The capillary was then fixed inside the thermoregulated measurement vessel, with two photon sensors. By turning the vessel, the pellet descends through the liquid, passing by the first and second photon sensor. Knowing the size and density of the pellet, as well as the density of the liquid, the viscosity is calculated automatically by applying Stokes' law.

Since the measurements were made at constant temperatures, the samples had to be thermoregulated all the time. Furthermore the stock solutions, as well as the capillary had to be equilibrated at the desired temperature.

d. Dynamic light scattering

The scattering experiments were performed with a 3D-LS spectrometer from LSinstruments, equipped with a Helium Neon Laser (633nm) and thermoregulated with a Julaba CF131 thermostat. The 3D-Cross Correlation function suppresses multiple light scattering, allowing the investigation of concentrated samples. As index-matching liquid decalin was used (RI = 1.47 at 633 nm).

The stock solution and the empty test tube were attached into a thermoregulated water bath at the desired temperature. Then approximately 3 mL of the mixture was transferred into the test tube, which was then closed with a cap and given to the thermostated measurement vessel of the spectrometer. Before the measurement was executed, the sample was left for 15 minutes to balance possible disequilibration during the transfer process from stock solution to test tube. The previously measured refractive index and viscosity were entered into the control panel. The measurement took then place at an angle of 90° for 120 s. The scattered light was detected and then transformed into the correlation function (**Figure 136**). The latter was analysed with a second order cumulant fit, which in turn gave the diffusion coefficient of the aggregates. The hydrodynamic radius R_h was then automatically calculated with the Stoke-Einstein equation. Each measurement was performed three times.

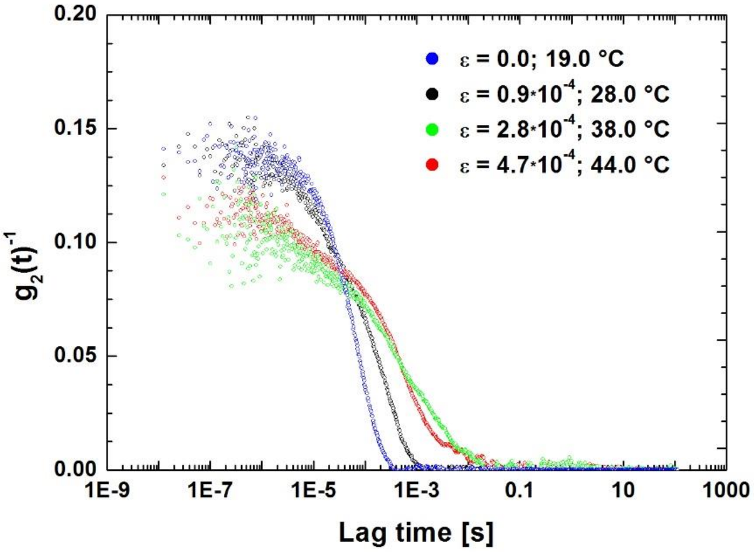

Figure 136 Correlation function measured by dynamic light scattering for varying ε and T.

4.6.5. Surface tension measurement

Surface tensions were measured with the tensiometer K11 (Krüss) using the Wilhelmy plate method. Aqueous concentrated solutions of the surfactant(s) were prepared and diluted in several samples in order to obtain a concentration range (Millipore water, σ = 72.6 mN.m-1 at 22 °C). Surface tension was recorded after equilibration for each mixture. The precision of the force transducer of the surface tension apparatus was 0.1 mN m-1 and before each experiment, the platinum plate was cleaned in blue-coloured flame. The temperature was stabilized at 22.0 ± 0.1°C with the thermo-regulated bath Julaba F12.

4.6.6. Gaschromatographic analysis

A Thermofisher GC Trace equipped with an AI 3000 injector connected to Thermofisher DSQ II simple quadrupole detector was used for the GC-MS analysis of the essential oils. Compound separation was achieved on a 30 m, DB5MS with 0.25 mm i.d. and 0.25 µm film thickness gas chromatographic column (J&W Scientific, Folsom, CA, USA). Carrier gas (ultra-pure helium) flow rate was 1.0 mL/min and the injector, the transfer line and the ion source were maintained at 220 °C respectively. The MS detector was used in the EI mode with an ionization voltage of 70 eV. The column was held at 70 °C for 2 min and then programmed at 10 °C/min to 285 °C and maintained for 15 min. The samples were diluted in cyclohexane and injected in the split mode with a ratio of 12. The NIST 2008 database was used to identify the chemical compounds.

An Agilent GC Trace equipped with an injector Series 7683 connected to an Agilent detector6890N/G1530N was used for the Gas chromatography-FID analyses. Compound separation was achieved on a 30 m HP-1 with 0.32 µm i.d. and 0.25 µm film thickness gas chromatographic column (J&W Scientific, Folsom, CA, USA). Carrier gas (N2) flow rate is 1.0 ml/mi. The injector was held at 70 °C for 2 min and then programmed at 60 °C/min to 280 °C and maintained for 6 min and then programmed at 20 °C/min to 70 °C. The ion source was maintained at 280 °C. The column was held at 70 °C for 2 min and then programmed at 10 °C/min to 220 °C and maintained for 5 min. The samples were diluted in cyclohexane.

General Conclusion

Nowadays ethanol and various other solvents represent the standard form of solubilising fragrances. However, due to regulations by the European Union and health issues, it is desired to find systems, which are able to replace those volatile organic compounds. It was thus part of this thesis to investigate the potential of non-ionic short-chain amphiphiles for aqueous fragrance solubilisation. Thereby several important aspects of these aqueous formulations were investigated, concerning the phase behaviour of short-chain amphiphiles in aqueous solution and their hydrophilic-lipophilic nature, as well as the hydrophobicity of fragrances. At last the findings are combined in order to explain the efficient solubilisation of fragrances in water.

In the first part of the thesis, the surfactant and solvent characteristics of solvo-surfactants were investigated. It was shown that they exhibit aqueous properties, concerning miscibility and aggregation, which can be extrapolated to real surfactants. However this is not valid for amphiphiles with $C_i \leq 4$. Furthermore the synergism between ionic and solvo-surfactants was investigated. It was demonstrated that the addition of SDS, DHS, etc. has a beneficial effect on the temperature stability of solvo-surfactants, as well as on the critical concentration, which induces the formation of mixed micelles. Especially at low solvo-surfactant content, traces of ionic surfactant have an enormous influence on the temperature interval, wherein a monophasic mixture is obtained. This region is of particular interest for aqueous fragrance solubilisation. In this context the hydrophilic-lipophilic nature of short-chain amphiphiles was investigated with respect to the reference system $C_{10}E_4$/*n*-octane/NaCl (aq). Thereby amphiphiles with $C_i \leq 5$ turned out to exhibit a strong dependency from the $C_{10}E_4$ mass concentration. Only for amphiphiles with $C_i \geq 6$, the variation can be neglected. Consequently it was found, that C_6E_4 is the most hydrophilic solvo-surfactant, which is favourable for the solubilisation of highly polar oils.

In the following the volatility and olfactory properties of short-chain amphiphiles were investigated, by determining their $T_{50\%}$ value. It is known that dimethyl isosorbide defines very well the frontier between VOCs and Non-VOCs ($T_{50\%}$ = 140 °C). Between this border another classification was introduced. The so-called “semi volatile organic compounds” (SVOC) represent molecules, which are not touched by EU regulations, but exhibit still acceptable volatile properties. For instance, the frontier was determined at $T_{50\%}$ = 180 °C for the perfume solvent triethyl citrate. Consequently various amphiphiles were found, which can be classified as SVOC, such as C_6E_3, C_6E_4, C_5Gly, etc. (**Figure 137**).

Eventually the olfactory properties of several interesting amphiphiles were investigated and classified according to their odour intensity and pleasantness. Thereby C_5E_3, C_6E_3, C_6E_4 and C_8E_3 turned out to be particularly interesting, since they exhibit relatively low odour intensity and their pleasantness was classified as neither particularly good, nor bad. Furthermore they represent SVOCs, which makes them particularly interesting for applications in perfumery, cosmetics or hard surface cleaning. The green alternative C_4Gly shows also acceptable results concerning odour intensity and pleasantness, however with the drawback of being classified as a VOC. In contrast its longer chained homologue

C_5Gly represents a SVOC. Unfortunately the odour perception is very strong, connected with a very unpleasant rancid scent.

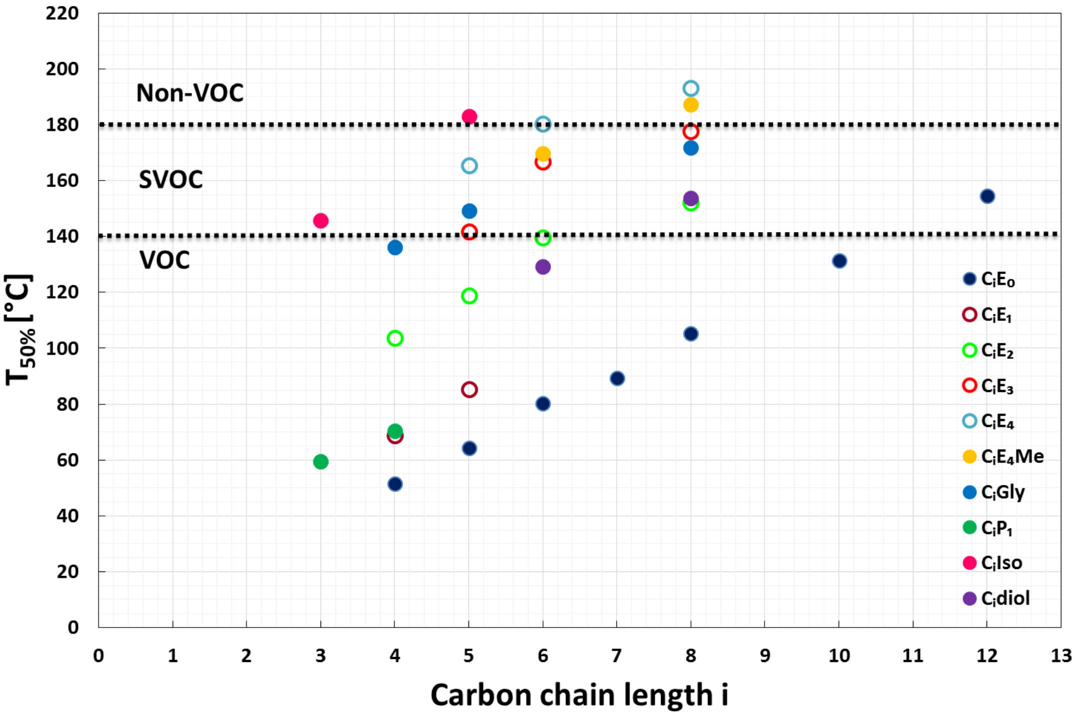

Figure 137 $T_{50\%}$ as a function of the carbon chain length *i*. The SVOCs can be found between 140 – 180 °C.

The phase behaviour of an aqueous fragrance formulation depends besides on the amphiphile, also on the hydrophobicity of the fragrance. A good possibility to classify an oil according to its hydrophobicity is the equivalent alkane carbon number (EACN). 46 new oils were investigated within **Chapter 3** and, together with the EACNs from literature, the influence of the functional group on the hydrophobicity of the oil was rationalised according to the effective packing parameter.

$$\bar{P} = \frac{(\nu_s + \tau\nu_o)}{(\sigma_s + \tau\sigma_o)l} \qquad \textbf{(58)}$$

The EACN was illustrated as a function of the carbon chain length for each functionalization (**Figure 138**). Each of them decreases the EACN. Thereby the strength is mainly determined by τ, which represents the number of oil molecules in relation to the number of amphiphile molecules at the interface. Consequently, the higher the polarity of the functional group, or the smaller the molecule, the easier it can penetrate into the interface and τ increases. Since σ_o can be neglected, the oil contribution to the effective volume of the amphiphile ($+\tau\nu_o$) augments the effective packing parameter, which in turn represents a decrease in EACN.

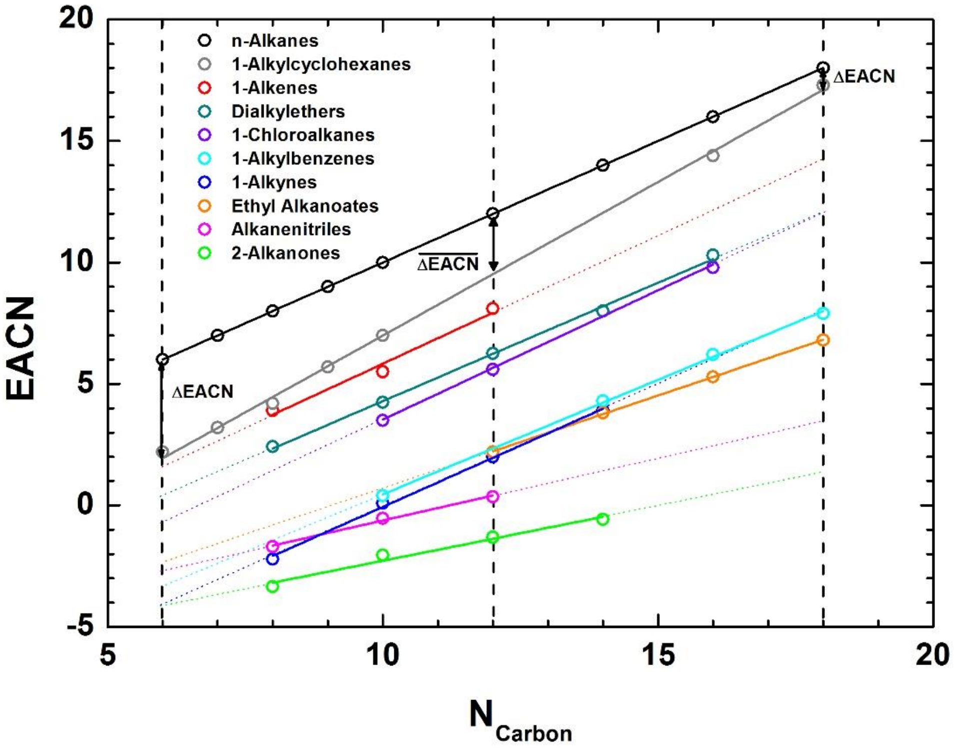

Figure 138 The EACN as a function of N_{Carbon} for several series of functionalised linear hydrocarbon oils.

The strong decrease in EACN upon functionalization highlights the importance of the oil polarity, concerning its influence on the phase behaviour in a SOW system. Since the determination of the EACN can be very time consuming, a QSPR model was established, with experimentally determined EACN values as dependent variables and COSMO-RS σ-moments as independent variables. Seven models where created, whereof two are of particular interest. Prediction *P6* represents a two-descriptor model, which is described by the surface area M_0^X and the overall polarity M_2^X of the molecule (**Equation 59**).

$$EACN_{pred6}^{X} = -5.1 + 0.065M_0^X - 0.22M_2^X \qquad \textbf{(59)}$$

This model is able to predict the EACN of each hydrocarbon oil adequately, which contains no strong hydrogen bond donors. M_0^X is connected to a positive coefficient, indicating the increase in EACN with augmenting molecular size. M_2^X on the other hand is linked to a negative coefficient. Thus the more polar the molecule, the lower the EACN. Consequently the model makes also physically sense and furthermore it proved its statistical relevance with $R^2 = 0.948$ and SEE = 1.35.

The second noteworthy model *P7* is represented by the pseudo-descriptor $M_{0/2}^X$, additionally to M_0^X and M_2^X (**Equation 60)**. There is no easy explanation for this descriptor, but it offers the possibility to distinguish between oils without and with a polar functional group.

$$EACN^{X}_{pred7} = -8.6 + 0.057M^{X}_{0} - 0.14M^{X}_{2} + 0.25M^{X}_{0/2} \qquad \textbf{(60)}$$

The pseudo-desriptor represents thus a rather correctional factor, which results in a better correlation ($R^2 = 0.968$) and a smaller error (SEE = 1.06). It was shown that $P7$ is especially good for the prediction of fragrances, where SEE was reduced to 0.90. Thus the latter model may find an application in fine perfumery.

Knowing the hydrophilic-lipophilic nature of the amphiphile, as well as the EACN of the fragrance, the phase behaviour can be anticipated. Thereby it was shown in **Chapter 4** that the optimum formulation in a water-rich system depends in the same way on the formulation variables as at WOR = 1. Since in a solvo-surfactant/fragrance/water system, the three-phase region is relatively narrow, the HLD equation can also be applied to approximate the optimum formulation in the water-rich corner of the ternary phase prism. However in aqueous fragrance solubilisation, it is desired to obtain a huge temperature insensitive monophasic region. This was achieved with the addition of traces of ionic surfactants, such as DHS or SDS. It was shown that the efficiency of the system to solubilise fragrance augments until the three-phase region disappears. From this point on, the mixed surfactant turns too hydrophilic and is not able to form an interfacial film with zero curvature. Consequently the efficiency decreases with further increasing ionic surfactant content. Another problem is the high monomeric solubility of solvo-surfactants in highly polar oils. With decreasing EACN less amphiphile is found at the interface. Hence for very polar oils, the efficiency may even decrease in comparison to the systems without ionic surfactant. Nevertheless in either case, the temperature stability augments constantly with augmenting ionic surfactant content, allowing the solubilisation of high amounts of fragrance, within a temperature interval of 50 °C and more. Consequently a compromise has to be made between efficiency and high temperature stability, since the latter is usually linked to a system, which is far away from zero curvature.

It can thus be summarized that solvo-surfactants are applicable for the solubilisation of fragrances in water. Especially C_6E_3 and C_6E_4 turned out to be predestined for such applications, since they are classified as SVOCs, have acceptable olfactory properties and show strong synergistic interactions with ionic surfactants, which permits an efficient solubilisation of fragrances within the formed mixed micelles. The best solubilisations were found with them at $w = 0.1$. A very temperature stable aqueous formulation (5 – 50 °C), which can solubilise 5.3 wt.% of fragrance mixture, can be obtained with the system C_6E_4/β-pinene+linalool/SDS (aq) with $\xi = 0.35$ and $\varepsilon = 2.8 * 10^{-4}$. The best system to solubilise 10 wt.% fragrance is C_6E_3/β-pinene/DHS (aq) with $\varepsilon = 4.7 * 10^{-4}$, within 33 – 48 °C.

The green alternative C_5Gly is barely able to replace the glycols within this context, since much more of it is necessary in order to obtain an efficient solubilisation and due to its strong hydrophilic head group it is only applicable to oils within a small EACN interval (0.7 – 1.9). The best system to solubilise 10 wt.% of fragrance was obtained for C_5Gly/ω-hexadecenlactone/SDS (aq), with $\varepsilon = 2.8 * 10^{-4}$ and $w = 0.2$, within 45 – 62 °C. Furthermore the olfactory properties were not favourable.

References

(1) Edwards, I. E. S. *Tutankhamun, His Tomb and Its Treasures*; Metropolitan Museum of Art, 1976.

(2) Tour Egypt : Egypt: Ancient Egyptian Beauty - Tutankhamun - 2011.

(3) Fortineau, A.-D. Chemistry Perfumes Your Daily Life. *J. Chem. Educ.* **2004**, *81* (1), 45.

(4) Firmenich. Facts & Figures. *Webpage*.

(5) Slomkowski, S.; Alemán, J. V.; Gilbert, R. G.; Hess, M.; Horie, K.; Jones, R. G.; Kubisa, P.; Meisel, I.; Mormann, W.; Penczek, S.; et al. Terminology of Polymers and Polymerization Processes in Dispersed Systems (IUPAC Recommendations 2011). *Pure Appl. Chem.* **2011**, *83* (12), 2229–2259.

(6) Shinoda, K.; Arai, H. The Correlation between Phase Inversion Temperature In Emulsion and Cloud Point in Solution of Nonionic Emulsifier. *J. Phys. Chem.* **1964**, *68* (12), 3485–3490.

(7) Shinoda, K. The Comparison between PIT System and the HLB-Value System to Emulsifier Selection. *Proc. 5th Int. Congr. Surf. Act.* **1969**, *2*, 275–283.

(8) Ontiveros, J. F.; Pierlot, C.; Catté, M.; Molinier, V.; Salager, J.-L.; Aubry, J.-M. A Simple Method to Assess the Hydrophilic Lipophilic Balance of Food and Cosmetic Surfactants Using the Phase Inversion Temperature of $C_{10}E_4$/*n*-Octane/water Emulsions. *Colloids Surf. Physicochem. Eng. Asp.* **2014**, *458*, 32–39.

(9) Holland, P. M.; Rubingh, D. N. Nonideal Multicomponent Mixed Micelle Model. *J. Phys. Chem.* **1983**, *87* (11), 1984–1990.

(10) Herrmann, A. Controlled Release of Volatiles under Mild Reaction Conditions: From Nature to Everyday Products. *Angew. Chem. Int. Ed.* **2007**, *46* (31), 5836–5863.

(11) Griffin, W. C. Classification of Surface-Active Agents by "HLB." *J. Soc. Cosmet. Chem.* **1949**, *1*, 311–326.

(12) Griffin, W. C. Calculation of HLB Values of Non-Ionic Surfactants. *J. Soc. Cosmet. Chem.* **1954**, *5*, 249–256.

(13) Davies, J. T. A Quantitive Kinetic Theory of Emulsion Type, I, Physical Chemistry of the Emulsifying Agent. Gas/Liquid and Liquid/Liquid Interface. *Proc. Int. Congr. Surf. Act.* **1957**, *Vol 1*, 426–438.

(14) Winsor, P. A. Hydrotropy, Solubilisation and Related Emulsification Processes. *Trans. Faraday Soc.* **1948**, *44*, 376–398.

(15) Winsor, P. A. *Solvent Properties of Amphiphilic Compounds*; Butterworths Scientific Publications: London, 1954.

(16) Bourrel, M.; Chambu, C. The Rules for Achieving High Solubilization of Brine and Oil by Amphiphilic Molecules. *Soc. Pet. Eng. J.* **1983**, *23* (02), 327–338.

(17) Shinoda, K.; Kunieda, H. The Effect of Salt Concentration, Temperature, and Additives on the Solvent Property of Aerosol OT Solution. *J. Colloid Interface Sci.* **1987**, *118* (2), 586–589.

(18) Salager, J.-L.; Marquez, L.; Pena, A. A.; Rondon, M.; Silva, F.; Tyrode, E. Current Phenomenological Know-How and Modeling of Emulsion Inversion. In *Industrial & Engineering Chemistry Research*; Industrial & Engineering Chemistry Research, 2000; Vol. 39:8, s. 2665-2676.

(19) Matsumoto, S.; Sherman, P. A DTA Technique for Identifying the Phase Inversion Temperature of O/W Emulsions. *J. Colloid Interface Sci.* **1970**, *33* (2), 294–298.

(20) Enever, R. P. Correlation of Phase Inversion Temperature with Kinetics of Globule Coalescence for Emulsions Stabilized by a Polyoxyethylene Alkyl Ether. *J. Pharm. Sci.* **1976**, *65* (4), 517–520.

(21) Reed, R. L.; Healy, R. N. Some Physicochemical Aspects of Microemulsion Flooding: A Review. *Improv. Oil Recovery Surfactant Polym. Flooding* **1977**, 383–437.

(22) Salager, J.-L. Physico-Chemical Properties of Surfactant-Water-Oil Mixtures: Phase Behavior, Microemulsion Formation and Interfacial Tension, University of Texas, Austin, 1977.

(23) Salager, J. L.; Morgan, J. C.; Schechter, R. S.; Wade, W. H.; Vasquez, E. Optimum Formulation of Surfactant/Water/Oil Systems for Minimum Interfacial Tension or Phase Behavior. *Soc. Pet. Eng. J.* **1979**, *19* (02), 107–115.

(24) Bourrel, M.; Salager, J. L.; Schechter, R. S.; Wade, W. H. A Correlation for Phase Behavior of Nonionic Surfactants. *J. Colloid Interface Sci.* **1980**, *75* (2), 451–461.

(25) Salager, J.-L.; Forgiarini, A. M.; Bullón, J. How to Attain Ultralow Interfacial Tension and Three-Phase Behavior with Surfactant Formulation for Enhanced Oil Recovery: A Review. Part 1. Optimum Formulation for Simple Surfactant–Oil–Water Ternary Systems. *J. Surfactants Deterg.* **2013**, *16* (4), 449–472.

(26) Salager, J.-L.; Antón, R.; Andérez, J.; Aubry, J.-M. Formulation Des Microémulsions Par La Méthode Du HLD. **2001**, *Techniques de l'Ingenieur*.

(27) Witthayapanyanon, A.; Harwell, J. H.; Sabatini, D. A. Hydrophilic–lipophilic Deviation (HLD) Method for Characterizing Conventional and Extended Surfactants. *J. Colloid Interface Sci.* **2008**, *325* (1), 259–266.

(28) Acosta, E. J.; Yuan, J. S.; Bhakta, A. S. The Characteristic Curvature of Ionic Surfactants. *J. Surfactants Deterg.* **2008**, *11* (2), 145–158.

(29) Acosta, E. J. The HLD–NAC Equation of State for Microemulsions Formulated with Nonionic Alcohol Ethoxylate and Alkylphenol Ethoxylate Surfactants. *Colloids Surf. Physicochem. Eng. Asp.* **2008**, *320* (1–3), 193–204.

(30) Yang, Z. Z.; Xu, Y. Z.; Zhao, D. L.; Xu, M. Preparation of Waterborne Dispersions of Epoxy Resin by the Phase-Inversion Emulsification Technique. 1. Experimental Study on the Phase-Inversion Process. *Colloid Polym. Sci.* **2000**, *278* (12), 1164–1171.

(31) Salager, J.-L.; Forgiarini, A.; Márquez, L.; Peña, A.; Pizzino, A.; Rodriguez, M. P.; Rondón-González, M. Using Emulsion Inversion in Industrial Processes. *Adv. Colloid Interface Sci.* **2004**, *108–109*, 259–272.

(32) Miller, C. A.; Raney, K. H. Solubilization—emulsification Mechanisms of Detergency. *Colloids Surf. Physicochem. Eng. Asp.* **1993**, *74* (2–3), 169–215.

(33) Israelachvili, J. N.; Mitchell, D. J.; Ninham, B. W. Theory of Self-Assembly of Hydrocarbon Amphiphiles into Micelles and Bilayers. *J. Chem. Soc. Faraday Trans. 2* **1976**, *72*, 1525.

(34) Imae, T.; Ikeda, S. Sphere-Rod Transition of Micelles of Tetradecyltrimethylammonium Halides in Aqueous Sodium Halide Solutions and Flexibility and Entanglement of Long Rodlike Micelles. *J. Phys. Chem.* **1986**, *90* (21), 5216–5223.

(35) Lin, Z.; Cai, J. J.; Scriven, L. E.; Davis, H. T. Spherical-to-Wormlike Micelle Transition in CTAB Solutions. *J. Phys. Chem.* **1994**, *98* (23), 5984–5993.

(36) Missel, P. J.; Mazer, N. A.; Benedek, G. B.; Carey, M. C. Influence of Chain Length on the Sphere-to-Rod Transition in Alkyl Sulfate Micelles. *J. Phys. Chem.* **1983**, *87* (7), 1264–1277.

(37) Imae, T.; Kamiya, R.; Ikeda, S. Formation of Spherical and Rod-like Micelles of Cetyltrimethylammonium Bromide in Aqueous NaBr Solutions. *J. Colloid Interface Sci.* **1985**, *108* (1), 215–225.

(38) Renoncourt, A.; Vlachy, N.; Bauduin, P.; Drechsler, M.; Touraud, D.; Verbavatz, J.-M.; Dubois, M.; Kunz, W.; Ninham, B. W. Specific Alkali Cation Effects in the Transition from Micelles to Vesicles through Salt Addition. *Langmuir* **2007**, *23* (5), 2376–2381.

(39) Vlachy, N.; Drechsler, M.; Verbavatz, J.-M.; Touraud, D.; Kunz, W. Role of the Surfactant Headgroup on the Counterion Specificity in the Micelle-to-Vesicle Transition through Salt Addition. *J. Colloid Interface Sci.* **2008**, *319* (2), 542–548.

(40) Singh, H. N.; Saleem, S. M.; Singh, R. P.; Birdi, K. S. Micelle Formation of Ionic Surfactants in Polar Nonaqueous Solvents. *J. Phys. Chem.* **1980**, *84* (17), 2191–2194.

(41) Akhter, M. S. Studies on Solvophobic Interactions and Micelle Formation in Non Aqueous Solvents. *Colloids Surf. Physicochem. Eng. Asp.* **1999**, *150* (1–3), 25–30.

(42) Nagarajan, R. Molecular Packing Parameter and Surfactant Self-Assembly: The Neglected Role of the Surfactant Tail†. *Langmuir* **2002**, *18* (1), 31–38.

(43) Tchakalova, V.; Testard, F.; Wong, K.; Parker, A.; Benczédi, D.; Zemb, T. Solubilization and Interfacial Curvature in Microemulsions. *Colloids Surf. Physicochem. Eng. Asp.* **2008**, *331* (1-2), 31–39.

(44) Tchakalova, V.; Testard, F.; Wong, K.; Parker, A.; Benczédi, D.; Zemb, T. Solubilization and Interfacial Curvature in Microemulsions: II. Surfactant Efficiency and PIT. *Colloids Surf. Physicochem. Eng. Asp.* **2008**, *331* (1–2), 40–47.

(45) Ontiveros, J. F.; Pierlot, C.; Catté, M.; Molinier, V.; Salager, J.-L.; Aubry, J.-M. Structure–interfacial Properties Relationship and Quantification of the Amphiphilicity of Well-Defined Ionic and Non-Ionic Surfactants Using the PIT-Slope Method. *J. Colloid Interface Sci.* **2015**, *448*, 222–230.

(46) Schreinemakers, F. A. H. *Die Heterogenen Gleichgewichte*; Vieweg; Braunschweig, 1913.

(47) Herrmann, C.-U.; Klar, G.; Kahlweit, M. On the Phase Inversion in H2O-Oil-Nonionic Surfactant Systems and Related Phenomena. *J. Colloid Interface Sci.* **1981**, *82* (1), 6–13.

(48) Kahlweit, M. The Phase Behavior of Systems of the Type H2O-Oil—nonionic Surfactant—electrolyte. *J. Colloid Interface Sci.* **1982**, *90* (1), 197–202.

(49) Kahlweit, M.; Strey, R. Phase Behavior of Ternary Systems of the Type H2O-Oil-Nonionic Amphiphile (Microemulsions). *Angew. Chem. Int. Ed. Engl.* **1985**, *24* (8), 654–668.

(50) Kahlweit, M.; Strey, R.; Firman, P.; Haase, D.; Jen, J.; Schomaecker, R. General Patterns of the Phase Behavior of Mixtures of Water, Nonpolar Solvents, Amphiphiles, and Electrolytes. 1. *Langmuir* **1988**, *4* (3), 499–511.

(51) Stubenrauch, C. *Microemulsions: Background, New Concepts, Applications, Perspectives*; Wiley, 2009.

(52) Kunieda, H.; Shinoda, K. Phase Behavior in Systemes of Nonionic Surfactant/ Water/ Oil around the Hydrophile-Lipophile-Balance-Temperature (HLB-Temperature). *J. Dispers. Sci. Technol.* **1982**, *3* (3), 233–244.

(53) Kahlweit, M.; Lessner, E.; Strey, R. Influence of the Properties of the Oil and the Surfactant on the Phase Behavior of Systems of the Type Water-Oil-Nonionic Surfactant. *J. Phys. Chem.* **1983**, *87* (24), 5032–5040.

(54) Tadros, T. F. *Self-Organized Surfactant Structures*; John Wiley & Sons, 2011.

(55) Pizzino, A.; Molinier, V.; Catté, M.; Ontiveros, J. F.; Salager, J.-L.; Aubry, J.-M. Relationship between Phase Behavior and Emulsion Inversion for a Well-Defined Surfactant (C10E4)/n-Octane/Water Ternary System at Different Temperatures and Water/Oil Ratios. *Ind. Eng. Chem. Res.* **2013**, *52* (12), 4527–4538.

(56) Burauer, S.; Sachert, T.; Sottmann, T.; Strey, R. On Microemulsion Phase Behavior and the Monomeric Solubility of Surfactant. *Phys. Chem. Chem. Phys.* **1999**, *1* (18), 4299–4306.

(57) Burauer, S.; Sottmann, T.; Strey, R. Nonionic Microemulsions with Cyclic Oils. *Tenside Surfactants Deterg.* **2000**, *37* (1), 8–16.

(58) Lade, O.; Beizai, K.; Sottmann, T.; Strey, R. Polymerizable Nonionic Microemulsions: Phase Behavior of H_2O − *n*-Alkyl Methacrylate − *n*-Alkyl Poly(ethylene Glycol) Ether (C_iE_j). *Langmuir* **2000**, *16* (9), 4122–4130.

(59) Balogh, J.; Olsson, U.; Jan, S. P.; Kaper, H.; Wennerström, H.; Schillén, K.; Miguel, M. Nonionic Microemulsions: Dependence of Oil Chain Length and Active Component (Lidocaine). In *Self-Organized Surfactant Structures*; Tadros, T. F., Ed.; Wiley-VCH Verlag GmbH & Co. KGaA, 2010; pp 59–87.

(60) Balogh, J. Determining Scaling in Known Phase Diagrams of Nonionic Microemulsions to Aid Constructing Unknown. *Adv. Colloid Interface Sci.* **2010**, *159* (1), 22–31.

(61) Kanei, N.; Tamura, Y.; Kunieda, H. Effect of Types of Perfume Compounds on the Hydrophile–lipophile Balance Temperature. *J. Colloid Interface Sci.* **1999**, *218* (1), 13–22.

(62) Ontiveros, J. F.; Bouton, F.; Durand, M.; Pierlot, C.; Quellet, C.; Nardello-Rataj, V.; Aubry, J.-M. Dramatic Influence of Fragrance Alcohols and Phenols on the Phase Inversion Temperature of the Brij30/*n*-Octane/water System. *Colloids Surf. Physicochem. Eng. Asp.* **2015**, *478*, 54–61.

(63) Rieger, M.; Rhein, L. D. *Surfactants in Cosmetics, Second Edition,*; CRC Press, 1997.

(64) Friberg, S. E.; Huang, T.; Fei, L.; Vona, S. A.; Aikens, P. A. Vapor Pressure of Phenethyl Alcohol in the System with Water, and Polyoxyethylene, 4, Lauryl Ether (Brij® 30). In *Interfaces, Surfactants and Colloids in Engineering*; Jacobasch, H.-J., Ed.; Progress in Colloid & Polymer Science; Steinkopff, 1996; pp 18–22.

(65) Friberg, S. E.; Fei, L.; Campbell, S.; Yang, H.; Lu, Y. Vapor Pressure of Phenethyl Alcohol in an Aqueous Hydrotrope Solution. *Colloids Surf. Physicochem. Eng. Asp.* **1997**, *127* (1–3), 233–239.

(66) Friberg, S. E.; Fei, L. Vapor Pressures of Phenethyl Alcohol and Phenethyl Acetate in Aqueous Solutions of Sodium Xylene Sulfonate and Polyvinylpyrrolidone. In *Horizons 2000 – aspects of colloid and interface science at the turn of the millenium*; Lagaly, G., Ed.; Progress in Colloid & Polymer Science; Steinkopff, 1998; pp 93–100.

(67) Friberg, S. E.; Bawab, A. Al-; Sandburg, J. D.; Barber, J. L.; Yin, Q.; Aikens, P. A. Phase Behavior of a Fragrance Compound System: Water/phenethyl Alcohol/laureth 4/glycerol. *J. Surfactants Deterg.* **1999**, *2* (2), 159–165.

(68) Ge, L.; Friberg, S. E.; Guo, R. Constant Vapour Pressure Evaporation from a Fragrance Emulsion—effect of Solubility of Surfactant in the Fragrance Compound. *Flavour Fragr. J.* **2009**, *24* (1), 7–12.

(69) Saito∗, Y.; Miura, K.; Tokuoka, Y.; Kondo, Y.; Abe, M.; Sato, T. Volatility and Solubilization of Synthetic Fragrances by Pluronic P-85. *J. Dispers. Sci. Technol.* **1996**, *17* (6), 567–576.

(70) Tokuoka, Y.; Uchiyama, H.; Abe, M. Phase Diagrams of Surfactant/water/synthetic Perfume Ternary Systems. *Colloid Polym. Sci.* **1994**, *272* (3), 317–323.

(71) Behan, J. M.; Ness, J. N.; Traas, P. C.; Vitsas, J. S.; Willis, B. J. Aqueous Perfume Oil Microemulsions. US5374614 A, December 20, 1994.

(72) Shick, R. A.; Tucker, C. J.; Piechocki, C.; Gatz, L. A. Ethanol-Free Aqueous Perfume Composition. US20130101531 A1, April 25, 2013.

(73) Rataj, N. V.; Aubry, J.-M. Volatile Aqueous Microemulsions of Perfumes and Essential Oils Based on the Use of Solvo-Surfactants. WO2014080150 A1, May 30, 2014.

(74) Kahlweit, M.; Strey, R. Phase Behavior of Quinary Systems: Tracing the Three-Phase Body. *J. Phys. Chem.* **1987**, *91* (6), 1553–1557.

(75) Kahlweit, M.; Strey, R. Phase Behavior of Quinary Mixtures of the Type Water-Oil-Nonionic Amphiphile-Ionic Amphiphile-Salt. *J. Phys. Chem.* **1988**, *92* (6), 1557–1563.

(76) Aramaki, K.; Ozawa, K.; Kunieda, H. Effect of Temperature on the Phase Behavior of Ionic–Nonionic Microemulsions. *J. Colloid Interface Sci.* **1997**, *196* (1), 74–78.

(77) Neuberg, C. Hydrotropic Phenomena I. *Biochem. Z.* **1916**, *76*, 101.

(78) McKee, R. H. Use of Hydrotropic Solutions in Industry. *Ind. Eng. Chem.* **1946**, *38* (4), 382–384.

(79) Friberg, S. E.; Rydhag, L. Solubility and Association Conditions of Hydrotropic Substances. *Tenside* **1970**, *7* (2), 80.

(80) Saleh, A. M.; El-Khordagui, L. K. Hydrotropic Agents: A New Definition. *Int. J. Pharm.* **1985**, *24* (2–3), 231–238.

(81) Balasubramanian, D.; Srinivas, V.; Gaikar, V. G.; Sharma, M. M. Aggregation Behavior of Hydrotropic Compounds in Aqueous Solution. *J. Phys. Chem.* **1989**, *93* (9), 3865–3870.

(82) Srinivas, V.; Rodley, G. A.; Ravikumar, K.; Robinson, W. T.; Turnbull, M. M. Molecular Organization in Hydrotrope Assemblies. *Langmuir* **1997**, *13* (12), 3235–3239.

(83) Arrigo, G. D'; Giordano, R.; Teixeira, J. Small-Angle Neutron Scattering Studies of Aqueous Solutions of Short-Chain Amphiphiles. *Eur. Phys. J. E* **2003**, *10* (2), 135–142.

(84) Zhu, Y.; Fournial, A.-G.; Molinier, V.; Azaroual, N.; Vermeersch, G.; Aubry, J.-M. Self-Association of Short-Chain Nonionic Amphiphiles in Binary and Ternary Systems: Comparison between the Cleavable Ethylene Glycol Monobutyrate and Its Ether Counterparts. *Langmuir* **2009**, *25* (2), 761–768.

(85) Neumann, M. G.; Schmitt, C. C.; Prieto, K. R.; Goi, B. E. The Photophysical Determination of the Minimum Hydrotrope Concentration of Aromatic Hydrotropes. *J. Colloid Interface Sci.* **2007**, *315* (2), 810–813.

(86) Lunkenheimer, K.; Schrödle, S.; Kunz, W. Dowanol DPnB in Water as an Example of a Solvo-Surfactant System: Adsorption and Foam Properties. In *Trends in Colloid and Interface Science XVII*; Progress in Colloid and Polymer Science; Springer Berlin Heidelberg, 2004; pp 14–20.

(87) Kennedy, A. W. Diacetone Alcohol, 2-Ethoxyethanol, 2-Butoxyethanol as Flaking Medium. US4026710 A, May 31, 1977.

(88) Flaningam, O. L.; Moore, J. A.; Williams, D. E. Containing 2-Butoxyethanol, 2-Methylcyclohexanol or Isopropyl Lactate; Cleaning, Rinsing or Drying Surfaces. US5456856 A, October 10, 1995.

(89) Etiemble, J. Les éthers de glycol : Une toxicité variable selon les composés. *Actual. Chim.* **2003**, No. 11-12, 145–149.

(90) Burlew, J. O. Industrial Cleaner Dispersant Formulation. US6100227 A, August 8, 2000.

(91) Walsum, A. V.; Ruizendaal, J.-W. Z.; Boden, R. M.; Crossman, A. J.; White, M. J. R. A Wipe Containing Perfume and a Mixture of Two Glycol Ether Compounds,. US6506723 B1, January 14, 2003.

(92) Vanlerberghe, G.; Sebag, H. 1,2-Alkanediol Derivatives in Cosmetic Compositions as an Excipient Therefor. US4303639 A, December 1, 1981.

(93) Lee, E.; An, S.; Cho, S.-A.; Yun, Y.; Han, J.; Hwang, Y. K.; Kim, H. K.; Lee, T. R. The Influence of Alkane Chain Length on the Skin Irritation Potential of 1,2-Alkanediols. *Int. J. Cosmet. Sci.* **2011**, *33* (5), 421–425.

(94) Pillai, R.; Roeding, J.; Lange, S.; Schmaus, G. Synergistic Mixtures of 1,2-Hexanediol and 1,2-Octanediol and Also a Further Preservative. WO2006045743 A1, May 4, 2006.

(95) Roeding, J.; Lange, S.; Schmaus, G. Synergistic Mixtures of at Least One 1,2 Alkanediol such as 1,2-Hexanediol and 1,2-Octanediol with a Further Compound Having Antimicrobial Properties. US 20070265352 A1.

(96) Hasegawa, R.; Hayashi, K. Polyester Containing Impure 1,2-Butanediol. US4596886 A, June 24, 1986.

(97) Hanessian, S. *Total Synthesis of Natural Products: The" Chiron" Approach*; Pergamon Press Oxford, 1983; Vol. 3.

(98) Moity, L.; Shi, Y.; Molinier, V.; Dayoub, W.; Lemaire, M.; Aubry, J.-M. Hydrotropic Properties of Alkyl and Aryl Glycerol Monoethers. *J. Phys. Chem. B* **2013**, *117* (31), 9262–9272.

(99) Shi, Y.; Dayoub, W.; Favre-Réguillon, A.; Chen, G.-R.; Lemaire, M. Straightforward Selective Synthesis of Linear 1-O-Alkyl Glycerol and Di-Glycerol Monoethers. *Tetrahedron Lett.* **2009**, *50* (49), 6891–6893.

(100) Shi, Y.; Dayoub, W.; Chen, G.-R.; Lemaire, M. Selective Synthesis of 1-O-Alkyl Glycerol and Diglycerol Ethers by Reductive Alkylation of Alcohols. *Green Chem.* **2010**, *12* (12), 2189–2195.

(101) Shi, Y.; Dayoub, W.; Chen, G.-R.; Lemaire, M. One-Step Selective Synthesis of Branched 1-O-Alkyl-Glycerol/diglycerol Monoethers by Catalytic Reductive Alkylation of Ketones. *Sci. China Chem.* **2010**, *53* (9), 1953–1956.

(102) Sutter, M.; Dayoub, W.; Métay, E.; Raoul, Y.; Lemaire, M. Selective Synthesis of 1-O-Alkyl(poly)glycerol Ethers by Catalytic Reductive Alkylation of Carboxylic Acids with a Recyclable Catalytic System. *ChemSusChem* **2012**, *5* (12), 2397–2409.

(103) Moity, L. Conception, Modeélisation et Caractérisation de Solvants Agro-Sourcés, Université de Sciences et Technologies Lille: Villeneuve d'Ascq, 2013.

(104) Schnell, E.; Touraud, D.; Gick, R.; Kunz, W. Properties of a New Hydrotrope Hydrophobic Molecule and Its Potential Applications. *Int. J. Cosmet. Sci.* **2008**, *30* (5), 347–351.

(105) Valentin, R.; Alignan, M.; Giacinti, G.; Renaud, F. N. R.; Raymond, B.; Mouloungui, Z. Pure Short-Chain Glycerol Fatty Acid Esters and Glycerylic Cyclocarbonic Fatty Acid Esters as Surface Active and Antimicrobial Coagels Protecting Surfaces by Promoting Superhydrophilicity. *J. Colloid Interface Sci.* **2012**, *365* (1), 280–288.

(106) Valentin, R.; Mouloungui, Z. Superhydrophilic Surfaces from Short and Medium Chain Solvo-Surfactants. *Ol. Corps Gras Lipides* **2013**, *20* (1), 33–44.

(107) Queste, S.; Salager, J. L.; Strey, R.; Aubry, J. M. The EACN Scale for Oil Classification Revisited Thanks to Fish Diagrams. *J. Colloid Interface Sci.* **2007**, *312* (1), 98–107.

(108) Mitchell, D. J.; Tiddy, G. J. T.; Waring, L.; Bostock, T.; McDonald, M. P. Phase Behaviour of Polyoxyethylene Surfactants with Water. Mesophase Structures and Partial Miscibility (cloud Points). *J. Chem. Soc. Faraday Trans. 1 Phys. Chem. Condens. Phases* **1983**, *79* (4), 975.

(109) Aveyard, R.; Binks, B. P.; Clark, S.; Fletcher, P. D. I. Cloud Points, Solubilisation and Interfacial Tensions in Systems Containing Nonionic Surfactants. *J. Chem. Technol. Biotechnol.* **1990**, *48* (2), 161–171.

(110) Schubert, K.-V.; Strey, R.; Kahlweit, M. A New Purification Technique for Alkyl Polyglycol Ethers and Miscibility Gaps for Water-CiEj. *J. Colloid Interface Sci.* **1991**, *141* (1), 21–29.

(111) Browarzik, C.; Browarzik, D. Liquid–liquid Equilibrium Calculation in Binary Water + Nonionic Surfactant C_iE_j Systems with a New Mass-Action Law Model Based on Continuous Thermodynamics. *Fluid Phase Equilibria* **2005**, *235* (2), 127–138.

(112) Queste, S.; Bauduin, P.; Touraud, D.; Kunz, W.; Aubry, J.-M. Short Chain Glycerol 1-Monoethers: A New Class of Green Solvo-Surfactants. *Green Chem.* **2006**, *8* (9), 822.

(113) Kahlweit, M.; Strey, R.; Busse, G. Weakly to Strongly Structured Mixtures. *Phys. Rev. E* **1993**, *47* (6), 4197.

(114) Kunieda, H.; Solans, C. How to Prepare Microemulsions : Temperature-Insensitive Micoremulsions. *Surfactant Sci. Ser.* **1997**, *66*, 21–45.

(115) Binks, B. P.; Fletcher, P. D. I.; Taylor, D. J. F. Temperature Insensitive Microemulsions. *Langmuir* **1997**, *13* (26), 7030–7038.

(116) Zhu, Y.; Durand, M.; Molinier, V.; Aubry, J.-M. Isosorbide as a Novel Polar Head Derived from Renewable Resources. Application to the Design of Short-Chain Amphiphiles with Hydrotropic Properties. *Green Chem.* **2008**, *10* (5), 532.

(117) Ciccarelli, D.; Costantino, L.; Errico, G. D'; Paduano, L.; Vitagliano, V. Mixed Micellar Aggregates of Anionic and Nonionic Surfactants with Short Hydrophobic Tails. A PGSE-NMR Study. *Langmuir* **1998**, *14* (25), 7130–7139.

(118) Cui, X.; Jiang, Y.; Yang, C.; Lu, X.; Chen, H.; Mao, S.; Liu, M.; Yuan, H.; Luo, P.; Du, Y. Mechanism of the Mixed Surfactant Micelle Formation. *J. Phys. Chem. B* **2010**, *114* (23), 7808–7816.

(119) Karlstroem, G.; Carlsson, A.; Lindman, B. Phase Diagrams of Nonionic Polymer-Water Systems: Experimental and Theoretical Studies of the Effects of Surfactants and Other Cosolutes. *J. Phys. Chem.* **1990**, *94* (12), 5005–5015.

(120) Gu, T.; Galera-Gómez, P. A. Clouding of Triton X-114: The Effect of Added Electrolytes on the Cloud Point of Triton X-114 in the Presence of Ionic Surfactants. *Colloids Surf. Physicochem. Eng. Asp.* **1995**, *104* (2–3), 307–312.

(121) Marszall, L. The Effect of Electrolytes on the Cloud Point of Ionic-Nonionic Surfactant Solutions. *Colloids Surf.* **1987**, *25* (2–4), 279–285.

(122) Smith, S.; Wiseman, P.; Boudreau, L.; Marangoni, G.; Palepu, R. Effect of Microheterogeneity on Bulk and Surface Properties of Binary Mixtures of Polyoxyethene Glycol Monobutyl Ethers with Water. *J. Solut. Chem.* **1994**, *23* (2), 207–222.

(123) Frindi, M.; Michels, B.; Zana, R. Ultrasonic Absorption Studies of Surfactant Exchange between Micelles and Bulk Phase in Aqueous Micellar Solutions of Nonionic Surfactants with a Short Alkyl Chain. 2. C6E3, C6E5, C8E4, and C8E8. *J. Phys. Chem.* **1992**, *96* (14), 6095–6102.

(124) Inoue, T.; Maema, K. Self-Aggregation of Nonionic Surfactants in Imidazolium-Based Ionic Liquids with Trifluoromethanesulfonate Anion. *Colloid Polym. Sci.* **2011**, *289* (10), 1167–1175.

(125) Chakraborty, T.; Ghosh, S. A Unified Survey of Applicability of Theories of Mixed Adsorbed Film and Mixed Micellization. *J. Surfactants Deterg.* **2008**, *11* (4), 323–334.

(126) Sohrabi, B.; Gharibi, H.; Tajik, B.; Javadian, S.; Hashemianzadeh, M. Molecular Interactions of Cationic and Anionic Surfactants in Mixed Monolayers and Aggregates. *J. Phys. Chem. B* **2008**, *112* (47), 14869–14876.

(127) Shiloach, A.; Blankschtein, D. Measurement and Prediction of Ionic/Nonionic Mixed Micelle Formation and Growth. *Langmuir* **1998**, *14* (25), 7166–7182.

(128) Rubingh, D. N. Mixed Micelle Solutions. In *Solution Chemistry of Surfactants*; Mittal, K. L., Ed.; Springer New York, 1979; pp 337–354.

(129) Rauwel, G.; Leclercq, L.; Criquelion, J.; Aubry, J.-M.; Nardello-Rataj, V. Aqueous Mixtures of Di-N-Decyldimethylammonium Chloride/polyoxyethylene Alkyl Ether: Dramatic Influence of Tail/tail and Head/head Interactions on Co-Micellization and Biocidal Activity. *J. Colloid Interface Sci.* **2012**, *374* (1), 176–186.

(130) Lange, H.; Beck, D. K.-H. Zur Mizellbildung in Mischlösungen homologer und nichthomologer Tenside. *Kolloid-Z. Z. Für Polym.* **1973**, *251* (6), 424–431.

(131) Holland, P. M.; Rubingh, D. N. Mixed Surfactant Systems; American Chemical Society, 1992.

(132) Strey, R.; Viisanen, Y.; Aratono, M.; Kratohvil, J. P.; Yin, Q.; Friberg, S. E. On the Necessity of Using Activities in the Gibbs Equation. *J. Phys. Chem. B* **1999**, *103* (43), 9112–9116.

(133) Kahlweit, M.; Strey, R.; Haase, D.; Firman, P. Properties of the Three-Phase Bodies in Water-Oil-Nonionic Amphiphile Mixtures. *Langmuir* **1988**, *4* (4), 785–790.

(134) Kahlweit, M.; Strey, R.; Schomaecker, R.; Haase, D. General Patterns of the Phase Behavior of Mixtures of Water, Nonpolar Solvents, Amphiphiles, and Electrolytes. 2. *Langmuir* **1989**, *5* (2), 305–315.

(135) Ontiveros, J. F. Classification Des Tensioactifs et Huiles Biocompatibles Par Mesure de La Température D'inversion de Phase (PIT) et Comparaison Des Diagrammes Des Phases, Université de Sciences et Technologies Lille: Villeneuve d'Ascq, 2014.

(136) The Council of the European Union. Council Directive 1999/13/EC of 11 March 1999 on the limitation of emissions of volatile organic compounds due to the use of organic solvents in certain activities and installations. Official Journal L 085.

(137) Millqvist, E. The Airway Sensory Hyperreactivity Syndrome. *Pulm. Pharmacol. Ther.* **2011**, *24* (3), 263–266.

(138) Ternesten-Hasséus, E.; Lowhagen, O.; Millqvist, E. Quality of Life and Capsaicin Sensitivity in Patients with Airway Symptoms Induced by Chemicals and Scents: A Longitudinal Study. *Environ. Health Perspect.* **2007**, *115* (3), 425–429.

(139) Millqvist, E.; Ternesten-Hasséus, E.; Bende, M. Inhaled Ethanol Potentiates the Cough Response to Capsaicin in Patients with Airway Sensory Hyperreactivity. *Pulm. Pharmacol. Ther.* **2008**, *21* (5), 794–797.

(140) Ophaswongse, S.; Maibach, H. I. Alcohol Dermatitis: Allergic Contact Dermatitis and Contact Urticaria Syndrome. *Contact Dermatitis* **1994**, *30* (1), 1–6.

(141) Durand, M. *Propriétés Physico-Chimiques, Fonctionnelles et Applicatives Des Ethers Courts d'Isosorbide*; PhD Thesis; Université de Lille 1, France, 2010.

(142) Lukacs, A.; Korting, H. C.; Braun-Falco, O.; Stanzl, K. Efficacy of a Deodorant and Its Components: Triethylcitrate and Perfume. *J. Cosmet. Sci.* **1991**, *42*, 159–166.

(143) Perring, K. D.; Evans, M. G. Perfume Compositions. US 8821847 B2.

(144) Kobayashi, T.; Tsuruta, H. Perfume Composition. US 4434306 A.

(145) Guenin, E.; Trotzinka, K. A. Alcohol Free Perfume. US 5468725 A.

(146) Vlad, F. J.; Mounier, R.; Jouault, A. D.; Herd, T. Solubilizing Systems for Flavors and Fragrances. US 7846889 B2.

(147) Meilgaard, M. C.; Carr, B. T.; Civille, G. V. *Sensory Evaluation Techniques, Fourth Edition*; CRC Press, 2006.

(148) Pfenninger, H. B. Methods of Quality Control in Brewing. *Schweiz. Brau.-Rundsch.* **1979**, *90*, 121.

(149) Pangborn, R. M. Individuality in Response to Stimuli. *Criteria Food Accept. Man Chooses What He Eats* **1981**, *Forster-Verlag*, 177.

(150) Schiffman, H. R. *Sensation and Perception: An Integrated Approach (3rd Ed.)*; John Wiley & Sons: Oxford, England, 1990; Vol. 21.

(151) Firestein, S. How the Olfactory System Makes Sense of Scents. *Nature* **2001**, *413* (6852), 211–218.

(152) Menini, A.; Lagostena, L.; Boccaccio, A. Olfaction: From Odorant Molecules to the Olfactory Cortex. *Physiology* **2004**, *19* (3), 101–104.

(153) Mécanisme de L'olfaction et Récepteurs. *Dossier chimique du Centre National de la Recherche Scientifique (CNRS).*

(154) Buck, L.; Axel, R. A Novel Multigene Family May Encode Odorant Receptors: A Molecular Basis for Odor Recognition. *Cell* **1991**, *65* (1), 175–187.

(155) Meierhenrich, U. J.; Golebiowski, J.; Fernandez, X.; Cabrol-Bass, D. De la molécule à l'odeur : Les bases moléculaires des premières étapes de l'olfaction. *Actual. Chim.* **2005**, No. 289, 29–40.

(156) Buck, L. B. The Molecular Architecture of Odor and Pheromone Sensing in Mammals. *Cell* **2000**, *100* (6), 611–618.

(157) Morrison, E. E.; Costanzo, R. M. Morphology of the Human Olfactory Epithelium. *J. Comp. Neurol.* **1990**, *297* (1), 1–13.

(158) Pick, H.; Etter, S.; Baud, O.; Schmauder, R.; Bordoli, L.; Schwede, T.; Vogel, H. Dual Activities of Odorants on Olfactory and Nuclear Hormone Receptors. *J. Biol. Chem.* **2009**, *284* (44), 30547–30555.

(159) Teixeira, M. A.; Rodríguez, O.; Mota, F. L.; Macedo, E. A.; Rodrigues, A. E. Evaluation of Group-Contribution Methods To Predict VLE and Odor Intensity of Fragrances. *Ind. Eng. Chem. Res.* **2011**, *50* (15), 9390–9402.

(160) Sell, C. S. On the Unpredictability of Odor. *Angew. Chem. Int. Ed.* **2006**, *45* (38), 6254–6261.

(161) Robbers, J. E.; Bhatia, V. N. Technique for the Rapid Determination of HLB and Required-HLB Values. *J. Pharm. Sci.* **1961**, *50* (8), 708–709.

(162) Orafidiya, L. O.; Oladimeji, F. A. Determination of the Required HLB Values of Some Essential Oils. *Int. J. Pharm.* **2002**, *237* (1–2), 241–249.

(163) Santos, O. D. H. dos; Miotto, J. V.; Morais, J. M. de; da Rocha-Filho, P. A.; Oliveira, W. P. de. Attainment of Emulsions with Liquid Crystal from Marigold Oil Using the Required HLB Method. *J. Dispers. Sci. Technol.* **2005**, *26* (2), 243–249.

(164) Morais, J. M. de; Santos, O. D. H. dos; Delicato, T.; Gonçalves, R. A.; da Rocha-Filho, P. A. Physicochemical Characterization of Canola Oil/Water Nano-emulsions Obtained by Determination of Required HLB Number and Emulsion Phase Inversion Methods. *J. Dispers. Sci. Technol.* **2006**, *27* (1), 109–115.

(165) Cash, L.; Cayias, J. L.; Fournier, G.; Macallister, D.; Schares, T.; Schechter, R. S.; Wade, W. H. The Application of Low Interfacial Tension Scaling Rules to Binary Hydrocarbon Mixtures. *J. Colloid Interface Sci.* **1977**, *59* (1), 39–44.

(166) Ontiveros, J. F.; Pierlot, C.; Catté, M.; Molinier, V.; Pizzino, A.; Salager, J.-L.; Aubry, J.-M. Classification of Ester Oils according to Their Equivalent Alkane Carbon Number (EACN) and Asymmetry of Fish Diagrams of $C_{10}E_4$/ester Oil/water Systems. *J. Colloid Interface Sci.* **2013**, *403*, 67–76.

(167) Queste, S. Classement Absolu Des Huilles et Des Amphiphiles Par La Methode de La Formulation Optimale, L'universuté des Sciences et technologies de Lille: Villeneuve d'Ascq, 2006.

(168) Bouton, F.; Durand, M.; Nardello-Rataj, V.; Serry, M.; Aubry, J.-M. Classification of Terpene Oils Using the Fish Diagrams and the Equivalent Alkane Carbon (EACN) Scale. *Colloids Surf. Physicochem. Eng. Asp.* **2009**, *338* (1–3), 142–147.

(169) Graciaa, A.; Lachaise, J.; Cucuphat, C.; Bourrel, M.; Salager, J. L. Interfacial Segregation of an Ethyl Oleate/hexadecane Oil Mixture in Microemulsion Systems. *Langmuir* **1993**, *9* (6), 1473–1478.

(170) Tchakalova, V.; Fieber, W. Classification of Fragrances and Fragrance Mixtures Based on Interfacial Solubilization. *J. Surfactants Deterg.* **2012**, *15* (2), 167–177.

(171) Bouton, F.; Durand, M.; Nardello-Rataj, V.; Borosy, A. P.; Quellet, C.; Aubry, J.-M. A QSPR Model for the Prediction of the "Fish-Tail" Temperature of CiE4/Water/Polar Hydrocarbon Oil Systems. *Langmuir* **2010**, *26* (11), 7962–7970.

(172) Leo, A.; Hansch, C.; Elkins, D. Partition Coefficients and Their Uses. *Chem. Rev.* **1971**, *71* (6), 525–616.

(173) Nielloud, F. *Pharmaceutical Emulsions and Suspensions: Second Edition, Revised and Expanded*; CRC Press, 2000.

(174) Miñana-Perez, M.; Graciaa, A.; Lachaise, J.; Salager, J.-L. Solubilization of Polar Oils with Extended Surfactants. *Colloids Surf. Physicochem. Eng. Asp.* **1995**, *100*, 217–224.

(175) Baran Jr., J. R.; Pope, G. A.; Wade, W. H.; Weerasooriya, V.; Yapa, A. Microemulsion Formation with Mixed Chlorinated Hydrocarbon Liquids. *J. Colloid Interface Sci.* **1994**, *168* (1), 67–72.

(176) Bourrel, M.; Schechter, R. S. *Microemulsions and Related Systems*; Marcel Dekker, 1998; Vol. Microemulsions and related systems.

(177) Salager, J.-L.; Antón, R.; Forgiarini, A.; Márquez, L. *Microemulsions: Formulation of Microemulsions*; Wiley, 2009.

(178) Chen, S. J.; Evans, D. F.; Ninham, B. W.; Mitchell, D. J.; Blum, F. D.; Pickup, S. Curvature as a Determinant of Microstructure and Microemulsions. *J. Phys. Chem.* **1986**, *90* (5), 842–847.

(179) Kunz, W.; Testard, F.; Zemb, T. Correspondence between Curvature, Packing Parameter, and Hydrophilic−Lipophilic Deviation Scales around the Phase-Inversion Temperature. *Langmuir* **2009**, *25* (1), 112–115.

(180) Appel, M.; Spehr, T. L.; Wipf, R.; Stühn, B. Water–AOT–alkylbenzene Microemulsions: Influence of Alkyl Chain Length on Structure and Percolation Behavior. *J. Colloid Interface Sci.* **2012**, *376* (1), 140–145.

(181) Fletcher, P. D. I.; Nicholls, R. J. Alkylbenzenes in Diiodomethane. A Novel, “Primitive” Micelle-Forming Surfactant System. *Langmuir* **2000**, *16* (3), 1050–1056.

(182) Kunieda, H.; Shinoda, K. Evaluation of the Hydrophile-Lipophile Balance (HLB) of Nonionic Surfactants. 1.Multisurfactant Systems. *J. Colloid Interface Sci.* **1985**, *107* (1), 107–121.

(183) Kunieda, H.; Horii, M.; Koyama, M.; Sakamoto, K. Solubilization of Polar Oils in Surfactant Self-Organized Structures. *J. Colloid Interface Sci.* **2001**, *236* (1), 78–84.

(184) Kallmayer, V.; Kröpke, R.; Lüttig, K. Kosmetische Zubereitung Mit Natriumcetearylsulfat. DE 102010063745 A1, 2012.

(185) Behrens, S.; Bleckmann, A.; Boenisch, A. Selbstbräunungsmittel Mit (2-Hydroxyethyl)harnstoff. DE 102006034532 A1, 2008.

(186) Alder, B. J.; Wainwright, T. E. Studies in Molecular Dynamics. I. General Method. *J. Chem. Phys.* **1959**, *31* (2), 459–466.

(187) Car, R.; Parrinello, M. Unified Approach for Molecular Dynamics and Density-Functional Theory. *Phys. Rev. Lett.* **1985**, *55* (22), 2471–2474.

(188) Metropolis, N.; Ulam, S. The Monte Carlo Method. *J. Am. Stat. Assoc.* **1949**, *44* (247), 335–341.

(189) Fredenslund, A.; Jones, R. L.; Prausnitz, J. M. Group-Contribution Estimation of Activity Coefficients in Nonideal Liquid Mixtures. *AIChE J.* **1975**, *21* (6), 1086–1099.

(190) Gmehling, J.; Li, J.; Schiller, M. A Modified UNIFAC Model. 2. Present Parameter Matrix and Results for Different Thermodynamic Properties. *Ind. Eng. Chem. Res.* **1993**, *32* (1), 178–193.

(191) Klamt, A.; Schüürmann, G. COSMO: A New Approach to Dielectric Screening in Solvents with Explicit Expressions for the Screening Energy and Its Gradient. *J. Chem. Soc. Perkin Trans. 2* **1993**, No. 5, 799.

(192) Klamt, A. *COSMO-RS: From Quantum Chemistry to Fluid PhaseThermodynamics and Drug Design*; Elsevier, 2005.

(193) Klamt, A. Conductor-like Screening Model for Real Solvents: A New Approach to the Quantitative Calculation of Solvation Phenomena. *J. Phys. Chem.* **1995**, *99* (7), 2224–2235.

(194) Wichmann, K.; Diedenhofen, M.; Klamt, A. Prediction of Blood-Brain Partitioning and Human Serum Albumin Binding Based on COSMO-RS σ-Moments. *J. Chem. Inf. Model.* **2007**, *47* (1), 228–233.

(195) Benazzouz, A.; Moity, L.; Pierlot, C.; Molinier, V.; Aubry, J.-M. Hansen Approach versus COSMO-RS for Predicting the Solubility of an Organic UV Filter in Cosmetic Solvents. *Colloids Surf. Physicochem. Eng. Asp.* **2014**, *458*, 101–109.

(196) Mokrushina, L.; Buggert, M.; Smirnova, I.; Arlt, W.; Schomäcker, R. COSMO-RS and UNIFAC in Prediction of Micelle/Water Partition Coefficients. *Ind. Eng. Chem. Res.* **2007**, *46* (20), 6501–6509.

(197) Mehling, T.; Ingram, T.; Smirnova, I. Experimental Methods and Prediction with COSMO-RS to Determine Partition Coefficients in Complex Surfactant Systems. *Langmuir ACS J. Surf. Colloids* **2012**, *28* (1), 118–124.

(198) Ingram, T.; Storm, S.; Kloss, L.; Mehling, T.; Jakobtorweihen, S.; Smirnova, I. Prediction of Micelle/Water and Liposome/Water Partition Coefficients Based on Molecular Dynamics Simulations, COSMO-RS, and COSMOmic. *Langmuir* **2013**, *29* (11), 3527–3537.

(199) Klamt, A.; Eckert, F.; Hornig, M. COSMO-RS: A Novel View to Physiological Solvation and Partition Questions. *J. Comput. Aided Mol. Des.* **2001**, *15* (4), 355–365.

(200) Kondor, A.; Járvás, G.; Kontos, J.; Dallos, A. Temperature Dependent Surface Tension Estimation Using COSMO-RS Sigma Moments. *Chem. Eng. Res. Des.* **2014**, *Article in Press*.

(201) Zissimos, A. M.; Abraham, M. H.; Klamt, A.; Eckert, F.; Wood, J. A Comparison between the Two General Sets of Linear Free Energy Descriptors of Abraham and Klamt. *J. Chem. Inf. Comput. Sci.* **2002**, *42* (6), 1320–1331.

(202) *IUPAC Compendium of Chemical Terminology: Gold Book*, 2.1.0 ed.; Nič, M., Jirát, J., Košata, B., Jenkins, A., McNaught, A., Eds.; IUPAC: Research Triagle Park, NC, 2009.

(203) Kubinyi, H. Variable Selection in QSAR Studies. I. An Evolutionary Algorithm. *Quant. Struct.-Act. Relatsh.* **1994**, *13* (3), 285–294.

(204) Dickey, D. A.; Fuller, W. A. Distribution of the Estimators for Autoregressive Time Series with a Unit Root. *J. Am. Stat. Assoc.* **1979**, *74* (366a), 427–431.

(205) Wormuth, K. R.; Kaler, E. W. Microemulsifying Polar Oils. *J. Phys. Chem.* **1989**, *93* (12), 4855–4861.

(206) Buggert, M.; Cadena, C.; Mokrushina, L.; Smirnova, I.; Maginn, E. J.; Arlt, W. COSMO-RS Calculations of Partition Coefficients: Different Tools for Conformation Search. *Chem. Eng. Technol.* **2009**, *32* (6), 977–986.

(207) Kahlweit, M.; Strey, R. Phasenverhalten Ternärer Systeme Des Typs H2O–Öl–nichtionisches Amphiphil (Mikroemulsionen). *Angew. Chem.* **1985**, *97* (8), 655–669.

(208) Pybus, D.; Sell, C. *The Chemistry of Fragrances*; Royal Society of Chemistry, 1999.

(209) Moyler, D. A. Extraction of Essential Oils with Carbon Dioxide. *Flavour Fragr. J.* **1993**, *8* (5), 235–247.

(210) Reverchon, E. Supercritical Fluid Extraction and Fractionation of Essential Oils and Related Products. *J. Supercrit. Fluids* **1997**, *10* (1), 1–37.

(211) Reverchon, E.; Porta, G. D.; Senatore, F. Supercritical CO2 Extraction and Fractionation of Lavender Essential Oil and Waxes. *J. Agric. Food Chem.* **1995**, *43* (6), 1654–1658.

(212) Marcus, J.; Klossek, M. L.; Touraud, D.; Kunz, W. Nano-Droplet Formation in Fragrance Tinctures. *Flavour Fragr. J.* **2013**, *28* (5), 294–299.

(213) Numanoğlu, U.; Şen, T.; Tarimci, N.; Kartal, M.; Koo, O. M. Y.; Önyüksel, H. Use of Cyclodextrins as a Cosmetic Delivery System for Fragrance Materials: Linalool and Benzyl Acetate. *AAPS PharmSciTech* **2007**, *8* (4), 34–42.

(214) Wang, C. X.; Chen, S. L. Fragrance-Release Property of β-Cyclodextrin Inclusion Compounds and Their Application in Aromatherapy. *J. Ind. Text.* **2005**, *34* (3), 157–166.

(215) Uyar, T.; Hacaloglu, J.; Besenbacher, F. Electrospun Polystyrene Fibers Containing High Temperature Stable Volatile Fragrance/flavor Facilitated by Cyclodextrin Inclusion Complexes. *React. Funct. Polym.* **2009**, *69* (3), 145–150.

(216) Sansukcharearnpon, A.; Wanichwecharungruang, S.; Leepipatpaiboon, N.; Kerdcharoen, T.; Arayachukeat, S. High Loading Fragrance Encapsulation Based on a Polymer-Blend: Preparation and Release Behavior. *Int. J. Pharm.* **2010**, *391* (1–2), 267–273.

(217) Ternat, C.; Kreutzer, G.; Plummer, C. J. G.; Nguyen, T. Q.; Herrmann, A.; Ouali, L.; Sommer, H.; Fieber, W.; Velazco, M. I.; Klok, H.-A.; et al. Amphiphilic Multi-Arm Star-Block Copolymers for Encapsulation of Fragrance Molecules. *Macromol. Chem. Phys.* **2007**, *208* (2), 131–145.

(218) Theisinger, S.; Schoeller, K.; Osborn, B.; Sarkar, M.; Landfester, K. Encapsulation of a Fragrance via Miniemulsion Polymerization for Temperature-Controlled Release. *Macromol. Chem. Phys.* **2009**, *210* (6), 411–420.

(219) Schobel, A. Encapsulated Fragrances and Flavors and Process Therefor. US 4568560 A, 1986.

(220) Friberg, S. E. Fragrance Compounds and Amphiphilic Association Structures. *Adv. Colloid Interface Sci.* **1998**, *75* (3), 181–214.

(221) Vona Jr., S. A.; Friberg, S. E.; Brin, A.-J. Location of Fragrance Molecules within Lamellar Liquid Crystals. *Colloids Surf. Physicochem. Eng. Asp.* **1998**, *137* (1–3), 79–89.

(222) Kayali, I.; Khan, A.; Lindman, B. Solubilization and Location of Phenethylalcohol, Benzaldehyde, and Limonene in Lamellar Liquid Crystal Formed with Block Copolymer and Water. *J. Colloid Interface Sci.* **2006**, *297* (2), 792–796.

(223) Fraser, S.; Warr, J.; Regniez, C. Fragrance Microemulsion Compositions. EP2340804 A1, July 6, 2011.

(224) Skrzecz, A.; Shaw, D. G.; Maczynski, A.; Skrzecz, A. IUPAC-NIST Solubility Data Series 69. Ternary Alcohol–Hydrocarbon–Water Systems. *J. Phys. Chem. Ref. Data* **1999**, *28* (4), 983–1235.

(225) Durand, M.; Stoppa, A.; Molinier, V.; Touraud, D.; Aubry, J.-M. Toward the Rationalization of Facilitated Hydrotropy: Investigation with the Ternary Dimethyl Isosorbide / Benzyl Alcohol / Water System. *J. Solut. Chem.* **2012**, *41* (3), 555–565.

(226) Kahlweit, M.; Strey, R.; Firman, P. Search for Tricritical Points in Ternary Systems: Water-Oil-Nonionic Amphiphile. *J. Phys. Chem.* **1986**, *90* (4), 671–677.

(227) Kahlweit, M.; Lessner, E.; Strey, R. Über Das Phasenverhalten Ternärer Systeme Des Typs H2O-Öl-Nichtionisches Tensid. *Colloid Polym. Sci.* **1983**, *261* (11), 954–964.

(228) Lyklema, J. *Fundamentals of Interface and Colloid Science: Soft Colloids*; Academic Press, 2005.

(229) Kahlweit, M.; Faulhaber, B.; Busse, G. Microemulsions with Mixtures of Nonionic and Ionic Amphiphiles. *Langmuir* **1994**, *10* (8), 2528–2532.

(230) Kahlweit, M.; Strey, R.; Firman, P.; Haase, D. Phase Behavior of Ternary Systems: Water-Oil-Nonionic Surfactant as a near-Tricritical Phenomenon. *Langmuir* **1985**, *1* (3), 281–288.

(231) Kunz, W.; Nostro, P. Lo; Ninham, B. W. The Present State of Affairs with Hofmeister Effects. *Curr. Opin. Colloid Interface Sci.* **2004**, *9* (1–2), 1–18.

(232) Schott, H.; Royce, A. E. Effect of Inorganic Additives on Solutions of Nonionic Surfactants VI: Further Cloud Point Relations. *J. Pharm. Sci.* **1984**, *73* (6), 793–799.

(233) Schott, H.; Royce, A. E.; Han, S. K. Effect of Inorganic Additives on Solutions of Nonionic Surfactants: VII. Cloud Point Shift Values of Individual Ions. *J. Colloid Interface Sci.* **1984**, *98* (1), 196–201.

(234) Kunieda, H.; Ozawa, K.; Huang, K.-L. Effect of Oil on the Surfactant Molecular Curvatures in Liquid Crystals. *J. Phys. Chem. B* **1998**, *102* (5), 831–838.

(235) Hill, K.; Rhode, O. Sugar-Based Surfactants for Consumer Products and Technical Applications. *Lipid Fett* **1999**, *101* (1), 25–33.

(236) Sottmann, T.; Kluge, K.; Strey, R.; Reimer, J.; Söderman, O. General Patterns of the Phase Behavior of Mixtures of H_2O, Alkanes, Alkyl Glucosides, and Cosurfactants. *Langmuir* **2002**, *18* (8), 3058–3067.

(237) Unilever. Aqueous Parfume Oil Microemulsions. EP0571677 A1, December 1, 1993.

(238) De Salvo Souza, L.; Corti, M.; Cantú, L.; Degiorgio, V. Observation of a Vanishing Miscibility Loop in the Phase Diagram of Solutions of a Mixed Non-Ionic-Ionic Amphiphile. *Chem. Phys. Lett.* **1986**, *131*, 160–164.

(239) Kuriyama, K. Temperature Dependence of Micellar Weight of Non-Ionic Surfactant in the Presence of Various Additives. *Kolloid-Z. Z. Für Polym.* **1962**, *180* (1), 55–64.

(240) Maclay, W. N. Factors Affecting the Solubility of Nonionic Emulsifiers. *J. Colloid Sci.* **1956**, *11* (3), 272–285.

(241) Graciaa, A.; Andérez, J.; Bracho, C.; Lachaise, J.; Salager, J.-L.; Tolosa, L.; Ysambertt, F. The Selective Partitioning of the Oligomers of Polyethoxylated Surfactant Mixtures between Interface and Oil and Water Bulk Phases. *Adv. Colloid Interface Sci.* **2006**, *123-126*, 63–73.

(242) Kunieda, H.; Shigeta, K.; Ozawa, K.; Suzuki, M. Self-Organizing Structures in Poly (oxyethylene) Oleyl Ether-Water System. *J. Phys. Chem. B* **1997**, *101* (40), 7952–7957.

(243) Garti, N.; Yaghmur, A.; Leser, M. E.; Clement, V.; Watzke, H. J. Improved Oil Solubilization in Oil/Water Food Grade Microemulsions in the Presence of Polyols and Ethanol. *J. Agric. Food Chem.* **2001**, *49* (5), 2552–2562.

(244) Stubenrauch, C.; Paeplow, B.; Findenegg, G. H. Microemulsions Supported by Octyl Monoglucoside and Geraniol. 1. The Role of the Alcohol in the Interfacial Layer. *Langmuir* **1997**, *13* (14), 3652–3658.

(245) Stubenrauch, C.; Findenegg, G. H. Microemulsions Supported by Octyl Monoglucoside and Geraniol. 2. An NMR Self-Diffusion Study of the Microstructure. *Langmuir* **1998**, *14* (21), 6005–6012.

(246) Tchakalova, V.; Testard, F.; Wong, K.; Parker, A.; Benczédi, D.; Zemb, T. Solubilization and Interfacial Curvature in Microemulsions: I. Interfacial Expansion and Co-Extraction of Oil. *Colloids Surf. Physicochem. Eng. Asp.* **2008**, *331* (1–2), 31–39.

Appendix 1

Table 23 Summary of all relevant σ-moments M_i^X for the hydrocarbon oils used in the multilinear regression analysis.

Compound	M_0^X	M_2^X	M_3^X	M_4^X	M_5^X	M_6^X	M_{acc}^X	M_{don}^X
Octacosane	595.55	25.79	2.30	2.51	0.46	0.32	0.00	0.00
Tetracosane	516.26	22.54	1.96	2.19	0.39	0.27	0.00	0.00
Eicosane	436.48	19.27	1.62	1.87	0.32	0.23	0.00	0.00
Octadecane	396.57	17.64	1.45	1.71	0.29	0.21	0.00	0.00
Hexadecane	356.86	16.00	1.27	1.55	0.25	0.19	0.00	0.00
Tetradecane	316.59	14.42	1.12	1.40	0.22	0.17	0.00	0.00
Dodecane	276.64	12.80	0.95	1.24	0.18	0.15	0.00	0.00
Decane	236.78	11.14	0.78	1.08	0.15	0.13	0.00	0.00
Nonane	216.79	10.36	0.69	1.00	0.13	0.12	0.00	0.00
Octane	196.84	9.50	0.59	0.91	0.11	0.11	0.00	0.00
Heptane	176.89	8.67	0.47	0.83	0.09	0.10	0.00	0.00
Hexane	156.90	7.92	0.43	0.76	0.08	0.09	0.00	0.00
Squalane	587.44	28.94	1.67	2.79	0.30	0.33	0.00	0.00
Dodecylcyclohexane	367.61	15.50	1.08	1.39	0.21	0.16	0.00	0.00
Decylcyclohexane	327.82	13.95	0.95	1.26	0.18	0.15	0.00	0.00
Butylcyclohexane	207.97	9.18	0.53	0.81	0.10	0.09	0.00	0.00
Propylcyclohexane	186.65	8.34	0.45	0.72	0.08	0.08	0.00	0.00
Cyclodecane	191.14	8.83	0.37	0.83	0.06	0.10	0.00	0.00
cis-Decalin	180.73	7.64	0.54	0.65	0.10	0.07	0.00	0.00
Isopropylcyclohexane	183.19	8.65	0.37	0.78	0.06	0.09	0.00	0.00
1,4-Dimethylcyclohexane	168.79	8.04	0.49	0.76	0.09	0.09	0.00	0.00
Ethylcyclohexane	168.08	7.65	0.39	0.67	0.07	0.07	0.00	0.00
Cyclooctane	162.27	7.14	0.44	0.62	0.09	0.07	0.00	0.00
1,2-Dimethylcyclohexane	163.93	7.97	0.43	0.73	0.08	0.08	0.00	0.00
Methylcyclohexane	148.89	7.11	0.41	0.64	0.08	0.07	0.00	0.00
Cyclohexane	131.49	5.70	0.35	0.48	0.06	0.05	0.00	0.00
1-Chlorohexadecane	375.07	35.19	4.74	11.54	3.04	5.67	0.01	0.00
1-Chlorotetradecane	336.98	33.19	5.04	11.02	3.20	5.41	0.00	0.00
1-Chlorododecane	295.24	31.95	4.45	11.23	3.01	5.61	0.01	0.00
1-Chlorodecane	252.91	30.08	4.51	10.86	3.07	5.48	0.01	0.00
1-Bromo-3-methylpropan	136.50	26.17	3.08	10.49	2.30	5.30	0.01	0.00
Squalene	542.30	70.95	18.97	27.91	17.97	18.78	0.57	0.00
1-Octadecene	391.54	27.99	5.35	7.61	3.98	4.13	0.08	0.00
1-Dodecene	272.29	23.10	4.81	7.11	3.85	4.05	0.08	0.00
1-Decene	232.04	21.54	4.70	6.99	3.85	4.06	0.08	0.00
1-Octene	192.22	19.99	4.62	6.98	4.00	4.26	0.10	0.00
cis-Cyclooctene	158.70	15.24	4.54	5.85	4.26	4.36	0.17	0.00
1-Methyl-1-cyclohexene	148.75	15.24	4.75	5.89	4.28	4.18	0.14	0.00
4-Methyl-1-cyclohexene	148.35	16.76	5.41	7.02	5.09	5.15	0.18	0.00
3-Methyl-1-cyclohexene	148.04	16.54	5.36	6.89	5.04	5.10	0.19	0.00
Cyclohexene	129.65	15.91	5.70	7.30	5.57	5.68	0.22	0.00
1-Tetradecyne	308.41	39.76	2.03	23.15	-2.94	22.06	0.17	0.81

1-Dodecyne	268.31	38.70	2.22	23.55	-2.53	22.64	0.21	0.82
1-Decyne	228.52	37.05	2.08	23.31	-2.52	22.50	0.21	0.82
1-Octyne	188.67	35.41	1.66	23.17	-3.00	22.57	0.18	0.84
Dodecylbenzene	357.91	36.21	3.12	9.77	1.58	3.60	0.00	0.00
Decylbenzene	317.88	34.65	2.94	9.72	1.56	3.67	0.00	0.00
Octylbenzene	278.05	33.05	2.76	9.54	1.52	3.63	0.00	0.00
Butylbenzene	198.60	29.91	2.44	9.23	1.46	3.58	0.00	0.00
p-Xylene	160.45	27.44	2.73	8.74	2.01	3.46	0.00	0.00
Phenyl-1-butyne	192.75	40.76	0.30	14.85	0.66	6.72	0.00	0.00
Longifolene	234.48	18.96	3.21	4.63	2.32	2.26	0.03	0.00
p-Menthane	197.61	10.05	0.44	0.95	0.07	0.11	0.00	0.00
Caryiophyllene	250.11	28.28	7.90	10.83	7.51	7.76	0.29	0.00
Pinane	185.99	10.57	0.29	1.08	0.04	0.13	0.00	0.00
α-Pinene	182.79	17.39	2.82	4.99	2.60	2.90	0.09	0.00
p-Menth-2-ene	199.01	19.12	5.21	6.95	4.78	4.89	0.18	0.00
Δ-3-Carene	187.24	19.03	3.95	5.57	3.06	2.97	0.06	0.00
β-Pinene	182.98	19.97	4.86	7.16	4.62	4.82	0.15	0.00
Limonene	193.07	25.77	7.45	10.31	6.70	6.74	0.18	0.00
γ-Terpinene	197.46	25.18	6.98	9.40	6.02	5.87	0.14	0.00
α-Terpinene	193.84	25.23	7.98	10.93	7.84	8.00	0.27	0.00
Terpinolene	195.95	25.77	7.10	10.38	6.73	6.97	0.20	0.00
p-Cymene	194.19	28.89	3.23	8.71	2.20	3.41	0.00	0.00
Ethyl decanoate	288.26	54.68	36.37	58.68	70.34	98.52	5.08	0.00
Ethyl dodecanoate	331.27	57.38	36.63	59.19	70.07	97.82	5.08	0.00
Decyl butyrate	331.75	56.26	36.74	57.58	68.50	94.51	4.96	0.00
Ethyl myristate	371.25	58.79	36.72	59.15	69.91	97.51	5.05	0.00
Hexyl octanoate	329.18	53.72	35.04	54.35	64.30	88.21	4.69	0.00
Myristyl propanoate	381.07	56.61	36.38	58.45	71.11	100.33	5.10	0.00
Ethyl palmitate	411.62	61.29	37.35	60.05	70.88	99.07	5.10	0.00
Butyl dodecanoate	363.60	56.33	36.88	58.43	71.07	99.74	5.09	0.00
Isopropyl myristate	388.70	57.60	36.60	57.44	68.92	95.41	4.95	0.00
Ethyl oleate	446.53	70.52	40.79	63.96	73.05	100.37	5.08	0.00
Octyloctanoate	361.81	60.02	39.36	64.98	78.81	113.62	5.63	0.01
Hexyl dodecanoate	401.58	57.13	36.72	58.48	71.23	100.28	5.12	0.00
Dibutylether	205.62	27.55	23.70	39.69	62.75	105.57	3.23	0.00
Dipentyl ther	246.43	29.41	24.48	41.70	67.54	116.95	3.28	0.00
Dihexylether	284.98	31.48	25.69	43.30	69.38	118.65	3.46	0.00
Diheptylether	321.24	31.76	23.66	39.46	62.23	105.73	3.15	0.00
Dioctylether	360.64	33.28	23.49	37.90	56.95	91.48	3.17	0.00
2-Octanone	200.61	48.51	35.86	62.50	80.45	121.03	5.43	0.00
2-Decanone	240.24	50.53	36.54	63.80	82.36	124.65	5.52	0.00
2-Undecanone	258.36	51.30	37.60	64.67	84.01	126.58	5.63	0.00
2-Dodecanone	278.59	52.12	37.30	64.24	83.14	125.39	5.54	0.00
Octanenitril	202.07	49.04	23.97	47.63	44.82	68.40	3.41	0.05
Decanenitrile	241.70	51.06	24.14	48.19	44.97	69.05	3.42	0.06
Dodecanenitril	281.66	52.30	24.25	47.93	44.81	68.39	3.41	0.05
Rose oxide	213.60	41.45	33.29	56.69	84.71	138.70	4.42	0.00

Geranyl acetate	267.57	69.36	36.24	64.49	67.75	96.37	4.82	0.00
Linalyl acetate	253.50	62.47	32.19	57.90	62.07	89.04	4.36	0.00
Citronellyl acetate	263.14	62.34	38.58	65.31	76.02	108.55	5.38	0.00
Menthyl acetate	245.54	55.32	39.43	66.56	81.98	119.92	5.78	0.00
Eucalyptol	191.56	35.87	35.70	63.96	105.63	183.05	5.01	0.00
D-Carvone	198.48	62.29	49.84	86.72	120.25	187.83	7.32	0.00
Damascone	237.74	54.81	36.88	65.67	84.32	128.43	5.59	0.01
β-Ionone	242.89	61.46	47.87	85.21	117.19	183.18	7.41	0.00
ω-Hexadecenlactone	283.05	55.80	37.37	59.03	70.86	98.84	5.01	0.00
Menthone	202.80	43.60	34.73	55.26	73.70	107.74	4.95	0.00
Methyl cedryl ether	258.07	33.17	24.92	44.72	70.34	119.51	3.55	0.00
Methyl dihydrojasmonate	224.89	56.51	47.30	83.23	117.02	183.41	7.28	0.00
Ethylene brassylate	297.17	88.09	52.51	95.72	100.62	145.33	7.78	0.01
Dipropoxybutane	256.83	48.24	47.47	79.20	124.51	205.96	6.61	0.00
Dibutoxyethane	262.29	53.29	48.60	76.42	109.47	165.66	6.88	0.00
Dipropoxyethane	216.46	43.75	38.01	61.63	89.27	138.25	5.36	0.00
Hexylmethacrylate	241.99	49.62	30.10	51.05	58.55	82.29	4.44	0.00

Appendix 2

Table 24 Composition of the essential oils *pinus sylvestris* and *pinus pinaster*, as well as of the fragrance mixture.

Compounds	Chemical structures	*Pinus sylvestris*	*Pinus pinaster*	Fragrance mixture	EACN
		Terpenes			
α-Pinene	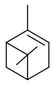	39.0	1.1	1.4	3.4
β-Pinene	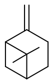	20.2	-	1.5	2.2
α-Phellandrene	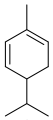	-	0.6	-	-
Limonene	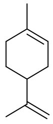	-	15.5	1.7	2.0
β-Terpinene	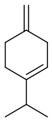	-	0.6	-	-
γ-Terpinene	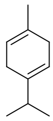	-	4.2	-	1.8
Terpinolene	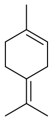	0.4	28.3	-	1.0
Camphene	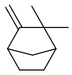	1.6	1.9	0.4	-
3-Carene	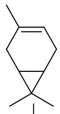	17.0	-	-	2.5
Camphor	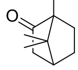	-	-	7.7	-
Cineole	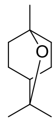	-	19.4	21.3	-1.6
β-Myrcene	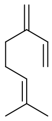	2.3	-	-	-
Ocimene	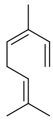	-	-	2.7	-
β-Caryophyllene	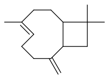	2.3	-	-	5.6
α-Caryophyllene	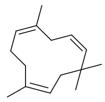	0.5	-	-	-

Longifolene	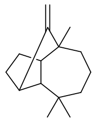	1.1	-	-	6.5
Terpene alcohols					
Fenchol	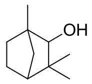	-	0.4	-	-
1-Terpineol	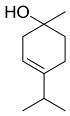	-	1.1	-	-
β-Terpineol	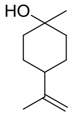	-	1.7	-	-
α-Terpineol	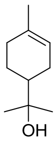	-	0.4	-	-
Linalool	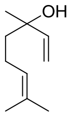	-	-	36.7	-11.4
Terpene acetates					
Bornyl acetate	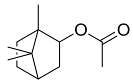	2.3	-	-	-
β-Terpenyl acetate	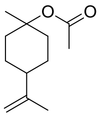	11.1	-	-	-
Linalyl acetate	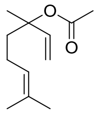	-	-	7.4	-0.8
Aromatic compounds					
o-Cymene	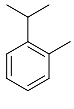	1.3	1.1	-	-
m-Cymene	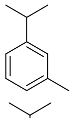	1.0	23.4	-	-
p-Cymene	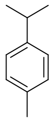	-	-	-	-0.4
p-α-Dimethyl styrene	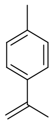	-	0.4	-	-
Solvent					
Dipropylene glycol	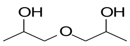	-	-	19.2	-

Appendix 3

Rationalization and Prediction of the Equivalent Alkane Carbon Number (EACN) of Polar Hydrocarbon Oils with COSMO-RS σ-Moments

Langmuir
Article
pubs.acs.org/Langmuir

Rationalization and Prediction of the Equivalent Alkane Carbon Number (EACN) of Polar Hydrocarbon Oils with COSMO-RS σ-Moments

Thomas Lukowicz, Adrien Benazzouz, Véronique Nardello-Rataj, and Jean-Marie Aubry*

[†]Unité de Catalyse et de Chimie du Solide, CNRS UMR 8181, Université Lille 1 and ENSCL, Equipe CÏSCO, Cité Scientifique F-59655 Villeneuve d'Ascq, France

Supporting Information

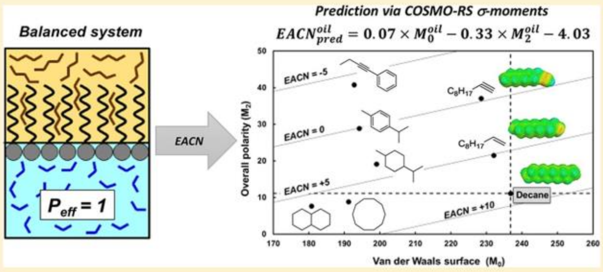

ABSTRACT: The equivalent alkane carbon numbers (EACNs) of 20 polar hydrocarbon oils are determined by the fishtail method. These values supplemented by 43 already reported EACNs of other hydrocarbons are rationalized by using the COSMO-RS σ-moments as descriptors for a QSPR analysis. A reliable model, with only two meaningful physicochemical parameters, namely the surface area (M_0^X) and the overall polarity (M_2^X) of the oil X, is able to predict the EACN values of a large variety of oils including (cyclo)alkanes, (cyclo)alkenes, terpenes, aromatics, alkynes, and chloroalkanes and to rationalize structural effects on EACNs. Furthermore, the dependence of the EACN of homologous oils on the chain length provides some molecular insight into how the different oils penetrate into the interfacial film of surfactants.

■ INTRODUCTION

The phase behavior of a surfactant/oil/water (SOW) system is driven by the relative proportion of each constituent, the temperature, and the nature of surfactant and oil as well as the presence of additives.[1−4] While HLB and packing parameter P express the hydrophilic/lipophilic balance of the surfactant, the hydrophobicity of the oil can be described by its equivalent alkane carbon number (EACN),[5] a dimensionless number which reflects the ability of oil molecules to penetrate the interfacial film and modify its spontaneous curvature.[6−10] By definition, the EACN value of an oil is equal to the number of carbons of the *n*-alkane exhibiting the same fishtail temperature T^*. EACN is an effective conceptual tool to predict whether a given oil may lead to Winsor-type I, II, and III microemulsions in a SOW system at equilibrium.[11,12] Many reliable EACN values have been determined by the so-called fishtail method[13] for various types of oils such as triglycerides[14] and other esters,[15] aliphatic and aromatic hydrocarbons,[13] and terpenes.[16] However, the experimental determination of EACNs may be lengthy and requires a significant amount of costly monodisperse C_iE_j surfactants. Nevertheless, when EACNs are measured for a large set of compounds within a given chemical family, a chemometric treatment of the data can provide an empirical model able to predict the EACN of any unknown oil belonging to the same family. For instance, Bouton et al. have established an effective QSPR model to predict the EACN of terpenes with the modeling software Molecular Operating Environment (MOE).[17,18] It can calculate hundreds of descriptors for a molecule, including physical properties, topological indices, or structural keys. Among this huge amount of descriptors, two were selected, namely "Kier A3" and "average negative softness". They were able to predict the EACN of polar hydrocarbon oils. But they have no clear and simple structural or physicochemical meaning. In order to get some deeper insight into the molecular factors influencing the EACN of oils and to get a sounded and predictive model, we used herein the COSMO-RS model as an alternative approach to rationalize the EACN values of a large set of hydrocarbon oils including (cyclo)alkanes, (cyclo)alkenes, terpenes, aromatics, 1-alkynes, and 1-chloroalkanes. COSMO-RS is an effective method for the prediction of physicochemical properties of liquid systems that combine exact statistical

Received: July 10, 2015
Revised: September 3, 2015

DOI: 10.1021/acs.langmuir.5b02545
Langmuir XXXX, XXX, XXX−XXX

thermodynamics with quantum chemistry. Unlike the hundreds of cryptic descriptors used in conventional QSPR analysis, the COSMO-RS method generates only nine clearly defined descriptors and provides in-depth interpretation of molecular parameters influencing EACNs.

■ EXPERIMENTAL SECTION

Materials. Tetraethylene glycol monoalkyl ethers (C_6E_j, j = 6, 10) were synthesized according to a known procedure.[13] Purity was ≥99%, verified by GC-FID. 1-Octadecene (≥95%), 1-dodecene (99%), 1-decene (97%), 1-octene (98%), cyclooctane (≥99%), cyclodecane (95%), 1-tetradecyne (≥97%), *cis*-cyclooctene (95%), 1-chlorohexadecane (95%), 1-chlorotetradecane (98%), 1-chlorododecane (≥97%), 1-chlorodecane (98%), 1-bromo-3-methylpropane (99%), and butylbenzene (≥99%) were obtained from Sigma-Aldrich. 1-Phenylbutyne (98%), *p*-xylene (99%), 1-octyne (98%), 1-decyne (98%), and 1-dodecyne (97%) were obtained from Alfa Aesar, whereas *cis*-decalin (≥98%) was purchased from TCI. All compounds were used as received. Millipore water was used.

Sample Preparation for the Determination of the "Fishtail" Temperature T^*. The "fishtail" temperature T^* was determined by investigating the phase behavior of the C_iE_4/oil/water (i = 6, 10) systems at a constant water-to-oil ratio (WOR = 1, w/w) as a function of temperature (ordinate) and surfactant mass fraction $\gamma = m_{\mathrm{surf}}/m_{\mathrm{total}}$ (abscissa). T^* was determined by observing the alterations of the phase behavior with decreasing temperature at different mass fractions of surfactant. Thereby water, oil, and surfactant were introduced in a thin glass tube (ϕ = 0.8 mm) and closed with a screw cap. The samples were gently shaken and placed into a thermostatic water bath. Temperature was altered in 0.1 °C steps, and the equilibration time was from 30 min to 2 days depending on the surfactant and the attainment of the equilibrium. Tubes were weighed from time to time to verify that no mass loss occurred. Oils with a high T^* (>50 °C) were added to tubes which were sealed by flame after freezing in liquid nitrogen to avoid any mass loss.

COSMO-RS Calculations. The modeling program ArgusLab (v. 4.0.1, Planaria Software LLC, Seattle, WA) was used to draw the molecules. Conformations of a molecule greatly impact the quality of the prediction of physicochemical properties. In order to depict such effects, conformational analysis has been carried out using the COSMOconf script.[19] It involves semiempirical AM1 (program: MOPAC 7, locally modified by COSMOlogic) calculations followed by a more accurate density functional (DFT) treatment of the most important AM1 conformers. Molecular geometries were then optimized by DFT/COSMO calculations, carried out with the quantum chemical program TURBOMOLE (TURBOMOLE GmbH, Karlsruhe, Germany) using a triple-ζ valence polarization basis set and the B88-PW86 exchange-correlation functionals. Eventually COSMOtherm (C30_1301 version, COSMOlogic, Leverkusen, Germany) was used for the generation of the σ-profiles and σ-moments.

■ RESULTS AND DISCUSSION

Determination of "Fishtail" Temperatures T^*. Hydrophobicity of oils can be estimated through the determination of the "optimal formulation" of SOW systems.[11,20] It corresponds to the particular state where the surfactant has the same affinity for the water and oil phase, with a zero spontaneous curvature of the interfacial film and a minimum value for the O/W interfacial tension.[21] Any changes in the system such as temperature, type of surfactant, and oil then lead to a departure from this reference state. Queste et al. used the so-called "fish diagrams" of C_iE_j/oil/water systems to determine the hydrophobicity of oils.[13] The boundaries of Winsor III and Winsor IV regions shape a fish and intersect at the characteristic point defined by the optimal temperature T^* and the critical mass fraction γ^* (Figure 1).

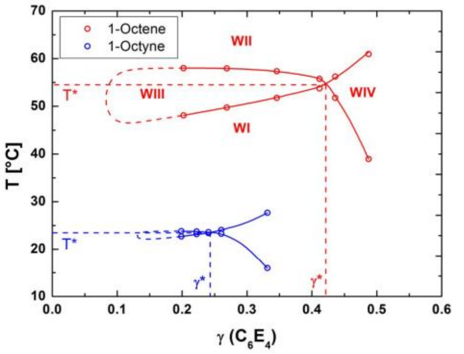

Figure 1. "Fish cuts" of C_6E_4/1-octene/water and C_6E_4/1-octyne/water systems obtained by fixing the water-to-oil weight ratio at 1. The "fishtail" is the characteristic point at T^* and γ^* where the one-phase (Winsor IV), the two-phase (Winsor I and II), and the three-phase (Winsor III) regions meet.

The value of T^* is characteristic of a given oil but depends on the chemical structure of the surfactant C_iE_j.[17] T^* is lower for the weakly hydrophilic $C_{10}E_4$ and higher for the strongly hydrophilic C_6E_4. $C_{10}E_4$ is suitable to investigate very hydrophobic oils such as *n*-octacosane (*n*-$C_{28}H_{58}$) while C_6E_4 is appropriate to more polar oils such as cyclohexene.[17] Experimental values of T^* and γ^* determined in this work for a series of 20 newly investigated oils are summarized in Table 1.

Influence of the Length of Homologous Oils on T^* and EACN. Figure 2 shows the evolution of T^* of different families of hydrocarbons according to the number of carbon atoms (N_C) in the oils. Thereby the newly determined T^* values were completed by existing values from literature, resulting in a total number of 62 oils.[13,17] As already known, there is a linear relationship between T^* and N_C for the series of *n*-alkanes. Interestingly, the evolutions of T^* for 1-alkenes, 1-alkynes, and 1-chloroalkanes are parallel to the straight line of *n*-alkanes. On the other hand, the fishtail temperatures T^* of *n*-alkylcyclohexanes approximates those of *n*-alkanes for increasing N_C; i.e., long *n*-alkylcyclohexanes ($N_C \gtrsim 20$) have approximately the same influence on the phase behavior as *n*-alkanes with the same number of carbons.

n-Alkanes are used as reference oils to calibrate the EACN scale by extrapolating the straight line to lower temperatures (dashed lines in Figure 2). The equations to calculate the experimental EACN are obtained from the literature.[17] It is generally a noninteger number and may even be negative for very polar oils (see Table 1). As the EACN values express the intrinsic hydrophobicity of oils, it does not depend on the structure of the surfactant as checked by Bouton et al. for 34 slightly polar oils. However, we study here more polar oils such as 1-alkyne, so we verified that the EACN of 1-octyne measured with a surfactant having a longer chain, such as $C_{12}E_6$ (T^* = 16.2 °C → $\mathrm{EACN_{exp}}$= −2.6), was actually close to the value determined with C_6E_4 (T^* = 23.3 °C → $\mathrm{EACN_{exp}}$= −1.8). Bouton et al. found deviations up to 1 between EACN values of a given oil measured with different amphiphiles. The averaged error of all these oils is ±0.4 EACN units, within an EACN range of 0−10. Since most EACN values are obtained by extrapolation of the *n*-alkane calibration curve, the deviation may occur due to errors in the slope of the latter. Especially

DOI: 10.1021/acs.langmuir.5b02545
Langmuir XXXX, XXX, XXX−XXX

Table 1. Fishtail Temperature T^*, Minimum Surfactant Mass Fraction γ^*, Experimental and Predicted EACN, and σ-Moments M_0^{oil} and M_2^{oil} of 20 Polar Hydrocarbon Oils[a]

hydrocarbon oil	$T^* \pm 0.8$ [°C] C_6E_4	$T^* \pm 0.8$ [°C] $C_{10}E_4$	$\gamma^* \pm 0.01$	$EACN_{exp}$	$EACN_{pred}$	M_0^{oil} [Å^2]	M_2^{oil} [e^2/Å^2]
1-octene	54.6		0.42	3.9	2.8	192.2	20.0
1-decene	63.2		0.44	5.5	5.1	232.0	21.5
1-dodecene	77.7		0.55	8.1	7.4	272.3	23.1
1-octadecene[b]		42.4	0.37	14.2	14.1	391.5	28.0
1-octyne	23.3		0.24	−1.8	−2.5	188.7	35.4
1-decyne	33.8		0.25	0.1	−0.2	228.5	37.0
1-dodecyne	44.0		0.30	2.0	2.0	268.3	38.7
1-tetradecyne	54.3		0.34	3.5	4.5	308.4	39.8
cis-cyclooctene[b]	41.6		0.26	1.6	2.0	158.7	15.2
cyclooctane	55.5		0.34	4.1	5.0	162.3	7.1
cyclodecane	63.0		0.38	5.5	6.4	191.1	8.8
cis-decalin[b]	62.3		0.40	5.3	6.1	180.7	7.6
butylbenzene	35.2		0.27	0.4	0.0	198.6	29.9
p-xylene[b]	20.2		0.24	−2.3	−1.8	160.4	27.4
phenyl-1-butyne[b]	15.1		0.28	−3.3	−4.0	192.7	40.8
1-chlorodecane		12.5	0.10	3.5	3.8	252.9	30.1
1-chlorododecane		18.5	0.14	5.6	6.1	295.2	31.9
1-chlorotetradecane		25.0	0.17	8.0	8.6	337.0	33.2
1-chlorohexadecane		30.0	0.23	9.8	10.6	375.1	35.2
1-bromo-3-methylpropane[b]	14.8		0.23	−3.3	−3.1	136.5	26.2

[a] The averaged error for the determination of T^* is ±0.8 °C, and for γ^* it is ±0.01. [b] Compounds used in the validation set.

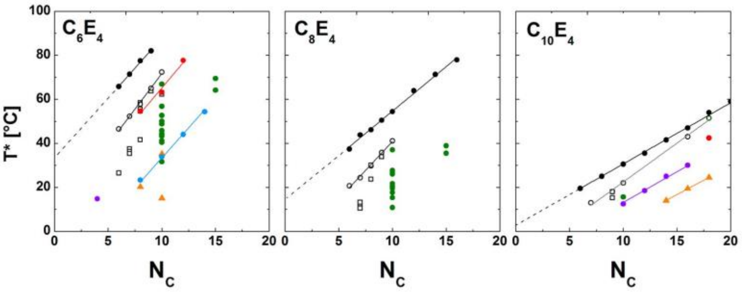

Figure 2. Evolution of the fishtail temperature T^* against the number of carbon atoms N_{carbon} for various families of oils: *n*-alkanes (black ●), *n*-alkylcyclohexanes (○), cycloalkanes (□), 1-alkenes (red ●), 1-alkynes (blue ●), terpenes (green ●), aromatics (yellow ▲), chloro- and bromoalkanes (purple ●). The dots corresponding to homologous series of oils are connected by straight lines to show the trends when N_C increases.

very polar oils are influenced by this source of error because their T^* value is much lower than of those in the range of *n*-alkanes. Furthermore, polar impurities contained in the oil, in particular those arising from air autoxidation, may alter T^*. Short-chain amphiphiles equilibrate rapidly, and thus the fishtail can be traced within few days. However, long-chain amphiphiles need more time for equilibration. In that case argon-saturated water shall be used, and the gaseous space in the tube shall be filled with argon. Within this work, no argon was used, since the systems were equilibrating rapidly and/or the oils were barely sensitive to oxidation. Another error, which affects the EACN, occurs from the geometric method used to determine the critical point. In our case an averaged geometrical error of ±0.8 °C for T^* and ±0.01 for γ^* were found which correspond to an error of ±0.1 for the EACN determined with C_6E_4 and ±0.3 for $C_{10}E_4$. Taking into account all the sources of error discussed above, we expect that EACNs are known to an accuracy of approximately 1.0 EACN unit for oils with EACN $\gtrsim 0$ and 1.5 EACN units for significantly more polar oils (EACN $\lesssim 0$).

Dependency of T^* on Oil Penetration. The evolution of the T^* values according to the chemical structure of the oil and the hydrophilicity of the surfactant can be rationalized in terms of the so-called "effective packing parameter" P_{eff}. P_{eff} is an extension, for SOW-T ternary systems, of the "packing parameter" P of a surfactant defined as $P = \nu_{surf}/a_{surf}l_{surf}$ where ν_{surf} and l_{surf} are the volume and the length of the hydrophobic tail respectively, while a_{surf} is the equilibrium area per surfactant molecule in the micellar interface.[22] For SOW systems, the penetration of the oil into the interfacial film influence the "effective" packing parameter of the surfactant. Tchakalova et al. have shown that in this case P must be replaced by P_{eff} (eq 1).[23,24]

DOI: 10.1021/acs.langmuir.5b02545
Langmuir XXXX, XXX, XXX−XXX

$$P_{\text{eff}} = \frac{\nu_{\text{surf}} + \tau\nu_{\text{oil}}}{(a_{\text{surf}} + \tau a_{\text{oil}})l_{\text{surf}}} \qquad (1)$$

where ν_{oil} is the known molecular volume of the oil, a_{oil} is the area occupied by each oil molecule located at the S/W interface, and $\tau = N_{\text{oil}}/N_{\text{surf}}$ is the number of oil molecules per the number of surfactant molecules at the interface. Depending on its affinity for the interfacial layer, the oil penetrates into the surfactant layer.[6,25,26] The higher the polarity of the oil (low EACN), the higher is τ. As the value of a_{oil} for nonpolar oils is much smaller than a_{surf}, the penetration of the oil will mainly increase the numerator of eq 1. Thus, starting from a balanced microemulsion system at T^* having an interfacial film with zero mean curvature (i.e., $P_{\text{eff}} = 1$), a penetrating oil will increase the curvature toward water ($P_{\text{eff}} > 1$), whereas a decrease of temperature will dramatically increase the hydrophilicity of ethylene oxide groups and thus a_{surf}, which induces a curvature toward the oil phase ($P_{\text{eff}} < 1$) as illustrated in Figure 3. The lower the EACN of an oil, the more it penetrates into the interfacial film and the lower is the temperature T^* required to restore a balanced system. This behavior is illustrated in Figure 1 with fish diagrams of 1-octene and 1-octyne. Since the latter is more polar, the penetration—and thus τ—increases, which in turn results in a larger P_{eff}. Consequently, the fish diagram is shifted to lower temperatures with respect to 1-octene. Remarkably is the strong decrease in the area of the three-phase body, which is due to the higher affinity of C_6E_4 for 1-octyne.

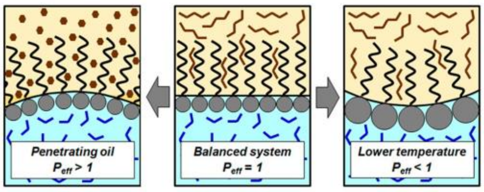

Figure 3. Effect of more penetrating oil (left) and lower temperature (right) on the spontaneous curvature of the interfacial film of a balanced C_iE_j/oil/water microemulsion system.

QSPR Analysis of EACN Values with COSMO-RS Descriptors of Oils. In an attempt to go further in our understanding of factors influencing EACN values of oil, we used the COSMO-RS model, which is implemented in the COSMOtherm software. It has the ability to compute the chemical potential μ of a given solute in a liquid phase.[19,27] This chemical potential can then be transformed into relevant physicochemical properties such as the partition coefficient of compounds between two phases or between an aqueous phase and a micelle.[28,29] So, if we consider the ternary SOW system, COSMOtherm should be able to calculate the amount of a given oil penetrating into the interfacial film of surfactant considered as a pseudophase. However, the chemical potential μ of the oil inside the interfacial film cannot be directly calculated because the COSMO-RS model is only able to describe bulk liquid phases and no interfaces. For such complex systems,[30] an alternative approach based on descriptors provided by COSMOtherm, the COSMO-RS σ-moments, enables an indirect treatment. Starting from the molecular structure, COSMOtherm generates the so-called σ-surface, a slightly increased van der Waals surface of X that can be projected in the σ-profiles $p^X(\sigma)$ histograms. They describe the distribution of the screening charge density σ on the molecular surface and thus offer a detailed quantitative description of the polarity and hydrogen bonding features of molecules.[31] Figure 4 shows the σ-profiles of n-decane, 1-decene, and 1-decyne, demonstrating differences in their overall polarity.

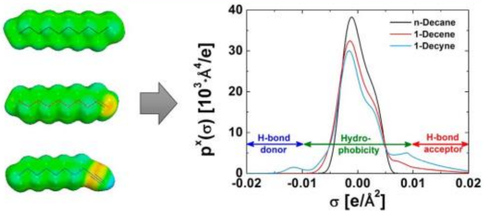

Figure 4. Main steps used by COSMO-RS model to convert molecular structures of n-octane (black), 1-octene (red), and 1-octyne (blue) into their σ-surfaces and then into the σ-profiles.

As shown by Klamt,[19] the partition coefficient K of a solute X between two phases can be written as a function of its σ-moments M_i^X according to eq 2.

$$RT \ln K = c_{\text{acc}}M_{\text{acc}}^X + c_{\text{don}}M_{\text{don}}^X + \sum_{i=0}^{m} c_i M_i^X \qquad (2)$$

where M_i^X are calculated from the σ-profile $p^X(\sigma)$ of the molecule according to eqs 3–5.

$$M_{\text{acc}}^X = \int_{+\sigma_{\text{hb}}}^{+\infty} p^X(\sigma)(\sigma - \sigma_{\text{hb}})\,d\sigma \qquad (3)$$

$$M_{\text{don}}^X = \int_{-\infty}^{-\sigma_{\text{hb}}} p^X(\sigma)(-\sigma - \sigma_{\text{hb}})\,d\sigma \qquad (4)$$

$$M_i^X = \int_{-\infty}^{+\infty} p^X(\sigma)\sigma^i\,d\sigma \qquad (5)$$

Since the units of $p^X(\sigma)$, σ, and dσ are expressed in $[10^3\ \text{Å}^4/\text{e}]$, $[\text{e}/\text{Å}^{-2}]$, and $[10^{-3}\ \text{e}/\text{Å}^{-2}]$, respectively, the units of the σ-moments M_i^X are expressed in $[\text{Å}^{2-2i}\ \text{e}^i]$. In particular, the zero-order σ-moment M_0^X is expressed in $[\text{Å}^2]$ and the first-order moment M_1^X as well as both hydrogen-bond moments M_{acc}^X and M_{don}^X are expressed in [e], whereas the second-order moment M_2^X is expressed in $[\text{e}^2/\text{Å}^2]$.

The two "hydrogen-bonding" σ-moments M_{acc}^X and M_{don}^X express the ability of X to interact as a hydrogen-bond acceptor and donor, respectively. They have a nonzero value only when the σ-profile of X exceeds the range $[-\sigma_{\text{hb}}, +\sigma_{\text{hb}}]$, where σ_{hb} is an appropriate value of the hydrogen-bond cutoff equal to 0.01 e/Å^2. Among hydrocarbon oils investigated here, only alkynes exhibit a significant acidity expressed in the σ-profile as a small peak at −0.012 e/Å^2 (Figure 4). The remaining M_i^X are obtained from the statistical moments of the σ-profile $p^X(\sigma)$ according to eq 5. Usually a mere development of the series up to $m = 6$ is sufficient to adequately describe the partition coefficient K (eq 2). The first σ-moments M_i^X have a simple physical meaning. The zero-order moment M_0^X is equal to the total surface area of solute X. The first-order moment M_1^X is the total polarization charge on the σ-surface of the solute and is equal to zero for uncharged compounds including all the compounds considered in this paper. The second-order

DOI: 10.1021/acs.langmuir.5b02545
Langmuir XXXX, XXX, XXX−XXX

moment M_2^X expresses the overall polarity of the compound. Usually, a molecule is called polar when it has a permanent dipole moment. Actually, the concept of chemical polarity is broader since it refers to a separation of electric charge in molecules having an electric dipole *or multipole* moment. As σ-profiles result from a projection of the screening charge density of σ-surfaces in two-dimensional graphs, a part of the initial 3D information is lost. Consequently, σ-profiles do not allow to calculate dipole moments, but they provide a detailed quantitative description of the polarity of each bond of the molecules. According to the definition of M_2^X given in eq 5, all nonzero values of $p^X(\sigma)$ will contribute to M_2^X. Thus, molecules such as CO_2, C_6H_6, or CCl_4, which do not have permanent electric dipole moments, lead to significant M_2^X values because they have multipole moments. The third-order moment M_3^X is a measure of the asymmetry of the σ-profile. Higher σ-moments possess only a mathematical interpretation. The σ-moment approach was already successfully applied for the prediction of Hansen solubility parameters,[32] temperature-dependent surface tensions,[33] and blood−brain partition coefficients.[34]

The EACN is strongly related to the partition coefficient of the oil into the surfactant layer and eventually to its affinity for the interfacial film and to its molecular volume through eq 1. The σ-moments are thus expected to be good descriptors for a QSPR analysis. Therefore, a multilinear regression analysis was performed with the experimental EACN values as dependent variable and the eight σ-moments $M_{\text{acc}}^{\text{oil}}$, $M_{\text{don}}^{\text{oil}}$, M_0^{oil}, and M_i^{oil} (with $i = 2-6$) as independent variables. In a first step, the 62 investigated hydrocarbons were split into a training (56 candidates) and a test (6 candidates) set. The training set was used in a regression analysis, and the significance of each parameter was then verified according to the *t*-test. The most insignificant descriptor was then removed, and the regression analysis was repeated until only one descriptor was left. Since the coefficient of determination offers no information about the optimal number of descriptors for a predictive model, the fitness function was applied in order to obtain the best model.[35] It relates the quality of a regression to the number of descriptors. Consequently, six uninformative σ-moments were eliminated leading to a predictive model that involves only the two descriptors M_0^{oil} and M_2^{oil}. At a second stage, the robustness of the model was evaluated with the test set of hydrocarbons verifying that the predicted values were close to the experimental ones ($\Delta(\text{EACN}) \leq 0.8$). Finally, the model was refined using the entire data set leading to best fit reported in eq 6.

$$\text{EACN}_{\text{pred}}^{\text{oil}} = 0.07M_0^{\text{oil}} - 0.33M_2^{\text{oil}} - 4.03 \qquad (6)$$

Table 1 and Figure 5 show the good linearity between experimental and predicted EACN values with an outstanding coefficient of determination ($R^2 = 0.98$) and a standard error of the estimate SEE of 0.82.

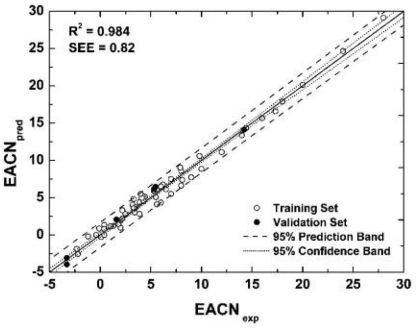

Figure 5. Comparison of predicted vs experimental EACNs of polar hydrocarbon oils. 56 oils were used for the training set and 6 oils for the validation set. The latter lie well inside the 95% prediction band.

Molecular Interpretation of the Factors Influencing EACNs of Oils. The chemical structure and the presence of polar functions have a distinct effect on the EACN value of oils. As a rule of thumb, nonlinear and functionalized oils exhibit EACN values lower than that of *n*-alkanes with the same number of carbon atoms. Branching has a relatively weak influence on the EACN, while cyclization and unsaturation result in a significant decrease of the EACN. Furthermore, aromaticity or the presence of polar groups such as esters or ethers dramatically reduces EACN values.[13−15] Additionally, it has been shown that the hydrophobicity of oils also depends on the location of the functional group within the molecule;[15] e.g., the two isomeric esters, ethyl myristate and octyl octanoate, exhibit EACN values equal to 5.3 and 8.1, respectively. All these findings are based on empirical observations of measured EACNs.

Actually, there has been so far no quantitative interpretation of structural parameters influencing EACNs of oils. To shed some light to this issue with the QSPR model, 11 oils having the same number of carbon atoms (C_{10}) were selected and positioned in Figure 6 as a function of their van der Waals surface M_0 (*X*-axis) and their overall polarity M_2 (*Y*-axis). The four inclined straight lines correspond to the *iso*-EACN curves calculated from eq 6 for EACN values equal to −5, 0, +5, and +10. *n*-Decane is used as a reference oil for identifying oils having a smaller or larger area than it, depending on whether they are located to the left or right of the dotted vertical line. Here, only the 1-chlorodecane has a greater area than *n*-decane due to the fact that chlorine atoms are much larger than hydrogen atoms. On the other side, 1-decene and 1-decyne have a slightly smaller area than *n*-decane while cyclic oils have a much smaller one. The dashed horizontal line separates, in turn, saturated (cyclo)alkanes from unsaturated and chlorinated oils that are significantly more polar than *n*-decane.

Comparing experimental EACNs of alkanes and cycloalkanes in Figure 6, one notes that they vary substantially from 5.3 (*cis*-decalin) to 10.0 (*n*-decane) while they have approximately the same polarity (M_2) as *n*-decane. The lower EACN values of cyclic oils do not come from their greater polarity as we had previously suggested.[17] It is simply due to a smaller van der Waals surface which decreases their interactions with surrounding oil molecules and increases its partition coefficient toward the interfacial film of surfactants. In the same way, it is worth comparing the EACN of *p*-menthane with that of the three unsaturated and aromatic derivatives (*p*-menth-2-ene, α-terpinene, and *p*-cymene) located above it in Figure 6. Actually, these four molecules have virtually identical surfaces but differ markedly with regard to their polarity as well as their EACN that follow the same trend starting from *p*-menthane (EACN = +6.0) to *p*-cymene (EACN = −0.4). The same argument can be applied to *n*-decane, 1-decene, and 1-chlorodecane that exhibit fairly similar M_0, but their EACNs greatly diminish as a result of increasing M_2. To summarize, the more polar functional groups are present in the oil, the lower is its EACN: alkanes < alkenes

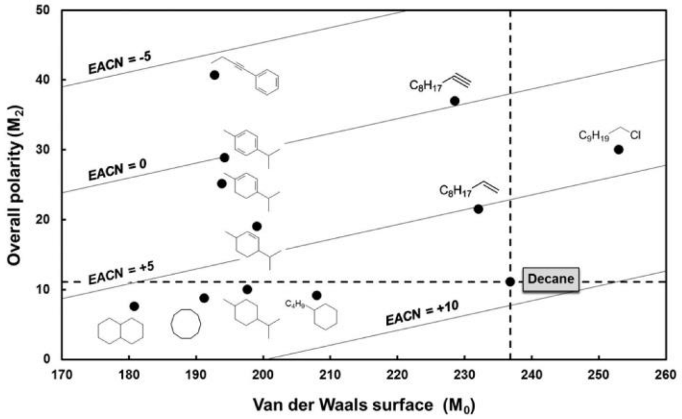

Figure 6. Position of a selection of various oil molecules with 10 carbons as a function of their van der Waals surface (M_0) and their overall polarity (M_2). Inclined straight lines correspond to the *iso*-EACN curves calculated from eq 6.

< dienes < aromatics ≈ chloroalkanes < alkynes. Therefore, one understands why a hydrocarbon such as phenyl-1-butyne combining a small area and two polar moieties (alkyne and aromatic) exhibit a particularly low EACN (−3.3).

Note that *n*-alkanes are not very well predicted by eq 6. Actually M_0 alone would be sufficient for a perfect correlation. Consequently, M_2 imposes a slight polarity dependence, which comes from the tetrahedral arrangement of the $-CH_2-$ segments and is increasing with augmenting N_C.

If we now focus at the influence of N_C on the EACNs of different sets of homologous oils (*n*-alkyl-R), two types of behavior appear in Figure 2. When R is a nonpolar group such as cyclohexane, the EACNs of alkylcyclohexanes approximate the straight line of *n*-alkanes when N_C increases whereas for more polar oils such as 1-alkenes, 1-alkynes, *n*-alkylbenzene, and 1-chloroalkanes, the tendency remains parallel to that of *n*-alkanes. These observations may be explained on the basis of the difference in polarity of R groups. When the R unit has the same polarity as the *n*-alkyl part of the oil, there is no reason that R first enters the interfacial film. In the case of short chain *n*-alkylcyclohexanes, it is just statistically more likely, that the small cyclohexane group enters the interface. This augments the effective volume of the hydrophobic tail ($\nu_{\text{surf}} + \tau\nu_{\text{oil}}$) and thus increases P_{eff}. If the alkyl chain increases in size, the probability for the cyclohexane group to penetrate between the surfactant tails decreases. It can be pictured as a higher dilution of the cyclohexane group between the alkyl chains, with increasing carbon chain length. Consequently, an oil with a nonpolar R group such as cyclohexane will increasingly penetrate the interfacial film by the *n*-alkyl end when N_C increases. Therefore, its EACN will then tend to approach that of *n*-alkanes. It can be assumed that same conclusions are valid for branched hydrocarbons. *Per contra*, when R is significantly more polar than the *n*-alkyl moiety, oil molecules preferentially penetrate into the interfacial film in order to localize polar R groups close to the transition zone between the alkyl chains C_i and the hydrophilic heads E_j of surfactants to minimize their energy. In this case, the contribution to the effective equilibrium area ($a_{\text{surf}} + \tau a_{\text{oil}}$) augments, which in turn decreases P_{eff}. Furthermore, the effective volume of the hydrophobic tail remains constant, since R is directed toward the interface. Consequently, the evolution of EACN as a function of N_C is parallel to that of the *n*-alkanes.

■ CONCLUSIONS

This work highlights the connection of the EACN of hydrocarbon oils with the van der Waals surface and the overall polarity of the oil. These two understandable descriptors (σ-moments M_0 and M_2) are readily generated by COSMO-therm and lead to an equation able to predict the EACN values of a large variety of hydrocarbon oils. The σ-moments approach turned out to be a fast and accurate tool for the estimation of the EACN of hydrocarbon oils, which do not contain strong hydrogen bond acceptor or donor groups. Research is currently underway to extend this approach to polar oils having functional groups including fragrances, triglycerides, and monomers.

■ ASSOCIATED CONTENT

Supporting Information

The Supporting Information is available free of charge on the ACS Publications website at DOI: 10.1021/acs.langmuir.5b02545.

Table of experimental and predicted EACN of all relevant oils, as well as their σ-moments M_0^X and M_2^X, which were used to build up the QSPR model (PDF)

■ AUTHOR INFORMATION

Corresponding Author

*E-mail Jean-Marie.Aubry@univ-lille1.fr (J.-M.A.).

Notes

The authors declare no competing financial interest.

■ ACKNOWLEDGMENTS

The authors thank Prof. Andreas Klamt and Prof. Steven Abbott for helpful discussions, which were most appreciated during this work.

REFERENCES

(1) Kahlweit, M.; Strey, R.; Firman, P.; Haase, D.; Jen, J.; Schomaecker, R. General Patterns of the Phase Behavior of Mixtures of Water, Nonpolar Solvents, Amphiphiles, and Electrolytes. 1. *Langmuir* **1988**, *4*, 499−511.

(2) Kahlweit, M.; Strey, R.; Haase, D.; Firman, P. Properties of the Three-Phase Bodies in Water-Oil-Nonionic Amphiphile Mixtures. *Langmuir* **1988**, *4*, 785−790.

(3) Kahlweit, M.; Strey, R.; Schomaecker, R.; Haase, D. General Patterns of the Phase Behavior of Mixtures of Water, Nonpolar Solvents, Amphiphiles, and Electrolytes. 2. *Langmuir* **1989**, *5*, 305−315.

(4) Aramaki, K.; Kunieda, H.; Ishitobi, M.; Tagawa, T. Effect of Added Salt on Three-Phase Behavior in a Sucrose Monoalkanoate System. *Langmuir* **1997**, *13*, 2266−2270.

(5) Cash, L.; Cayias, J. L.; Fournier, G.; Macallister, D.; Schares, T.; Schechter, R. S.; Wade, W. H. The Application of Low Interfacial Tension Scaling Rules to Binary Hydrocarbon Mixtures. *J. Colloid Interface Sci.* **1977**, *59*, 39−44.

(6) Kanei, N.; Tamura, Y.; Kunieda, H. Effect of Types of Perfume Compounds on the Hydrophile−lipophile Balance Temperature. *J. Colloid Interface Sci.* **1999**, *218*, 13−22.

(7) Tchakalova, V.; Fieber, W. Classification of Fragrances and Fragrance Mixtures Based on Interfacial Solubilization. *J. Surfactants Deterg.* **2012**, *15*, 167−177.

(8) Hyde, S.; Blum, Z.; Landh, T.; Lidin, S.; Ninham, B. W.; Andersson, S.; Larsson, K. *The Language of Shape: The Role of Curvature in Condensed Matter: Physics, Chemistry and Biology*; Elsevier: Amsterdam, 1996.

(9) Testard, F.; Zemb, T. Solute Effect on Connectivity of Water-in-Oil Microemulsions. *Langmuir* **2000**, *16*, 332−339.

(10) Testard, F.; Zemb, T. Excess of Solubilization and Curvature in Nonionic Microemulsions. *J. Colloid Interface Sci.* **1999**, *219*, 11−19.

(11) Salager, J.-L.; Forgiarini, A. M.; Bullón, J. How to Attain Ultralow Interfacial Tension and Three-Phase Behavior with Surfactant Formulation for Enhanced Oil Recovery: A Review. Part 1. Optimum Formulation for Simple Surfactant−Oil−Water Ternary Systems. *J. Surfactants Deterg.* **2013**, *16*, 449−472.

(12) Salager, J.-L.; Forgiarini, A. M.; Márquez, L.; Manchego, L.; Bullón, J. How to Attain an Ultralow Interfacial Tension and a Three-Phase Behavior with a Surfactant Formulation for Enhanced Oil Recovery: A Review. Part 2. Performance Improvement Trends from Winsor's Premise to Currently Proposed Inter- and Intra-Molecular Mixtures. *J. Surfactants Deterg.* **2013**, *16*, 631−663.

(13) Queste, S.; Salager, J. L.; Strey, R.; Aubry, J. M. The EACN Scale for Oil Classification Revisited Thanks to Fish Diagrams. *J. Colloid Interface Sci.* **2007**, *312*, 98−107.

(14) Engelskirchen, S.; Elsner, N.; Sottmann, T.; Strey, R. Triacylglycerol Microemulsions Stabilized by Alkyl Ethoxylate surfactants—A Basic Study: Phase Behavior, Interfacial Tension and Microstructure. *J. Colloid Interface Sci.* **2007**, *312*, 114−121.

(15) Ontiveros, J. F.; Pierlot, C.; Catté, M.; Molinier, V.; Pizzino, A.; Salager, J.-L.; Aubry, J.-M. Classification of Ester Oils according to Their Equivalent Alkane Carbon Number (EACN) and Asymmetry of Fish Diagrams of C10E4/ester Oil/water Systems. *J. Colloid Interface Sci.* **2013**, *403*, 67−76.

(16) Bouton, F.; Durand, M.; Nardello-Rataj, V.; Serry, M.; Aubry, J.-M. Classification of Terpene Oils Using the Fish Diagrams and the Equivalent Alkane Carbon (EACN) Scale. *Colloids Surf., A* **2009**, *338*, 142−147.

(17) Bouton, F.; Durand, M.; Nardello-Rataj, V.; Borosy, A. P.; Quellet, C.; Aubry, J.-M. A QSPR Model for the Prediction of the "Fish-Tail" Temperature of CiE4/Water/Polar Hydrocarbon Oil Systems. *Langmuir* **2010**, *26*, 7962−7970.

(18) *Molecular Operating Environment*; 1010 Sherbooke St. West, Suite #910; Chemical Computing Group Inc., Montreal, QC, Canada, 2007.

(19) Klamt, A. *COSMO-RS: From Quantum Chemistry to Fluid Phase Thermodynamics and Drug Design*; Elsevier: Amsterdam, 2005.

(20) Salager, J. L.; Morgan, J. C.; Schechter, R. S.; Wade, W. H.; Vasquez, E. Optimum Formulation of Surfactant/Water/Oil Systems for Minimum Interfacial Tension or Phase Behavior. *SPEJ, Soc. Pet. Eng. J.* **1979**, *19*, 107−115.

(21) Sottmann, T.; Strey, R. Ultralow Interfacial Tensions in Water−n-Alkane−surfactant Systems. *J. Chem. Phys.* **1997**, *106*, 8606−8615.

(22) Israelachvili, J. N.; Mitchell, D. J.; Ninham, B. W. Theory of Self-Assembly of Hydrocarbon Amphiphiles into Micelles and Bilayers. *J. Chem. Soc., Faraday Trans. 2* **1976**, *72*, 1525.

(23) Tchakalova, V.; Testard, F.; Wong, K.; Parker, A.; Benczédi, D.; Zemb, T. Solubilization and Interfacial Curvature in Microemulsions. *Colloids Surf., A* **2008**, *331*, 31−39.

(24) Tchakalova, V.; Testard, F.; Wong, K.; Parker, A.; Benczédi, D.; Zemb, T. Solubilization and Interfacial Curvature in Microemulsions: II. Surfactant Efficiency and PIT. *Colloids Surf., A* **2008**, *331*, 40−47.

(25) Uddin, M. H.; Kanei, N.; Kunieda, H. Solubilization and Emulsification of Perfume in Discontinuous Cubic Phase. *Langmuir* **2000**, *16*, 6891−6897.

(26) Kamada, M.; Shimizu, S.; Aramaki, K. Manipulation of the Viscosity Behavior of Wormlike Micellar Gels by Changing the Molecular Structure of Added Perfumes. *Colloids Surf., A* **2014**, *458*, 110−116.

(27) Benazzouz, A.; Moity, L.; Pierlot, C.; Molinier, V.; Aubry, J.-M. Hansen Approach versus COSMO-RS for Predicting the Solubility of an Organic UV Filter in Cosmetic Solvents. *Colloids Surf., A* **2014**, *458*, 101−109.

(28) Ingram, T.; Storm, S.; Kloss, L.; Mehling, T.; Jakobtorweihen, S.; Smirnova, I. Prediction of Micelle/Water and Liposome/Water Partition Coefficients Based on Molecular Dynamics Simulations, COSMO-RS, and COSMOmic. *Langmuir* **2013**, *29*, 3527−3537.

(29) Mehling, T.; Ingram, T.; Smirnova, I. Experimental Methods and Prediction with COSMO-RS to Determine Partition Coefficients in Complex Surfactant Systems. *Langmuir* **2012**, *28*, 118−124.

(30) Masuch, K.; Fatemi, A.; Murrenhoff, H.; Leonhard, K. A COSMO-RS Based QSPR Model for the Lubricity of Biodiesel and Petrodiesel Components: Quantitative Structure-Property Relationship Lubricity. *Lubr. Sci.* **2011**, *23*, 249−262.

(31) Klamt, A.; Eckert, F.; Hornig, M. COSMO-RS: A Novel View to Physiological Solvation and Partition Questions. *J. Comput.-Aided Mol. Des.* **2001**, *15*, 355−365.

(32) Járvás, G.; Quellet, C.; Dallos, A. Estimation of Hansen Solubility Parameters Using Multivariate Nonlinear QSPR Modeling with COSMO Screening Charge Density Moments. *Fluid Phase Equilib.* **2011**, *309*, 8−14.

(33) Kondor, A.; Járvás, G.; Kontos, J.; Dallos, A. Temperature Dependent Surface Tension Estimation Using COSMO-RS Sigma Moments. *Chem. Eng. Res. Des.* **2014**, *92*, 2867−2872.

(34) Wichmann, K.; Diedenhofen, M.; Klamt, A. Prediction of Blood-Brain Partitioning and Human Serum Albumin Binding Based on COSMO-RS σ-Moments. *J. Chem. Inf. Model.* **2007**, *47*, 228−233.

(35) Kubinyi, H. Variable Selection in QSAR Studies. I. An Evolutionary Algorithm. *Quant. Struct.-Act. Relat.* **1994**, *13*, 285−294.

Appendix 4

Fragrance solubilisation in temperature insensitive aqueous microemulsions based on synergistic mixtures of non-ionic and anionic surfactants

Colloids and Surfaces A: Physicochem. Eng. Aspects 458 (2014) 85–95

Contents lists available at ScienceDirect

Colloids and Surfaces A: Physicochemical and Engineering Aspects

journal homepage: www.elsevier.com/locate/colsurfa

Fragrance solubilization in temperature insensitive aqueous microemulsions based on synergistic mixtures of nonionic and anionic surfactants

Thomas Lukowicz, Roberto Company Maldonado, Valérie Molinier,
Jean-Marie Aubry, Véronique Nardello-Rataj*

Université Lille 1 and ENSCL, EA 4478 Chimie Moléculaire et Formulation, Equipe Oxydation et Physicochimie de la Formulation, F-59655 Villeneuve d'Ascq, France

HIGHLIGHTS

- 1% ionic surfactant boosts the solubilizing properties of nonionic surfactants.
- 10% of Dehydol/SDS solubilizes up to 7 wt.% β-pinene in water.
- The water-rich microemulsion is almost temperature insensitive.
- Compared to pure C_8E_4, the polydisperse C_8E_4 leads to a broader one-phase region.
- Terpene alcohols penetrate the interface and increase the solubilization capacity.

GRAPHICAL ABSTRACT

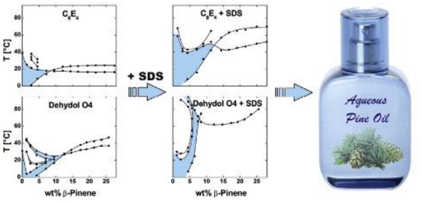

ARTICLE INFO

Article history:
Received 12 September 2013
Received in revised form 5 November 2013
Accepted 19 November 2013
Available online 28 November 2013

Keywords:
Fragrance solubilisation
Essential oils
Polyoxyethylene alkyl ether
Binary surfactant systems
Optimal temperature
Temperature insensitive microemulsion

ABSTRACT

Well-defined tetraethylene glycol monooctylether (C_8E_4) and its commercial polydispersed counterpart (Dehydol® O4) were used to solubilize fragrances. Addition of small amounts (≤1 wt.%) of the ionic surfactants, sodium dodecylsulfate (SDS) or sodium lauryl ether sulfate (SLES), permits the formulation of temperature insensitive fragrance in water microemulsions. The investigation of the pseudo-ternary surfactants/β-pinene/water systems allows the determination of the optimum temperature T^* as well as the assessment of the efficiency of the surfactant mixtures to solubilize β-pinene. A mixture of Dehydol O4 and SDS (9/1 wt.%) can solubilize 6.5 wt.% of β-pinene in water within the temperature range of 25–80 °C. This synergistic formulation was also applied to the solubilization of *p*-cymene, the essential oils *pinus pinaster* and *pinus sylvestris* and a true fragrant mixture composed of 9 terpenes and terpenoids in dipropylene glycol.

1. Introduction

Synergistic effects between surfactants (S) are very common. They are strong between nonionic and ionic, very strong between cationic and anionic and rather weak between nonionic surfactants [1–5]. While the effect of ionic surfactants on well-defined nonionic surfactants such as polyethoxylated fatty alcohols abbreviated as C_iE_j (i = number of carbons of the alkyl chain and j = number of ethoxy units) is well described [6], the effect on commercial surfactant blends is rarely investigated from a physicochemical viewpoint due to their complexity. However, polyethoxylated surfactant blends with a size distribution both in chain lengths and in number of ethoxy units exhibit better performances than monomolecular C_iE_j and are ubiquitous in end-use products such as detergents or

---

* Corresponding author. Tel.: +33 3 20 33 63 69.
E-mail address: veronique.rataj@univ-lille1.fr (V. Nardello-Rataj).

0927-7757/$ – see front matter © 2013 Elsevier B.V. All rights reserved.
http://dx.doi.org/10.1016/j.colsurfa.2013.11.024

cosmetics [7]. Moreover, they are often combined with ionic surfactants because of the synergistic effects resulting from a non-ideal behaviour on mixing. Indeed, such binary surfactant systems form mixed aggregates leading to lower surface tensions and improved foaming, emulsification, solubilization, wetting and detergency [8,9].

Ionic surfactants for example tend to increase the monophasic region in the water-rich corner of the ternary nonionic–S/O/W systems [10]. This causes the mixture to become more effective towards the solubilization of oils in aqueous solutions. Moreover, the hydrophilicity of ionic surfactants increases with temperature in contrast to ethoxylated surfactants [11]. Hence, an appropriate mixture of nonionic and ionic surfactants allows the preparation of temperature insensitive microemulsions despite the temperature sensitivity of polyethoxylated surfactants [12]. Such systems could be of great interest regarding the aqueous solubilization of fragrances (F) since one of the challenges in fine perfumery is to replace the VOC ethanol with an aqueous solution containing the minimum amount of additives.

The phase behaviour of C_iE_j/O/W systems strongly depends on temperature [13]. If the amphiphilicity of the surfactant is high enough and its hydrophilic/lipophilic balance is in accordance with the hydrophobicity of the oil, the solubilization of a given oil in a nonionic surfactant solution reaches its maximum at the so-called "optimal temperature", noted T^*. At this temperature, a bicontinuous microemulsion with a zero mean curvature coexists with excess oil (O) and water (W) phases. The location of T^* depends both on the hydrophilic/lipophilic balance of the surfactant and on the lipophilicity of the oil, as well as on salt and alcohol content [14]. It is known that increasing the hydrophilicity of the surfactant or the lipophilicity of the oil increases T^* [15,16]. The solubilization of fragrances in $C_{12}E_8$/F/W systems has already been reported and the effect of molecular structures of fragrances on T^* has been studied [17]. However, the microemulsions turned out to be very temperature sensitive limiting their practical use. Moreover, liquid crystal phases are formed at the expense of the monophasic fluid phase.

In the present work, the effect of an ionic surfactant on the solubilization efficiency of well-defined C_8E_4 and of its commercial counterpart Dehydol O4 is investigated. Two terpenes, two essential oils and one true fragrant composition have been chosen to compare the solubilization capacity of the systems in a broad temperature range, i.e. 5–50 °C. In order to identify the best conditions allowing the solubilization of the maximum amount of a given fragrance, the temperature dependent phase behaviour has been determined in the W/S cut through the ternary phase prism S/F/W where S is either one of the non-ionic surfactants alone (10 wt.%) or a mixture with one of the anionic surfactants (1 wt.%).

2. Experimental

2.1. Analytical methods

A Thermofisher GC Trace equipped with an AI 3000 injector connected to Thermofisher DSQ II simple quadrupole detector was used for the GC–MS analysis. Compound separation was achieved on a 30 m, DB5MS with 0.25 mm i.d. and 0.25 μm film thickness gas chromatographic column (J&W Scientific, Folsom, CA, USA). Carrier gas (ultra-pure helium) flow rate was 1.0 mL min^{-1} and the injector, the transfer line and the ion source were maintained at 220 °C respectively. The MS detector was used in the EI mode with an ionization voltage of 70 eV. The column was held at 70 °C for 2 min and then programmed at 10 °C min^{-1} to 285 °C and maintained for 15 min. The samples were diluted in cyclohexane and injected in the split mode with a ratio of 12. The NIST 2008 was used to identify the chemical compounds.

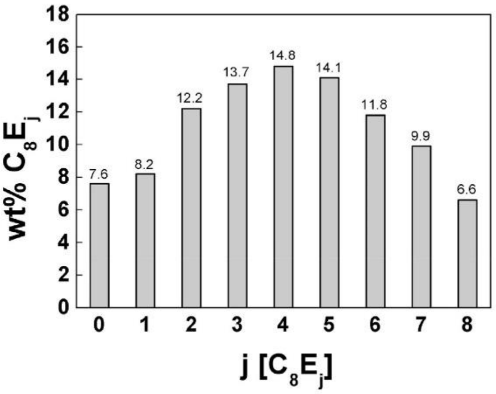

Fig. 1. Composition of Dehydol O4® determined by GC–MS. It can be seen that the arrangement of the peaks resembles a Poisson distribution, which has its maximum at 14.8 wt.% of C_8E_4.

An Agilent GC Trace equipped with an injector Series 7683 connected to an Agilent detector 6890N/G1530N was used for the Gas chromatography-FID analyses. Compound separation was achieved on a 30 m HP-1 with 0.32 μm i.d. and 0.25 μm film thickness gas chromatographic column (J&W Scientific, Folsom, CA, USA). Carrier gas (N_2) flow rate was 1.0 ml min^{-1}. The injector was held at 70 °C for 2 min and then programmed at 60 °C min^{-1} to 280 °C and maintained for 6 min and then programmed at 20 °C min^{-1} to 70 °C. The ion source was maintained at 280 °C. The column was held at 70 °C for 2 min and then programmed at 10 °C min^{-1} to 220 °C and maintained for 5 min. The samples were diluted in cyclohexane.

2.2. Materials

Dehydol O4® (≈307 g/mol) and sodium lauryl ether sulfate or Texapon® (SLES) (27 wt.% in aqueous solution, 2–3 ethoxy units) were a gift from Cognis. The composition of Dehydol® O4, determined by GC–MS, is shown in Fig. 1. Its molar mass was determined by integration of the peaks in the MS–chromatogram and verified with high resolution NMR [18].

β-Pinene (99%), *p*-cymene (99%), α-pinene (98%), camphene (95%), cineole (≥85%), camphor (98%), linalyl acetate (≥97%), limonene (97%), ocimene (≥90%), dipropylene glycol (99%) and sodium dodecylsulfate (SDS) (99%, 288.38 g/mol) were purchased from Sigma–Aldrich. SDS was recrystallized three times from ethanol and lyophilized in order to avoid the deep minimum around the critical micelle concentration caused by impurities like dodecanol. The fragrant mixture was prepared from literature [19]. Linalool (97%) was obtained from Alfa Aesar. The essential oils *pinus sylvestris* and *pinus pinaster* were obtained from Cooper. While the first was obtained from extraction of leaves and arms, the latter was composed of a synthetic mixture of terpenic compounds. Their compositions, determined by GC–MS, are shown in Table 1. C_8E_4 (97%, 306.44 g/mol) was synthesized from tetraethylene glycol and octylbromide according to known procedure [20]. The purity was verified by GC-FID at 285 °C.

2.3. Surface tension measurements

Surface tensions were measured with the tensiometer K11 (Krüss) using the Wilhelmy plate method. Aqueous concentrated solutions of the surfactant(s) were prepared and diluted in several samples in order to obtain a concentration range (Millipore

Table 1
Composition (wt.%) of the essential oils *pinus sylvestris, pinus pinaster* and the fragrant mixture. The Equivalent Alkane Carbon Numbers (EACN) of some terpenes are also reported [21,22].

Compounds	Chemical structures	*Pinus sylvestris*	*Pinus pinaster*	Fragrant mixture	EACN
Terpenes					
α-Pinene	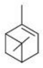	39.0	1.1	1.4	3.4
β-Pinene	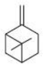	20.2	–	1.5	2.2
α-Phellandrene	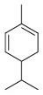	–	0.6	–	–
Limonene	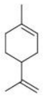	–	15.5	1.7	2.0
β-Terpinene	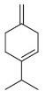	–	0.6	–	–
γ-Terpinene	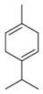	–	4.2	–	1.8
Terpinolene	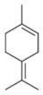	0.4	28.3	–	1.0
Camphene		1.6	1.9	0.4	–
3-Carene		17.0	–	–	2.5
Camphor	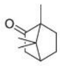	–	–	7.7	–
Cineole	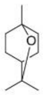	–	19.4	21.3	–
β-Myrcene	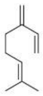	2.3	–	–	–
Ocimene	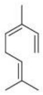	–	–	2.7	–
β-Caryophyllene	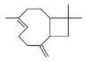	2.3	–	–	5.6
α-Caryophyllene	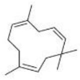	0.5	–	–	–

Table 1 (*Continued*)

Compounds	Chemical structures	*Pinus sylvestris*	*Pinus pinaster*	Fragrant mixture	EACN
Longifolene		1.1	–	–	6.5
Terpene alcohols					
Fenchol	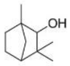	–	0.4	–	–
1-Terpineol	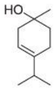	–	1.1	–	–
β-Terpineol	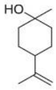	–	1.7	–	–
α-Terpineol	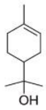	–	0.4	–	–
Linalool	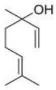	–	–	36.7	–
Terpene acetates					
Bornyl acetate	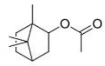	2.3	–	–	–
β-Terpenyl acetate	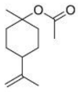	11.1	–	–	–
Linaly acetate	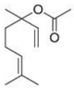	–	–	7.4	–
Aromatic compounds					
o-Cymene	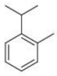	1.3	1.1	–	–
m-Cymene	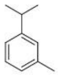	1.0	23.4	–	–
p-Cymene	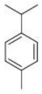	–	–	–	−0.4
p-α-Dimethyl styrene	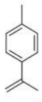	–	0.4	–	–
Solvent					
Dipropylene glycol	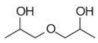	–	–	19.2	–

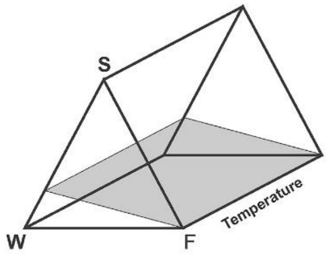

Fig. 2. Temperature dependent cut through the pseudo-ternary water (W)/fragrance (F)/surfactant (S) diagram, also called Lund cut.

water, $\sigma = 72.6\,\text{mN}\,\text{m}^{-1}$ at 22 °C). Surface tension was recorded after equilibration for each mixture. The precision of the force transducer of the surface tension apparatus was $0.1\,\text{mN}\,\text{m}^{-1}$ and before each experiment, the platinum plate was cleaned in blue-coloured flame. The temperature was stabilized at 22.0 ± 0.1 °C with the thermo-regulated bath Julaba F12.

2.4. Binary phase behaviour

The (pseudo-)binary phase diagrams were determined by visual inspection of the phase behaviour of the mixtures at different temperatures between 0 and 100 °C. Several samples of Dehydol O4 or well-defined C_8E_4 in water and in aqueous SDS (1 wt.%) solution were prepared and sealed. The overall sample size was 1.0 g. Afterwards the samples were placed into a thermo-regulated bath and the temperature was changed in 1 °C steps. The phase behaviour was observed after an equilibration time of approximately 30 min after each temperature change. Near the critical line, the steps were decreased to 0.1 °C in order to determine the border more precisely and equilibration time was increased to at least 1 h.

2.5. Ternary phase behaviour

A cut through the phase prism S/F/W-temperature at a constant W/S ratio, the so-called Lund cut, was performed (see Fig. 2), in order to determine the "optimal" temperature T^* and to assess the efficiency of a given system to solubilize β-pinene. Thereby, aqueous stock solutions containing 10 wt.% of well-defined C_8E_4 or Dehydol O4 were prepared and 1.0 g samples were distributed into several vials. Various quantities of β-pinene were added and the samples were sealed and gently shaken avoiding emulsification of the mixture. The samples were maintained in a thermo-regulated water-bath at the desired temperature (±0.1 °C). The same procedure was repeated by replacing 1.0 wt.% of the nonionic surfactant in the stock solution with 1.0 wt.% of SDS. The phase behaviour was observed visually by increasing the temperature in 1 °C steps. Depending on the sample, 1 h to two days were necessary to reach equilibrium. Liquid crystalline phases were detected with a polarized optical microscope.

2.6. Fragrance solubilization

The pseudo-ternary diagrams of the Dehydol O4 + SDS/F/W systems were constructed at different temperatures. In particular, the temperature range, in which the mixture appears as a clear monophasic microemulsion, was determined for several oils. Thereby, several samples were prepared, consisting of 9.0 wt.% Dehydol O4, 1.0 wt.% SDS, 5–7 wt.% fragrance and water. The terpenes β-pinene and *p*-cymene were chosen as simple model oils because they have different EACNs (2.2 and −0.4 respectively) [21]. The two essential oils *pinus sylvestris* and *pinus pinaster* were also investigated as complex oils. Finally, a fragrant mixture was reformulated to mimic a true fragrant composition (see Table 1). All experiments were also performed with 1 wt.% SLES instead of SDS in order to see the impact of another ionic surfactant on the temperature range of the monophasic region.

2.7. Modelling non-ideal micellisation

From a theoretical point of view, mixed surfactant systems first form mixed monolayers at the air–water interface and then, once the surface is saturated, they aggregate in the bulk phase to form mixed micelles. According to Holland and Rubingh, the critical micelle concentration of a surfactant mixture (C^*) is given by the subsequent equation (Eq. (1)) [6].

$$\frac{1}{C^*} = \Sigma i = 1n\left(\frac{\alpha_i}{f_i \cdot C_i}\right) \tag{1}$$

where α_i, C_i and f_i are respectively the stoichiometric mole fraction, the critical micelle concentration (CMC) and the activity coefficient of the *i*th component in the mixture ($i = 1$ for the nonionic surfactant and 2 for the anionic surfactant) [6]. From Eq. (1), the CMC of an ideal mixture ($f_i = 1$), noted C^*_{calc}, can be calculated. When the experimental C^* is lower than C^*_{calc}, the system exhibits a non-ideal behaviour corresponding to a synergistic effect (i.e. $f_i < 1$). It results from an attractive interaction between the two surfactants located in the surface monolayer and into the mixed micelles [23,24]. In this case, the regular solution theory must be invoked and the activity coefficient f_i of the *i*th surfactant is expressed as follows [23,25]:

$$\ln f_i = \beta \cdot (1 - X_i)^2 \tag{2}$$

where X_i is the mole fraction of the *i*th surfactant in the mixed micelle and β is an interaction parameter related to the molecular interactions between the surfactant molecules in the mixed micelles. The interaction parameter β is an indication of the degree of interaction between the two surfactants. A negative β value indicates a synergism meaning that the attractive interaction between the two different surfactants is stronger than the one between identical molecules of surfactants. From Eqs. (1) and (2), the following relationship can be deduced [26]:

$$C^* = \frac{C_1 \cdot C_2 \cdot e^{\beta\cdot(-1+X_1)^2 + \beta\cdot X_1^2}}{\alpha_1 (C_2 \cdot e^{\beta\cdot X_1^2} - C_1 \cdot e^{\beta\cdot(-1+X_1)^2}) + C_1 \cdot e^{\beta\cdot(-1+X_1)^2}} \tag{3}$$

Moreover, the mole fraction of the ionic surfactant in the aggregated pseudo-phase, X_1, can be solved iteratively for each α_1 from Eq. (4) [23,25].

$$\frac{X_1^2 \cdot \ln(\alpha_1 \cdot C^*/X_1 \cdot C_1)}{(1 - X_1)^2 \cdot \ln[(1 - \alpha_1) \cdot C^*/(1 - X_1) \cdot C_2]} = 1 \tag{4}$$

Hence, for each α_1, the theoretical C^* can be calculated, from Eqs. (2) and (3), in order to determine X_1 and consequently to fit the adjustable parameters (β) with an algorithm.

3. Results and discussion

3.1. Mixed micellisation and interaction parameter β

The surface tensions of aqueous solutions containing different ratios of Dehydol O4 and SDS, as well as C_8E_4 and SDS, have been measured. The results are illustrated in Fig. 3. The CMC of single-component C_8E_4 is 7.7 mmol/L, while its polydisperse counterpart Dehydol O4 has a value of 5.3 mmol/L. Addition of C_8E_4 or Dehydol O4 to aqueous solutions of SDS leads to a slight decrease of the CMCs, i.e. from 7.9 mmol/L for single-component SDS to 3.4 mmol/L for C_8E_4/SDS with $\alpha_1 = 0.25$ and from

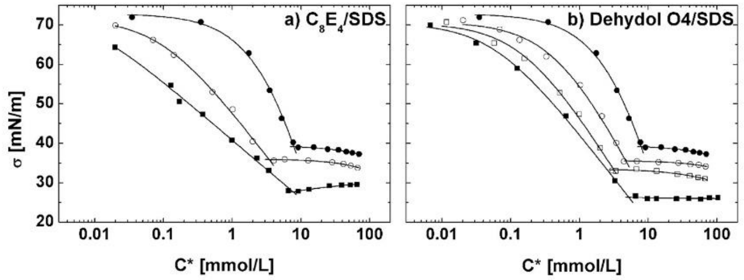

Fig. 3. Surface tension measurements of two mixed surfactant systems. (a) C_8E_4/SDS: $\alpha_1 = 0.00$ (●), $\alpha_1 = 1.00$ (■), $\alpha_1 = 0.24$ (○). (b) Dehydol O4/SDS: $\alpha_1 = 0.00$ (●), $\alpha_1 = 1.00$ (■), $\alpha_1 = 0.10$ (○), $\alpha_1 = 0.40$ (□). For the sake of clarity not all performed measurements were displayed here.

7.9 mmol/L to 4.7 mmol/L and to 3.2 mmol/L for Dehydol O4/SDS with $\alpha_1 = 0.1$ and 0.4 respectively, indicating a synergistic interaction between the amphiphiles. Furthermore, the surface tensions of surfactant mixtures are lower than the value obtained for single-component SDS in water and the curves approach the curve of single-component nonionic surfactant when its mole fraction increases. Ionic surfactants have usually higher surface tensions than nonionic surfactants due to electrostatic interactions at the surface. However, added nonionic surfactant molecules migrate to the water/air surface, resulting in a decrease of the electrostatic interactions. Hence, the surface tension diminishes, which is desirable for processes like emulsification, solubilization, and surface wetting. It is also noteworthy that the aqueous solution of Dehydol O4 separates in two phases just above the CMC and merges to one phase again with increasing concentration. This is in accordance with the binary phase diagram of Dehydol O4 in water (see Section 3.2).

The experimental values of C^* for each ratio of the nonionic/anionic surfactant mixture are displayed in Fig. 4. The non-ideal curve fits were determined according to the model developed by Holland and Rubingh for mixed micelles (see Section 2.7) and compared with the ideal mixing curve.

While the ideal curve fit results in a marginal decrease of C^*, the nonideal curve fit of the experimental values shows a pronounced decrease. Its minimum of the mixed surfactant system C_8E_4/SDS is located at $\alpha_1 = 0.5$ with a CMC of 2.7 mmol/L, compared to 7.8 mmol/L for the ideal curve fit. Dehydol O4/SDS has its minimum at $\alpha_1 = 0.55$ at the CMC of 2.9 mmol/L, compared to 6.2 mmol/L for the ideal curve fit. The interaction parameter β calculated for the C_8E_4/SDS system is equal to −4.2. Lange and Beck have reported a value of −4.1 for C_8E_6/SDS; −3.9 for $C_{12}E_8$/SDS and −4.3 for $C_{10}E_6$/sodium pentadecylsulfate [25]. Rubingh and Holland found a β value of −3.6 for $C_{10}E_4$/SDS and −4.1 for C_8E_4/sodium decylsulfate respectively [7]. Although chain lengths and number of ethoxy units of the C_iE_j vary between 8–12 and 4–8 respectively, β changes only slightly and remains between −3.6 and −4.2. This indicates that the interaction between SDS and C_iE_j is more affected by the nature of the polar head group of the ionic surfactant rather than by the lengths of the hydrophilic and hydrophobic parts of C_iE_j. Indeed, the interaction parameter β of C_8E_4 with decyltrimethylammonium bromide is equal to −1.8 which is quite different from the above values [6]. So, the interaction parameter between Dehydol O4 and SDS is expected to be close to the value between C_8E_4 and SDS. However, the β value of −3.1 significantly differs from −4.2. Packing constraints in mixed micelle formation may have an influence on the interaction parameter since the different lengths of the polyethoxylated chains may produce unwanted antagonistic effects. Hence, the best fit for the mixture Dehydol O4/SDS does not fit well the measured values for high Dehydol concentrations. Calculating the interaction parameter for $\alpha_1 = 0.8$ and 0.9 results in β values of −3.7 for both mole fractions, which in turn lies in the range of the above values. From the measurement of the β value, it is difficult to predict the influence of the interaction between SDS and C_8E_4 or Dehydol O4 on the solubilization of oils.

Table 2
Critical temperature T_c and critical composition γ_c of C_8E_4 and Dehydol O4 in pure water and in aqueous solution of SDS (1 wt.%).

Compound(s)	γ_c (wt.%)	T_c (°C)
C_8E_4	4.8	38.3
C_8E_4 + SDS	48.5	72.9
Dehydol O4	0.9	16.3
Dehydol O4 + SDS	42.3	60.2

3.2. Binary phase behaviour

The pseudo-binary phase diagrams of Dehydol and C_8E_4 in water and in an aqueous SDS solution are shown in Fig. 5. γ is the weight fraction of non-ionic surfactant in the mixture.

The phase diagram of the C_8E_4/water system shows the expected miscibility gap around 40 °C. With increasing amounts of C_8E_4, the phase separation temperature increases accordingly because a higher concentration results in an increase of ethoxy group concentration that has to be dehydrated. The addition of 1 wt.% SDS to the water phase charges the micelles and thus more energy in form of temperature increase has to be added to overcome – besides the dehydration of ethoxy groups – the electrostatic repulsion between micelles, until phase separation occurs [27–29]. Therefore, the critical temperature T_c, also known as cloud point evolves towards higher temperatures, as well as higher mass concentrations of C_8E_4 (see Table 2). Since at low nonionic surfactant concentrations, more SDS is available, and thus more ionic surfactant is distributed to each micelle, the increase is more pronounced in this region. With increasing amounts of C_8E_4, the curve passes through a minimum and eventually the dehydration of the ethoxy groups dominates again the curve slope change, as in the case without SDS. Roughly speaking, the same phenomena take place for the Dehydol O4/water system, with and without SDS. However, a noticeable profound minimum in the curve of the binary system is observed at very low concentration, as well as a break in the curve of the pseudo-binary system at $\gamma = 0.3$, $T = 72$ °C in the presence of SDS. Dehydol O4 is a surfactant mixture, consisting of C_8E_j with j ranging from 0 to 8. The low homologues ($j = 0–2$) are not miscible with water above 0 °C, so that they probably solubilize in the core of the micelles formed by the higher homologues. Since the minimum is located slightly above the CMC ($\gamma = 0.0016$, $T = 22$ °C), it can

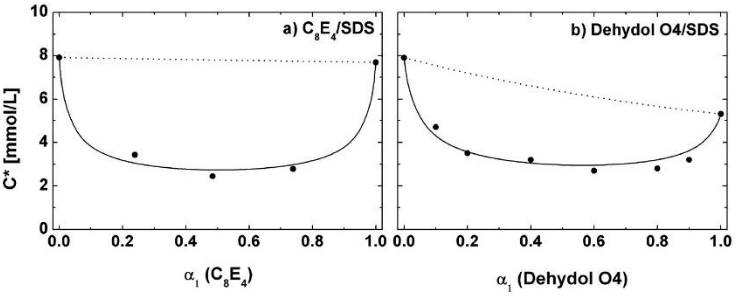

Fig. 4. Mixed critical micelle concentration C^* as a function of the mole fraction α_1 of the nonionic surfactant in the surfactant mixture. The dotted lines correspond to the ideal behaviour ($\beta = 0$) and the solid lines to the best non-ideal fit. (a) C_8E_4/SDS with $\beta = -4.2$. (b) Dehydol O4/SDS with $\beta = -3.1$.

be assumed that the very first micelles are not able to solubilize all lower homologues. Then, at higher concentrations of Dehydol O4, the second phase disappears, because there are enough micelles of C_8E_j ($j > 3$) to solubilize the non-water soluble homologous C_8E_j ($j < 3$). In the presence of SDS, an anomaly is also visible. A break in the curve ($\gamma = 0.3$, $T = 72$ °C) occurs at higher temperatures, probably caused as well by the different solubilities of C_8E_j in water. As already shown, the interaction parameter β between C_8E_4 and SDS is higher than the one between Dehydol O4 and SDS. Hence, by increasing the concentration of Dehydol O4 – and at the same time by decreasing the concentration of SDS – the phase separation temperature diminishes. At the break point, probably one of the homologues in Dehydol O4 returns to the surfactant layer due to hydration of the ethoxy units and thus reduces the interaction parameter between Dehydol O4 and SDS due to unfavourable packing in the mixed micelle. Eventually the curve drops faster towards lower temperatures until the dehydration of the ethoxy units overcomes this effect. It is foreseeable that the differences between the pseudo-binary phase diagrams of C_8E_4 and Dehydol O4 will induce distinct effects on the solubilization of fragrances. Table 2 summarizes the critical temperature (T_c) and the critical compositions (γ_c) obtained from the determination of the (pseudo-)binary phase diagrams.

The C_8E_4/SDS mixture has the highest critical temperature T_c of all investigated systems, followed by Dehydol O4/SDS. Pure Dehydol O4 has the lowest critical temperature and the lowest critical composition, owing to its polydispersity. The critical temperature and composition of a polyethoxylated glycol decrease with decreasing number of ethoxy units [30].

3.3. Lund cuts of the surfactant(s)/fragrance/water-temperature phase prism

The solubilization of β-pinene in the presence of different surfactant systems was investigated by constructing the T-β-pinene diagrams, i.e. the so-called Lund cuts of the surfactant(s)/fragrance/water-temperature phase prism [31]. The Lund cuts for the C_8E_4/β-pinene/water, C_8E_4 + SDS/β-pinene/water, Dehydol O4/β-pinene/water and Dehydol O4 + SDS/β-pinene/water systems are displayed in Fig. 6. C_8E_4 alone is capable of solubilizing β-pinene at low temperatures in a reduced monophasic region. At the optimal temperature T^* (18.0 °C), 8.9 wt.% of fragrance can be solubilized. Obviously the system is very temperature sensitive and no monophasic region is obtained above ≈20 °C since increase of T gives a two-phase system. However, due to the relatively short alkyl chain length of C_8E_4, the system exhibits a very limited zone of liquid crystals. By replacing 1.0 wt.% nonionic surfactant with SDS, the efficiency increases up to 12.5 wt.% of fragrance and T^* to 49.2 °C. Indeed, the ionic surfactant interacts with the nonionic surfactant and thus, shifts the miscibility gap in the W/S binary phase diagram to higher temperatures due to the presence of negative charges on the micelles. Since the phase behaviour in a S/F/W Gibb's triangle is mainly determined by the superposition of the miscibility gaps of its S/W, S/F and F/W binary phase diagrams, the increase of the cloud point in the S/W binary system results in a shrinking of the three-phase region and hence, the monophasic region in the water rich corner expands [10]. This results in a higher efficiency of the mixed surfactant system in comparison with the single surfactant system. The higher T^* can be explained by the increase of the

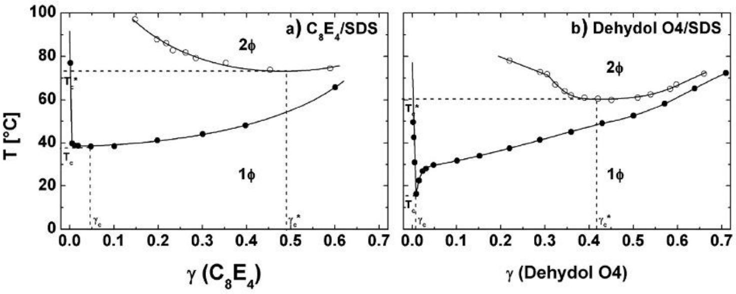

Fig. 5. Pseudo-binary phase diagrams. (a) C_8E_4 in pure water (●) and C_8E_4 in SDS_{aq} (○). (b) Dehydol O4 in pure water (●) and Dehydol O4 in SDS_{aq} (○). T_c and γ_c correspond to the critical temperature and composition respectively of the nonionic surfactants in water, whereas T_c^* and γ_c^* correspond to the critical temperature and composition respectively in SDS_{aq} (1 wt.%).

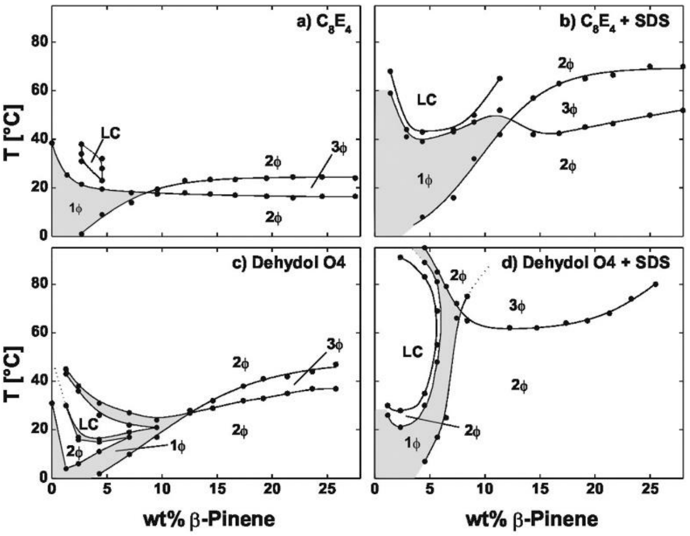

Fig. 6. Lund cut through the SOW-T phase prism at a constant water-to-surfactant ratio. β-Pinene is added to an aqueous surfactant solution containing (a) 10 wt.% C_8E_4, (b) 9 wt.% C_8E_4 + 1 wt.% SDS, (c) 10 wt.% Dehydol O4, (d) 9 wt.% Dehydol O4 + 1 wt.% SDS. The monophasic regions are shaded in grey. *Abbreviations*: 1ϕ, 2ϕ and 3ϕ correspond to 1, 2 and 3 phases respectively, LC = liquid crystalline phase.

effective hydrophilicity of the surfactant system in the presence of SDS. Due to the anionic surfactant the amphiphilic film is stronger curved. Therefore, more energy in form of temperature increase has to be transmitted into the system, in order to obtain a zero curvature. This turns the mixed surfactant system more hydrophobic due to dehydration of the ethoxy groups, and thus more fragrance of the excess oil phase can be solubilized in the O/W microemulsion until T^* is reached and the micellar solution inverts by squeezing out water. Noticeable is the huge expanded area of the liquid crystalline phase after addition of SDS. Since strong interaction occurs between the ionic and nonionic surfactants, a more expanded rigid surfactant interface may form between the water and oil phase.

The ternary Dehydol O4/β-pinene/W system shows more complicated phase behaviour. The binary phase diagram of Dehydol O4 in water has already set apart from the expected behaviour and obviously it affects fragrance solubilization as well. In particular, the efficiency and T^* increase to 12.5 wt.% and 26.4 °C respectively compared to 8.9 wt.% and 18.0 °C with C_8E_4. The liquid crystalline phase lies now at lower temperatures and lower fragrance concentrations, surrounded by a monophasic region. Furthermore, another two-phase region is found at low temperatures (between 5 and 20 °C) and low β-pinene concentrations (<5 wt.%), which is probably affected by the minimum in the binary phase diagram of Dehydol O4/water. By increasing temperature, a narrow one-phase region appears which results finally in a liquid crystalline phase. Further increase of the temperature leads to the melting of the liquid crystalline phase and above the narrow monophasic region, another two-phase region appears. Due to the polydispersity of Dehydol O4, the surfactants partition between the oil phase, water phase and interface [32]. With increasing temperature, the lower homologues become increasingly hydrophobic and migrate in the oil phase. The surfactants remaining at the interface have longer ethoxylated polar heads. This promotes the deformation of liquid crystalline phases, since a more hydrophilic head group results in a more curved micelle. Therefore transitions from hexagonal or lamellar liquid crystalline phases to isotropic micellar phases are possible [33].

In Fig. 6d, the liquid crystalline phase strongly expands as a function of T for β-pinene lower than ≈5 wt.%, which is due to the same reason as in the case of C_8E_4 and SDS. Moreover, T^* increases up to 69.0 °C while the efficiency dramatically decreases to 7.9 wt.%. Actually, an increase in efficiency was expected, as it occurred for C_8E_4 in combination with SDS. As already brought up, the various glycols in Dehydol O4 partition differently between the phases. Thus, by increasing the temperature, the lower homologues migrate from the interface to the oil phase while the higher homologues migrate from the water phase to the interface. With the addition of SDS, an almost temperature-insensitive surfactant is introduced to the mixture. As in the pseudo-binary system, the ionic surfactant increases also the temperature stability of the nonionic surfactant in the pseudo-ternary system. Therefore, the partition of the homologues surfactants occurs over a larger temperature range than in the case of Dehydol O4 alone, and thus less surfactant is available at the interface. Consequently, less fragrance can be solubilized with the Dehydol O4/SDS mixture compared to Dehydol O4 alone. However there is to some extent a constant amount of surfactant at the interface over the whole temperature interval, which results in the steep ascent of the phase boundary and thus an almost temperature insensitive microemulsion can be formed.

3.4. Solubilization of terpenes and essential oils

β-Pinene and *p*-cymene, as well as the essential oils *pinus sylvestris* and *pinus pinaster* were mixed with various aqueous solutions of surfactants. The phase diagrams were built as a function of temperature and weight percentages of terpene oil in the mixture in order to determine the one-phase microemulsion region. The diagrams were investigated solely in the range between 5 and 7 wt.% of oil because it is the concentration of fragrance required for practical applications. As shown previously in Fig. 6, the one-phase

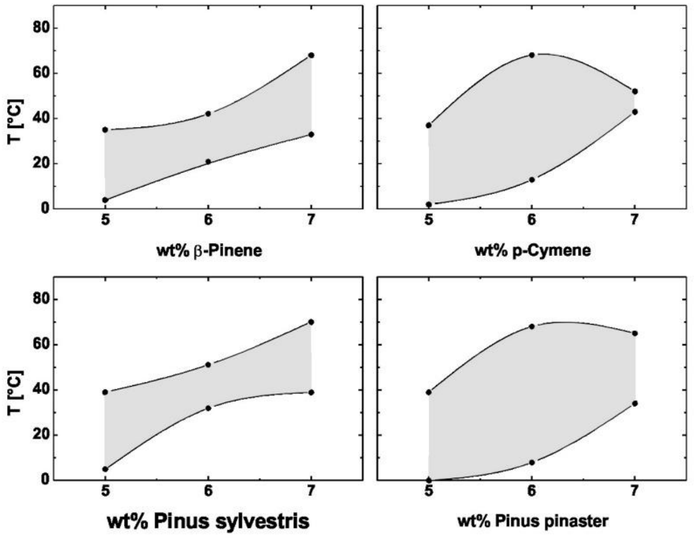

Fig. 7. Phase diagrams of the Dehydol O4 (9 wt.%) + SDS (1 wt.%)/fragrance/water systems. The one-phase regions are shaded in grey.

region obtained with 10 wt.% of Dehydol O4 alone is rather limited and fractionated in two parts by a LC zone whereas an aqueous surfactant mixture with 9 wt.% Dehydol O4 and 1 wt.% SDS is able to solubilize 6.5 wt.% of oil between 25 and 80 °C. Therefore, we studied here the solubilizing properties of two binary surfactant mixtures consisting of 9 wt.% of Dehydol O4 and 1 wt.% of SDS or SLES as solubilization enhancers in order to solubilize terpenes, as well as more complex fragrant mixtures. SLES was chosen because it is milder to skin than SDS. The one phase regions obtained with the four terpene oils are indicated in grey in Figs. 7 and 8 respectively.

The width of the monophasic regions depends on the hydrophobicity of the oil and the hydrophilicity of the ionic surfactant. It can be seen that *pinus sylvestris* behaves similarly to β-pinene, while *pinus pinaster* behaves similarly to *p*-cymene. This indicates that the apparent hydrophobicity of a multicomponent essential oil is related to the hydrophobicity and the ratio of each component in the mixture. A relevant parameter introduced by Cash et al. in 1977 to quantify the hydrophobicity of an oil is the equivalent alkane carbon number (EACN) value [34,35]. The EACN of a monomolecular or complex oil corresponds to the number of carbon atoms of

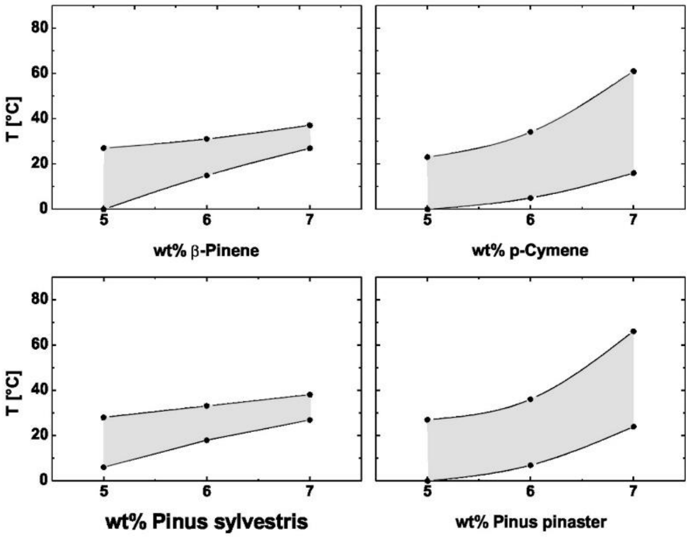

Fig. 8. Phase diagrams of the Dehydol O4 (9 wt.%) + SLES (1 wt.%)/fragrance/water systems. The monophasic regions are shaded in grey.

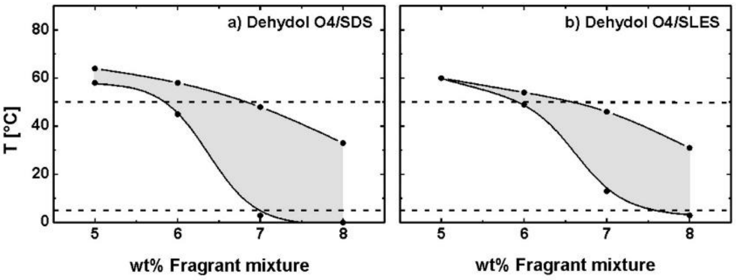

Fig. 9. Phase diagrams of Dehydol O4 (9 wt.%) + SDS (a) or SLES (b) (1 wt.%)/fragrant mixture/water. The monophasic regions are shaded in grey. The dashed lines indicate the temperature interval wherein water based perfume shall be one-phase.

the linear alkane that exhibits an equivalent hydrophobicity. It is known that branching, cyclisation [36], unsaturation or aromatization of the oil and the presence of a polar function in its chemical structure play a major role on the polarity of a given oil and thus impact its capability to be solubilized. Ontiveros et al. have recently reported the influence of the location of the —C(O)O— function on the EACN of ester oils [37]. Bouton et al. have assessed the EACN of β-pinene and *p*-cymene to 2.2 and −0.4 respectively, indicating that *p*-cymene is significantly more polar than β-pinene [21]. In both cases – with SDS and SLES – the solubilization of the more polar oil is easier as expected. Based on the oil composition (see Table 1) and on the hypothesis that EACNs are additives, an average EACN value equal to 3.0 can be calculated for *pinus sylvestris*. The average EACN value of *pinus pinaster* is expected to be much lower since it contains 23.4% of *m*-cymene (to which we assign an EACN close to that of *p*-cymene, i.e. −0.4) and 19.4% of the polar oil cineole (for which the EACN is unknown). Therefore, it is understandable that *pinus sylvestris* and *pinus pinaster* behave similarly to β-pinene and *p*-cymene respectively.

3.5. Fragrance solubilization

For practical application such as non-alcoholic perfumes, it is necessary to formulate aqueous solutions of complex fragrances which remain stable in a large temperature range, i.e. 5–50 °C. As shown in Fig. 9, a stable microemulsion containing 7 wt.% of a true fragrant composition (see Table 1) can be prepared with the binary Dehydol O4/SDS surfactant system.

It is striking that in contrast to previous terpene oils, the temperature interval of stability of the microemulsion increases with the amount of oil. The one-phase region starts at high temperature (≈60 °C) and expands with higher amounts of oil to lower temperatures. The main difference between the fragrant composition and the terpene oils (see Fig. 8) is the presence of large amounts of linalool (36.7 wt.%), a fragrant alcohol, and of the solvent dipropylene glycol (19.2 wt.%). Depending on their chemical functionalities, terpene oils can solubilize in the interfacial surfactant monolayer between oil and water and alter the curvature [38]. Especially terpene alcohols, which can be used both as a co-solvent and as a co-surfactant in a microemulsion formulation, are good for solubilization in the surfactant palisade. Garti et al. have shown that ethanol, propylene glycol and glycerol are able to increase the monophasic region in the water rich corner [39]. Stubenrauch et al. have already pointed out that the fragrance molecule geraniol is effective as a co-surfactant, which penetrates the interface and a as a co-solvent [40,41]. Tchakalova et al. stated that in the interface solubilized polar oils alter the curvature, thus leaving energetically unfavourable holes, which can be filled by co-extraction of more hydrophobic compounds of the oil mixture [42]. Therefore it can be concluded that linalool acts as a co-surfactant which solubilizes in the interface and co-extracts more hydrophobic compounds closer to the palisade layer. Furthermore, dipropylene glycol acts as a co-solvent, which supports solubilization as well. Thus it is possible to obtain an enlarged monophasic region with increasing amount of oil. Finally, it is noteworthy that in the absence of the ionic surfactant, the monophasic region, surrounded by liquid crystalline structures, is obtained only below 10 °C for 5 wt.% of the fragrant mixture. Linalool probably penetrates the interface and makes the nonionic surfactant effectively more hydrophobic, which results in a shift of the whole monophasic region to lower temperatures. The effect of the ionic surfactant is thus remarkable, because it is able to shift the monophasic region to ambient temperatures by simultaneously increasing its expanded area.

4. Conclusion

A clear, non-viscous microemulsion, containing 5–7 wt.% of fragrance or essential oil and stable in a wide range of temperatures, i.e. from 5 to 50 °C, may be of great interest for perfumery and personal care industries. In this work, it is shown that small amounts of SDS or SLES (≤1 wt.%) improve the ability of monodispersed C_8E_4 and polydispersed Dehydol O4 to solubilize terpene oils and fragrances in fragrance-in-water temperature insensitive microemulsions. The differences between well-defined and commercial C_8E_4 arise from the change with temperature of the partition of homologous C_8E_j between the water phase, the oil phase and the interfacial pseudo-phase. The location and the width of the monophasic region are influenced by the hydrophilicity of the ionic surfactant and the EACN of the oil as well as its co-surfactant properties. Ionic surfactants and polar oils shift the monophasic region to higher temperatures because they increase the effective hydrophilicity of the interfacial film. Aromatic polar oils and terpene alcohols are better solubilized than terpene oils and in a wider temperature range because they penetrate into the interfacial films and increase their flexibilities. Furthermore, they create holes in the palisade layer, wherein more hydrophobic oil can be co-extracted, hence resulting in a more expanded one-phase region in the case of fragrant mixtures.

References

[1] A.M. Misselyn-Bauduin, A. Thibaut, J. Grandjean, G. Broze, R. Jérome, Mixed micelles of anionic–nonionic and anionic–zwitterionic surfactants analyzed by pulsed field gradient NMR, Langmuir 16 (2000) 4430–4435.

[2] I.A. Khan, A.J. Khanam, Z.A. Khan, Kabir-ud-Din, Mixing behaviour of anionic hydrotropes with cationic Gemini surfactants, J. Chem. Eng. Data 55 (2010) 4775–4779.

[3] C. Treiner, M. Nortz, C. Vaution, Micellar solubilisation in strongly interacting binary surfactant systems, Langmuir 6 (1990) 1211–1216.

[4] J.D. Hines, R.K. Thomas, P.R. Garret, G.K. Rennie, J. Penfold, Investigation of mixing in binary surfactant solutions by surface tension and neutron reflection: anionic/nonionic and zwitterionic/nonionic mixtures, J. Phys. Chem. B 101 (1997) 9215–9223.

[5] Q. Zhou, M.J. Rosen, Molecular interactions of surfactants in mixed monolayers at the air/aqueous solution interface and in mixed micelles in aqueous media: the regular solution approach, Langmuir 19 (2003) 4555–4562.

[6] P.M. Holland, D.N. Rubingh, Nonideal multicomponent mixed micelle model, J. Phys. Chem. 87 (1983) 1984–1990.

[7] R.M. Holland, D.N. Rubingh, Mixed Surfactant Systems, American Chemical Society, Washington, DC, 1992.

[8] H. Matsubara, A. Ohta, M. Kameda, N. Ikeda, M. Aratono, Interaction between ionic and nonionic surfactants in the absorbed film and micelle. Dodecylammonium chloride and tetraethylene glycol monooctyl ether, Langmuir 16 (2000) 7589–7596.

[9] H. Matsubara, S. Muroi, M. Kameda, N. Ikeda, A. Ohta, M. Aratono, Interaction between ionic and nonionic surfactants in the adsorbed film and micelle. 3. Sodium dodecyl sulfate and tetraethylene glycol monooctyl ether, Langmuir 17 (2001) 7752–7757.

[10] M. Kahlweit, B. Faulhaber, G. Busse, Microemulsions with mixtures of nonionic and ionic amphiphiles, Langmuir 10 (1994) 2528–2532.

[11] T. Sottmann, Phase behaviour, interfacial tension and microstructure of microemulsions, in: C. Stubenrauch (Ed.), Microemulsions, Wiley-Blackwell, 2009, pp. 1–47.

[12] M. Kahlweit, R. Strey, Phase behavior of quinary mixtures of the type H_2O–oil–nonionic amphiphile-ionic amphiphile-salt, J. Phys. Chem. 92 (1988) 1557–1563.

[13] H. Kunieda, K. Shinoda, Phase behavior in systems of nonionic surfactant/water/oil around the hydrophile–lipophile-balance-temperature (HLB-temperature), J. Disper. Sci. Technol. 3 (1982) 233–244.

[14] A. Graciaa, Y. Barakat, R.S. Schechter, W.H. Wade, S. Yiv, Emulsion stability and phase behavior for ethoxylated nonyl phenol surfactants, J. Colloid Interface Sci. 89 (1982) 217–225.

[15] K. Aramaki, K. Ozawa, H. Kunieda, Effect of temperature on the phase behavior of ionic–nonionic microemulsions, J. Colloid Interface Sci. 196 (1997) 74–78.

[16] S. Queste, J.L. Salager, R. Strey, J.M. Aubry, The EACN scale for oil classification revisited thanks to fish diagrams, J. Colloid Interface Sci. 312 (2007) 98–107.

[17] N. Kanei, Y. Tamura, H. Kunieda, Effect of types of perfume compounds on the hydrophile–lipophile balance temperature, J. Colloid Interface Sci. 218 (1999) 13–22.

[18] A.G. Fournial, V. Molinier, G. Vermeersch, J.M. Aubry, N. Azaroual, High resolution NMR for the direct characterization of complex polyoxyethoxylated alcohols (C_iE_j) mixtures, Colloid Surf. A: Physicochem. Eng. Aspects 331 (2008) 16–24.

[19] PLC, Unilever, Aqueous perfume oil microemulsions, European Patent Office (1992), 0 571 677 A1.

[20] M. Stejerndahl, K. Holmberg, Synthesis and chemical hydrolysis of surface-active esters, J. Surfactants Deterg. 6 (2003) 311–318.

[21] F. Bouton, M. Durand, V. Nardello-Rataj, A.P. Borosy, C. Quellet, J.-M. Aubry, A QSPR model for the prediction of the "Fish-Tail" temperature of C_iE_4/water/polar hydrocarbon oil systems, Langmuir 26 (2010) 7962–7970.

[22] F. Bouton, M. Durand, V. Nardello-Rataj, M. Serry, J.-M. Aubry, Classification of terpene oils using the fish diagrams and the Equivalent Alkane Carbon (EACN) scale, Colloid Surf. A: Physicochem. Eng. Aspects 338 (2009) 142–147.

[23] T. Chakraborty, S. Ghosh, A unified survey of applicability of theories of mixed adsorbed film and mixed micellization, J. Surfactants Deterg. 11 (2008) 323–334.

[24] B. Soharbi, H. Gharibi, B. Tajik, S. Javadian, M. Hashemianzadeh, Molecular interactions of cationic and anionic surfactants in mixed monolayers and aggregates, J. Phys. Chem. B 112 (2008) 14869–14876.

[25] H. Lange, K.H. Beck, Zur Mizellbildung in Mischlösungen homologer und nichthomologer Tenside, Kolloid Z. -Z. Polym. 251 (1973) 424–431.

[26] G. Rauwel, L. Leclerq, J. Criquelion, J.-M. Aubry, V. Nardello-Rataj, Aqueous mixtures of di-n-decyldimethylammonium chloride/polyoxyethylene alkyl ether: dramatic influence of tail/tail and head/head interactions on co-micellization and biocidal activity, J. Colloid Interface Sci. 374 (2012) 176–186.

[27] L. De Salvo Souza, M. Corti, L. Cantú, V. Degiorgio, Observation of a vanishing miscibility loop in the phase diagram of solutions of a mixed non-ionic–ionic amphiphile, Chem. Phys. Lett. 131 (1986) 160–164.

[28] K. Kuriyama, H. Inoue, T. Nakagawa, Temperature dependence of micellar weight of nonionic surfactant in the presence of various additives. III. Addition of sodium dodecyl sulfate, Kolloid Z. 183 (1962) 68–71.

[29] W.N. Maclay, Factors affecting the solubility of nonionic emulsifiers, J. Colloid Sci. 11 (1956) 272–285.

[30] K.-V. Schubert, R. Strey, M. Kahlweit, A new purification technique for alkyl polyglycol ethers and miscibility gaps for water–C_iE_j, J. Colloid Interface Sci. 141 (1990) 21–29.

[31] J. Balogh, Determining scaling in known phase diagrams of nonionic microemulsions to aid constructing unknown, Adv. Colloid Interface 159 (2010) 22–31.

[32] A. Graciaa, J. Andérez, C. Bracho, J. Lachaise, J.-L. Salager, L. Tolosa, F. Ysambertt, The selective partitioning of the oligomers of polyethoxylated surfactant mixtures between interface and oil and water bulk phases, Adv. Colloid Interface 123 (2006) 63–73.

[33] H. Kunieda, K. Shigeta, K. Ozawa, M. Suzuki, Self-organizing structures in poly(oxyethylene) oleyl ether–water system, J. Phys. Chem. B 101 (1997) 7952–7957.

[34] L. Cash, J.L. Cayias, G. Fournier, D. McAllister, T. Schatz, R.S. Schechter, W. Wade, The application of low interfacial tension scaling rules to binary hydrocarbon mixtures, J. Colloid Interface Sci. 59 (1977) 39–44.

[35] M.E. Hayes, M. Bourrel, M.M. El-Emary, R.S. Schechter, W.H. Wade, Interfacial tension and behaviour of nonionic surfactants, Soc. Petrol. Eng. J. 19 (1979) 349–356.

[36] S. Burauer, T. Sottmann, R. Strey, Nonionic microemulsions with cyclic oils, Tenside Surfactants Deterg. 37 (2000) 8–16.

[37] J.F. Ontiveros, C. Pierlot, M. Catté, V. Molinier, A. Pizzino, J.-L. Salager, J.-M. Aubry, Classification of ester oils according to their Equivalent Alkane Carbon Number (EACN) and asymmetry of fish diagrams of $C_{10}E_4$/ester oil/water systems, J. Colloid Interface Sci. 403 (2013) 67–76.

[38] V. Tchakalova, W. Fieber, Classification of fragrances and fragrance mixtures based on interfacial solubilization, J. Surfactants Deterg. 15 (2012) 167–177.

[39] N. Garti, A. Yaghmur, M.E. Leser, V. Clement, H.J. Watzke, Improved oil solubilization in oil/water food grade microemulsions in the presence of polyols and ethanol, J. Agric. Food Chem. 49 (2001) 2552–2562.

[40] C. Stubenrauch, B. Paeplow, G. Findenegg, Microemulsions supported by octyl monoglucoside and geraniol. 1. The role of the alcohol in the interfacial layer, Langmuir 13 (1997) 3652–3658.

[41] C. Stubenrauch, G. Findenegg, Microemulsions supported by octyl monoglucoside and geraniol. 2. An NMR self-diffusion study of the microstructure, Langmuir 14 (1998) 6005–6012.

[42] V. Tchakalova, F. Testard, K. Wong, A. Parker, D. Benczédi, T. Zemb, Solubilisation and interfacial curvature in microemulsions. I. Interfacial expansion and co-extraction of oil, Colloid Surf. A: Physicochem. Eng. Aspects 331 (2008) 31–39.